Universitat Autònoma de Barcelona

# GENE THERAPY FOR THE TREATMENT OF NEUROLOGIC AND SOMATIC MUCOPOLYSACCHARIDOSIS TYPE II (HUNTER SYNDROME)

**SANDRA MOTAS MALLOL**

Universitat Autònoma de Barcelona

DEPARTMENT OF BIOCHEMISTRY AND MOLECULAR BIOLOGY
SCHOOL OF VETERINARY MEDECINE

CENTER OF ANIMAL BIOTECHNOLOGY AND GENE THERAPY

# GENE THERAPY FOR THE TREATMENT OF NEUROLOGIC AND SOMATIC MUCOPOLYSACCHARIDOSIS TYPE II (HUNTER SYNDROME)

SANDRA MOTAS MALLOL

This PhD thesis has been carried out under the direction of Dr. Fàtima Bosch Tubert and Dr. Virginia A. Haurigot at the Biochemistry and Molecular Biology Department of the Veterinary School of Medicine and at the Center of Animal Biotechnology and Gene Therapy (CBATEG).

**SANDRA MOTAS MALLOL**

**FÀTIMA BOSCH TUBERT** **VIRGINIA A. HAURIGOT**

**JULY 2016**

**BELLATERRA**

*Als meus pares*

Cada nova etapa de la vida es comença amb molta il·lusió i entusiasme, però també amb respecte i una mica d'incertesa i por per no saber què passarà, i aquesta tesi doctoral no n'ha sigut una excepció. Però per sort, durant el llarg camí d'aquesta tesi molta gent m'ha guiat, ajudat i acompanyat dia rere dia. Aquesta tesi té una petita part de cada un d'ells, i és per això, que ara només puc tenir paraules d'agraïment.

En primer lloc, m'agradaria agrair a la Dra. Fàtima Bosch haver-me donat l'oportunitat de poder realitzat la tesi doctoral en el seu grup d'investigació. Gràcies per la confiança dipositada en mi i per tota l'energia i passió que m'has transmès per aquest projecte i per la ciència. He aprés molt de la teva vitalitat.

Dra. Virginia A. Haurigot, és a dir, Vicky, gràcies per ensenyar-me que l'esforç i el treball constant tenen la seva recompensa. Sempre has tingut les paraules justes i els consells oportuns per mi, gràcies per guiar-me durant tots aquests anys.

Vull donar les gràcies també a tots els companys de laboratori que m'han acompanyat, ajudat, i sobretot aguantat durant aquest camí. Gràcies per tots els moments inoblidables que hem viscut al laboratori (i fora del laboratori) i sobretot, per haver fet agradables els moments més difícils.

Pilar, moltes, moltíssimes gràcies per iniciar-me en el món de la investigació. M'has ensenyat a ser crítica, i sobretot, a no rendir-me i ser persistent per aconseguir el que vulgui. Simplement, no tinc paraules per expressar el meu agraïment per tot el que et dec.

Sara, Albert i Carles, gràcies per ser els meus mestres MPSs. M'heu ensenyat a sobreviure als moments més estressants i sempre heu estat disponibles al 110% per ajudar-me en qualsevol cosa. Gràcies equip!

Xavi, el meu axó, no et pots arribar a imaginar com m'has ajudat i facilitat el treball d'aquests últims anys, mil gràcies! Sé que aconseguiràs tot el que et proposis.

A la resta de MPSeros, Víctor, Joan, Sara *petita* i Jenny, gràcies per tota l'ajuda i per ser l'alegria de l'equip, us dec molts somriures.

Estefania i Iris, no podia haver tingut millors companyes d'inici d'aquesta aventura. Mai oblidaré els berenars a la primera planta o les excursions a l'escola de postgrau per entregar papers. Maria, sempre hi has estat, apunt per ajudar tant amb un clonning, amb una matança improvisada com amb consells de com fer una bufanda amb mitja, gràcies per estar sempre disponible. Miquel, sé que a vegades sóc molt pesada, però sempre has trobat 10 minuts per dedicar-me i ajudar-me en qualsevol tema, moltes gràcies. Xavi León,

gràcies per saludar-me matí sí, matí també. A la resta de joves i adorables C., Clàudia, Victor adipo, Jordi i Marisa, moltes gràcies per acompanyar-me i sobretot, per totes les rialles. Tami, gràcies per tots els dinars que vam compartir. Alba i Cristina, les noies de pàncrees, gràcies perquè sempre m'heu escoltat i aconsellat sàviament. Gràcies també a la resta de companys de laboratori: Luca, Vero, Sergio, Meritxell, Tura, Laia, Ivet i Sylvie; i també a tots els ex-companys amb qui vaig compartir alguna estona de laboratori: Miquel Calero, Andrés, Calle, Edu, Ricardo i Efrén.

M'agradaria agrair també tota l'ajuda rebuda del Dr. Jesús Ruberte i tot el seu equip: Lorena, David, Ángel i Vero. Gràcies per totes les hores dedicades a matances, immunos i microscopi.

Moltes gràcies també a tot l'equip tècnic: Marta, per totes les immunos d'última hora; i Jenny i Lídia, les cuineres, per totes les solucions i comandes. Gràcies també a tota la gent de l'estabulari SER-CBATEG, en especial a en Pedro i la Marta, per tota la feinada que han portat els 30.000. No pot faltar també, agrair la simpatia i els bons ànims de les noies de la UAT, Anna Pujol, Anna Arbós i Sandra. Gràcies a la Rosmi i la Montse, el vostre suport administratiu ha sigut clau durant tots aquests anys, a en Carles Ros i al seu equip de manteniment, a l'SPLIPI i als companys de seguretat i neteja.

Però sobretot vull agrair aquesta tesi a la meva família. Gràcies mama i gràcies papa per haver-m'ho donat tot en aquesta vida. Sempre m'heu recolzat i animat a seguir endavant, gràcies a vosaltres he aconseguit tot el que m'he proposat. Mireia, *Caipi*, sempre has vetllat perquè no em falti de res i m'has donat suport incondicional en tot. I és gràcies a tu que va començar tota aquesta aventura de venir a estudiar a Barcelona. Josep, gràcies per aquests últims anys, has sigut una incorporació molt valuosa a la família. Avi, iaia, sé que heu lluitat perquè no perdi la lletra, gràcies. Gràcies també família Caballé Moreno, perquè des del primer dia m'heu acollit amb els braços oberts i m'heu fet sentir com una més de la família. Aquesta etapa ha sigut molt més fàcil al tenir-vos a tots vosaltres al meu costat, moltes gràcies de tot cor.

Aquesta tesi també ha estat possible gràcies a la Montse, en Jaume i la Sílvia, a les nenes de Torroella, gràcies per haver seguit al meu costat tot i la distància, i a les princeses de Girona, gràcies per haver-me acollit com una amiga més de tota la vida. Valèria i Anna, gràcies pels dinars a ciències i les *nombroses* visites al SAF.

Per últim, l'agraïment més important és per en Marc. Amb molta paciència, no t'has cansat de fer-me somriure dia rere dia. Ets tot el que necessito. M'has acompanyat en els moment bons però sobretot en els moments més difícils, i mai t'ho podré agrair prou. Simplement, gràcies per fer-me feliç.

I gratefully acknowledge the predoctoral fellowship received during 3 years of my PhD from Generalitat de Catalunya, Spain. The studies have been supported by funding from: Plan Nacional I+D+I from the Ministerio de Economía y Competitividad (INNPACTO IPT-2012-0772-300000 and SAF 2014-54866-R), Generalitat de Catalunya (2014SGR-1669), MPS España Foundation, Spain, and from the European Union through Regional Development Funds (ERDF). This work is also part of a Public-Private Partnership on Gene Therapy between UAB and Laboratorios ESTEVE S.A.

| | |
|---|---|
| **6MWT** | Six-minute walk test |
| **A** | Adenine |
| **AAP** | Assembly-activating protein |
| **AAV** | Adeno-associated virus |
| **ADA-SCID** | Severe combined immunodeficiency due to adenosine deaminase deficiency |
| **Ad** | Adenovirus |
| **AM** | Ante meridiem |
| **ANOVA** | Analysis of variance |
| **AO** | Antisense oligonucleotide |
| **APE1** | Apurinic endonuclease 1 |
| **ARRIVE** | Animal Research Reporting In Vivo Experiments |
| **ATP** | Adenosine triphosphate |
| **BBB** | Blood-brain barrier |
| **bGeo/Puro** | beta-galactosidase/neomycin, puromycine |
| **BMT** | Bone marrow transplantation |
| **BMP** | Bone morphogenetic protein |
| **bp** | Base pair |
| **BSA** | Bovine serum albumin |
| **BSI-B4** | Lectin from *Bandeiraea simplicifolia* (*Griffonia simplicifolia*), Isolectin B4 |
| **C** | Cytosine |
| **CAG** | Hybrid promoter composed of the cytomegalovirus (CMV) early enhancer, the chicken β-actin promoter, the chiken β-actin exon, the chimeric intron composed of the chicken β-actin intron and the rabbit β-globin intron, and the rabbit β-globin exon |
| **CBATEG** | Center of Animal Biotechnology and Gene Therapy |
| **cDNA** | Complementary deoxyribonucleic acid |
| **CDS** | Coding sequence |
| **cm** | Centimetre |
| **CMT** | Calcium modulating therapy |
| **CMV** | Cytomegalovirus |
| **CNS** | Central nervous system |
| **CP** | Choroid plexuses |
| **CRT** | Cholesterol removing therapy |
| **CsCl** | Cesium cloride |
| **CSF** | Cerebrospinal fluid |
| **CT** | Chaperon therapy |
| **CTEN** | Cell Type Enrichment |
| **CTS** | Carpal tunnel syndrome |
| **Cu/ZnSOD** | Copper/zinc superoxide dismutase |
| **DBS** | Dried blood spots |
| **DNA** | Deoxyribonucleic acid |
| **DNase** | Deoxyribonuclease |

| | |
|---|---|
| **dNTP** | Deoxynucleoside trifosfate |
| **DMMB** | Dimethyl methylene blue |
| **ds** | Double stranded |
| **DS** | Dermatan sulfate |
| ***E. coli*** | *Escherichia coli* |
| **EDTA** | Ethylendiaminetetraacetic acid |
| **EF** | Elongation factor 1-a |
| **e.g.** | *Exempli gratia* (for example) |
| **EMA** | European Medicines Agency |
| **ERT** | Enzyme replacement therapy |
| **FDA** | Food and Drug Administration |
| **FGF** | Fibroblast growth factor |
| **FGFR** | Fibroblast growth factor receptor |
| **FGly** | FormylGlycine |
| **Fw** | Forward |
| ***g*** | Gravity |
| **g** | Gram |
| ***G*** | Gauge |
| **G** | Guanine |
| **GAG** | Glycosaminoglycan |
| **GALNS** | N-Acetylgalactosamine-6-sulfate-sulfatase |
| **GFAP** | Glial fibrillary acidic protein |
| **GFP** | Green fluorescent protein |
| **GM2** | Monosialodihexosylganglioside 2 |
| **GM3** | Monosialodihexosylganglioside 3 |
| **GMP** | Good Manufacturing Practice |
| **GO** | Gene Ontology |
| **GUSB** | β-Glucoronidase |
| **HGF/SF** | Hepatocyte growth factor/scatter factor |
| **HGSNAT** | Heparan α-glucosaminide N-acetyltransferase |
| **h** | Hour |
| **h*IDS*** | Human *Iduronate-2-sulfatase* gene |
| **HIR** | Human insulin receptor |
| **HS** | Heparan sulfate |
| **HSCT** | Hematopoietic stem cell transplantation |
| **Iba1** | Ionized calcium-binding adapter molecule 1 |
| **IDDD** | Intrathecal drug delivery device |
| ***Ids*** | *Iduronate-2-sulfatase* (murine gene) |
| ***IDS*** | *Iduronate-2-sulfatase* (human gene) |
| **IDS** | Iduronate-2-sulfatase (protein) |
| **IDUA** | α-L-Iduronidase |
| **i.e.** | *Id est* (that is) |
| **IQ** | Intelligence quotient |

| | |
|---|---|
| **IR** | Insulin receptor |
| **IT** | Intrathecal |
| **ITR** | Inverted terminal repeats |
| **kb** | Kilobase |
| **kDa** | KiloDalton |
| **kg** | Kilogram |
| **KO** | Knock-out |
| **LAMP1** | Lysosome-associated membrane protein 1 |
| **LAMP2** | Lysosome-associated membrane protein 2 |
| **LEBT** | Lysosomal enzymes purified from bovine testis |
| **LIMP2** | Lysosomal integral membrane protein 2 |
| **LPLD** | Lipoprotein lipase deficiency |
| **LPS** | Lipopolysaccharide |
| **LSD** | Lysosomal storage disease |
| **LV** | Lentivirus |
| **M** | Molar concentration (mol/l) |
| **M6P** | Mannose-6-phosphate |
| **M6PR** | Mannose-6-phosphate receptor |
| **MAb** | Monoclonal antibody |
| **MCS** | Multiple-cloning site |
| **MDS** | Multiple sulfatase deficiency |
| **mer** | Repeat unit |
| **mg** | Miligram |
| **m*Ids*** | murine *Iduronate-2-sulfatase* gene |
| **ml** | Millilitre |
| **mM** | Millimolar |
| **$mm^3$** | Cubic millimetre |
| **MnSOD** | Manganese superoxide dismutase |
| **MPS** | Mucopolysaccharidosis |
| **mRNA** | Messenger RNA |
| **MTH** | Molecular Trojan horse |
| **MU** | Methylumbelliferone |
| **N** | Number of animals |
| **NAGLU** | α-N-Acetylglucosaminidase |
| **NCL** | Neuronal ceroid lipofuscinoses |
| **NeuN** | Neuronal nuclei |
| **ng** | Nanogram |
| **nm** | Nanometre |
| **ODD** | Orphan Drug Designation |
| **oh*IDS*** | optimized human *Iduronate-2-sulfatase* gene |
| **Oligo-dT** | Oligo deoxitimine |
| **om*Ids*** | optimized murine *Iduronate-2-sulfatase* gene |
| **ORF** | Open reading frame |

| | |
|---|---|
| **OSA** | Obstructive sleep apnoea |
| ***P*** | Statistic *P*-value |
| **P2** | Postnatal day 2 |
| **PAMP** | Pathogen-associated molecular pattern |
| **PBL** | Peripheral blood lymphocytes |
| **PBS** | Phosphate-buffered saline |
| **PCR** | Polymerase chain reaction |
| **PEG** | Polyethylene glycol |
| **PG** | Proteoglycan |
| **pH** | Potential hydrogen |
| **PM** | Post meridiem |
| **PNS** | Peripheral nervous system |
| **qPCR** | Quantitative polymerase chain reaction |
| **RB** | Roller bottle |
| **RER** | Rough endoplasmic reticulum |
| **RMA** | Robusst Multiarray Averaging |
| **RNA** | Ribonucleic acid |
| **RNase** | Ribonuclease |
| **ROM** | Range of motion |
| **rpm** | Revolutions per minute |
| **Rv** | Reverse |
| **s** | Second |
| **SEM** | Standard error of the mean |
| **SER-CBATEG** | Servei Estabulari Ratolins - Center of Animal Biotechnology and Gene Therapy |
| **SGSH** | Sulfoglucosamine N-sulfohydrolase |
| **SPF** | Specific pathogen-free |
| **SRT** | Substrate reduction therapy |
| **ss** | Single stranded |
| **SUMF1** | Sulfatase-modifying factor 1 |
| **T** | Thymine |
| **TBG** | Thyroxin-binding globulin |
| **TEM** | Transmission electron microscopy |
| **TFEB** | Transcription factor EB |
| **TfR** | Transferrin receptor |
| **TLR4** | Toll-like receptor 4 |
| **U** | Unit |
| **UAB** | Universitat Autònoma de Barcelona |
| **USA** | United States of America |
| **UV** | Ultraviolet |
| **V** | Volt |
| **vg** | Vector genome |
| **vg/dg** | Vector genome copy number/diploid genome |

| | |
|---|---|
| ***vs.*** | Versus |
| **v/v** | Volume/volume |
| **W** | Watt |
| **WPRE** | Woodchuck hepatitis virus post-transcriptional regulatory element |
| **WT** | Wild-type |
| **w/v** | Weight/volume |
| **XCI** | X-chromosome inactivation |
| **ºC** | Degree centigrade |
| **Å** | Angstrom |
| **β-HEXO** | β-hexosaminidase |
| **µg** | Microgram |
| **µl** | Microliter |
| **µm** | Micrometre |
| **$** | Dollar sign |

# I. PRESENTATION

Mucopolysaccharidosis type II (MPSII), or Hunter syndrome, is an X-linked recessive lysosomal storage disease (LSD) caused by the deficiency in Iduronate-2-sulfatase (IDS), an enzyme involved in the stepwise degradation of the glycosaminoglycans (GAGs) heparan sulfate (HS) and dermatan sulfate (DS). The pathological accumulation of undegraded HS and DS in the lysosomes leads to cell dysfunction, causing severe neurologic and somatic disease. The most severe and most prevalent form of Hunter syndrome is characterized by chronic and progressive neurodegeneration of the central nervous system (CNS) and multisystem dysfunction; patients usually die during the second decade of life. To date, weekly intravenous enzyme replacement therapy (ERT) constitutes the only approved therapeutic option for MPSII. However, the inability of recombinant IDS to efficiently cross the blood-brain barrier (BBB) limits the efficacy of ERT in treating neurological symptoms. The therapy has several other drawbacks. Thus, an efficient therapy for the treatment of the neurodegeneration of MPSII disease represents a highly unmet medical need. *In vivo* gene therapy with adeno-associated vectors offers the possibility of lifelong therapeutic benefit following a single administration.

Therefore, the present work was focused on the development of a new gene therapy approach for MPSII based on the delivery of vectors to the cerebrospinal fluid (CSF) and aimed at counteracting simultaneously the neurological and somatic pathology characteristic of the disease. Adeno-associated virus serotype 9 vectors (AAV9) containing the murine *Ids* gene were administered through a minimal invasive procedure to the CSF of 2-month-old MPSII mice, which already presented established pathology. The efficacy of AAV9-*Ids* vectors to counteract MPSII pathology after a single intra-CSF injection was evaluated 4 and 8 months after treatment. AAV9-mediated *Ids* gene transfer led to a significant increase in IDS activity throughout the encephalon, which resulted in full reversion of lysosomal storage lesions. In addition, correction of lysosomal dysfunction in the CNS, normalization of brain transcriptomic signature and disappearance of neuroinflammation were achieved after gene transfer. Moreover, after AAV9-*Ids* delivery to the CSF, vectors also transduced the liver, providing a peripheral source of the therapeutic protein that corrected storage pathology in visceral organs of treated MPSII mice. The reversion of the pathology in non-transduced somatic organs provided evidence of cross-correction by circulating enzyme. Importantly, AAV9-*Ids* treatment also resulted in normalization of behavioural deficits and considerably prolonged the survival of treated MPSII mice.

The efficacy of the intra-CSF administration of AAV9 vectors containing the human *IDS* coding sequence was also evaluated in MPSII mice. One and a half months after gene transfer, a significant increase in IDS activity was documented throughout the encephalon, an in the liver and serum of treated MPSII mice. Consequently, pathological GAG content was reduced, or even normalized, in the CNS and in most somatic tissues of MPSII mice that received the vectors.

Altogether, the results obtained in the present work provide a strong proof of concept that supports the clinical translation of the intra-CSF AAV9-*IDS* gene therapy for the treatment of Hunter patients with cognitive impairment.

# II. INTRODUCTION

# 1. LYSOSOMAL STORAGE DISEASES

Lysosomal storage diseases (LSDs) are a group of rare, inherited, metabolic disorders characterized by the accumulation of partially or non-degraded compounds as a consequence of deficiencies in normal lysosomal function (Parenti et al., 2015). The first LSD described was Gaucher disease in 1882 (Gaucher, 1882), followed by the description of Fabry disease in 1898 (Fabry, 1898). However, the concept of LSD was not established until 1965, when the deficiency in α-glucosidase was causally associated to Pompe disease (Hers, 1965).

## 1.1. Lysosomes and lysosomal enzymes

The term "lysosome" was originally proposed by C. de Duve, and makes reference to the Greek word "digestive body" (de Duve et al., 1955; de Duve, 2005). Lysosomes are intracellular membrane-bound organelles that contain nearly 60 acidic hydrolases, including glycosidases, sulfatases, proteases, peptidases, phosphatases, lipases and nucleases. These hydrolases are involved in the degradation and recycling of intra- and extracellular macromolecules, such as glycosaminoglycans, sphingolipids, glycogen and proteins (Appelqvist et al., 2013; Parenti et al., 2015). Lysosomes have an acidic lumen (pH 4.5-5.0) provided by $H^+$-ATPase transmembrane pumps, which use the energy from ATP hydrolysis to pump protons from the cytosol into the lumen of the lysosome (Appelqvist et al., 2013). This acidic environment is not only optimal for the activity of the hydrolytic enzymes, but also contributes to the degradation process by facilitating the loss of structures of the substrates (Appelqvist et al., 2013).

The synthesis of the lysosomal enzymes takes place in the rough endoplasmic reticulum (RER), where native conformation is adopted and some post-translational modifications are performed, such as the modification of a highly conserved cysteine residue to formylglycine (FGly) in all enzymes of the lysosomal sulfatase family (Braulke and Bonifacino, 2009; Paretin et al., 2015a). By vesicular transport, lysosomal enzymes reach the Golgi apparatus. At this stage, the majority of the lysosomal enzymes are tagged with mannose-6-phosphate (M6P) residues by the sequential action of two enzymes: N-acetylglucosaminyl-1-phosphotransferase and N-acetylglucosamine-1-phosphodiester α N-acetyl-glucosaminidase (Vellodi, 2005; Braulke and Bonifacino, 2009). In the trans-Golgi

compartment, M6P receptors (M6PR) specifically recognize the M6P tag and package the hydrolases into clathrin-coated vesicles to transport them to late endosomes, which later form lysosomes (Braulke and Bonifacino, 2009). The low pH present in lysosomes results in the dissociation of the hydrolase from the M6PR. Then, M6PR are either recycled to the Golgi to pick up other ligands, or transported to the plasma membrane to internalize exogenous M6P-tagged enzymes (Figure 1) (Vellodi, 2005). However, some lysosomal enzymes are independent of the M6PR pathway and their delivery into the lysosomes is mediated by other mechanisms, such as those mediated by the lysosomal integral membrane protein 2 (LIMP2), or the alternative receptor protein sortilin (Braulke and Bonifacino, 2009). Finally, lysosomal enzymes may be modified in the lysosome by proteolysis, folding and aggregation to become fully functional hydrolases (Vellodi, 2005).

On the contrary, different routes are involved in the transport and internalization of macromolecules into lysosomes to be subsequently degraded. Autophagy is the main route of entry for intracellular materials, while microorganisms and cellular debris are internalized by phagocytosis (Vellodi, 2005; Appelqvist et al., 2013; Parenti et al., 2015).

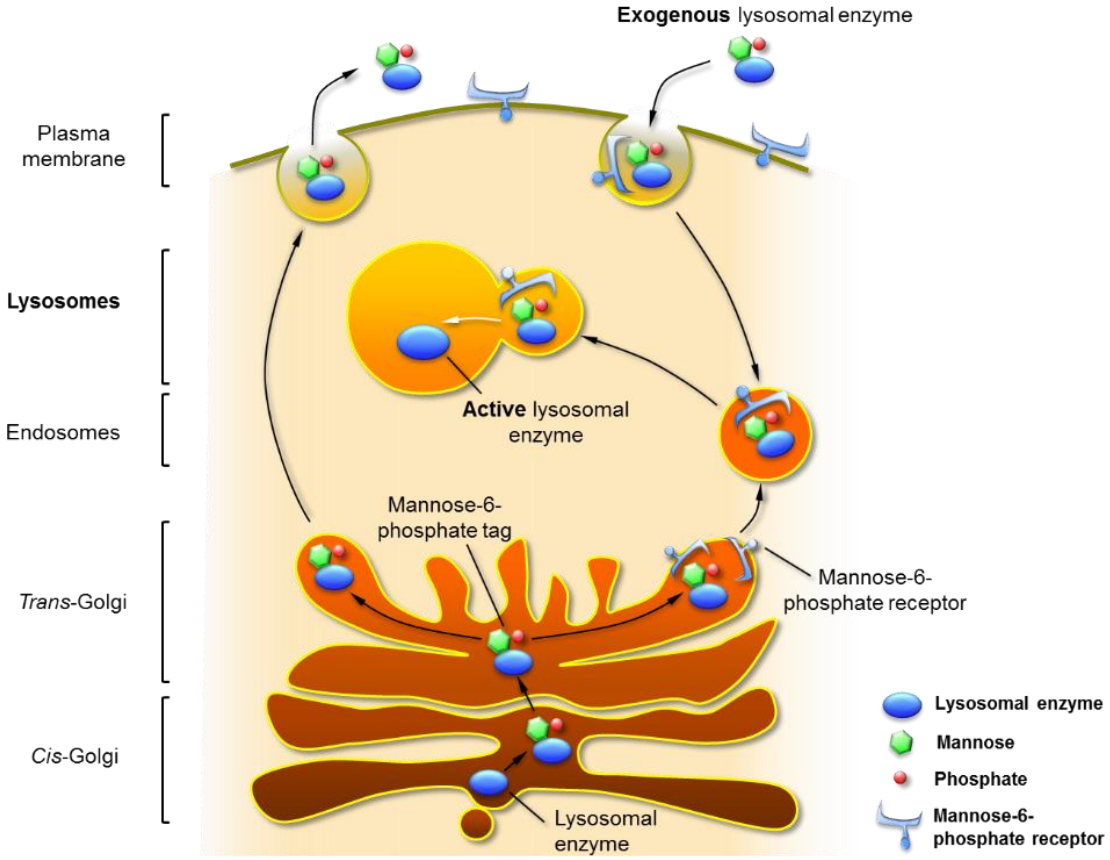


**Figure 1. Trafficking pathways of lysosomal enzymes inside the cell.** Lysosomal enzymes can be targeted to the lysosomes from the Golgi compartment and from the plasma membrane via M6PRs.

Apart from their crucial catabolic function, lysosomes are also considered key regulators of cell homeostasis and play a role in essential cellular functions, such as nutrient sensing, cell-signalling, vesicle trafficking or cellular growth (Appelqvist et al., 2013; Parenti et al., 2015).

### 1.2. Lysosomal storage diseases

Lysosomal storage diseases comprise a group of about 70 inherited metabolic disorders caused by dysfunction of lysosomal breakdown mechanisms (Cox and Cachón-González, 2012). Most LSDs are caused by deficiency in soluble acidic hydrolases. However, a minority are due to defects in lysosomal membrane proteins, transporter proteins, activator proteins or non-lysosomal proteins required for lysosomal catabolic function (Ballabio and Gieselmann, 2009; Parenti et al., 2015). As a consequence, progressive accumulation of undegraded compounds within virtually all lysosomes occurs. The secondary alteration of other lysosome-related pathway also contributes to tissue and organ dysfunction and multisystemic pathology (Platt et al., 2012; Alroy et al., 2014).

Most LSDs are caused by a single hydrolase deficiency. Nonetheless, some are the result of the deficiency in a common activator essential for the activity of a group of lysosomal enzymes, as it occurs in Multiple Sulfatase Deficiency (MSD), in which the absence of sulfatase-modifying factor 1 (SUMF-1) leads to simultaneous deficiency in the activation of all lysosomal sulfatases (Futerman and van Meer, 2004; Parenti et al., 2015).

Although each LSD is considered individually as a rare disease, the combined prevalence of LSDs may be as high as 1 in 5000 births (Vitner et al., 2010), being LSDs approximately 14% of all inherited metabolic diseases (Wolf et al., 2015).

The majority of LSDs are inherited in an autosomal recessive manner, with the exception of Fabry disease and Mucopolysaccharidosis type II (MPSII), which present an X-linked recessive inheritance; and Danon disease, which is X-linked dominant inherited (Fuller et al., 2006; Alroy et al., 2014). Several disease-causing mutations have been identified for each gene associated to a particular LSD. It is difficult, however, to establish clear genotype-phenotype correlations for most of these diseases, and the clinical course cannot be accurately predicted (Futerman and van Meer, 2004).

### 1.3. Classification of lysosomal storage diseases

LSDs were originally classified according to the nature of the major accumulated substrate: LSDs in which glycosaminoglycans (GAGs, previously known as mucopolysaccharides) were accumulated, were classified as mucopolysaccharidoses (MPSs); those with sphingolipids storage, as sphingolipidoses; and oligosaccharidoses were those disorders in which oligosaccharides were primary accumulated (Ballabio and Gieselmann, 2009; Vitner et al., 2010). However, it is noteworthy that in most LSDs more than one compound is stored or the accumulated material is heterogeneous (Ballabio and Gieselmann, 2009). Thus, a less restrictive classification is currently used (Table 1).

**Table 1. Classification of lysosomal storage diseases** *(Part I)*

| Disease | Defective enzyme or protein | Main storage materials |
|---|---|---|
| **Mucopolysaccharidoses: deficiency in glycosaminoglycan catabolism** | | |
| MPSI *(Hurler, Hurler/Scheie, Scheie)* | α-L-Iduronidase | Dermatan sulfate, heparan sulfate |
| MPSII *(Hunter)* | Iduronate-2-sulfatase | Dermatan sulfate, heparan sulfate |
| MPSIIIA *(Sanfilippo A)* | Sulfoglucosamine N-sulfohydrolase | Heparan sulfate |
| MPSIIIB *(Sanfilippo B)* | α -N-Acetylglucosaminidase | Heparan sulfate, |
| MPSIIIC *(Sanfilippo C)* | Heparan α-glucosaminide N-acetyltransferase | Heparan sulfate |
| MPSIIID *(Sanfilippo D)* | N-Acetylglucosamine-6-sulfatase | Heparan sulfate |
| *MPSIIIE** | N-Sulfoglucosamine 3-O-sulfatase | Heparan sulfate |
| MPSIVA *(Morquio A)* | N-Acetylgalactosamine-6-sulfate-sulfatase | Keratan sulfate, chondroitin-6-sulfate |
| MPSIVB *(Morquio B)* | β-Galactosidase | Keratan sulfate |
| *MPSV (Scheie)*** | α-L-Iduronidase | Dermatan sulfate, heparan sulfate |
| MPSVI *(Maroteaux-Lamy)* | N-Acetylgalactosamine-4-sulfatase | Dermatan sulfate |
| MPSVII *(Sly)* | β-Glucoronidase | Heparan sulfate, dermatan sulfate, chondroitin-4- and -6-sulfates |
| *MPSVIII**** | *N-acetylglucosamine-6-sulfate sulfatase* | - |
| MPSIX *(Natowicz)* | Hyaluronidase | Hyaluronic acid |
| **Oligosaccharidoses and glycoproteinoses: deficiency in the degradation of glycanproteins** | | |
| Aspartylglucosaminuria | Aspartylglucosaminidase | Aspartylglucosamine |
| Mucolipidosis I or Sialidosis (*Type I and II*) | Sialidase | Sialyloligosaccharides and sialyglycopeptides |
| α-N-acetylgalactosaminidase: Schindler (*Type I and III*) Kanzaki (*Type II*) | α-N-Acetylgalactosaminidase | Glyco-conjugates containing α-N-acetylgalactosaminyl |
| α-Fucosidosis (*Type I and II*) | α-L-Fucosidase | Fucose-containing oligosaccharides |
| α-Mannosidosis (*Type I and II*) | α-Mannosidase | Mannose-containing oligosaccharides |
| β-Mannosidosis | β-Mannosidase | Man(β1→4)GlcNAc disaccaride |
| **Glycogenoses: deficiency in glycogen degradation** | | |
| Glycogenosis type II *(Pompe)* | α-Glucosidase | Glycogen |
| **Deficiency in polypeptide degradation** | | |
| Pycnodysostosis | Cathepsin K | Bone proteins including collagen fibrils |

**Continuation Table 1. Classification of lysosomal storage diseases** *(Part II)*

| Disease | Defective enzyme or protein | Main storage materials |
|---|---|---|
| **Sphingolipidoses: deficiency in sphingolipid metabolism** | | |
| Fabry | α-Galactosidase A | Globotriaosylceramide, |
| Farber lipogranulomatosis | Ceramidase | Ceramide |
| Gaucher *(Type I)* | β-Glucosidase | Glucosylceramide, |
| *variant (Type II and III)* | Saposin-C activator | Glucosylceramide |
| GM1 gangliosidosis *(Type I, II and III)* | β-Galactosidase | GM1 and related glycolipids |
| GM2 gangliosidosis: | | |
| Tay-Sachs | β-Hexosaminidase A | GM2 and related glycolipids |
| Sandhoff | β-Hexosaminidase A and B | GM2 and related glycolipids |
| variant AB | GM2-activator protein | GM2 and related glycolipids |
| Globoid cell leukodystrophy: | | |
| Krabbe | Galactocerebroside β-galactosidase | Galactosylceramide |
| *variant* | Saposin A | Galactosylceramide |
| Metachromatic leukodystrophy | Arylsulfatase A | Sulfatides |
| *variant* | Saposin-B activator | Sulfatides |
| Niemann-Pick *(Type A and B)* | Sphingomyelinase | Sphingomyelin |
| Sphingolipid-activator deficiency | Sphingolipid activator | Glycolipids |
| **Deficiency in degradation or transport of cholesterol or other complex lipids** | | |
| Cholesteryl ester storage disease | Acid lipase | Cholesterol esters and triglycerides |
| Neuronal ceroid lipofuscinosis *(NCL)*[#]*:* | | |
| NCL1 *(INCL, LINCL, JNCL, ANCL)* | Palmitoyl-protein thioesterase-1 | Lipofuscin |
| NCL2 *(LINCL and JNCL)* | Tripeptidyl peptidase-1 | Lipofuscin |
| NCL3 *(Batten, JNCL)* | CLN3 (battenin) | Lipofuscin |
| NCL4 *(ANCL)* | CLN4 | Lipofuscin |
| NCL5 *(LINCL, JNCL, ANCL; previously CLN9)* | CLN5 | Lipofuscin |
| NCL6 *(LINCL, ANCL)* | CLN6 | Lipofuscin |
| NCL7 *(LINCL, JNCL, ANCL)* | MFSD8 | Lipofuscin |
| NCL8 *(Northern epilepsy, LINCL)* | CLN8 | Lipofuscin |
| NCL10 *(LINCL and ANCL)* | Cathepsin D | Lipofuscin |
| NCL11 *(ANCL)* | Granulin precursor | Lipofuscin |
| NCL12 *(JNCL)* | ATP13A2 | Lipofuscin |
| NCL13 *(ANCL)* | Cathepsin F | Lipofuscin |
| NCL14 *(INCL)* | KCTD7 | Lipofuscin |
| Niemann-Pick type C *(Type 1 and 2)* | NPC1 and 2 | Cholesterol and sphingolipids |
| Wolman | Acid lipase | Cholesterol esters and triglycerides |
| **Deficiency in multiple lysosomal enzymes** | | |
| Galactosialidosis | Cathepsin A | Sialyloligosaccharaides |
| Mucolipidosis *(Type II and III)* | GlcNAc-1-phosphotransferase | Oligosaccharides, mucopolysaccharides and lipids |
| Multiple sulfatase deficiency *(MSD)* | SUMF-1 | Heparan sulfate, dermatan sulfate, chondroitin-sulfates, sulfolipids |
| **Deficiency in lysosomal transmembrane proteins, transport and trafficking** | | |
| Cystinosis | Cystinosin | Cystine |
| Danon disease | LAMP2 | Cytoplasmic debris and glycogen |
| Hermansky-Pudlak | HPS1-4 | Ceroid lipofuscin |
| Infantile sialic-acid-storage disease | Sialin | Sialic acid |
| Mucolipidosis type IV | Mucolipin-1 | Lipids and acid mucopolysaccharides |

*MPSIIIE: enzymatic deficiency only described in mice (Kowalewski et al., 2012).

**MPSV: the deficiency in α-L-Iduronidase observed in MPSV patient was similar to the one observed in MPSI (Dekaban et al., 1976). Subsequently, MPSV was renamed as MPSI-Scheie syndrome.

***MPSVIII: the description of N-acetylglucosamine-6-sulfate sulfatase deficiency was suspected of misdiagnosis (Di Ferrante, 1980); therefore, MPSVIII designation was retired and the next MPS described was designated as MPSIX.

GM1, ganglioside; GM2, ganglioside 2.

[#]INCL, LINCL, JNCL and ANCL correspond to infantile-, late infantile-, juvenile- and adult-NCL, respectively.

Adapted from Futerman and van Meer, 2004; Ballabio and Gieselmann, 2009; Vitner et al., 2010; Alroy et al., 2014.

### 1.4. Mucopolysaccharidoses

Mucopolysaccharidoses (MPSs) are a group of rare genetic disorders that comprise around 30% of all LSD patients (Wolf et al., 2015). MPSs are caused by deficiencis in lysosomal enzymes involved in the degradation of glycosaminoglycans. To date, the deficiency in 11 different enzymes has resulted in 7 distinct MPS diseases (Table 1). Due to the lack of activity of these enzymes, undegraded GAGs are accumulated within the lysosomes of virtually all cells, leading to cell dysfunction and death (Neufeld and Muenzer, 2001).

Although each MPS results from a different enzyme deficiency and accumulates distinctive GAGs (dermatan sulfate, heparan sulfate, keratan slfate, chondroitin sulfate or hyaluronan), MPSs share common biochemical and clinical features. MPSs frequently involve cardiorespiratory impairment, organomegaly, multisystem pathology and skeletal, hearing and vision alterations (Neufeld and Muenzer, 2001). Severely affected patients of some forms of MPSs, such as MPSI, MPSII, MPSIII and MPSVII, also show pathology in the central and peripheral nervous systems (CNS and PNS), leading to neuronal degeneration, behavioural disturbances and premature death (Neufeld and Muenzer, 2001).

The heterogeneity of phenotypes together with the low prevalence of MPSs hinder their clinical diagnosis. For this reason, screening panels on urine or blood samples have been developed as a first filter to facilitate the rapid diagnosis of MPSs (Muenzer, 2011). Importantly, an early diagnosis is essential for those forms that have an approved therapy because the earlier the treatment begins, the better efficacy is expected (Muenzer, 2011).

Despite there is no cure for most MPSs, several approaches have been recently developed. Enzyme replacement therapy (ERT) has provided therapeutic benefit in some MPSs when the recombinant deficient enzyme is periodically infused to patients. ERT is already commercially available for MPSI (ALDURAZYME®, Genzyme), MPSII (ELAPRASE®, Shire), MPSIVA (VIMIZIN®, BioMarin) and MPSVI (NAGLAZYME®, BioMarin). However, the main limitations of ERT are: 1) the inability of recombinant enzyme to cross the blood-brain barrier (BBB) and reach CNS following intravenous delivery, limiting the potential applicability to treat neurological symptoms; 2) the adverse events related with infusions; and 2) the high cost of the therapy (Biffi, 2015). Other approaches under consideration are bone marrow transplantation (BMT), hematopoietic stem cell transplantation (HSCT), substrate reduction therapy (SRT) and cell and gene therapy (Giugliani et al., 2016).

# 2. MUCOPOLYSACCHARIDOSIS TYPE II (HUNTER SYNDROME)

## 2.1. History of MPSII

Mucopolysaccharidosis type II (OMIM 309900) is an X-linked recessive inherited disorder that courses with variable, progressive and multisystemic pathology. MPSII is caused by deficiency in the enzyme Iduronte-2-sulfatase, resulting in pathological accumulation of the glycosaminoglycans heparan sulfate (HS) and dermatan sulfate (DS) within virtually all lysosomes of the body (Neufeld and Muenzer, 2001).

In 1917, Charles Hunter described for the first time a rare disease in two brothers of 8 and 10 years, who presented with coarse face, throat abnormalities, hearing impairment, undersize, inguinal hernia, hepatosplenomegaly, prominent abdomen, limitations of the joint movements, audible breathing and alterations in heart and bones (Hunter, 1917). Soon after this, two unrelated patients who suffered from similar symptoms to those reported by C. Hunter and additionally with corneal clouding and mental impairment were described (Hurler, 1919). Both cases were considered the same disease, bearing the name of who Hurler-Hunter syndrome (Martin et al., 2008). This syndrome was also referred to as “gargoylism” (Ellis et al., 1936). The X-linked recessive inheritance and the absence of corneal clouding later became key features to discriminate between Hunter and Hurler syndrome (Nja, 1946; McKusick, 1956). Then, the excessive excretion of two acid mucopolysaccharides was reported in urine samples of Hurler patients, which gave these disorders the name of “mucopolysaccharidoses” (Brante, 1952; Dorfman and Lorincz, 1957). The term mucopolysaccharidoses arises from “muco”, which refers to the jelly-like appearance of these molecules; “poly”, meaning many; and “saccharide”, which is commonly used to refer to the sugar part of a molecule.

Initially, it was suggested that Hurler syndrome was the consequence of an excessive production of GAGs (Matalon and Dorfman, 1966). However, fibroblasts derived from the skin of Hurler and Hunter patients synthesized and secreted GAGs normally; their intracellular storage was due to an inadequate degradation (Fratantoni et al., 1968). Contemporarily, a congenital defect in one of the enzymes involved in the lysosomal digestion of GAGs was postulated as the cause of storage, a hypothesis confirmed after measuring the activity of acid hydrolases in liver samples from patients with different MPSs (Van Hoof and Hers, 1968). Thereafter, independent experimental works

demonstrated the correction of the metabolic defect in fibroblasts from Hunter patients mediated by some secreted factor obtained from cultured fibroblast of Hurler patients, with the backward assays also successful (Fratantoni et al., 1969; Neufeld and Cantz, 1971). These results led to the identification and isolation of the protein deficient in Hunter syndrome, designated as "Hunter corrective factor" (Cantz et al., 1972). Later, the Hunter corrective factor was identified as a sulfatase acting on sulfated iduronic acid residues, named Iduronate-2-sulfatase (IDS) (Bach et al., 1973).

### 2.2. Inheritance and incidence of MPSII

MPSII is inherited in an X-linked recessive manner, then, almost all MPSII patients are males. Nonetheless, some cases of women with well-documented Hunter syndrome have been reported in the literature (Neufeld and Muenzer, 2001).

Epidemiological data on MPSII disease have been collected in several countries and shows a highly variable prevalence (Table 2). Although the prevalence of MPSII varies depending on the geographical area under study, all publications agree that MPSII is a rare disease, as it affects less than 50 persons per 100,000 inhabitants (rarity definition according to the European legislation, http://www.orpha.net/orphacom/cahiers/docs/GB/List_of_rare_diseases_in_alphabetical_order.pdf).

**Table 2. Incidence and/or prevalence of MPSII in different geographic areas**

| Study group | Years of study | Incidence in 100,000 | | Prevalence in 100,000 inhabitants | Reference |
|---|---|---|---|---|---|
| | | live births | male live births | | |
| **Israel** | 1974-1979 | 1.48 | - | - | Schaap and Bach, 1980 |
| **British Columbia** | 1952-1986 | - | 0.901 | - | Lowry et al., 1990 |
| **Northern Ireland** | 1958-1985 | 0.71 | 1.39 | - | Nelson, 1997 |
| **Australia** | 1980-1996 | 0.62 | 0.73 | - | Meikle et al., 1999 |
| **The Netherlands** | 1970-1996 | 0.67 | 1.3 | - | Poorthuis et al., 1999 |
| **Western Australia** | 1969-1996 | 0.31 | 0.61 | - | Nelson et al., 2003 |
| **Northern Portugal** | 1967-2000 | 1.09 | - | - | Pinto et al., 2004 |
| **Germany** | 1980-1995 | 0.64 | 1.3 | - | Baehner et al., 2005 |
| **Sweden** | 1975-2004 | - | - | 0.27 | Malm et al., 2008 |
| **Norway** | 1979-2004 | - | - | 0.13 | Malm et al., 2008 |
| **Denmark** | 1975-2004 | - | - | 0.27 | Malm et al., 2008 |
| **Taiwan** | 1984-2004 | 1.07 | 2.05 | - | Lin et al., 2009 |
| **Czech Republic** | 1975-2008 | 0.43 | 0.83 | - | Poupetová et al., 2010 |
| **Estonia** | 1985-2006 | 2.16 | 4.2 | - | Krabbi et al., 2012 |
| **Poland** | 1970-2010 | 0.45 | - | - | Jurecka et al., 2015 |

Summary of the incidence (number of newly diagnosed live birth cases within a time period) or prevalence (total cases of the disease in a population at a particular time point) of MPSII.

Hunter syndrome has an average worldwide incidence of 0.30-0.71 cases/100,000 live births (Muenzer, 2011). It is the most prevalent MPS disorder in Asia, accounting for 60% of all MPSs documented cases in Japan and 52% of all MPSs cases diagnosed in Taiwan (Yamada et al., 1993; Lin et al., 2009; Okuyama et al., 2010).

## 2.3. Iduronate-2-sulfatase

### *2.3.1. The Iduronate-2-sulfatase gene*

The human Iduronate-2-sulfatase gene (*IDS*) is localized in the X chromosome, mapped to the region Xq27.3-q28 (Berg et al., 1968; Roberts et al., 1989). It spans approximately 24 kb from the translation start site to the polyadenylation site and contains nine exons ranging from 89 bp to 4.4 kb (Figure 2) (Flomen et al., 1993; Wilson et al., 1993). As it occurs for other lysosomal genes, differential polyadenilation of the mRNA of *IDS* resultes in three major RNA species of 2.1, 5.4 and 5.7 kb, and one minor specie of approximately 1.4 kb (Wilson et al., 1990). The homologous murine *Ids* gene (Figure 2), located in the same relative position on the X chromosome, presents high identity to the human *IDS* gene at both nucleotide and amino acid level, and contains the well conserved putative catalytic site (Faust et al., 1992; Daniele et al., 1993).


**Figure 2. Location and organization of the human and murine *Iduronate-2-sulfatase* genes.** Source: http://www.ncbi.nlm.nih.gov/gene/3423 and http://www.ncbi.nlm.nih.gov/gene/15931.

A human pseudogene (*IDS2*) is located 80 kb telomeric to the *IDS* locus and shows homology to exons 2 and 3, and introns 2, 3 and 7 of the *IDS* gene (Bondeson et al., 1995). Interactions between the *IDS* gene and the *IDS2* pseudogene have been associated to gross structural rearrangements, homologous recombinations and/or deletions (Timms et al., 1995; Bunge et al., 1998).

To date, more than 500 different mutations have been documented in the *IDS* gene, of which approximately 80-90% account for small gene alterations, while theremaining 10-20% involve large gene alterations (Froissart et al., 2007). Specifically, 51.7% of the IDS reported mutations are missense or nonsense, 9.2% affect splicing sites, 18.3% are small deletions, 7.9% are small insertions, 2% are small indels, 7.4% are gross indels, 0.7% are gross insertions or duplications, and 2.8% account for complex rearrangements (http://www.hgmd.cf.ac.uk/ac/gene.php?gene=IDS). The distribution of point mutations over the *IDS* gene presents a non-random pattern, with relatively frequent occurrence in exons 3, 8, and 9 (Gort et al., 1998; Li et al., 1999), whereas the distribution of small rearrangements, such as deletions, insertions and duplications tend to be random (Gort et al., 1998).

Because of the unique nature of most mutations observed in MPSII patients, the establishment of a comprehensive genotype-phenotype correlation is not feasible (Hopwood et al., 1993; Froissart et al., 2002; Froissart et al., 2007). Even in the case of patients carrying the same genetic alteration in the *IDS* gene, different phenotypes have been described (Yatziv et al., 1977; Froissart et al., 2007).

Nevertheless, large deletions, including multiple exons or whole-gene deletions, and complex rearrangements resulting from recombination between the *IDS* gene and *IDS2* pseudogene seem to be associated with severe MPSII phenotypes with CNS impairment (Hopwood et al., 1993; Gort et al., 1998; Froissart et al., 2007). However, it has also been reported that large deletions in the *IDS* gene can be associated with the mild form of MPSII disease (Bonuccelli et al., 1998; Filocamo et al., 2001). Similarly, abnormalities that result from a single amino acid mutation have been associated with a broad spectrum of phenotypes from sever to attenuated clinical presentation (Gort et al., 1998; Li et al., 1999; Vafiadaki et al., 1998; Moreira da Silva et al., 2001; Froissart et al., 2007).

### *2.3.2. The Iduronate-2-sulfatase enzyme*

The lysosomal enzyme Iduronate-2-sulfatase (IDS, EC 3.1.6.13) hydrolyses the 2-sulfate ester bond of L-iduronate 2-sulfate moieties from heparan sulfate, dermatan sulfate and

heparin (Froissart et al., 1995). As the majority of soluble lysosomal enzymes, IDS is transported to the lysosomes via the M6PR-mediated pathway (Wraith et al., 2008a).

The human *IDS* gene encodes a 550 amino acid protein that presents 8 potential N-glycosylation sites and has a 25 amino acid amino-terminal signal sequence (Millat et al., 1997; Martin et al., 2008). As all human sulfatases, IDS presents three highly conserved domains; amino acids 45 to 46, 84 to 88, and 127 to 135 (Diez-Roux and Ballabio, 2005). Cys84, which belongs to the CXPSR pentapeptide conserved region essential for the catalytic action of IDS, is post-translationally modified to a formylglycine (FGly) in the endoplasmic reticulum (Millat et al., 1997; Fraldi et al., 2007a). This modification is performed by the sulfatase-modifying factor 1, SUMF-1, an essential factor responsible for the modification of the cysteine residue in the active site of all sulfatases (Fraldi et al., 2007a).

Iduronate-2-sulfatase has been found in human placenta and other human tissues and body fluids in three different isoforms: form A, B and C (Di Natale and Ronsisvalle, 1981; Archer et al., 1982). Serum and amniotic fluid contain only the larger form, form C; whereas kidney only contains appreciable amounts of form A; and the less-anionic form, form B, is found in cultured fibroblast and urine (Archer et al., 1982).

Biosynthesis and maturation studies of IDS carried out in human fibroblast and hepatocyte cell lines reported an initial form of 73-78 kDa, which is converted in the Golgi apparatus into a phosphorylated 90 kDa precursor. After deglycosilation and proteolytic cleavage by thiol proteases, a 55 kDa intermediate is obtained, and the release of a 18 kDa polypeptide results in the 42-45 kDa IDS mature form containing hybrid and complex-type oligosaccharide chains (Wilson et al., 1990; Froissart et al., 1995).

The murine *Ids* gene encodes a 564 amino acid protein that shares 84.5% identical amino acid sequence with human IDS (Daniele et al., 1993). Both human and murine IDS proteins share the majority of amino acids involved in the catalytic site, as well as the majority of glycosylation sites, except for two that are lost in the mouse IDS protein (Daniele et al., 1993).

## 2.4. Molecular pathology of MPSII

IDS deficiency results in failure of the catabolism of heparan sulfate and dermatan sulfate in MPSII patients. These undegraded glycosaminoglycans are pathologically accumulated within cellular lysosomes (Neufeld and Muenzer, 2001).

### *2.4.1. Structure and function of heparan sulfate and dermatan sulfate*

GAGs are long, unbranched, negatively charged polysaccharides composed of repeating disaccharide units of an hexosamine (N-acetyl-D-glucosamine, D-GlcNAc; or N-acetyl-D-galactosamine, D-GalNAc) linked to an uronic acid (D-glucoronic acid, D-GlcA; or L-iduronic acid, L-IdoA) or a galactose (Taylor and Gallo, 2006). Specifically, HS is composed of alternating units of N-acetyl-D-glucosamine linked to an uronic acid residue (Figure 3) (Häcker et al., 2005). On the other hand, DS is composed of disaccharide units of N-acetyl-D-galactosamine and uronic acid residues (Figure 3) (Trowbridge and Gallo, 2002).

The synthesis of the GAG chain begins with the addition of an hexosamine to a tetrasaccharide linker, composed of xylose-galactose-galactose-uronic acid and attached to the core protein by an amino acid residue (Serine in the case of HS and DS) that is N-terminal to a glycine (Figure 3) (Häcker et al., 2005). The covalent union of HS or DS to the serine residue results in the formation of a proteoglycan (PG) (Rowlands et al., 2015). After synthesis, the polysaccharide chain may undergo various modifications. HS can be sulphated, including 6-O-sulfatation or 3-O-sulfatation of the N-acetyl-D-glucosamine subunits, or 2-O-sulfatation or occasionally 3-O-sulfatation of the D-GlcA/L-IdoA subunit (Taylor and Gallo, 2006; Rowlands et al., 2015). Sulfatations of DS can occur on the C2-hydroxyl moiety of the L-IdoA subunit, or on the C4-hydroxyl and/or C6-hydroxyl moiety of the N-acetyl-D-galactosamine subunit (Trowbridge and Gallo, 2002).

The variable total length of the HS and DS polysaccharide chains, the variable placement of uronic acid subunits, the different sulfatations that such component may undergoes, as well as the multiple alternatives for core proteins dictate the complexity level of these GAGs and the PGs formed (Trowbridge and Gallo, 2002). This structural diversity leads to a wide range of protein-binding motifs, allowing the modulation of numerous cellular signalling pathways. Certainly, besides the crucial structural role that GAGs play in the extracellular matrix, they are also involved in other essential biological

functions such as cell division, development, regulation of neuronal growth and plasticity, cell adhesion and migration, modulation of inflammatory responses and BBB support, to mention a few (Taylor and Gallo, 2006; Rowlands et al., 2015).

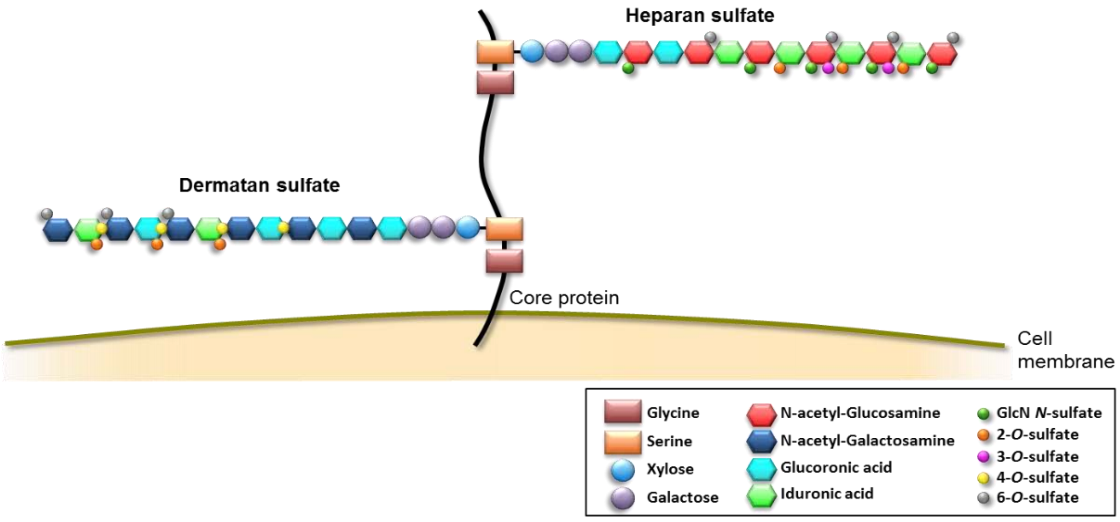


**Figure 3. Structure of heparan sulfate and dermatan sulfate.** Both HS and DS are attached to a serine residue on the core protein by a tetrasaccharide linker (xylose-galactose-galactose-uronic acid) onto which the polysaccharide chain is assembled and subsequently modified. Adapted from Häcker et al., 2005.

### *2.4.2. Heparan sulfate and dermatan sulfate degradation*

The first step in the catabolic pathway of HS and DS is the cleavage of the long polysaccharide chain from the PG core, which is mediated by heparanase or chondroitinase B, respectively (Ernst et al., 1995). Thereafter, HS and DS degradation proceeds from the non-reducing end by sequential action of several enzymes (Figure 4) (Neufeld and Muenzer, 2001). In HS catabolism three glycosidases (α-L-iduronidase, β-glucoronidase and α-N-acetylglucosaminidase), at least three sulfatases (Iduronate-2-sulfatase, sulfoglucosamine N-sulfohydrolase, glucoronate-2-sulfatase and N-acetylglucosamine-6-sulfatase) and one acetyltransferase (Heparan α-glucosaminide N-acetyltransferase) participate (Neufeld and Muenzer, 2001). On the other hand, DS degradation requires the action of three exo-glycosidases (α-L-iduronidase, β-hexosaminidase and β-glucoronidase) and two sulfatases (Iduronate-2-sulfatase and N-acetylgalactosamine-4-sulfatase). Hyaluronidase may also take in the catabolism of DS by cleaving the chain next to glucuronic acid residues (Neufeld and Muenzer, 2001).

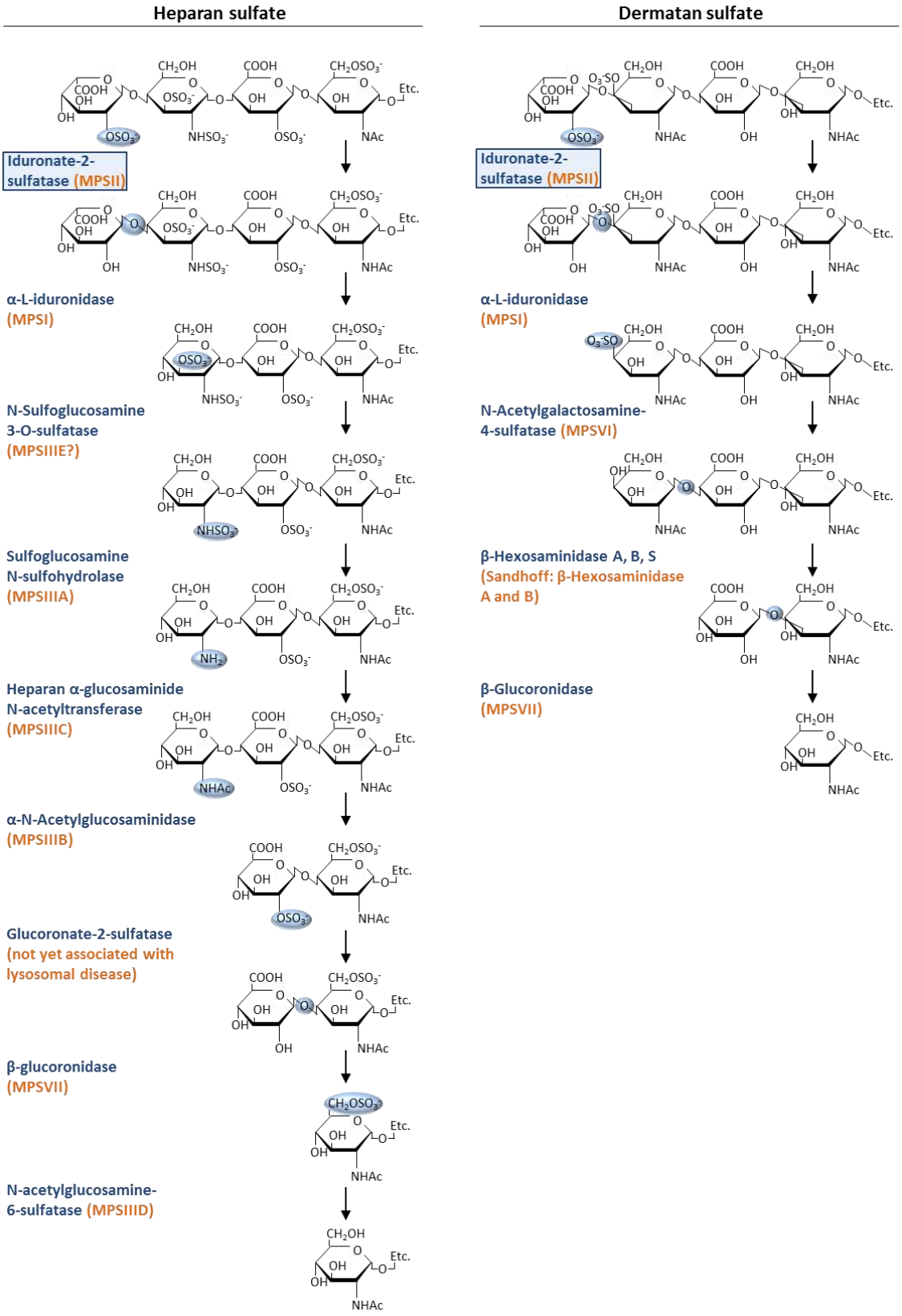


**Figure 4. Stepwise degradation of heparan sulfate and dermatan sulfate.** Blue circles indicate the moieties where each enzyme acts. In orange are denoted the human disease caused by the deficient of each enzyme. The schematic representation depicts all structures known to occur within HS and DS; it does not imply that they occur stoichiometrically. Iduronate-2-sulfatase specifically removes the 2-sulfate group of L-iduronic acid from HS and DS. Adapted from Neufeld and Muenzer, 2001 and Kowalewski et al., 2012.

### *2.4.3. Pathophysiology of heparan sulfate and dermatan sulfate accumulation*

Glycosaminoglycans, HS and DS among them, were historically thought to play an important role in the orientation and organization of the extracellular matrix in all cell types. More recently, however, a significant function in cell communication and the mechanical support of tissues has been highlighted, since glycosaminoglycans accumulate large volumes of water. Their contribution ito many other cellular functions, such as cell growth, immunity, defence against viral infections, coagulation or lipid metabolism has also been reported (Taylor and Gallo, 2006). Their implication in such a wide range of cellular precesses is a consequence of their capacity to bind to different proteins, such as proteases, growth factors and chemokines (Capila and Linhardt, 2002). Thus, the excess of HS and DS that is accumulated in lysosomes could interfere with the aforementioned processes, aggravating the MPSII disease (Vitner et al*.,* 2010). However, the cascade of pathological events that leads to cell dysfunction and death in MPSII is not completely known, although several theories try to explain the pathology observed, especially in the CNS disease.

HS has important functions in the development and plasticity of neural cells and is known to be a low-affinity receptor for members of the fibroblast growth factor (FGF) family, such as FGF-1, FGF-2 and FGFR (Yayon et al., 1991; Mulloy, 2005). The relative concentrations of HS and FGF-2 necessary to elicit a biological response appear to be inversely related. DS can also interact with FGF proteins, such as FGF-2, promoting their activity (Penc et al*.,* 1998). One of the key functions of the FGF-2/HS or FGF-2/DS complexes is to regulate astrocyte proliferation and function. Astrocytes have a critical role in maintaining brain homeostasis, particularly after insult or disease. In addition, FGF-2 acts as a neuroprotector and as an activator of proliferation for neurons and neuronal pregenitor cells (Gritti et al*.,* 1996; Ballabio and Gieselmann, 2009). Therefore, the accumulation of HS and DS may impair FGF function, which could explain the increased rate of glial cell apoptosis and the disorganized neuronal pattern observed in the brain of the murine Hunter model (Fusar Poli et al*.,* 2013). In addition, MPSII mice show a high density of reactive astrocytes in the brain (Polito et al*.,* 2010). Hence, the chronic accumulation of HS and DS may be responsible for the progressive increase in reactive astrocytes observed in MPSII.

In addition, HS and DS can bind, the latter with less affinity, to the activated hepatocyte growth factor/scatter factor (HGF/SF) (Lyon et al*.,* 1998; Malavaki et al*.,* 2008). Despite the fact that HGF/SF was originally described as a potent mitogen for hepatocytes, it has now become clear that this growth factor plays an important role in neuritogenesis, angiogenesis, morphogenesis and differentiation (Matsumoto and Nakamura, 1996; Li et al*.,* 2007). Imbalance of HS and DS may interfere with HGF/SF biological functions, contributing to Hunter pathology.

It is believed that the innate immune system could be activated by HS and DS-derived oligosaccharides through Toll-Like Receptor 4 (TLR4) signalling (Ballabio and Gieselmann, 2009). TLRs are receptors that are stimulated by a variety of conserved pathogen-associated molecular patterns (PAMPs) present in pathogens, but also by endogenous ligands related to tissue damage, such as extracellular matrix products (Carpentier et al., 2008). HS, DS and derived fragments, are known to be endogenous ligands for TLR4 (Ballabio and Gieselmann, 2009). Activation of microglial cells by TLR4 starts a signalling cascade through the adaptor protein MyD88 that leads to the production of inflammatory cytokines, such as TNFα, IL1β or TGF-β (Ballabio and Gieselmann, 2009), which are toxic for neurons (Block and Hong, 2005).

The presence of inflammatory cytokines has also been associated with the skeletal abnormalities described in some forms of MPSs (Simonaro et al., 2001; Simonaro et al., 2005; Simonaro et al., 2008). Because of the structural similarity between DS and bacterial lipopolysaccharide (LPS), it has been hypothesised the progressive accumulation of undegraded GAGs in MPS joints as a mechanism to explain skeletal impairment (Aldenhoven et al., 2009). In this regard, a high rate of apoptosis and release nitric oxide and inflammatory cytokines from articular chondrocytes has been reported in animal models of MPSVI, a disease in which DS is primarily accumulated (Simonaro et al., 2001). The increased apoptosis of articular chondrocytes leads to abnormal articular cartilage matrix, which in turn is exacerbated by mechanical forces placed on the joints, resulting in further inflammation (Simonaro et al., 2001; Simonaro et al., 2008). In addition, most of MPS chondrocytes are immature and do not mineralize into bone, a failure of ossification that contributes to the skeletal manifestations present in MPS patients (Simonaro et al., 2005).

Apart from HS and DS, neurons of Hunter patients accumulate GM2 and GM3 gangliosides (Ballabio and Gieselmann, 2009). This secondary accumulation also plays an important role in the neurologic pathology, since an intraneuronal accumulation of GM2 has been associated with ectopic dendritogenesis, a feature unique to LSDs, and with the formation of membranous bodies, also known as *zebra bodies* (Walkley, 1998). GM2 and to lesser extent GM3 storage, have also been associated with an impairment of calcium homeostasis, by decreasing the reuptake of calcium into the endoplasmic reticulum of affected neurons (Ginzburg et al., 2004; Lloyd-Evans et al., 2008; Vitner et al*.,* 2010).

Oxidative stress has also been reported as a secondary biochemical pathway that is altered in several LSDs (Vitner et al*.,* 2010). Evidence of oxidative stress has been documented in a variety of LSDs, such as the up-regulation of the DNA-reparing apurinic endonuclease 1 (APE1) in Gaucher syndrome (Deganuto et al*.,* 2007), the induction of nitric oxide synthase and the increased levels of nitrotyrosine and reactive oxygen species in Fabry disease (Shen et al*.,* 2008), and the increased oxidation of lipids, proteins and DNA in MPSIIIB (Villani et al*.,* 2009). Altogether, these findings suggest that oxidative stress plays an important role in the pathology of LSDs and are in agreement with the evidence of oxidative stress damage in MPSII patients. The post-mortem analysis of brains from Hunter patients revealed increased immunoreactivity of 8-Oxo-2'-deoxyguanosine (8-OHdG), a marker of DNA oxidative damage, as well as reduced expression of the antioxidants enzymes manganese superoxide dismutase (MnSOD) and copper/zinc superoxide dismutase (Cu/ZnSOD) in different brain areas (Hamano et al*.,* 2008).

Finally, the modulation of growth factor signalling may not only provide an explanation for the neurodegeneration observed in MPSII but also for the skeletal pathology. The growth factors bone morphogenetic proteins (BMPs), which belong to the TGF-β growth factor superfamily, play an important role in the proliferation, differentiation and apoptosis of several tissues, including brain, bone and cartilage (Chen et al*.,* 2004). An impairment of BMP-4 signalling due to GAG accumulation has been reported in multipotent stem cells obtained from Hurler patients (Khan et al*.,* 2008).

## 2.5. Clinical aspects of MPSII

The pathological HS and DS accumulation in MPSII patients results in damage of a broad range of tissue and organs (Martin et al., 2008). MPSII is a variable, chronic, progressive and multisystem disorder traditionally classified into two clinical phenotypes. The severe form, formerly known as MPSIIA, is characterized by CNS involvement, leading to severe cognitive impairment and behavioural disturbance. Somatic pathology and death during the second decade of life are also characteristics of MPSII patients with the severe form of the disease (Neufeld and Muenzer, 2001). On the other hand, the mild form, or MPSIIB, presents with attenuated somatic disease, absence or minimally intellectual deterioration and survival into adulthood; although premature mortality may occurs (Neufeld and Muenzer, 2001). The severe form of MPSII may be up to 3 times more prevalent than the mild form (Martin et al., 2008). Importantly, those patients diagnosed with the attenuated form may still present some cognitive deterioration and significant morbidity, disability and learning difficulties (Schwartz et al., 2007; Wraith et al., 2008a).

However, the classification of MPSII according to the degree of CNS involvement and the length of survival is a gross oversimplification. Hunter syndrome spans a wide spectrum of clinical severity and should be considered as a continuous of phenotypes between the two extremes, the severe and the attenuated form (Wraith et al., 2008a).

### *2.5.1. Presenting symptoms*

MPSII presents a variable age at onset, with a median age of symptoms of 1.5 years, as well as a variable rate of progression (Wraith et al., 2008b). Infants with MPSII appear normal at birth and early developmental milestones may be achieved (Wraith et al., 2008b). The clinical course of the severe form of MPSII generally begins with failing of hearing tests, speech delay and slow-progressive cognitive impairment (Wraith et al., 2008a). By 18-24 months of age, Hunter patients usually show developmental delay, followed by behavioural alterations and progressive intellectual decline (Neufeld and Muenzer, 2001; Wraith et al., 2008a). In addition, MPSII patients suffer from non-neurological alterations, including recurrent ear, nose, throat and chest infections, cardiac failure, coarse facial features, short stature, progressive joint stiffness, skeletal abnormalities that affect mobility, as well as hepatosplenomegaly (Neufeld and Muenzer,

2001). The age at onset and the prevalence of the most frequent symptoms presented by Hunter patients are listed in Figure 5.

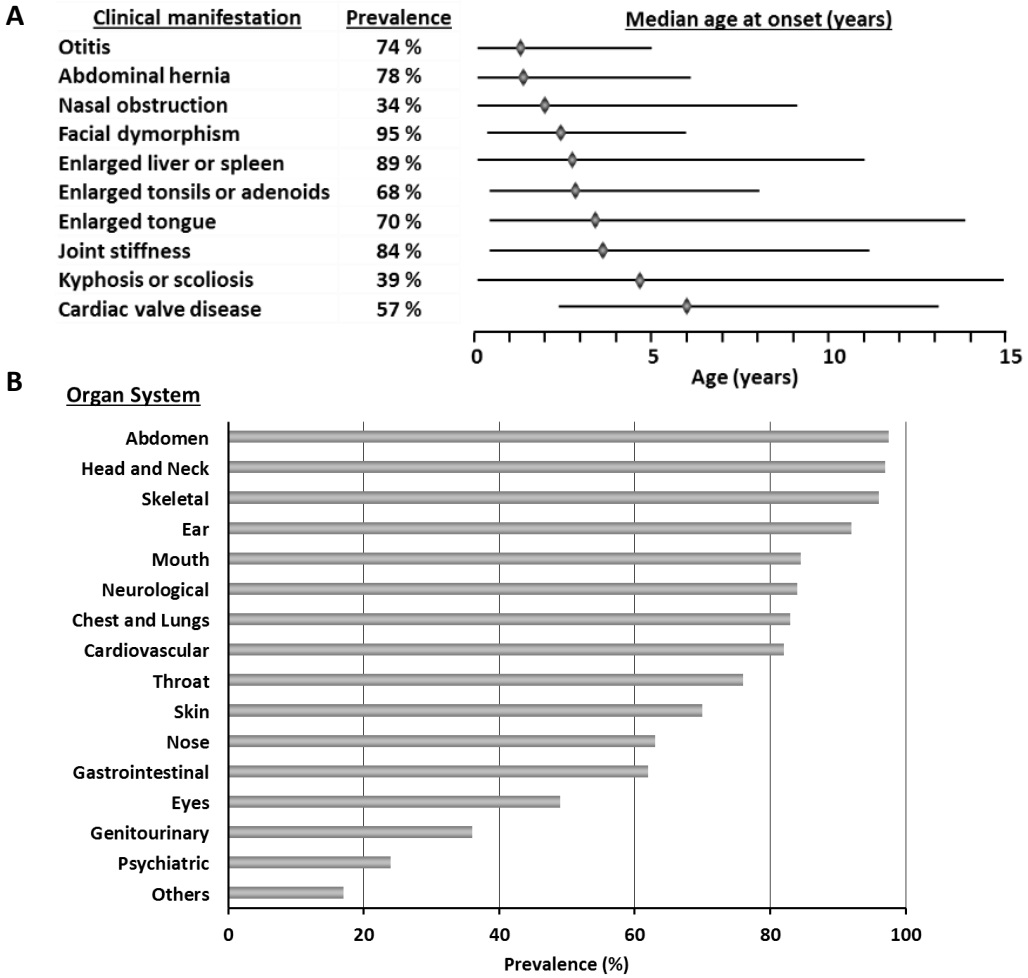


**Figure 5. Clinical aspects of MPSII patients.** (**A**) Prevalence of specific clinical manifestations reported in Hunter patients. Rhombuses indicate the median age at onset of each clinical sign. (**B**) Prevalence of organ systems affected in Hunter syndrome. Adapted from Wraith et al., 2008b.

### *2.5.2. Physical appearance*

The general appearance of newborns with MPSII is normal, however, typical facial features become apparent between 2 and 4 years of age in the severe form of the disease (Martin et al., 2008). As a consequence of GAG storage in soft tissues of the orofacial region and underlying facial bone dysostosis, Hunter patients present coarse facial features (Wraith et al., 2008a), including broad nose with flared nostrils, coarse hair, prominent supraorbital ridge and enlarged jowl (Schwartz et al., 2007; Martin et al., 2008; Scarpa et al., 2011). Thickened lips, hyperplasic and hypertrophic gingiva tissue, irregular and poorly formed teeth and enlarged tongue have also been reported and associated with impairment of the

speech in Hunter patients (Scarpa et al., 2011). Macrocephaly and short stature may also aoccur in these patietns. In addition, hepatosplenomegaly combined with lax abdominal muscles result in protuberant abdomen in these patients (Wraith et al., 2008a). As an early sing in some cases, patients also develop skin eruption with papules and nodules spreading throughout the trunk, the upper arms and thighs (Demitsu et al., 1999).

### *2.5.3. Skeletal abnormalities*

Skeletal abnormalities are commonly observed in LSDs and affect around 80% of Hunter patients, with a median age at presentation of 3.5 years (Link et al., 2010). Deposition of GAGs deposition within the cartilage, bone, soft and connective tissue, in combination with inflammation, which disrupts connective tissue homeostasis, lead to skeletal abnormalities, severe restriction of motion and impaired quality of life (Link et al., 2010). The skeletal abnormalities that characterize MPS disorters are collectively referred to as *dysostosis multiplex* and are manifested as abnormal thickness of all bones with irregular epiphyseal ossification centres of joints (Martin et al., 2008; Clarke and Hollak, 2015). Hunter patients usually display short thorax, wide and larger clavicles, macrocephaly, thickened skull and thickened ribs with unusual shape (Aldenhoven et al., 2009). Short stature as a consequence of disturbed ossification in the growth plate is also common in MPSII (Aldenhoven et al., 2009). Hands and wrist are also involved, including a decreased wrist range of motion, interphalangeal joint stiffness and curved fingers, resulting in a claw-like appearance of the hands (Martin et al., 2008; Link et al., 2010). Carpal tunnel syndrome (CTS) contributes also to a significant reduction in fine motor movements of the hand and loss of hand functionality (Wraith et al., 2008a).

In early childhood, joint stiffness and contractures of nearly all joints restrict mobility of Hunter patients. Spine stiffness and deformities, such as scoliosis or spinal cord compression, develop later in the disease (Link et al., 2010). The limited extension of the hip together with the extension deficits in knee and foot contribute to the abnormal gait of MPSII patients (Link et al., 2010). The hip joint appears to be especially vulnerable in these patients and the alterations of the hips can result in significant disability with early-onset arthritis (Aldenhoven et al., 2009). The use of a wheelchair is necessary in most cases at advanced stages of the disease because of hip pain (Wraith et al., 2008a).

The most common surgical intervention that MPSII patients may undergo is carpal tunnel decompression. Other palliative orthopaedic surgeries, such as surgery to alleviate spine fusion, femoral osteotomy and trigger finger release surgery are occasionally performed. (Link et al., 2010). Early surgical spinal decompression to prevent irreversible cord damage is also frequently performed in Hunter patients (Al Sawaf et al., 2008).

### *2.5.4. Neurological involvement and behavioural alterations*

CNS involvement is observed in approximately two thirds of MPSII patients (Wraith et al., 2008a). In a long-term observational study performed in a cohort of 263 Hunter patients, 84% of them presented some form of neurological involvement, being cognitive and behavioural alterations the most common symptoms with a median age at onset of 3.2 and 3.7 years, respectively (Wraith et al., 2008b). Behavioural problems are more common in patients who suffer from the severe form of MPSII, however, they have also been reported in the mild phenotype (Wraith et al., 2008b). At the initial stages of the disease, behavioural changes manifest as hyperactivity and aggressiveness in 51% and 45% of Hunter cases, respectively (Holt et al., 2011). Hypoactive behaviour occurs later in the disease, when severe neurological involvement and cognitive decline are evident (Holt et al., 2011). Developmental delay is usually apparent in severely affected MPSII patients by 18-24 months of age and reaches a plateau at nearly 4 years of age (Wraith et al., 2008a; Holt et al., 2011). Mental impairment is progressive and profound, with a median age of onset around 8 years (Martin et al., 2008). The decline in language skills often reflects the loss of cognitive function (Holt et al., 2011). In addition, impaired hearing and enlargement of the tongue contribute to a bad reading and verbal performance in these patients, who present highly variable IQ scores (Al Sawaf et al., 2008).

A broad spectrum of CNS abnormalities are reported in severe Hunter cases, being the most common findings regional atrophy, hydrocephalus and enlarged ventricles (Al Sawaf et al., 2008; Holt et al., 2011). Enlarged perivascular spaces, white-matter lesions, delayed myelination and elevated intracranial pressure -which may result in optic nerve atrophy- are also common findings in MPSII (Al Sawaf et al., 2008; Martin et al., 2008). Seizures are reported in more than half of Hunter patients with severe phenotype who reach 10 years of age, while they are uncommon in the mild form of MPSII (Martin et al., 2008).

MPSII patients suffer also from visual problems, such as retinopathy. Corneal clouding is not, however, a typical feature in Hunter patients as opposet to other forms of MPSs (Wraith et al., 2008a). Retinal dysfunction leads to a decrease in peripheral vision and to poor dark adaptation (Wraith et al., 2008a). Other ocular findings include optic nerve head swelling and atrophy in 20% and 11% of the cases, respectively. Ocular nerve atrophy is attributed to increased intracranial pressure (Al Sawaf et al., 2008; Fenzl et al., 2015). Bilateral pigmentary changes, glaucoma and sclera thickening -which may contribute to optic nerve compression- have also been described in MPSII (Ashworth et al., 2006; Martin et al., 2008). Regular ophthalmological assessment, including measurement of the intraocular pressure, is indicated for MPSII patients (Wraith et al., 2008a).

Finally, hearing loss is a common feature in Hunter syndrome, which courses with frequent middle ear disease, scarring of the tympanic membrane and damage to the eighth nerve (Wraith et al., 2008a). In most Hunter patients, deafness is the result of both conductive and sensorineural impairment, and an appropriated regular audiology assessment is required for MPSII patients (Al Sawaf et al., 2008; Wraith et al., 2008a).

Regarding the peripheral nervous system, carpal tunnel syndrome is the most common symptom in MPSII patients, and surgical decompression at an early stage results in partial or complete improvement in most patients (Wraith et al., 2008a).

Even in those patients who do not present cognitive involvement, some progressive decline in both gross and fine motor skills is reported (Holt et al., 2011).

### *2.5.5. Sleep alterations*

Hunter patients also suffer from sleep disturbances, characterized by obstructive sleep apnoea (OSA), altered sleep architecture and impaired gas exchange (Wooten et al., 2013). The most common manifestation, reported in 90% of MPSII patients, is OSA, which is caused by physical blockage of the upper and lower airways (Wooten et al., 2013; Moreira et al., 2014). Several factors have been accounted responsible of collapsing MPSII patients' airway, such as macrogliossia, adenotonsillar hypertrophy and GAG deposition within tracheobronchial mucosa (Kasapkara et al., 2014). The apnoeic events that MPSII patients suffer result in poor quality sleep with and repetitive pauses, behavioural problems, congestive heart failure and pulmonary and systemic hypertension (Moreira et al., 2014).

### *2.5.6. Somatic symptomatology*

Undegraded GAGs accumulate in virtually in all organs, however, certain tissues appear to be more affected. As a consequence of GAG storage, an enlargement of the liver and the spleen are commonly observed in Hunter patients, although a dysfunction of these two organs has not been reported (Martin et al., 2008; Wraith et al., 2008a). As a result of hepatosplenomegaly, umbilical and inguinal hernias are frequent manifestations in MPSII patients, who require surgical correction of hernias (Wraith et al., 2008a).

Cardiovascular pathology is an early feature in many MPSII patients, with a prevalence of 82%, being heart murmur and cardiac valve disease the most common signs (Wraith et al., 2008b). Cardiac complications, which are a major cause of morbidity and mortality in Hunter patients, include morphologic changes in the mitral and aortic valves, ventricular hypertrophy, coronary artery narrowing and/or occlusion, heart failure and hypertension (Braunlin et al., 2011; Sohn et al., 2012). Progressive cardiac valve dysfunction, reported in approximately 60% of the MPSII population, is the most prominent manifestation (Wraith et al., 2008b; Kampmann et al., 2011). Annual echocardiography and electrocardiography evaluation are essential, and surgical valve replacement may be necessary in severely affected MPSII patients (Braunlin et al., 2011).

Hunter patients also suffer from progressive airway disease, which is manifest firstly in the upper airways with frequent rhinitis and noisy breathing and gradually involves the lower airways (Martin et al., 2008; Wraith et al., 2008a). Other factors that contribute to chronic respiratory failure are airway obstruction during sleep, recurrent and prolonged ear and upper respiratory infections, pneumonia, weakness of the tracheal and bronchial walls, narrowed and abnormally shaped trachea and bronchi, as well as thick nasal and tracheal secretions (Martin et al., 2008). Oral findings are also present in MPSII, such as thickened vocal cords, macroglossia, enlargement of the tonsils and adenoids and restricted movement of the temporomandibular joints due to skeletal abnormalities in the jaw and neck (Martin et al., 2008; Wraith et al., 2008a). Tonsillectomy, adenoidectomy and the usage of ventilating tubes are recommended in severely affected patients to decrease airway obstruction and assist with breathing (Martin et al., 2008; Wraith et al., 2008a). As a direct consequence of airway complications, anaesthesia represents a major risk for Hunter patients and should be performed only by highly experienced anaesthesiologists under critical scenarios (Wraith et al., 2008a).

Difficulties in food intake are associated to the hyperplasia and hypertrophy of gingival tissue and to irregularly shaped teeth (Martin et al., 2008). The enlarged tongue and tonsils also contribute to the swallowing difficulty (Holt et al., 2011). As the disease progresses, diet becomes more restrictive and at late stages of the disease patients depend exclusively on gastric tubes for feeding (Holt et al., 2011).

Finally, Hunter patients suffer from periodic diarrhoea that has been attributed to an impairment of the autonomic nervous system due to the accumulation of GAGs within gut neural cells (Wraith et al., 2008a). In addition, with age Hunter patients may present constipation as a result of the loss of muscular strength in combination with physical inactivity (Wraith et al., 2008a). Bladder obstruction and urinary retention have also been observed in these patients (Martin et al., 2008).

#### *2.5.7. Death*

Hunter patients usually die from significantly compromised cardiac and respiratory functions due to valve dysfunction, myocardial thickening, coronary artery narrowing and pulmonary hypertension (Neufeld and Muenzer, 2001; Jones et al., 2009). The life expectancy of Hunter patients with cognitive involvement is significantly shorter than those without cognitive impairment (Jones et al., 2009). In the severe form of MPSII disease, death usually occurs in the mid-teenage years, although it may also occurs earlier (Neufeld and Muenzer, 2001). On the contrary, patients with the attenuated form of the disease commonly survive into adulthood, where death often occurs between 20 and 30 years of age. Some patients with the attenuated phenotype may, however, die earlier or survive into their fifth or sixth decade (Wraith et al., 2008a; Jones et al., 2009). A few of the patients with the mild form of the disease may have progeny and their life expectancy may be near normal (DiFerrante and Nichols, 1972; Wraith et al., 2008a), with the longest known survival in this cohort of patients being 87 years (Hobolth and Pedersen, 1978).

#### *2.5.8. Hunter syndrome in females*

As previously mentioned, MPSII is an X-linked recessive inherited LSD and affected patients are mainly males. Heterozygous females carrying a mutation in only one *IDS* allele are usually asymptomatic and present levels of urinary GAGs within normal limits, despite showing a slightly lower IDS activity in plasma and leukocytes (Schwartz et al., 2009; de

Camargo Pinto et al., 2011). Nevertheless, some heterozygous females present signs and symptoms of Hunter disease (Mossman et al., 1983; Broadhead et al., 1986; Clarke et al., 1991; Winchester et al., 1992; Sukegawa et al., 1997, Sukegawa et al., 1998; Cudry et al., 2000; Tuschl et al., 2005; Kloska et al., 2011; Jurecka et al., 2012; Guillén-Navarro et al., 2013; Piña-Aguilar et al., 2013). As in males, the disease in females shows a wide spectrum of clinical severity, ranging from the severe phenotype -with mental retardation, skeletal anomalies, severe systemic pathology and death during the mild-teenager ages- to the attenuated form.

To date, the most common mechanism that explains the existence of femals affected by Hunter is chromosomal rearrangement followed by skewed X-chromosome inactivation (XCI) of the parental *IDS* gene (Mossman et al., 1983; Broadhead et al., 1986; Clarke et al., 1991; Winchester et al., 1992; Sukegawa et al., 1997, Sukegawa et al., 1998; Cudry et al., 2000; Tuschl et al., 2005; Kloska et al., 2011; Jurecka et al., 2012; Guillén-Navarro et al., 2013; Piña-Aguilar et al., 2013). During the development of the female embryo, XCI occurs usually in a random and irreversible manner, resulting in the inactivation of the parental or maternal X chromosome in somatic cells (Lyon, 1961). Under a normal situation, a random X inactivation leads to females with a mosaic expression of approximately equal proportions of paternal and maternal X-chromosome alleles (50:50 or 60:40). Conversely, when non-random X-inactivation occurs, a skewing pattern (≥ 75:25) is observed, which, in the case of female carriers of an *IDS* mutation may leads clinically manifestations of Hunter syndrome (Guillén-Navarro et al., 2013). Depending on the individual *IDS* mutation and the degree of skewing of the X-chromosome inactivation, a wide range of severity of Hunter phenotype has been described in females (Martin et al., 2008).

Another mechanism much less frequent than skewed XCI was reported for the first time in an 11-year old girl, in whom both *IDS* genes were mutated (Cudry et al., 2000). A substitution event of T to C at cDNA position 246 in exon 2 was described in fibroblast samples from the patient, and after sequence analysis, the patient appeared to be homozygous for this substitution (Cudry et al., 2000). The only signs or symptoms shown by the girl were hepatomegaly and growth retardation, resulting in a mild form of the disease in a family of previously undiagnosed male members (Cudry et al., 2000).

## 2.6. Diagnosis of MPSII

The diagnosis of MSPII is often suspected in males with short stature, hepatosplenomegaly, joint contractures and coarse facial features. The median age of MPSII diagnosis is 3.5 years, being usually between 18 and 36 months in the most severe form of the disease, and between the age of 4 and 8 years for the attenuated phenotype (Wraith et al., 2008b).

### *2.6.1. Biochemical tests*

The first screening technique used when an MPS is suspected is the quantification of GAGs excreted in urine. To this aim, the most frequently used method is the dimethylmethylene blue (DMMB) test, based on the spectrophotometric measurement of the amount of DMMB dye that has bounded to the GAGs in the sample (de Jong et al., 1992; Bekri, 2006). A combination of the DMMB test with qualitative electrophoretic separation of excreted GAGs is needed to identify the excreted GAG and outline the diagnosis (Gray et al., 2007). Recently, a method based on the use of electrospray ionization-tandem mass spectrometry to identify the excreted GAG has been proposed for the diagnosis of MPSII (Nielsen et al., 2010). The presence of excess of HS and DS is indicative of MPSI, MPSII and MPSVII; a negative result in the urinary GAG test does not necessarily rule out the diagnosis of an MPS disorder (Burton and Giugliani, 2012). In addition, MPSII female carriers usually present GAG levels within the normal range, therefore, this method is not suitable to identify carriers and further analyses are required to confirm MPSII diagnosis in this group (Burton and Giugliani, 2012).

Confirmation of MPSII diagnosis can be made by demonstration of a deficiency in IDS enzymatic activity (Burton and Giugliani, 2012). IDS is present in all cells, except for mature red blood cells. Therefore, enzyme activity can be measured in a variety of cells and body fluids, such as cultured fibroblasts, leukocytes, plasma or serum, to mention the most frequently used (Neufeld and Muenzer, 2001; Voznyi et al., 2001; Martin et al., 2008). The choice of assay depends on the testing facility, but leukocytes are usually preferred when available (Martin et al., 2008). Analysis of IDS activity in dried blood spots (DBS) on filter paper is an especially useful screening tool, particularly in areas where transport of cells or serum samples is challenging (Civallero et al., 2006; Gelb et al., 2006; Scarpa et al., 2011). Recently, a small-scale pilot study showed that newborn screening for

Hunter disease using a fluorometric assay in DBS is feasible, allowing for the identification of infants with MPSII before clinical symptoms become evident and thus, enabling early intervention (Ruijter et al., 2014). Absent or low IDS activity in males is diagnostic of Hunter syndrome, provided that the activity of another sulfatase is measured and is normal, which would rule out multiple sulfatase deficiency (Burton and Giugliani, 2012).

Enzyme activity cannot be used to identify female carriers. Although on average IDS activity in female carriers is approximately 50% of that seen in non-affected individuals, considerable overlap exist (Martin et al., 2008).

### *2.6.2. Genetic testing*

Mutation analysis of the *IDS* locus is the only reliable method to confirm carrier status in female and may be used to confirm MPSII in males (Neufeld and Muenzer, 2001; Burton and Giugliani, 2012). Sequence analysis for the entire *IDS* coding region detects 82% of mutations in both males and females (Froissart et al., 2007). A variety of analyses are available to detect large -exonic or whole-gene- deletions in males and females, including quantitative PCR, long-range PCR, multiplex ligation-dependent probe amplification or targeted array gene/segment-specific. Southern blot analysis is used to detect complex rearrangements resulting from the recombination with the *IDS2* pseudogene or from other processes (Froissart et al., 2007).

### *2.6.3. Prenatal diagnosis*

Prenatal diagnosis by quantification of enzyme activity may be performed on cells that are cultured from amniotic fluid or in tissue from chorionic villus biopsies, and even in fetal blood, but this test is available at only a few laboratories worldwide (Martin et al., 2008). The assessment of enzymatic activity in uncultured chorionic villi allows early ($12^{th}$ week), rapid (2-3 days) and reliable results (Keulemans et al., 2002). In addition, prenatal diagnosis can be performed using molecular analysis on cells cultured from amniotic fluid or in chorionic villus biopsies if the specific mutation affecting the family are known. Preimplantation genetic diagnosis for MPSII has been reported but is not yet widely available (Altarescu et al., 2011).

## 2.7. Treatment for MPSII

Until recently, there were no specific approved therapies for MPSII and the only treatment available was focused on the management of Hunter syndrome complications. In the last few years, the development of new treatments, such as enzyme replacement therapy and hematopoietic stem cell transplantation, has provided therapeutic options for MPSII. The rational behind these therapeutic strategies is the principle of cross-correction: cells secrete M6P-tagged soluble lysosomal enzymes, such as IDS, which can be subsequently taken up from the extracellular compartment by other cells via M6P receptors located on the plasma membrane and targeted to their lysosomes (Enns and Huhn, 2008). In addition, a "critical threshold" of residual activity, generally as low as 10%, has been postulated. Above this threshold, the cell can cope with substrate influx and patients are not affected by the disease (Neufeld, 1991; Desnick, 2004). This fact suggests that a complete restoration of enzyme activity is not required to obtain a clinical benefit.

### *2.7.1. Supportive treatment*

Since clinical manifestations observed in MPSII patients belong to a wide range of medical areas, the management of these patients is extremely complex and requires multidisciplinary supportive therapies. Subspecialites involved in the symptomatic and palliative treatment for MPSII include otorhinolaryngology, neurosurgery, orthopaedics, cardiology, anesthesiology, pulmonology, physiotherapy, audiology, ophthalmology and others (Muenzer et al., 2009; Hollak and Wijburg, 2014).

In addition, a wide range of unspecific drugs are used for the prevention and management of complications, trying to preserve the health of MPSII patients (Giugliani et al., 2010). Antipsychotic agents, anticonvulsant therapies and attention stimulants are administered to manage behavioural issues associated with Hunter syndrome. There are not, however, any published studies on the efficacy of these agents in MPSII patients, so they should be prescribed with caution.

Many complications of Hunter patients require surgical interventions, such as hernia repair or carpal tunnel realise, to mention a few. However, anaesthetic procedures represent a high risk for MPSII patients due to the compromised airway as a consequence of GAG accumulation in soft tissues (Valayannopoulos and Wijburg, 2011). End-of-life

management of Hunter patients is based on palliative treatments that try to maintain the comfort of the patient, including pain medications when are indicated (Muenzer et al., 2009). Several guidelines and protocols for supportive care and general management of MPSII patients have been edited (Muenzer et al., 2009; Scarpa et al., 2011).

### *2.7.2. Enzyme replacement therapy*

To date, enzyme replacement therapy is commercially available for a few LSDs, such as Gaucher, Fabry, Pompe, MPSI, MPSIVA and MPSVI diseases (Baldo B, 2015). Since its approval by the Food and Drug Administration (FDA) in 2006 and by the European Medicines Agency (EMA) in 2007, recombinant human Iduronate-2-sulfatase (Idursulfase, ELAPRASE®, Shire Pharmaceuticals, Lexington, MA, USA) has been indicated for the treatment of patients with MPSII as an enzyme replacement therapy. This treatment is generally administered weekly at a dose of 0.5 mg/kg by intravenous infusion, with an average infusion time of 1-3 hours (Giugliani et al., 2010). ELAPRASE® was approved after a randomized, double-blind, placebo-controlled study in 96 Hunter patients with no cognitive decline at baseline and with moderately advanced disease (Muenzer et al., 2006; Muenzer et al., 2011). After one year of treatment, ELAPRASE®-treated patients showed an increase in the six-minute walk test (6MWT), an improvement in joint range of motion (ROM) as well as a reduction in liver and spleen volumes compared with those patients who received placebo (Muenzer et al., 2011). In addition, there was evidence of improved pulmonary function when neutralizing antibodies against Idursulfase were not present. The development of anti-IDS antibodies was reported in 50% of the long-term treated patients (Muenzer et al., 2011). To date, however, there is no evidence available in the literature demostrating that ERT provide any amelioration in growth, sleep apnoea, cardiac function, quality of life or mortality. More studies are necessary to obtain information related to the long-term efficacy of ERT for MPSII (da Silva et al., 2014).

As a consequence of possible hypersensitivity to ELAPRASE®, medical support has to be available during product administration. During the trial, the most severe adverse events described were anaphylactic reactions that appeared anytime during ELAPRASE® infusion or up to 24 hours after product administration (Muenzer et al., 2006; Muenzer et al., 2011). The post-marketing monitoring of ELAPRASE® has revealed that the anaphylactic reactions, which can compromise the life of the patients, include respiratory

distress, hypoxia, hypotension, urticaria and/or angioedema of throat or tongue (http://elaprase.com/), and some required interventions such as resuscitation or emergency tracheotomy, and treatment with inhaled beta-adrenergic agonists, epinephrine or intravenous corticosteroids (Burton and Whiteman, 2011). Apart from these severe infusion-related reactions, ERT presents other disadvantages: 1) the life-long dependence on weekly 1-3 hour-long intravenous infusions and the difficulty of performing this procedure in paediatric patients, many of whom suffering from mental illness (http://elaprase.com/); 2) the fact that 50% of patients treated with ELAPRASE® in clinical studies became positive for antibodies to Idursulfase of yet unknown clinical significance, but which might limit product efficacy in the long-term, as suggested by tests of pulmonary function (Muenzer et al., 2006; Muenzer et al., 2007; Muenzer et al., 2011; Muenzer, 2011); 3) the high cost of the therapy, estimated to be >$480,000/patient/year (Wyatt et al., 2012); and 4) the inability of intravenously administered recombinant IDS to reach the CNS, limiting the potential applicability of ERT to treat the neurodegeneration observed in severe Hunter patients (Muenzer, 2011; Muenzer et al., 2012).

In this regard, only a partial rescue of IDS brain activity was achieved in MPSII mice by weekly intravenous administration of higher doses of ELAPRASE® (1.2 or 10 mg/kg to 2 or 7 month-old animals, respectively) (Polito et al., 2010). Indeed, intravenous ERT also failed to correct GAG accumulation in the brain of an MPSII murine model (Garcia et al., 2007a). Furthermore, even at these high doses, circulating IDS activity returned to pre-treatment levels 72 hours post-administration (Polito et al., 2010).

Hence, the efficacy of ERT based on ELAPRASE® infusions is limited to the treatment of non-neurological complications of MPSII (Muenzer et al., 2012). For this reason, the decision to initiate an ERT protocol in MPSII patients with the severe form is complex and require many considerations, such as the clinical status of the patient, the benefit expected and the ERT-associated risks; not all patients with severe phenotype should be considered candidates for ERT (Muenzer et al., 2012).

To overcome the limited efficacy of intravenous ERT in counteracting CNS disease, a recent safety and dose ranging study based on the administration of Idursulfase to the cerebrospinal fluid (CSF) via an intrathecal drug delivery device (IDDD) to directly treat CNS pathology of Hunter patients was carried out (NCT00920647, www.clincialtrials.gov). The implantation of the IDDD was performed following a lumbar incision at the level of the L4-

L5 vertebrae (Muenzer et al., 2015). After 6 months of monthly infusion of Idursulfase, a reduction of approximately 80-90% in CSF GAG levels was observed (Muenzer et al., 2015). Despite these promising results, the therapy itself had a very high economic cost per patient/year and presented substantial risks and shortcomings associated to drug delivery. More than 85% of reported serious adverse events were related to the IDDD, including complications of device insertion, procedural pain, device dislocation, breakage, malfunction or implant site infection, which required IDDD surgical revision or removal in half of the treated patients (Muenzer et al., 2015).

A second ERT product based on the beta isoform of Idursulfase, named Hunterase® (Green Cross biopharmaceutical, Korea), has also been evaluated in a phase I/II study in 31 MPSII patients, and compared with the efficacy of ELAPRASE® (NCT01301898, http://clinicaltrials.gov). Both proteins were weekly administered intravenously to MPSII patients at a dose of 0.5 mg/kg for ELAPRASE® and 0.5 and 1.0 mg/kg for Hunterase® during 24 weeks. The results from Hunterase® treatment showed reduced urine GAG excretion and improved performance in the 6MWT, but none of the doses was able to mediate therapeutic efficacy in pulmonary function, cardiac function nor joint mobility (Sohn et al., 2013a). Hunterase® infusions were generally safe and well-tolerated, although a few adverse events, such as urticaria and skin rash, were reported (Sohn et al., 2013a). A phase III study to evaluate the safety and efficacy of Hutnerase® in Hunter patients younger than 6 years old has recently been completed (NCT01645189, http://clinicaltrials.gov), but results are not yet available.

The effectiveness of intermittent intrathecal (IT) ERT administration was also evaluated at pre-clinical stage. The delivery of the exogenous IDS enzyme directly to the CNS has been assessed in the MPSII mouse model. The stereotaxic injection of 20 μg of recombinant human IDS to the lateral ventricle of 5-month-old MPSII mice every 3 weeks increased IDS activity in cerebrum, cerebellum and somatic organs, such as liver, heart, kidney and testis (Higuchi et al., 2012). The restoration of IDS activity led to the recovery of short-term memory and locomotor activity and to a reduction in cellular vacuolation and lysosomal distention in cerebellum, liver and testis. However, therapeutic efficacy was partial; GAG content was not completely normalized and some behavioural alterations remained refractory to the treatment (Higuchi et al., 2012).

The transport of the therapeutic IDS protein from the CSF to the brain parenchyma after IT-lumbar administration was reported in healthy *Cynomolgus* monkeys and healthy *Beagle* dogs (Calias et al., 2012). In addition, the IT-lumbar administration of recombinant IDS to MPSII mice resulted in widespread enzyme distribution through the brain, including reduction in cellular vacuolation and in LAMP1 (Lysosomal-associated membrane protein1) immunoreactivity, a marker of lysosomal distention, in different brain areas analysed (Calias et al., 2012). Following this principle, the implantation of an IT osmotic pump in MPSII mice to achieve continuous IT enzyme replacement resulted in a decrease of GAG content and a reduction of vacuolation in the brain after 3 weeks of treatment (Sohn et al., 2013b). However, safety long-term studies in both mice and larger animal models should be performed to assess depth of enzyme penetration and the functional, biochemical, and morphological benefits of the treatment (Sohn et al., 2013b).

### *2.7.3. Bone marrow transplantation and hematopoietic stem cell transplantation*

In 1981, the first successful bone marrow transplantation (BMT) in a MPSI patient was reported (Hobbs et al., 1981). Since then, BMT and hematopoietic stem cell transplantation (HSCT) have been considered as a therapeutic option for MPSII. The principle underlying the correction by both approaches is that donor monocytes are able to cross the capillary wall, even at the BBB, after which they differentiate into tissue macrophages -microglia in the case of the CNS- and secrete the enzyme deficient in the disease (Krivit et al., 1995).

BMT performed in MPSII mice reduced GAG accumulation in a variety of somatic tissues, including liver, spleen and lung, but not in the CNS (Akiyama et al., 2014). When BMT was combined with ERT (0.5 mg Idursulfase/kg/weekly), an additive effect on GAG content in heart, kidney and lung was observed 7 months after treatment of MPSII mice. However, accumulation of GAGs in the CNS remained at pathological levels (Akiyama et al., 2014). Despite these results obtained in MPSII mice, the evidence for clinical efficacy has been not very strong in MPSII patients. The follow-up of 10 Hunter patients who received BMT between 1982 and 1991 showed highly varying degrees of success (Vellodi et al., 1999). Four of those patients died before 100 days post-BMT, and 3 more patients died before 7 years after the procedure. Among the 3 patients that survived more than 7 years after BMT, one of them reported no clinical benefit; a second patient showed a

minimal increase of IDS activity in plasma, and the third patient failed to normalize GAG content despite having a slight increase in IDS activity in plasma (Vellodi et al., 1999). In agreement, Magnetic Resonance Imaging (MRI) of the brain of MPSII patients after BMT resulted in variable outcomes (Seto et al., 2001). One MPSII patient with mild MPSII phenotype showed a slight decrease in the number of cystic lesions 2.5 years after BMT (Seto et al., 2001). However, the same study provided data on another Hunter patient with mild phenotype that did not show any improvement under MRI (Seto et al., 2001).

Therefore, clinical outcomes appear to be highly variable among Hunter patients (Giugliani et al., 2010; Valayannopoulos et al., 2011). Several factors have been suggested to influence the long-term outcomes, including the genotype, age and patient's clinical status at treatment -such as degree of neurological impairment-, donor status, donor chimerism, bone marrow or stem cell source and activity of the deficient enzyme reached with the treatment (Giugliani et al., 2010; Valayannopoulos et al., 2011). A plausible explanation to the failure of BMT and HSCT is the limited IDS expression in engrafted cells, leading to an insufficient IDS cross-correction in the CNS. In general, both BMT and HSCT approaches are not recommended for Hunter patients, due to the high rate of morbidity and mortality and the poor neurocognitive benefit obtained (Giugliani et al., 2010).

### *2.7.4. Other therapeutic options under research*

Despite the safety profile and significant improvements achieved by ERT and some cases of HSCT in MPSII, the existing therapeutic options still not constitute a cure for the disease. Hence, new therapeutic tools for MPSII have been developed during the last few years.

#### *2.7.4.1. Small molecules therapy*

Small molecules therapy has been developed to address the limitations of the other approaches mentioned above by using oral drugs that may present better distribution than infused enzyme and presumably can gain access to CNS (Valayannopoulos et al., 2011; Weinreb, 2013). In this regard, substrate reduction therapy (SRT) use compounds that restore the balance between synthesis and degradation of accumulated material in LSDs (Banecka-Majkutewicz et al., 2012; Hollak and Wijburg, 2014). SRT is based on the usage of specific inhibitors of the storage compounds synthesis, assuming that slowing down the synthesis pathway of these compounds may decrease the storage process, and

therefore, improve cell pathology (Banecka-Majkutewicz et al., 2012). A candidate for this approach is genistein, which is a natural soy isoflavone that significantly inhibits GAG synthesis when is added to cultured fibroblast of MPSI, MPSII, MPSIIIA and MPSIIIB patients (Piotrowska et al., 2006). Despite the decrease in GAG content observed after using genistein also in MPSII mice (Friso, 2010) and in a pilot study with Sanfilippo patients (Piotrowska et al., 2008), no clinical efficacy on total behavioural scores was reported in a randomized double-blind trial with Sanfilippo patients (de Ruijter et al., 2012).

#### *2.7.4.2. Molecular Trojan horses*

An alternative way to enable BBB penetration and reach the CNS is based on the systemic administration of a molecular trojan horse (MTH). MTH results from the fusion of a biological agent, such as a lysosomal enzyme, with the IgG part of a reengineered monoclonal antibody (MAb) against an endogenous BBB receptor, such the human insulin receptor (HIR) (Pardridge, 2015). Hence, the HIR-MAb domain of the resultant reengineered fusion protein binds the insulin receptor (IR) expressed on the BBB, a binding that triggers transport across the BBB (Pardridge, 2015).

Regarding MPSII disease, the insulin receptor antibody-iduronate 2-sulfatase fusion protein (HIRMAb-IDS) was tested. Weekly intravenous administrations of 3, 10 and 30 mg/kg of HIRMAb-IDS to healthy juvenile Rhesus monkeys during 26 weeks resulted in a HIRMAb-IDS brain uptake of 1% of the total injected dose (Boado et al., 2014). A phase I in adult MPSII patients to test the safety and dose-finding of HIRMAb-IDS is currently recruiting patients (NCT02262338, www.clincialtrials.gov).

#### *2.7.4.3. Cell microencapsulation*

An alternative route of IDS delivery is cell therapy based on the implantation of allogeneic microcapsules containing engineered cells that constitutively produce high levels of the deficient enzyme (Friso et al., 2005). Engineered cells are trapped in a semipermeable membrane, which prevents the access of the immune system to the cells avoiding immunosuppression and allows simultaneous exchange of metabolites and nutrients between the confined cells and the external environment (Giugliani et al., 2016). Microcapsules enclosing myoblasts over-expressing IDS were intraperitoneally implanted in MPSII mice (Friso et al., 2005). After 8 weeks of monitoring MPSII mice that had received approximately $1.5x10^6$ recombinant cells, an increase of 17-20% of wild-type IDS

activity in liver, kidney and spleen was observed in treated mice, which led to a moderated reduction of GAG content in the same somatic tissues and in urinary levels (Friso et al., 2005). Despite the modest efficacy obtained and the easy handling of the procedure, encapsulated cells could only survive for a few months, resulting in necessary re-administrations (Friso et al., 2005).

#### *2.7.4.4. Antisense oligonucleotides*

Around 9% of the mutations described to cause MPSII are based on single nucleotide substitutions that affect splice site signals, leading to abnormal or deficient IDS protein production (http://www.hgmd.cf.ac.uk/ac/gene.php?gene=IDS). Therefore, the modification of the splicing pattern by antisense oligonucleotides (AOs) can lead to the recovery of the production of normally spliced transcripts (Matos et al., 2015). In this regard, three different AO approaches were tested in fibroblast from MPSII patients, however, they resulted in the appearance of another aberrant splicing product, suggesting that further knowledge in the field is required (Matos et al., 2015).

## 2.8. MPSII animal models

In the study of human genetic diseases, the use of animal models that reproduce the human pathology is a useful option. Animal models are frequently selected not only because of their genetic, pathophysiology and anatomy similitude to the humans, but also because of their easy handling and genetic manipulation, accelerated lifespan, availability, reproducible results and relatively low associated cost. In addition, animal models are complex living systems that represent a valuable tool where new therapeutic approaches can be developed, tested and evaluated in terms of efficacy and safety (Haskins, 2007).

Until now, three different mouse models (Muenzer et al., 2002; Jung et al., 2010; Higuchi et al., 2012) and one canine case (Wilkerson et al., 1998) of mucopolysaccharidosis type II have been described in the literature.

### *2.8.1. MPSII mouse models*

In 2002, Muenzer *et al.* described the first knock-out mouse model of MPSII (IdS-KO) in C57BL/6 strain background and obtained by replacing exon 4 and part of exon 5 of the murine *Iduronate-2-sulfatase* gene with the neomycin resistance gene (Muenzer et al., 2002). At the age of 4-6 weeks, IdS-KO showed significantly elevated GAG urinary levels and evident GAG accumulation in several organs, like liver, kidney, lung and heart valves (Muenzer et al., 2002; Garcia et al., 2007b). By 10 weeks of age, coarse fur, sporadic alopecia and skeletal abnormalities were reported in the IdS-KO; and by 40 weeks, liver and spleen weight were significantly increased in the knock-out mice compared to wild-type mice (Garcia et al., 2007b). Radiographic studies revealed a progressive and severe involvement of bones and joints in the IdS-KO aged 40 weeks, such as enlarged skull, thickening of long bones in the hind limbs, increased bone density and severe calcification of the calcaneal tendon of the distal tibia (Garcia et al., 2007b). Histopathological analysis of IdS-KO aged 60 weeks showed foamy, vacuolated cell types infiltrating multiple organs and tissues (Muenzer et al., 2002; Garcia et al., 2007b). The deficiency of IDS activity was confirmed in brain, liver, spleen, kidney and serum extracts of the mouse model at the age of 10-12 months (Garcia et al., 2007b). The IdS-KO mouse model also presented shorter lifespan (1 year) compared to wild-type littermates (2.5 years) (Garcia et al., 2007b).

In 2010, Jung et al. characterized a novel knock-out MPSII mouse model (IDS KO) generated by replacing 1485 bp encompassing exon 2 and exon 3 of the murine Ids gene with the neomycin resistance gene (Jung et al., 2010). IDS KO showed no morphological differences compared to wild-type C57BL/6 littermates at birth. At the age of 4-5 weeks, the first morphological changes observed in IDS KO were coarse face and sporadic alopecia. Later on, knock-out mice aged 6 weeks showed elevated GAG content in several organs, including liver, kidney, lung, heart and brain; and by 7-8 weeks of age, mice presented limitations of the hind limb join (Jung et al., 2010). No IDS activity was detected in a variety of tissue extracts and serum from 16-week-old IDS KO mice. By 25-30 weeks of age, a decline in the physical activity was observed and by 38 week, IDS KO presented foamy cells and a prominent urinary GAG extraction (Jung et al., 2010). Most IDS KO mice had died before 1 year of age (Jung et al., 2010).

A third MPSII murine model (IDS-KO) was generated by JCR Pharmaceuticals Co., Ltd. (Hyogo, Japan) (Highuchi et al., 2012). In this case, the IDS-KO mouse, bread from a

C57BL/6 strain, resulted by the deletion from exon 2 to exon 5 of the murine Ids gene (Higuchi et al., 2012). By 21 weeks of age, IDS-KO mice presented coarse face and abnormal walking footprint pattern compared to wild-type littermates. IDS-KO male mice aged 33 weeks showed almost negligible IDS activity and elevated GAG content in different brain areas (Higuchi et al., 2012). At the age of 34 weeks, alterations in Y-maze test were detected in IDS-KO and by 40 weeks of age, many vacuolations in the cytosol of Purkinje and liver cells were reported (Higuchi et al., 2012).

### *2.8.2. MPSII canine model*

In 1998, Wilkerson *et al.* reported a case of Hunter syndrome in a Labrador retriever (Wilkerson et al., 1998). The male dog presented progressive incoordination at the age of 3 years, in combination with labial mucosal thickening, asymmetric ataxia and paresis affecting all limbs, hypermetria, sporadic and variable nystagmus, visual impairment, unilateral corneal dystrophy, generalized osteopenia, exercise intolerance, hepatomegaly and macrodactylia (Wilkerson et al., 1998). The MPSII diagnosis was confirmed by the positive urine spot test for heparan and dermatan sulfate, the presence of abundant intracytoplasmatic clear vacuoles in dermal fibroblast from skin biopsy and the deficiency in IDS activity in cultured dermal fibroblast. At the age of 5 years, the dog presented coarse facial features and enlarged tongue. In addition, by 5 years of age the medical records got worse due to progressive neurologic deterioration, severe asymmetric limb ataxia, tremors and nystagmus. Because of the progressive nature of the disease, the dog was euthanatized at the age of 5 years and no colony was established (Wilkerson et al., 1998). Therefore, a canine model of mucopolysaccharidosis type II is not available.

# 3. GENE THERAPY

## 3.1. Introduction to gene therapy

Gene therapy is a technology that mediates the transfer of foreign genetic material into target cells or tissues with therapeutic purposes, by counteracting or replacing a malfunctioning gene within the cells affected by a condition through gene editing, gene addition or knockdown technology (Naldini, 2015).

According to the delivery system used, gene therapy can be categorized into two types: *ex vivo* and *in vivo* gene therapy. While *ex vivo* gene therapy is based on the *in vitro* genetically modification of cultured cells extracted from the patient, which are then re-implanted into the patient; *in vivo* gene therapy transfers the genetic material by direct administration of therapeutic vectors to the patient (Chira et al., 2015).

Because of the great variety of possibilities that offers this technology, many gene therapy approaches are currently under investigation for a wide range of diseases and several are under clinical development, being two of them approved in European Union (Glybera®, Uniqure; and Strimvelis™, Gsk). In particular, LSDs have been proposed to be excellent candidates for gene therapy, due to the monogenic nature of these disorders, the low levels of enzymatic activity required to produce clinical benefit, and the possibility to cure the disease by cross-correction mechanism that allows widespread distribution of functional enzyme after secretion by engineered cells (Biffi, 2015; Parenti et al., 2015).

To achieve successful gene therapy outcomes, the development of efficient, safe, and innocuous gene transfer vehicles has become a key point. For both *ex vivo* and *in vivo* gene therapy, several vectors -classified as non-viral or viral vectors- have been used to introduce genetic material into the cells. Non-viral vectors are based on the use of physical and chemical systems to transfer the therapeutic gene expression cassette into the cells, including direct administration of naked DNA, minicircle vectors, transposons and microcapsules, among other delivery systems (Nayerossadat et al., 2012; Baldo et al., 2014; Ramamoorth and Narvekar, 2015). Although non-viral vectors are easily produced, display low inflammatory-associated complications and high capacity for carrying large DNA molecules, they do not show high transfection efficacy nor long-term transgene expression *in vivo* (Baldo et al., 2014; Ramamoorth and Narvekar, 2015). On the other hand, viral vectors systems take advantage of the inherent infectious capacity of virus to

enter into target cells, deliver their genetic material to the nucleus and express their proteins (Waehler et al., 2007).

### 3.2. Viral vectors

Viruses have become an attractive tool for therapeutic gene transfer due to their high transduction efficiency in a broad range of human cells (Chira et al., 2015). Because of the ability of viruses to enter in a host, to avoid its defence systems, to pass through physical barriers, to infect cells by active mechanism and to deliver their genetic direct to the nucleus of a cell (Pellett et al., 2014), virus-derived vectors have been proposed as natural vectors for the transfer of therapeutic foreign genetic material into diseased cells.

Naturally, the viral cycle can be divided in two temporally distinct phases: infection and replication. The entry of the virus into the host cell is mediated by the attachment of proteins of the virus surface to specific receptors on the cell surface, leading to its penetration (Pellett et al., 2014). Once inside the cell, uncoating of the virus occurs and the viral genome arrives to the nucleus where it replicate its own genome and express viral genes necessary for the assembly of new viral particles (Pellett et al., 2014).

Nevertheless, because of the pathogenic properties of viruses, its attenuation is required to guarantee safety in clinical applications. In this regard, viral vectors used in gene therapy protocols are genetically modified by replacing or deleting some of the viral genes involved in integrative and replicative mechanism (Nayerossadat et al., 2012; Baldo et al., 2014). Thus, viral vectors used in gene therapy carry a therapeutic gene construct instead of the whole wild-type viral genome, keeping the infectivity efficiency of viruses but without the ability to produce new viral particles.

Several viral vectors have been engineered, such as retroviral vectors, lentiviral vectors, adenoviral vectors, adeno-associated virus vectors, sendai virus vectors, baculovirus vectors and herpes simplex virus vectors, to mention some (Sands and Davidson, 2006). However, the most commonly used viral vectors for the treatment of mucopolysaccharidoses are retroviral, lentiviral, adenoviral and adeno-associated virus-derived vectors. The main characteristics of these vectors are summarized in Table 3.

**Table 3. General characteristics of the most commonly used viral vectors in gene therapy for mucopolysaccharidosis**

| Viral vector | Retroviral (RV) | Lentiviral (LV) | Adenoviral (Ad) | Adeno-associated (AAV) |
|---|---|---|---|---|
| **Family** | *Retroviridae* | *Retroviridae* | *Adenoviridae* | *Parvoviridae* |
| **Pathogenicity of parental virus** | Yes | Yes | Yes | No |
| **Genome** | ssRNA, lineal | ssRNA, lineal | dsDNA, lineal | ssDNA, lineal |
| **Maximum cloning capacity** | 8 kb | 8 kb | 36 kb | 4.7 kb |
| **Production at high titers** | Yes | No | Yes (lower titers with 3rd generation vectors) | Yes |
| **Insertion in host genome** | Yes, with preference for regulatory elements | Yes, but with no preference for regulatory elements | No | Yes, but randomly and with very low frequency, mainly episomal |
| **Innate immunity** | Yes | Yes | High for 1st and 2nd generation vectors | Very limited |
| **Target cells** | Dividing cells | Dividing and quiescent cells | Dividing and quiescent cells | Dividing and quiescent cells |
| **Transgene expression** | Long-lasting | Long-lasting | Short-lived, except for 3rd generation vectors | Long-lasting |
| **Main advantages** | Long-lasting expression in dividing cells<br>Production at high titers | Long-lasting expression in dividing cells | Episomal production at high titers (except for 3rd generation)<br>High levels of transduction *in vivo*.<br>High cloning capacity. | Episomal. Production at high titers<br>High levels of transduction *in vivo*<br>Non-pathogenic, low immunogenicity<br>Several serotypes with different tissue tropism |
| **Main disadvantages** | Infects only dividing cells<br>Limited cloning capacity<br>Risk of insertional mutagenesis | Limited cloning capacity<br>Risk of insertional mutagenesis but lower than RV vectors | Inflammatory and immune response to the viral proteins, limit persistence of transgene expression.<br>Diminished in 3rd generation vectors<br>Useful only for short-term studies<br>Unselective tropism | Limited cloning capacity |

## 3.3. Adeno-associated viral vectors

### *3.3.1. Biology of adeno-associated viruses*

Adeno-associated viruses belong to the family and genus *Parvoviridae Dependoparvovirus* and are dependent viruses that require co-infection by helper virus such as adenovirus or herpes simplex virus to complete their viral life cycle (Balakrishnan and Jayandharan, 2014; Wolf et al., 2015). AAVs are composed of a linear 4.7 kb single-stranded DNA genome within a nonenvoloped, icosahedral capsid with a diameter of 20-25 nm (Waehler et al., 2007; Kotterman et al., 2015). The wild-type AAV genome (Figure 6) contains two genes (*Rep* and *Cap*) and three open reading frames (ORFs) flanked by two hairpin palindromic repeat sequences designated as inverted terminal repeats (ITRs) of 145 bp, which behave as the viral origin of replication and the packaging signal (Chira et al., 2015; Kotterman et al., 2015). The *Rep* ORF encodes four non-structural proteins (Rep78, Rep68, Rep52 and Rep40), which are crucial for viral replication, transcriptional regulation, genomic integration and virion assembly and encapsidation (Kotterman et al., 2014; Kotterman et al., 2015; Lisowski et al., 2015). The *Cap* ORF encodes three structural proteins (VP1, VP2 and VP3) that assemble a 60-mer viral capsid (Kotterman et al., 2015). Lastly, an alternate third ORF within the *Cap* gene produces the essential assembly-activating protein (AAP), which localizes AAV capsid proteins to the nucleolus and participates in the process of capsid assembly (Kotterman et al., 2015; Lisowski et al., 2015).

In the absence of helper virus, wild-type AAVs tend to be mainly retained in circular episomal form or integrated with low frequency within a specific region of the human chromosome 19 (19q13.3-qter), the so-called AAVS1 site, by a mechanism that involves *Rep* proteins (Kotin et al., 1990; McCarty et al., 2004; Lisowski et al., 2015).

To date, 12 naturally occurring AAV serotypes and more than 100 human and non-human primate AAV variants have been identified (Balakrishnan and Jayandharan, 2014; Lisowski et al., 2015), being nearby 90% of the human population AAV seropositive for some of them (Calcedo et al., 2009; Calcedo et al., 2011; Boutin et al., 2010; Skubis-Zegadlo et al., 2013). However, no known pathogenesis has been linked to adeno-associated viruses in human beings (Lisowski et al., 2015).

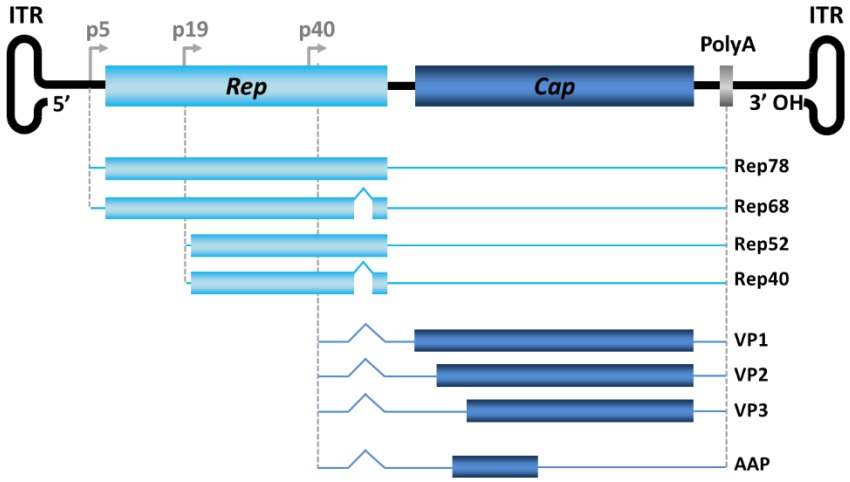


**Figure 6. Wild-type adeno-associated virus genome.** Schematic representation of the wild-type single-stranded DNA genome of an AAV, which contains two genes (*Rep* and *Cap*) and three open reading frames (ORF) flanked by inverted terminal repeats (ITRs). By alternative splicing, the *Rep* ORF encodes four non-structural proteins (Rep78, Rep68, Rep52 and Rep40) and the *Cap* ORF encodes three structural proteins (VP1, VP2 and VP3) and the assembly-activating protein (AAP). Rep78 and Rep68 are transcribed from the internal promoter p5, Rep52 and Rep40 from p19 promoter and *Cap* ORF from p40 promoter. Adapted from Balakrishnan and Jayandharan, 2014.

### *3.3.2. Recombinant adeno-associated viral vectors*

Recombinant adeno-associated viral vectors are generated by replacing both *Rep* and *Cap* genes by the transgene of interest between the ITRs to retain the packaging ability (Balakrishnan and Jayandharan, 2014). Despite the resulting vectors do not contain viral genes, AAV vectors can transduce both dividing and non-dividing cells with stable long-term transgene expression in the absence of helper virus (Balakrishnan and Jayandharan, 2014). Recombinant AAV vectors are maintained predominantly as episomal circular form, but can also undergo genomic integration in low frequency (Lisowski et al., 2015).

The manufacture and purification of recombinant AAV vectors can be achieved in high titers (Ayuso et al., 2010a) and is usually done by triple plasmid cotransfection into cell culture. The first plasmid holds the therapeutic construct of interest flanked by the ITRs; the second plasmid does not carry ITRs sequences but codifies for the genes encoding for both *Rep* and *Cap* genes, which are essential for the replication and the capsid assembly; and the third one is a helper plasmid which provides those adenoviral genes required for AAV replication (Matsushita et al., 1998; Balakrishnan and Jayandharan, 2014). To avoid possible recombination events during vector production, the packaging system used expresses the viral proteins *in trans* with the therapeutic gene (Baldo et al., 2014). After the triple cotransfection, transcription and translation of REP and VP proteins

occurs, the ITR flanked transgene cassette of the vector plasmid is replicated, and the single-stranded DNA molecules containing the construct of interest are encapsidated into preformed AAV capsids. Cells are later lysed to release the packaged vector particles, which are then separated from cellular debris by density gradient centrifugation (CsCl or iodixanol) and/or column chromatography (Ayuso et al., 2010b). The purified vector preparation also contains empty capsids, the amount of which depends on the packaging efficiency and the purification method, being separation of empty capsids from full capsids most efficiently achieved using CsCl density gradients (Ayuso et al., 2010b). Particularly, the polyethylene glycol (PEG) and CsCl-based purification protocol dramatically reduce empty AAV capsids and DNA and protein impurities from viral stock, increasing AAV vector purity, which ultimately results in higher transduction *in vivo* (Ayuso et al., 2010b).

To date, several serotypes of AAVs have been identified; Table 4 describes the main AAV serotypes used in gene therapy. These serotypes differ in the amino acidic sequences of the capsid proteins (VP1, VP2 and VP3), which determine the bind affinity to different cellular receptors and co-receptors, conferring to each AAV serotype specific physicochemical properties and diverse tissue tropism (Baldo et al., 2014; Balkrishnan and Jayandharan, 2014). Because AAV serotype 2 was the first isolated, and subsequently the most characterized AAV, most gene therapy approaches have been carried out using the AAV2 vector or the modified AAV2 genome and packaged within different capsid proteins of other serotypes (Balakrishnan and Jayandharan, 2014).

Since each AAV serotype displays different cell tropism, many efforts have been focused in the isolation and characterization of new serotypes with different tissue tropism and broaden the range of use of these vectors. This is the case of adeno-associated virus serotype 9 (AAV9) (Gao et al., 2004). AAV9, a serotype derived from non-human primates, seems to present different structure of some capsid proteins compared to AAV1-8, modifying the capsid-cell interaction and allowing the vector to cross the blood-brain barrier and transduce neurons and astrocytes in the CNS, among other cell types (Duque et al., 2009; Foust et al., 2009; Wang et al., 2010; Gray et al., 2011; Haurigot et al., 2013). However, the precise mechanism by which AAV9 vectors bypass the BBB is still unknown. In addition to the ability to penetrate to the CNS, AAV9 vectors have high tropism for liver and heart, present broad genome distribution and rapid-onset, leading to high protein expression levels compared to other AAV serotypes (Zincarelli et al., 2008).

**Table 4. Characteristics of the AAV serotypes 1-12.** Summary of the origin of each AAV serotype, their receptors and tissue tropism.

| Serotype | Origin | Receptor and co-receptors | Tissue tropism |
|---|---|---|---|
| AAV1 | Human or NHP | N-linked sialic acid | SM[1, 2, 3], CNS[1, 2], airway[1, 2], retina[1], pancreas[1], heart[1, 4], liver[1] |
| AAV2 | Human | HSPG, FGFR1, HGFR, LamR, CD9, integrin $\alpha_v\beta_5$, $\alpha_5\beta_1$, | SM[1], CNS[1, 5], liver[1], kidney[1], retina[1, 2, 3, 6] |
| AAV3 | Human or NHP | HSPG, FGFR, HGFR, LamR | HCC[6], SM[1], inner ear |
| AAV4 | NHP | O-linked sialic acid | CNS[1], retina[1, 3], lung[1, 2], kidney[1] |
| AAV5 | Human | N-linked sialic acid, PDGFR | SM[1], CNS[1, 3], lung[1], retina[1], liver |
| AAV6 | Human | HSPG, N-linked sialic acid | SM[1, 3], heart[1, 3, 4, 7], airway[1, 2, 3] |
| AAV7 | Rhesus macaque | Unknown | SM[1], retina[1], CNS[1], liver[1] |
| AAV8 | Rhesus macaque | LamR | Liver[1, 2, 3], CNS[1, 2, 3], retina[1, 3], heart[1], SM[1], pancreas[1], kidney[1], adipose tissue[1] |
| AAV9 | Human | N-linked glycans, LamR | Liver[1], heart[1, 2, 4], SM[1, 3], lung[1], pancreas[1], CNS[1, 2], retina[1, 2], testes[1], kidney[1], adipose tissue[1] |
| AAV10 | NHP | Unknown | Liver |
| AAVrh10 | Rhesus macaque | LamR | Liver[1], heart[1], SM[1, 3], lung[1], CNS[1, 8], pancreas[1], retina[1], kidney[1] |
| AAV11 | NHP | Unknown | Not described |
| AAV12 | NHP | Unknown | Not described |

Tissue tropism in [1]mouse, [2]NHP, [3]dog, [4]pig, [5]monkey, [6]human being, [7]sheep and [8]rat.
Abbreviations: NHP, non-human primate; HSPG, heparan sulfate proteoglycan; LamR, 37/67 kDa laminin receptor; FGFR1, fibroblast growth factor receptor 1; HGFR, hepatocyte growth factor receptor, PDGFR, platelet-derived growth factor receptor; EGFR, epidermal growth factor receptor; SM, skeletal muscle; CNS, central nervous system; HCC, hepatocellular carcinoma.
Adapted from Jimenez et al., 2013; Balakrishnan and Jayandharan, 2014 and Lisowski et al., 2015.

Because of the versatility of recombinant AAV vectors, their high efficient transduction of a broad range of cell types, and their ability to produce long-term expression of the desired therapeutic gene with low toxicity and low immunogenicity, recombinant AAV vectors have emerged as a very attractive tool for gene transfer. To date, numerous preclinical studies in large animal models (Rivera et al., 2005; Niemeyer et al., 2009; Callejas et al., 2013; Bainbridge et al., 2015) as well as several clinical trials (Hauswirth et al., 2008; Maguire et al., 2008; Maguire et al., 2009; Simonelli et al., 2010; Buchlis et al., 2012; Jacobson et al., 2012; Gaudet et al., 2013; Testa et al., 2013; Nathawani et al., 2014; Bainbridge et al., 2015) based on recombinant AAV-mediated gene transfer are ongoing with promising outcomes.

In 2012, EMA approved the first human gene therapy product licenced in the European Union, called Glybera®. This product is based on AAV1 vectors encoding for the lipoprotein lipase administered intramuscularly for the treatment of lipoprotein lipase deficiency (LPLD) (EMA product number: EMEA/H/C/002145).

## 3.4. Gene therapy for the treatment of MPSII

Given the limitations of current therapeutic options for MPSII, alternative and more effective approaches are needed. Gene therapy may overcome some of the problems mentioned previously, as it offers the possibility of a one-time treatment for MPSII and other inherited diseases, with the prospect of lifelong beneficial effects.

### 3.4.1. *Ex vivo gene therapy for MPSII*

In the 90's, *ex vivo* gene therapy based on retrovirus-mediated gene transfer of human *IDS* coding sequence into peripheral blood lymphocytes (PBL) from Hunter patients was tested (Braun et al., 1993; Braun et al., 1996). The approach achieved 1-5% of cell transduction, leading to a 10-70 fold increase of IDS activity and a reduction in GAG storage in cultured lymphocytes (Braun et al., 1996). In addition, 5 months after vector administration, IDS activity remained 2-log fold higher than non-transduced PBLs (Braun et al., 1996).

*Ex vivo* gene therapy approach based on lentiviral vectors coding for human *IDS* coding sequence was assessed to transduce bone marrow cells prior to their transplantation into MPSII mice, resulting in improved performance in the T-maze memory test 14 weeks post-transplant (Podetz-Pedersen et al., 2013). The feasibility of *ex vivo* hematopoietic stem cell gene therapy with lentiviral vectors in MPSII mice was also assessed (Wakabayashi et al., 2015). IDS-transduced hematopoietic stem cells increased IDS activity in liver, heart and slightly in the CNS, ameliorated the autophagic flux and resulted in better performance in the Y-maze test. However, GAG accumulation in brain remained (Wakabayashi et al., 2015). A plausible explanation to the failure of HSCT is the limited IDS expression achieved in engrafted cells, leading to an insufficient IDS cross-correction in the CNS (Podetz-Pedersen et al., 2013).

### 3.4.2. *In vivo gene therapy for MPSII*

*In vivo* gene therapy represents a promising therapeutic tool for rare genetic diseases, such as MPSII, as it may allow constant delivery of the deficient lysosomal enzyme direct to key organs after a single administration of the product. In addition, the number of cells required to be modified by gene therapy is relatively low, as low levels of the deficient

enzyme -generally around 10%- are sufficient to observe clinical benefit in LSDs (Neufeld, 1991; Desnick, 2004; de Carvalho et al., 2015).

To date, few gene therapy approaches based on intravenous delivery of viral vectors have been tested in MPSII disease, being all of them conducted at preclinical stage.

AAV serotype 5 vectors encoding for the human *IDS* gene under the control of the ubiquitous promoter CMV were systemically administered to the temporal vein of MPSII mouse pups (P2) (Polito and Cosma, 2009). Treated MPSII mice showed an increase of IDS activity in peripheral tissues and a moderated increase in brain, leading to a reduction of GAG content in somatic tissue and urinary up to 18 months post-treatment (Polito and Cosma, 2009). Moreover, this treatment prevented the CNS pathology by preventing neurodegeneration, astrogliosis and inflammation. The Open Field test assessed 18 months after gene transfer demonstrated an improvement in the gross motor phenotype of treated MPSII mice (Polito and Cosma, 2009).

AAV serotype 8 vectors encoding for the human *IDS* gene under the control of the liver-specific TBG promoter were also assessed in MPSII mice intravenously administered (Cardone et al., 2006). After 7 months of vector delivery, treated MPSII mice showed an increase in IDS activity in serum, liver, spleen, lung, heart, kidney and muscle, resulting in complete correction of GAG storage in these tissues (Cardone et al., 2006). However, very high dose ($4x10^{12}$ vector genomes/mouse) was required to achieve a slight increase in IDS activity and partial clearance of GAG accumulation in the brain (Cardone et al., 2006).

The intravenous delivery of AAV8 vectors encoding for the human *IDS* gene under the control of the ubiquitous elongation factor 1-a (EF) promoter to adult MPSII mice led to an increase of IDS activity in liver, heart, spleen and kidney 24 weeks after treatment, with full correction of GAG storage in these organs (Jung et al., 2010). Brain IDS activity was only increased in those mice sacrificed at short-term (6 weeks post-injection), however, this was not sufficient to normalize GAG content in the CNS (Jung et al., 2010).

Thus, none of the aforementioned approaches tested in MPSII mice have attained therapeutic enzyme levels and achieved full eradication of introcytoplasmatic inclusions in the CNS nor corrected all clinical sings of MPSII. Therefore, there is an unmet medical need for developing novel approaches for the treatment of MPSII at neurological as well as at somatic level that present better efficacy and safety profiles.

## 4. INTRA-CSF AAV-BASED GENE THERAPY FOR MUCOPOLYSACCHARIDOSES

### 4.1. Route of administration

Current therapeutic options for the treatment of MPSII do not achieve neurological benefit. When the therapy is administered systemically, the BBB blocks the lysosomal enzyme to cross it and therefore, IDS is not able to reach the CNS. Only when high doses of the treatment are systemically delivered, few enzyme is detected in the CNS with scarce neurological improvement. On the other hand, the efficacy of local administration of the IDS to the brain is restricted to the nearest areas surrounding the injection point.

Previously studies in our laboratory have demonstrated widespread transduction of the CNS -even in deep areas of the encephalon- after the administration of AAV vectors to the CSF using surgical procedures and equipment that are common practice in paediatric neurosurgery (Haurigot et al., 2013; Ribera et al., 2015). Hence, in order to genetically engineer the CNS, the administration of AAV vectors directly to the cerebrospinal fluid could become the ideal route of administration for MPSII disease.

Cerebrospinal fluid is a colourless body fluid that set up an independent circulatory system, named the “third circulation”, which baths the whole CNS (Spector et al., 2015). Its main function is not only to protect the CNS against traumas through hydromechanical stability, but it also plays a key role in the homeostasis, regulation of neuronal function, nutrition, metabolite regulation and brain development, to mention some (Sakka et al., 2011). The majority of the CSF is produced and secreted by ependymal cells of choroid plexuses (CP) in the lateral ventricles of the brain. It is then distributed from there to the third and fourth ventricle, moving latter to the central canal of the spinal cord or draining into the cisterna magna (cerebrollomedullary cistern) to subsequently flow to the subarachnoid space between the arachnoid mater and the pia mater (Figure 7) (Wright et al., 2012; Lehtinen et al., 2013). The CSF located in the subarachnoid space is then reabsorbed into the systemic circulation via the arachnoid villi (Wright et al., 2012). Thus, the CSF circulates from the sites where it is secreted to the sites where absorption occurs, following a rostrocaudally unidirectional flow in ventricular cavities and a multidirectional flow in subarachnoid spaces (Sakka et al., 2011). Hence, CSF-mediated delivery allows widespread distribution of the therapeutic vector throughout the whole CNS. To this aim, direct vector administration to the CSF can be accomplished with an injection to the cisterna magna, to the ventricles or through a lumbar puncture (Sorrentino et al., 2016).

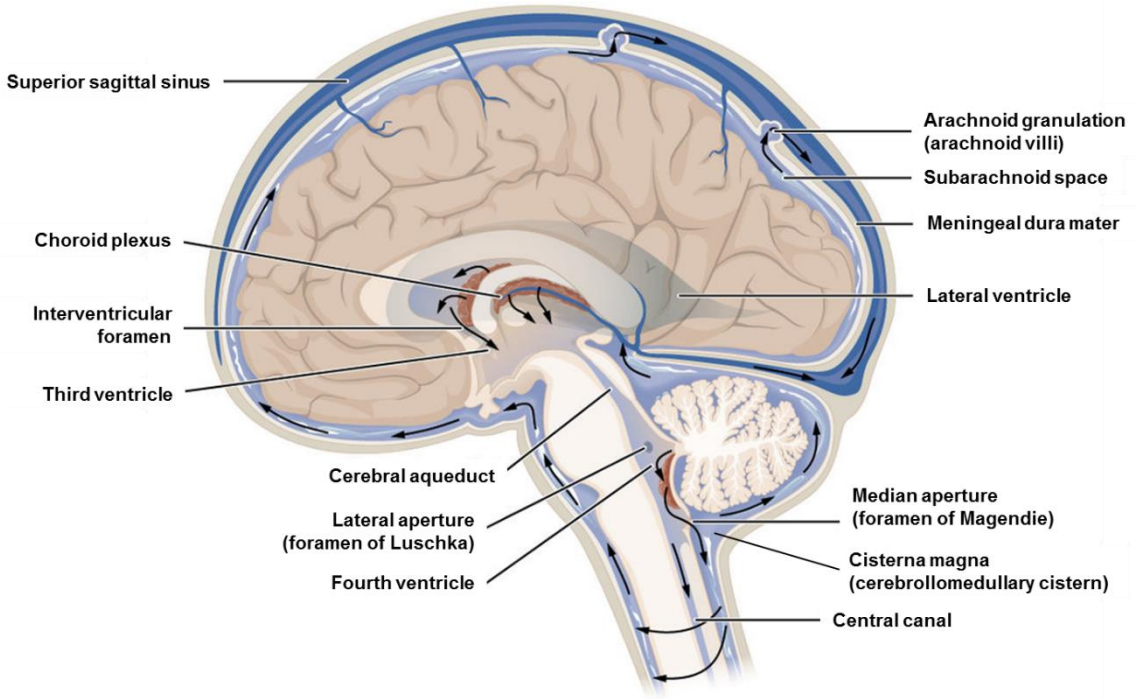


**Figure 7. Schematic representation of the secretion and flow of the CSF.** CSF is mainly produced by the choroid plexus (brown), which are located in each ventricle of the brain. CSF moves from lateral ventricles to the third ventricle via the interventricular foramen, and then from the third to the fourth ventricle via the cerebral aqueduct. Next, CSF can either continue within the ventricular system and moves through the spinal canal, or can flow to the subarachnoid space via the median aperture (foramen of Magendie) or via the lateral aperture (foramen of Luschka). Finally, the CSF that flows in the subarachnoid space, both cranial and spinal, is reabsorbed into the peripheral circulation by arachnoid granulation (arachnoid villi) in venous sinuses of the brain. Adapted from Wright et al., 2012. Illustration from Anatomy & Physiology, Connexions Web site (http://cnx.org/content/col11496/1.6/).

### 4.2. Choice of the AAV serotype

Apart from the common properties of AAV, such as the absence of human pathology and the ability to lead to stable transgene expression for years with both low toxicity and low immunogenicity, adeno-associated virus serotype 9 vector presents unique properties, which turn it into an ideal vector for the treatment of neurological diseases, such as MPSII. In addition to the ability to penetrate to the CNS, AAV9 vector stands out for its broad genome biodistribution as well as a rapid-onset, leading to high protein expression levels compared to other AAV serotypes (Zincarelli et al., 2008; Haurigot et al., 2013; Sorrentino et al., 2015).

Previously in our laboratory it has been demonstrated that the intra-CSF administration of AAV9 vectors encoding for the enzyme deficient in the disease of interest resulted in complete correction of both CNS and somatic pathology in mouse

models of two different MPSs, MPSIIIA and MPSIIIB (Haurigot et al., 2013; Ribera et al., 2015). When AAV9 vectors are administered intra-CSF, they are able to reach the bloodstream and transduce the liver, providing a peripheral source of the therapeutic protein (Gray et al., 2013; Haurigot et al., 2013; Ribera et al., 2015). Moreover, it has recently been demonstrated that intra-CSF delivery of AAV9 vectors is feasible and safe in large animal models, such as dogs and non-human primates (Samaranch et al., 2012; Gray et al., 2013; Haurigot et al., 2013; Hinderer et al., 2014a; Hinderer et al., 2015; Ribera et al., 2015; Gurda et al., 2016).

### 4.3. Mechanism of action

The design of the AAV9-based gene therapy approach for MPSII relies on the principle of cross-correction. After gene transfer to the CSF, transduced cells produce IDS enzyme and digest their own accumulated heparan sulfate and dermatan sulfate. In addition, genetically corrected cells continuously produce and secrete enzyme to the extracellular medium and to the CSF, from which it can be taken up by brain cells in other brain areas via mannose-6-phosphate receptor-mediated endocytosis (Enns and Huhn, 2008). Therefore, following this approach, a single administration of the vectors would result in correction of the disease in large areas of the brain in addition to long-term secretion of IDS to the CSF without the need of the surgical implantation of a pump to achieve a chronic delivery of the recombinant enzyme. Actually, during the last years the directly administration of AAV9 vectors to the CSF has become a rising route of delivery used for the treatment of several MPSs (Haurigot et al., 2013; Hinderer et al., 2014b, Hinderer et al., 2015; Ribera et al., 2015; Gurda et al., 2016

# III. OBJECTIVES

Mucopolysaccharidosis type II, or Hunter syndrome, is an X-linked recessive lysosomal storage disease caused by the deficiency in Iduronate-2-sulfatase, an enzyme essential for the catabolism of the glycosaminoglycans heparan sulfate and dermatan sulfate. Undegraded glycosaminoglycans accumulate within the lysosomes of virtually all cells of the body, leading to cell dysfunction. The most severe, and more prevalent, form of Hunter syndrome is characterized by chronic and progressive neuropathy of the central nervous system and multisystem dysfunction; patients usually die during the second decade of life. To date, weekly intravenous enzyme replacement therapy constitutes the only approved therapeutic option for MPSII. However, ERT infusions are not sufficient to correct neurological impairment, among other drawbacks. Thus, an efficacious therapy for the treatment of the neurodegeneration of MPSII disease represents a highly unmet medical need. *In vivo* gene therapy with adeno-associated virus vectors offers the possibility of lifelong therapeutic benefit following a single administration of the treatment, together with an excellent safety profile associated to the delivery of this type of vectors.

The *general aim* of this work was **to develop a new gene therapy approach based on the delivery of adeno-associated virus vectors to the CSF to simultaneously treat the neurologic and somatic pathology of MPSII**. This general aim was divided into three specific goals:

1. **To characterize the effects of *Ids* deletion on the brain and somatic organs of adult MPSII male mice.**

2. **To evaluate the therapeutic efficacy of the intra-CSF administration of adeno-associated virus serotype 9 vectors encoding for the murine *Iduronate-2-sulfatase* gene in the MPSII mouse model.**

3. **To design an optimize adeno-associated virus serotype 9 vectors encoding for human Iduronate-2-sulfatase as a frist step towards the clinical translation of this approach, and to test the therapeutic efficacy of the vectors carrying the human transgene in the MPSII mouse model.**

# IV. RESULTS

# PART I. Characterization of the effects of *Ids* deletion in male mice

The MPSII mouse model used in this work was obtained by targeted disruption of exons 2 to 5 of the murine *Iduronate-2-sulfatase* gene, located on chromosome X. There was no phenotypic description available for this animal model. Therefore, the first part of this work was focused on the phenotypic characterization of these mice. To this end, experiments were carried out to characterize the alterations resulting from thedeletion of *Ids* gene. Specifically, the phenotypic evaluation was performed on the CNS and somatic organs of 2-month-old MPSII male mice (Figure 8).

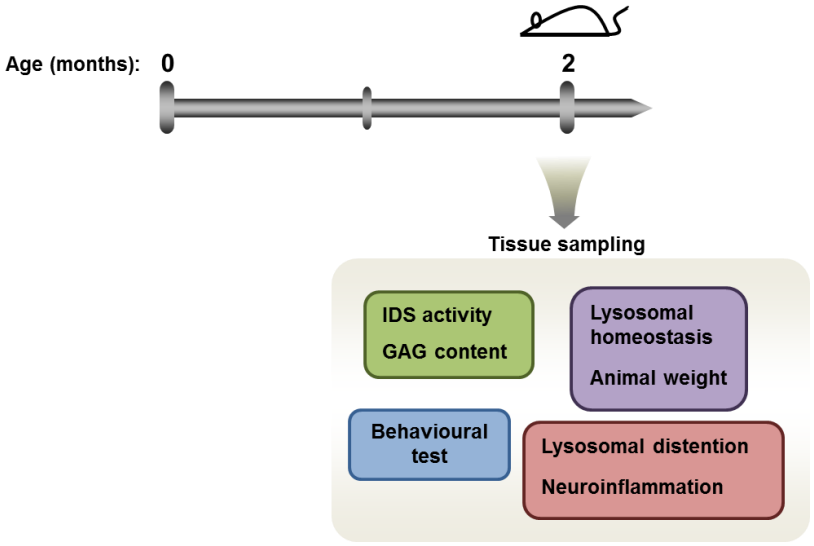


**Figure 8. Experimental design for the phenotypic characterization of the MPSII mouse model.** The study was performed in 2-month-old MPSII male mice and included several biochemical determinations, measurement of lysosomal-related parameters, assessment of neuroinflammation, performance of behavioural test amongst others.

## 1. PHENOTYPIC DESCRIPTION OF THE CNS PATHOLOGY OF ADULT MPSII MALE MICE

### 1.1. IDS activity and GAG content in the encephalon

The encephalon of 2-month-old WT and MSPII mice was dissected and sliced in 5 coronal sections, namely I to V, being section I the most frontal part of the encephalon, and section V the most caudal part. In each coronal section, IDS activity and GAG content were assessed (Figure 9). IDS activity was almost undetectable throughout the encephalon of IDS-deficient mice (Figure 9A); the low levels of IDS activity (<0.8%) measured corresponded to the background signal of the assay (Higuchi et al., 2012). As a consequence, all areas of the encephalon analysed presented an increase in GAG content, which ranged from 121% to 150% of WT values (Figure 9B).

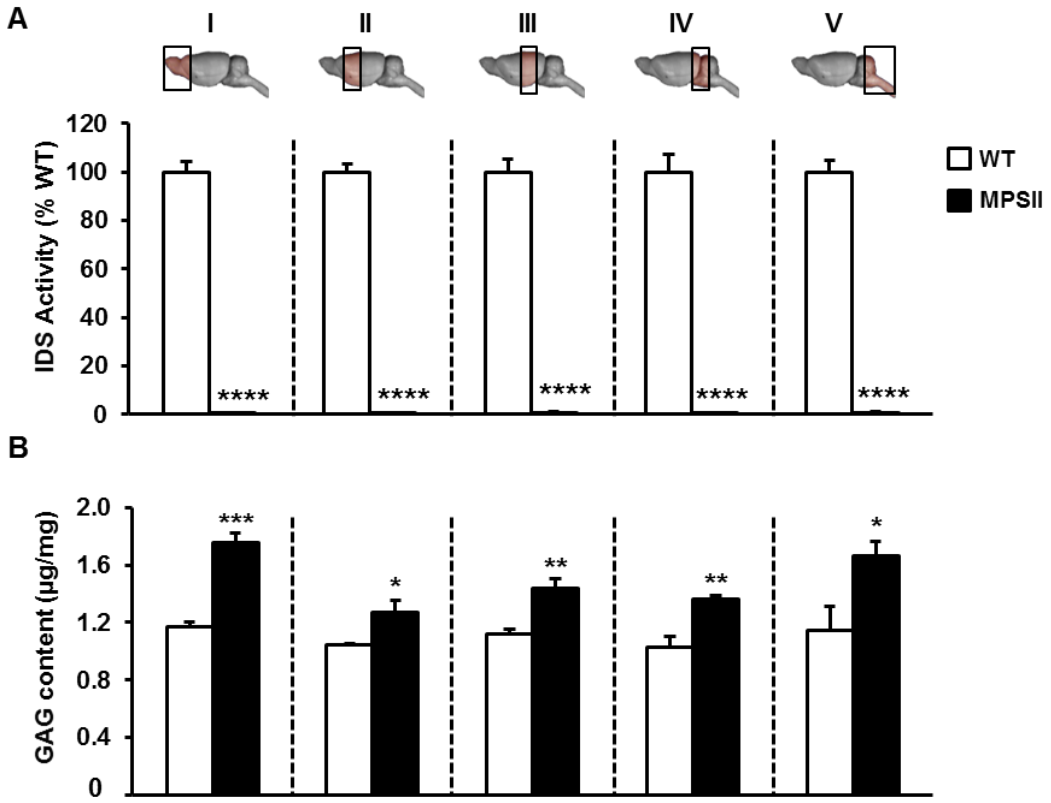


**Figure 9. IDS activity and GAG content in the CNS of IDS-deficient mice**. (**A**) Measurement of IDS activity in brain extracts obtained from wild-type (WT) and IDS-deficient (MPSII) mice. The encephalon of each animal was dissected and sectioned in 5 coronal sections (I to V), as indicated in the diagram above the plot. IDS activity of WT mice was set to 100%. IDS activity was practically undetectable in all brain areas analysed of IDS-deficient mice. (**B**) Quantification of GAG content in the same cohort of animals. At 2 months of age, IDS-deficient mice showed pathological accumulation of GAGs in all regions analysed. Data are shown as mean ± SEM of 4-5 animals/group. **P*<0.05, ***P*<0.01, ****P*<0.001 and *****P*<0.0001 *vs.* WT.

### 1.2. Assessment of lysosomal pathology in the CNS

The size of the lysosomal compartment of several brain regions was evaluated at histological level through immunostaining for the lysosomal marker lysosome-associated membrane protein 2 (LAMP2), a protein located on the lysosome, endosome and cell membrane. As indicated by the analysis of LAMP2 signal, the pathological accumulation of GAGs translated into an increase in the number and/or size of lysosomes in different areas of the encephalon of IDS-deficient mice in comparison with healthy WT littermates (Figure 10).

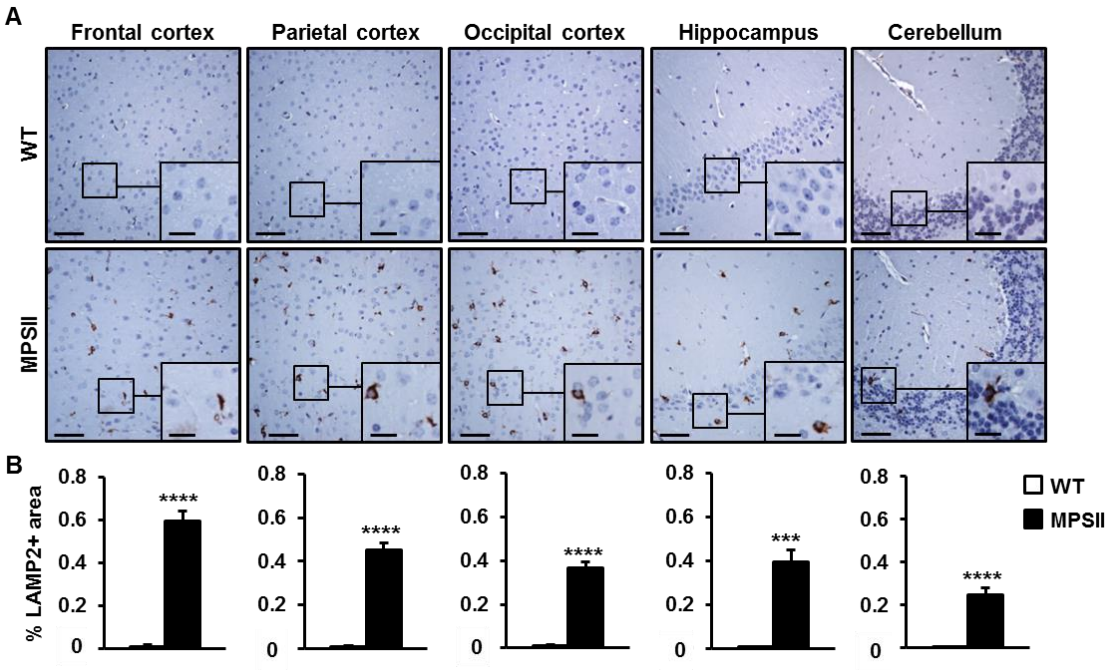


**Figure 10. Enlargement of the lysosomal compartment in the brain of IDS-deficient mice.** The size of the lysosomal compartment was analysed in different brain areas by immunostaining for the lysosomal marker LAMP2 at 2 months of age. (**A**) Representative photomicrographs obtained from different brain regions of wild-type (WT) and IDS-deficient (MPSII) mice. The encephalon of IDS-deficient male mice showed cells with intense LAMP2 staining, indicative of enlargement of the lysosomal compartment. Scale bars are 50 µm, and 20 µm for insets. (**B**) Histograms represent the quantification of the percentage of $LAMP2^+$ area in each brain region analysed. Data are shown as mean ± SEM of 4-5 animals/group. ***$P$<0.001 and ****$P$<0.0001 *vs.* WT.

In LSDs, the activity of several lysosomal enzymes aside from that directly affected by the inherited mutation can be altered secondary to the perturbation of normal lysosomal homeostasis (Tomatsu et al., 2005; Sardiello et al., 2009; Rowan et al., 2013). Therefore, the activities of several enzymes, such as Sulfoglucosamine N-sulfohydrolase (SGSH), Heparan α-glucosaminide N-acetyltransferase (HGSNAT), N-Acetylgalactosamine-6-sulfate-sulfatase (GALNS) and β-hexosaminidase (β-HEXO) were measured in brain extracts to determine whether *Ids* deletion affected lysosomal homeostasis in the CNS. In most cases, statistically significant differences were observed in the activities of these enzymes between IDS-deficient mice and healthy WT littermates (Figure 11). While HGSNAT and β-HEXO showed increased activity, the activities of SGSH and GALNS were reduced (Figure 11).

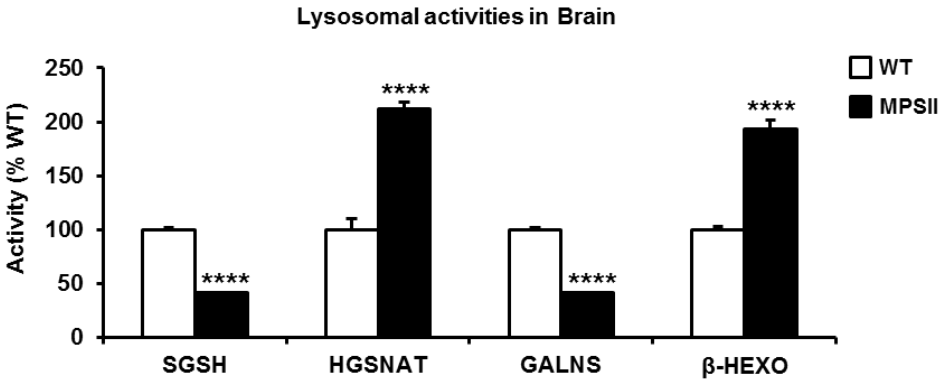


**Figure 11. Disruption of lysosomal homeostasis in the brain of IDS-deficient mice.** Measurement of the activity of other lysosomal enzymes different from IDS in brain extracts obtained from 2-month-old wild-type (WT) and IDS-deficient (MPSII) mice. Each enzymatic activity of WT mice was set to 100%. The activity of the enzyme Sulfoglucosamine N-sulfohydrolase (SGSH), Heparan α-glucosaminide N-acetyltransferase (HGSNAT), N-Acetylgalactosamine-6-sulfate-sulfatase (GALNS), and β-hexosaminidase (β-HEXO) were significantly altered in the brain of IDS-deficient males. Data are shown as mean ± SEM of 5 animals/group. ****$P$<0.0001 *vs.* WT.

### 1.3. Study of neuroinflammation

MPSII, as many other LSD with CNS involvement, is characterized by the presence of neuroinflammation, defined by chronic activation of glial cells (Constantopoulos et al., 1980; Hamano et al., 2008). Neuroinflammation was evaluated by specific immunostaining of paraffin-embeded brain sections for glial fibrillary acidic protein (GFAP) and by staining with lectin Isolectin B4 (BSI-B4) obtained from *Bandeiraea simplicifolia* (*Griffonia simplicifolia*). GFAP is a cytoplasmic intermediate filament protein upregulated upon activation of astrocytes (Eng and Ghirnikar, 1994). BSI-B4 recognizes α-D-galactose residues present on resting and activated microglia (Streit and Kreutzberg, 1987), but under the specific protocol used in this study, preferentially labels amoeboid activated microglia (Ruzo et al., 2012a, Ruzo et al., 2012b; Haurigot et al., 2013; Ribera et al., 2015). For both GFAP and BSI-B4, a strong positive signal was observed in all the different areas of the encephalon of IDS-deficient mice analysed; healthy WT littermates showed, however, weak labelling (Figure 12). This observation indicated the presence of astrocytosis (Figure 12A) and microgliosis (Figure 12B) in the brain of MPSII mice at the age of 2 months. The quantification of the percentage of positive signal for each staining confirmed this observation.

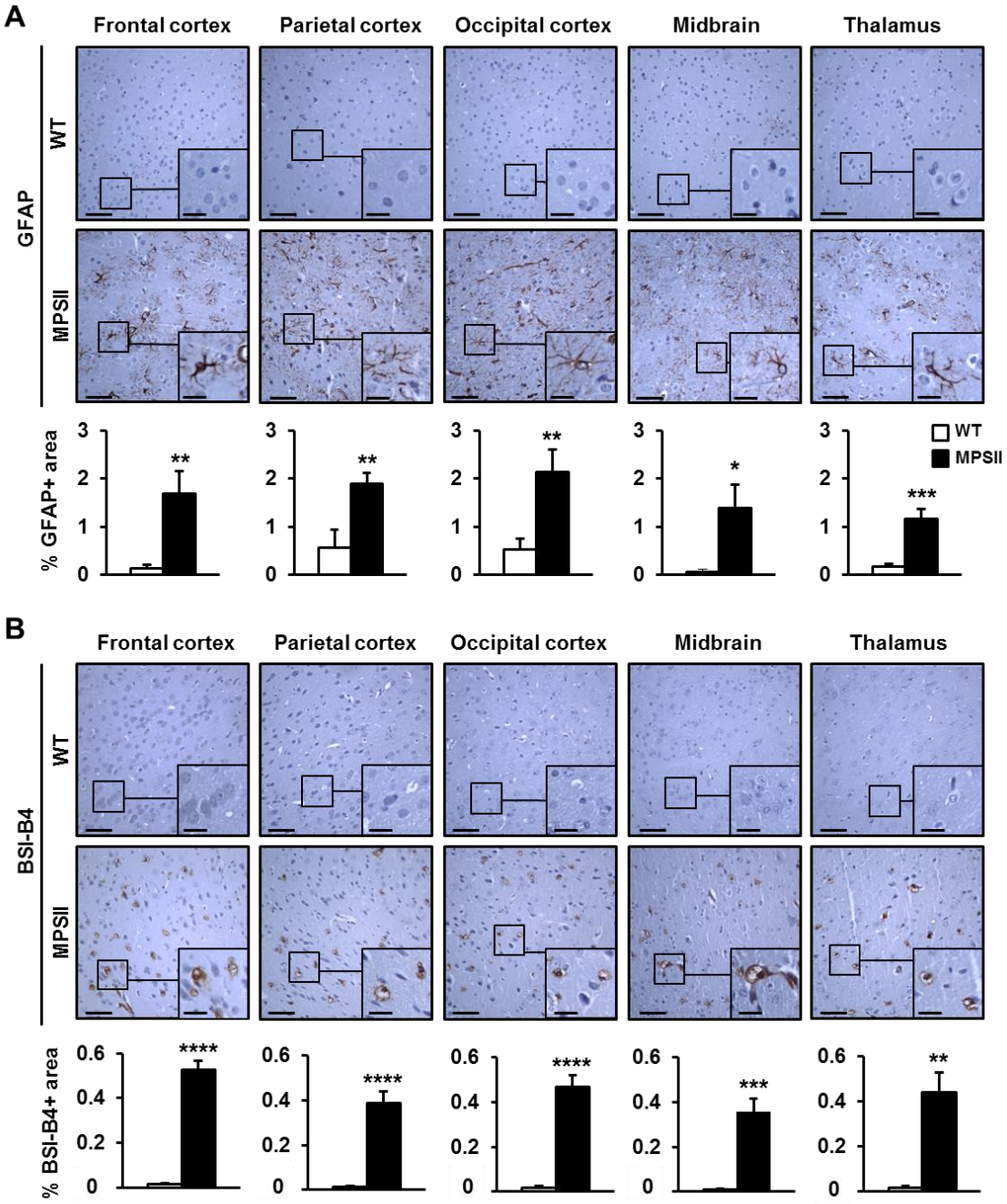


**Figure 12. Characterization of neuroinflammation in the brain of IDS-deficient mice**. (**A**) Immunostaining of paraffin-embeded sections of the encephalon from wild-type (WT) and IDS-deficient (MPSII) mice with anti-GFAP antibody, which labels activated astrocytes. (**B**) Staining of sections of the encephalon of wild-type (WT) and IDS-deficient mice with BSI-B4 lectin, a marker of microglia. Representative photomicrographs obtained from several brain regions are shown. Histograms depict the quantification of the percentage of positive signal area in each region of the brain in each cohort. At the age of 2 months, IDS-deficient mice showed signs of astrogliosis (A) and microgliosis (B) in all the encephalon areas analysed. Scale bars are 50 µm, and 20 µm for insets. Values are mean ± SEM of 5 animals/group. **P*<0.05, ***P*<0.01, ****P*<0.001 and *****P*<0.0001 *vs.* WT.

## 2. PHENOTYPIC DESCRIPTION OF THE SOMATIC PATHOLOGY OF ADULT MPSII MICE

### 2.1. IDS activity and GAG content in somatic tissues

Despite the fact that CNS involvement is a hallmark of the severe forms of Hunter syndrome, somatic pathology is also a major trait of the disease. Therefore, the effect of the deletion of the *Ids* gene was also evaluated at somatic level. To this aim, WT and IDS-deficient male mice were euthanized at the age of 2 months and samples of somatic organs were harvested and subsequently analysed.

The enzymatic activity of IDS was determined in liver extracts and serum samples (Figure 13). IDS-deficient mice showed practically undetectable IDS-activity in liver and serum, in comparison with values of heathy WT counterparts.

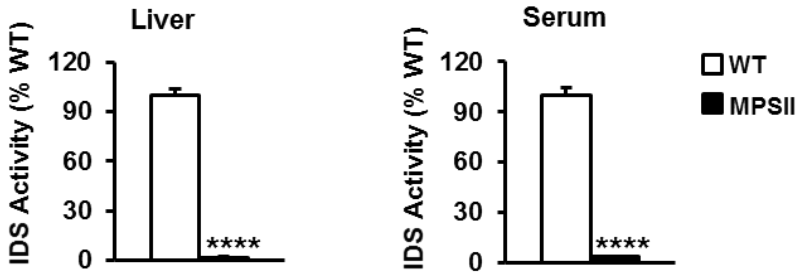


**Figure 13. Quantification of IDS activity in liver and serum of IDS-deficient mice**. Measurement of IDS activity in liver extracts and serum samples of wild-type (WT) and IDS-deficient (MPSII) mice at 2 months of age. IDS activity of WT mice was set to 100%. IDS activity was practically undetectable in liver and serum of IDS-deficient mice. Data are shown as mean ± SEM of 5 animals/group. ****$P$<0.0001 *vs.* WT.

The deficiency of IDS activity resulted in pathological accumulation of GAGs in several somatic organs, including liver, spleen, heart, lung, kidney, urinary bladder, testis, adipose tissue and skeletal muscle of MPSII mice (Figure 14). By far, the most noticeable increase was observed in the liver, in which GAG content reached almost 10-fold higher levels than those observed in WT littermates.

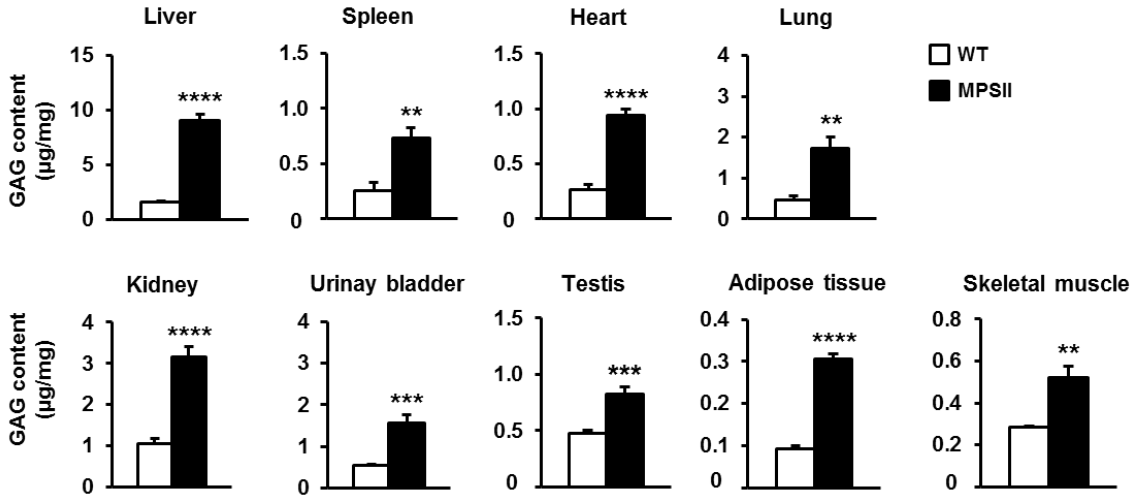


**Figure 14. Quantification of GAG storage in somatic organs of IDS-deficient mice**. Measurement of the amount of GAGs in several somatic organs of wild-type (WT) and IDS-deficient (MPSII) mice. IDS-deficient mice aged 2 months showed increased GAG content in all somatic tissues analysed, particularly in the liver. Values are shown as mean ± SEM of 5 animals/group. ***P*<0.01, ****P*<0.001 and *****P*<0.0001 *vs.* WT.

### 2.2. Study of the size of the lysosomal compartment in somatic organs

To evaluate the size of the lysosomal compartment in somatic tissues, liver, heart and lung paraffin-embeded sections were analysed by immunohistochemistry for the lysosomal marker lysosomal-associated membrane protein 1 (LAMP1), a transmembrane protein integral to the lysosomal membrane. Through LAMP1 immunostaining, the expansion of the lysosomal compartment was easily detectable in different somatic organs of IDS-deficient mice (Figure 15).

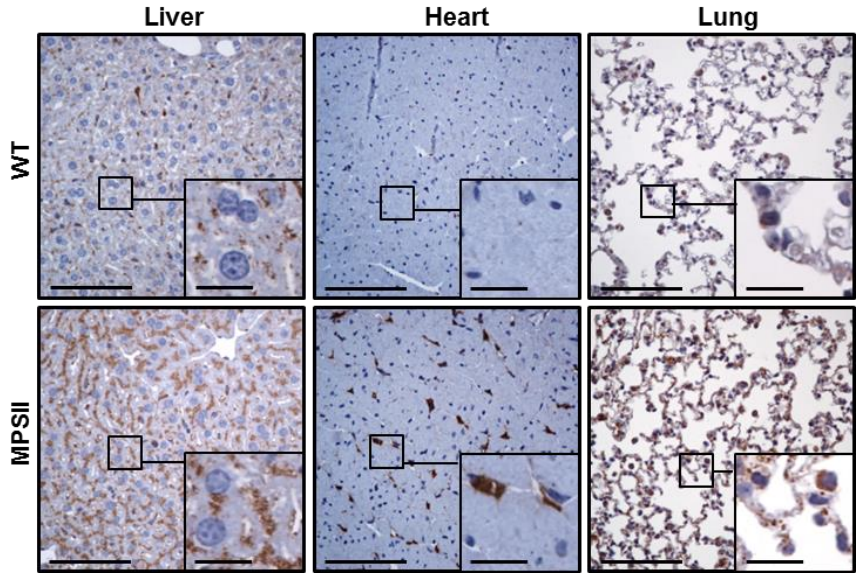


**Figure 15. Enlargement of lysosomal compartment in somatic organs of IDS-deficient mice**. The size of the lysosomal compartment was analysed in sections from somatic organs by immunostaining with the lysosomal marker LAMP1. Representative photomicrographs obtained from wild-type (WT) and IDS-deficient (MPSII) mice at 2 months of age are shown. At this age, IDS-deficient mice showed an enlargement of the lysosomal compartment in liver, heart and lung. Scale bars are 100 µm, and 20 µm for insets.

### 2.3. Evaluation of liver pathology

Because hepatomegaly is a common finding in Hunter patients (Hunter, 1917; Neufeld and Muenzer, 2001; Wraith et al., 2008a), the weight of the liver of IDS-deficient mice was also measured. The excessive storage of undegraded GAGs in liver resulted in a slight increase in the weight of this organ in IDS-deficient mice (Figure 16).

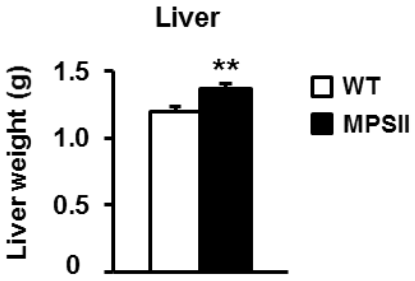


**Figure 16. Hepatomegaly in IDS-deficient mice**. The wet weight of the liver was measured in wild-type (WT) and IDS-deficient (MPSII) mice. At the age of 2 months, IDS-deficient mice presented a slight increase in liver weight. Data are shown as mean ± SEM of 17-18 animals/group. ***P*<0.01 *vs.* WT.

To evaluate lysosomal homeostasis in somatic organs, the activity of several lysosomal enzymes, different from IDS, was also assessed in liver extracts. Similar to the observations made the in brain, the activity of several lysosomal enzymes was altered in liver extracts; in the case of liver, however, the activites of α-L-Iduronidase (IDUA), α-N-Acetylglucosaminidase (NAGLU) and β-Glucoronidase (GUSB) were also considerably affected (Figure 17).

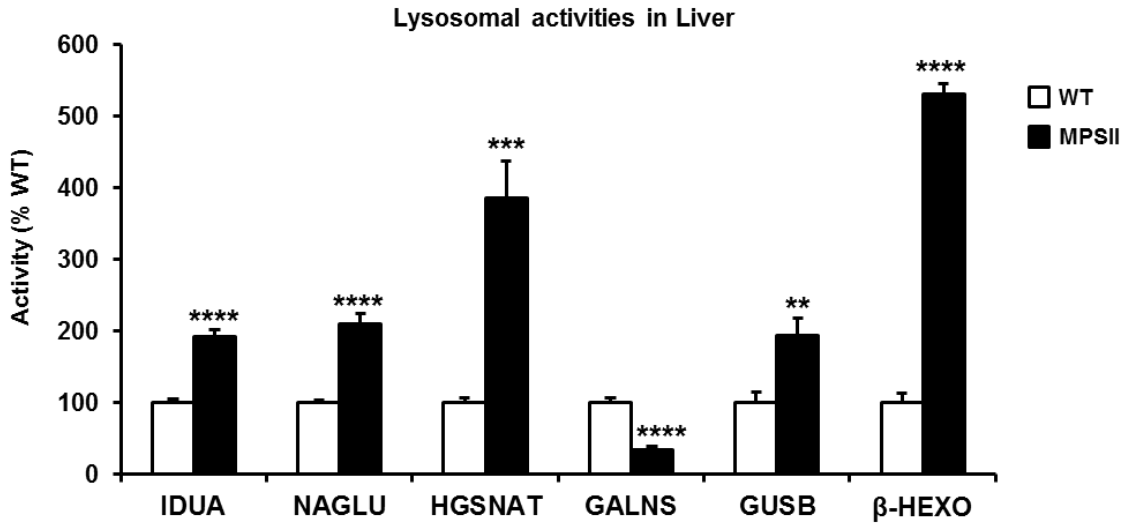


**Figure 17. Disruption of lysosomal homeostasis in the liver of IDS-deficient mice.** Measurement of enzymatic activities of other lysosomal enzymes different from IDS in liver extracts obtained from 2-month-old wild-type (WT) and IDS-deficient (MPSII) mice. Each enzymatic activity of WT mice was set to 100%. The activity of the enzymes α-L-Iduronidase (IDUA), α-N-Acetylglucosaminidase (NAGLU), Heparan α-glucosaminide N-acetyltransferase (HGSNAT), N-Acetylgalactosamine-6-sulfate-sulfatase (GALNS), β-Glucoronidase (GUSB), and β-hexosaminidase (β-HEXO) were significantly altered in the liver of IDS-deficient males. Data are shown as mean ± SEM of 5 animals/group. ***P*<0.01, ****P*<0.001 and *****P*<0.0001 *vs.* WT.

## 3. BEHAVIOURAL ALTERATIONS IN ADULT MPSII MALE MICE

As a consequence of disease progression, MPSII patients suffer also from behavioural alterations. In an attempt to determine whether the MPSII mouse model used in this work presented behavioural deficits, IDS-deficient mice, together with healthy WT littermates, were evaluated with the Open Field test. The Open Field test is a well-established test designed to measure locomotor activity and anxiety-related behaviour in mice (Bailey and Crawley, 2009). The area of the Open Field, where naïve mice are placed individually, is virtually divided into three concentric square regions: centre, periphery and border. Under healthy conditions, mice tend to avoid brightly illuminated, novel, open spaces. Thus, the

Open Field environment acts as an anxiogenic stimulus and allows the measurement of anxiety-induced locomotor activity and exploratory behaviours.

At 2 months of age, IDS-deficient mice did not show any statistically significant differences with healthy WT littermates in any of the parameters evaluated in the Open Field test (Figure 18), neither in exploratory activity (number of entries in centre, lines crossed and total movements) nor in anxiety-related behaviour (latency to the centre, time in centre and time in periphery). However, and despite the variability of the test at this age, IDS-deficient mice showed a tendency towards anxiety and reduced exploratory behaviour (Figure 18).

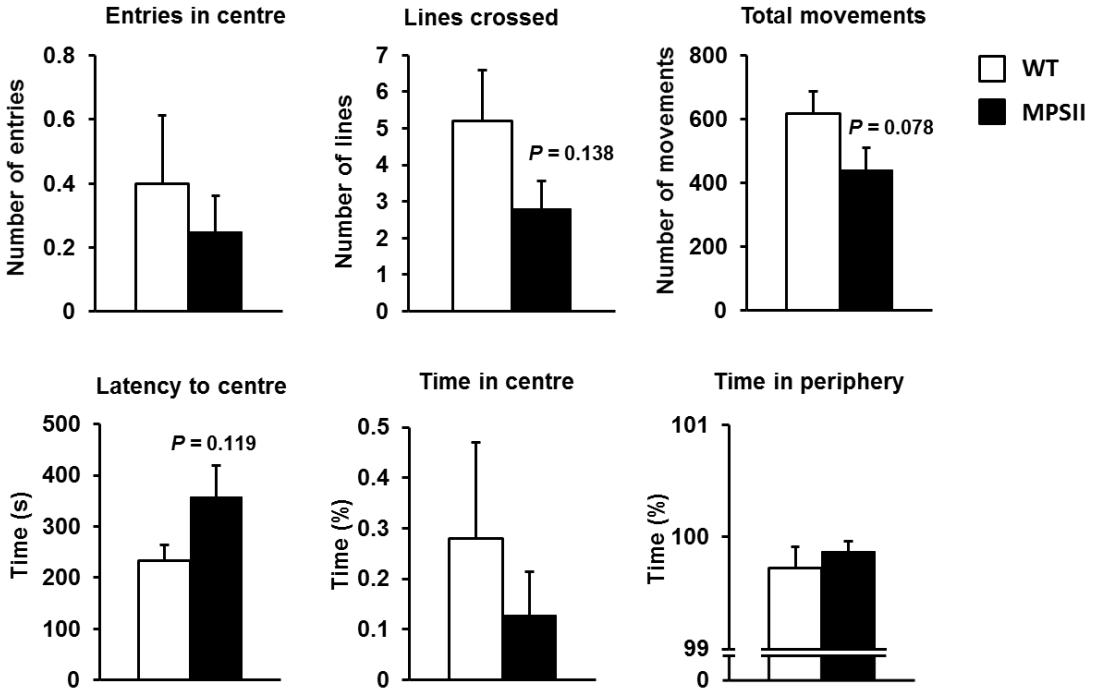


**Figure 18. Behavioural deficits in MPSII male mice.** Results of the Open Field test performed in naïve-tested healthy wild-type (WT) and IDS-deficient (MPSII) male mice at 2 months of age. Histograms represent the mean ± SEM obtained during the first 3 min of recording of each parameter in groups of 17–18 animals/cohort. *P* value *vs.* WT.

Overall, these results demonstrated that the MPSII mouse model used in the present work reproduced the main features of human Hunter syndrome. At the age of 2 months, the pathology was well established in both CNS and somatic organs. Thus, the MPSII mouse represents a suitable mouse model for the study of the efficacy of new therapeutic approaches.

## PART II. Evaluation of the therapeutic efficacy of the intra-CSF AAV9-*Ids* administration to adult MPSII mice

The second part of this work was centred on the development of a gene therapy approach for MPSII based on the delivery of adeno-associated virus serotype 9 (AAV9) vectors encoding for IDS enzyme. The efficacy of a single intra-CSF administration of these vectors in counteracting MPSII CNS and somatic pathology was tested in the MPSII mouse model.

## 1. SET-UP OF THE AAV9-BASED GENE THERAPY APPROACH FOR MPSII

### 1.1. AAV9 cell tropism in the CNS of MPSII mice after intra-CSF administration

To characterize the nature of the cells transduced in the CNS of MPSII mice after the delivery of AAV9 vectors to the CSF through the cisterna magna, co-localization studies with the reporter green fluorescent protein (GFP) were performed. At the age of 2 months, MPSII mice were administered intra-CSF with $5x10^{10}$ vector genomes (vg) of AAV9-CAG-GFP-WPRE, which mediates the expression of the GFP gene under the control of the ubiquitous hybrid promoter CAG. Ten days after the administration, animals were sacrificed and double-immunostaining against GFP and specific cell markers for neurons, astrocytes and microglia were performed. Neuronal cells were immunostained with NeuN (Neuronal nuclei), which is a DNA-binding, neuron-specific protein located mainly in neuronal nuclei, somas and some proximal neuronal processes (Mullen et al., 1992). Astrocytes were labelled with GFAP, and microglia with Iba1 (Ionized calcium-binding adapter molecule 1), a cytoplasmic protein highly and specifically expressed in microglia (Ito et al., 1998).

Co-localization studies performed in frontal cortex revealed that the majority of transduced cells were neurons, with transduction of few astrocytes and no transgene expression observed in microglia cells (Figure 19).

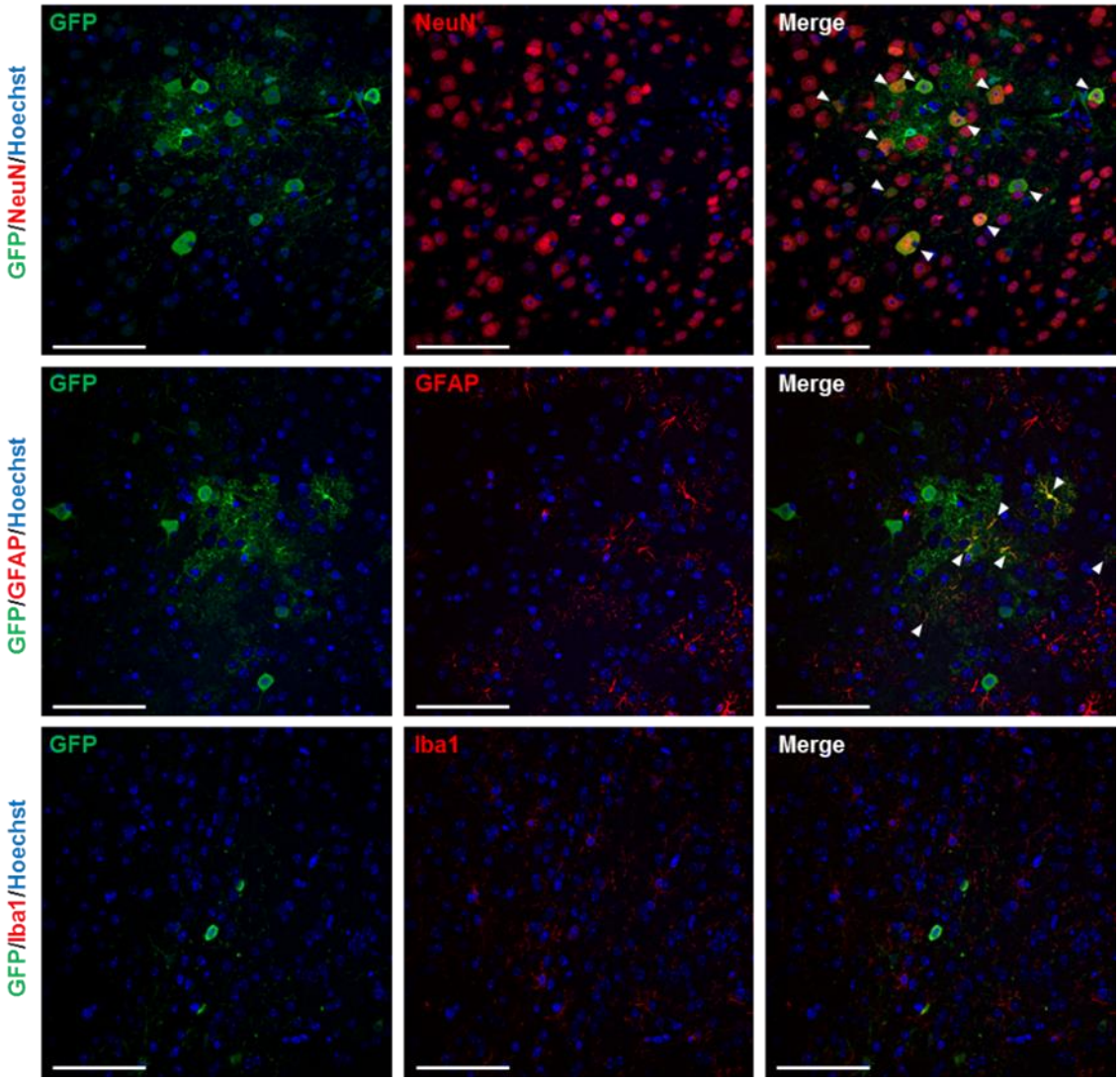


**Figure 19. AAV9 transduces predominantly neurons following intra-CSF delivery to MPSII mice.** Co-localization study on sections of the frontal cortex from 2-month-old MPSII mice administered intra-CSF with $5x10^{10}$ vg of AAV9-CAG-GFP-WPRE vector and analysed 10 days post-injection. Tissue sections were double-immunostained for GFP (*green*) and specific markers (*red*) for neurons (NeuN, *top panels*), astrocytes (GFAP, *central panels*) or microglia (Iba1, *bottom panels*). Nuclei were counterstained with Hoechst. Confocal microscopy images showed efficient transduction of neurons, occasional transduction of astrocytes and no transduction of microglia after intra-CSF AAV9-CAG-GFP-WPRE delivery to mice. Arrowheads indicate double-positive cells. Scale bars are 100 µm.

### 1.2. Choice of transgene construct

To develop a gene therapy protocol based on efficient AAV9-mediated IDS production, four different constructs encoding for murine IDS were generated to determine which one mediated the highest IDS production (Figure 20A). The first engineered construct contained the wild-type murine *Ids* coding sequence (CDS), while the rest of the constructs contained different optimized versions it. The optimization of the *Ids* CDS was based on algorithms that maximize the efficiency of IDS protein production in

mice through increasing RNA stability and optimizing codon usage and G/C content, among other modifications. The expression of all transgenes was under the control of the ubiquitous promoter CAG. The CAG promoter is a hybrid promoter composed of the early enhancer of cytomegalovirus (CMV), the chicken β-actin promoter and the chiken β-actin intron.

To determine which construct resulted in highest IDS enzyme activity, 30 µg of the plasmids pAAV-CAG-m*Ids*, pAAV-CAG-om*Ids*-v1, pAAV-CAG-om*Ids*-v2 and pAAV-CAG-om*Ids*-v3 were administered to 4.5-month-old MPSII mice via hydrodynamic tail vein injection. As a control of the technique, non-injected wild-type mice and MPSII mice injected with saline solution were used (Figure 20B). Animals were sacrificed 1 week after plasmid delivery and the activity of IDS was measured in liver protein extracts and serum samples.

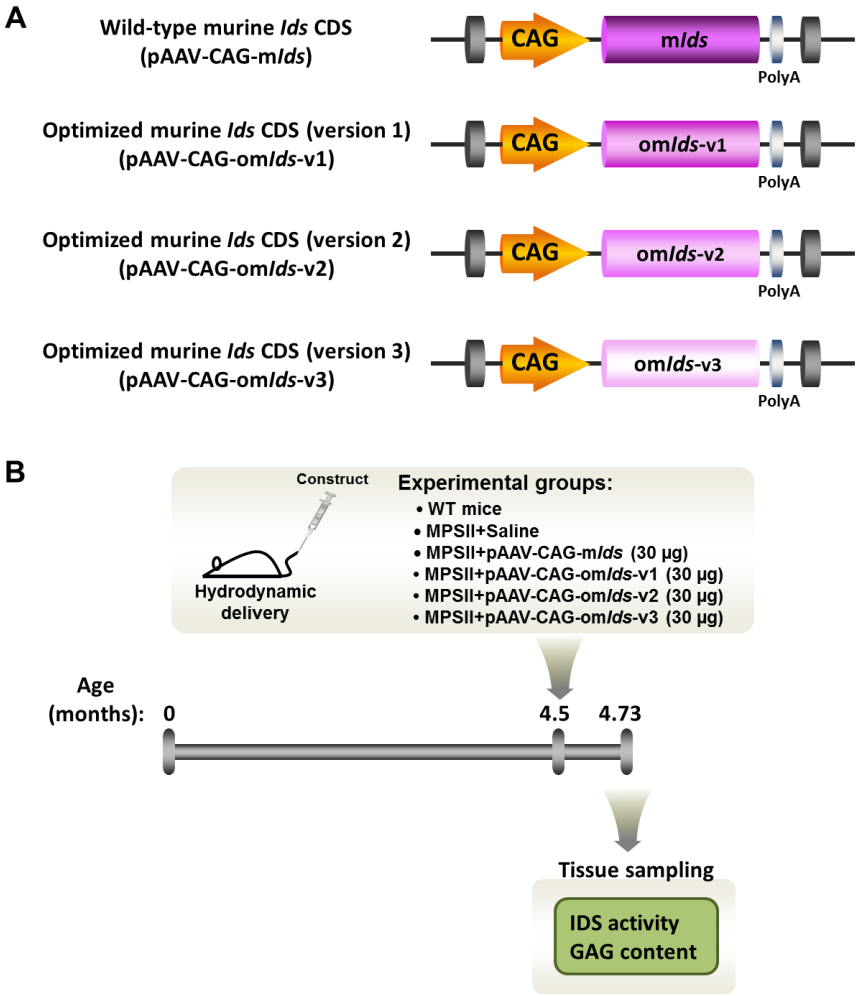


**Figure 20. Experimental design for the *in vivo* evaluation of the plasmids containing murine IDS-coding sequences.** (**A**) Schematic representation of the four generated constructs that contained the murine *Ids* coding sequence (CDS)**.** One plasmid containing the murine wild-type *Ids* CDS and three expression cassettes containing optimized versions of the murine *Ids* CDS were generated. CAG, hybrid CAG promoter. The schematic representation is not to scale. (**B**) Experimental design for the hydrodynamic administration of plasmids containing murine IDS-coding sequences to 4.5-month-old MPSII male mice. IDS activity and GAG content were evaluated 1 week after plasmid administration.

All four tested constructs led to a great increase over basal levels in IDS activity in both liver and serum samples (Figure 21), ranging from 500% to 800% of WT levels in liver, and from 800% to 1500% of WT values in serum. In both cases, the plasmid which resulted in the highest statistically significant increase of IDS activity was pAAV-CAG-om*Ids*-v1. Noteworthy, only the optimized version pAAV-CAG-om*Ids*-v1 of the murine *Ids* coding sequence seemed to work better than the wild-type murine *Ids* sequence (pAAV-CAG-m*Ids*). The other two sequence-optimized plasmids (pAAV-CAG-om*Ids*-v2 and pAAV-CAG-om*Ids*-v3) behaved similarly to the plasmid containing the wild-type sequence (Figure 21).

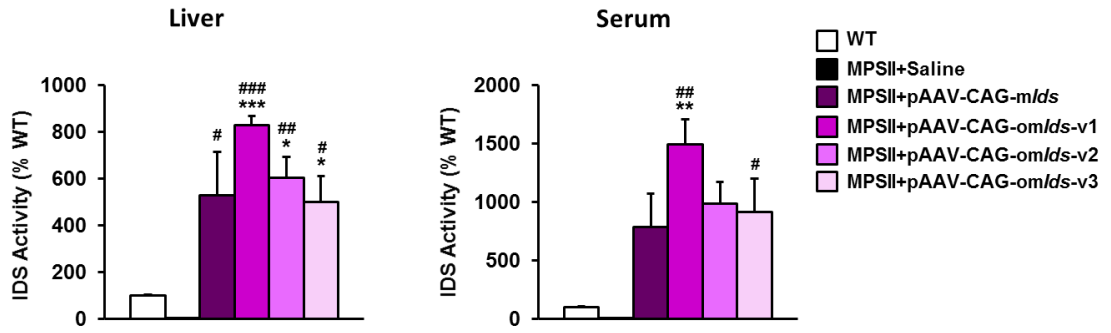


**Figure 21. IDS activity in liver and serum after hydrodynamic delivery of plasmids containing murine IDS-coding sequences to adult MPSII mice.** Measurement of IDS activity in liver extracts and serum samples 1 week after the administration of the plasmids. Wild-type (WT) and saline-injected MPSII mice were used as controls. IDS activity of WT mice was set to 100%. IDS activity considerably increased over basal levels in both liver and serum, being pAAV-CAG-om*Ids*-v1 the plasmid that led to the greatest rise in activity in both cases. Data are shown as mean ± SEM of 3-4 animals/group. **P*<0.05, ***P*<0.01 and ****P*<0.001 vs. WT. $^{\#}P$<0.05, $^{\#\#}P$<0.01 and $^{\#\#\#}P$<0.001 *vs.* MPSII+Saline.

Consistent with the high levels of IDS activity detected in liver and serum, GAG content was reduced in several somatic tissues after the administration of the constructs (Figure 22). In particular, all 4 IDS-containing plasmids led to complete normalization of pathological GAG accumulation in liver, spleen, heart and urinary bladder, with the exception of pAAV-CAG-om*Ids*-v3, which did not manage to fully normalize GAG content in the urinary bladder. In lung and kidney, the three expression cassettes containing optimized versions of the *Ids* CDS statistically reduced the levels of GAGs more efficiently than the plasmid containing the wild-type sequence, however, normal values of GAGs were not reached.

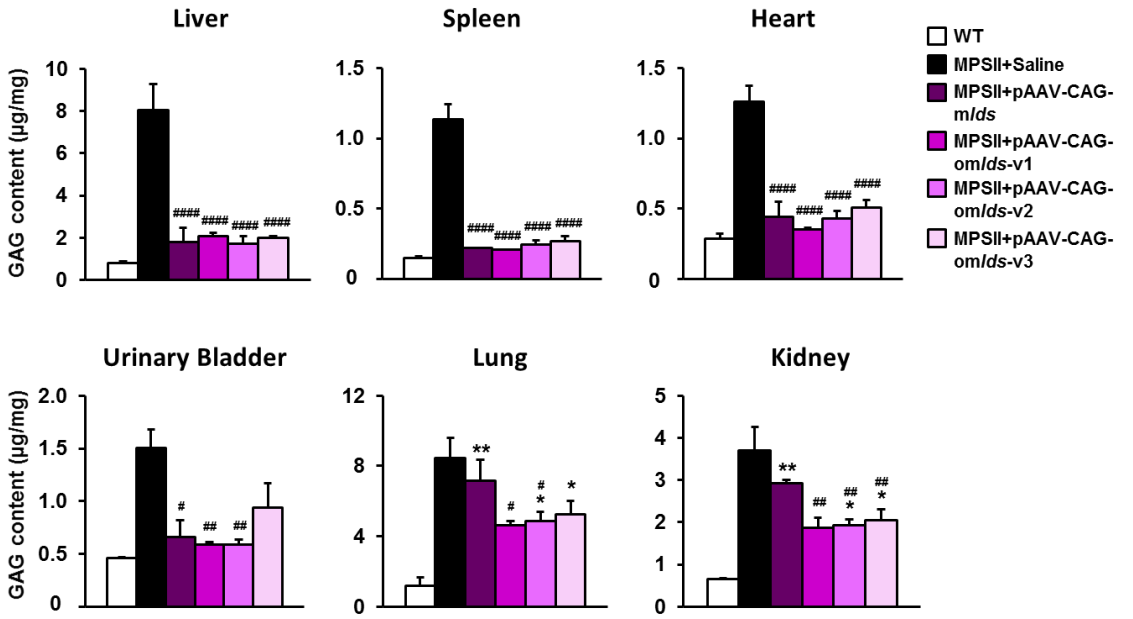


**Figure 22. GAG content after hydrodynamic delivery of plasmids containing murine IDS-coding sequences to adult MPSII mice.** Quantification of the amount of GAGs in liver, spleen, heart, urinary bladder, lung, and kidney 1 week after the administration of the plasmids. Wild-type (WT) and saline-injected MPSII mice were used as controls. All four IDS-containing plasmids resulted in almost complete normalization of the pathological GAG accumulation in liver, spleen, heart and urinary bladder; only a partial reduction in GAG content was observed in lung and kidney. Data are shown as mean ± SEM of 3-4 animals/group. **P*<0.05 and ***P*<0.01 *vs.* WT. $^{\#}P$<0.05, $^{\#\#}P$<0.01 and $^{\#\#\#\#}P$<0.0001 *vs.* MPSII+Saline.

Taking these results together, pAAV-CAG-om*Ids*-v1 was the construct that mediated the highest increase in IDS activity in liver and serum, which resulted in complete normalization or great improvement in GAG storage in all organs analysed. For these reasons, pAAV-CAG-om*Ids*-v1 was the construct selected to use in the production of adeno-associated virus serotype 9 vectors containing the murine *Ids* gene, referred from now on as AAV9-*Ids*.

### 1.3. Study of the biodistribution profile of AAV9-*Ids* vectors

To determine the biodistribution profile of AAV9 vectors after direct-CSF administration through the cisterna magna, MPSII male mice aged 2 months were injected with $5x10^{10}$ vg of AAV9-*Ids* vectors, which contain version 1 of optimized IDS coding sequence under the control of the ubiquitous promoter CAG. Vector genome copy number and *Ids* expression were analysed 2 months after vector delivery. A widespread distribution of the vector in the whole encephalon was observed, as indicated by the genome copy number/diploid genome quantified in each brain section (Figure 23A). Despite the delivery of vectors was

to the CSF, vector genomes were also detected in peripheral tissues, mainly in the liver (Figure 23A). This observation was in agreement with previous studies that reported a leakage of a portion of the administered vector to the circulation after intra-CSF administration, leading to liver transduction (Haurigot et al., 2013; Gray et al., 2013; Hinderer et al., 2014a; Hinderer et al., 2014b; Ribera et al., 2015).

Consistently, *Ids* expression showed a similar profile of distribution as vector genomes: transgene expression was broadly detectable throughout the CNS and peripheral *Ids* expression was detected mainly in the liver (Figure 23B). Noteworthy, lymph nodes and adrenal glands presented low but detectable vector genome copy numbers as well as *Ids* expression after gene transfer (Figure 23).

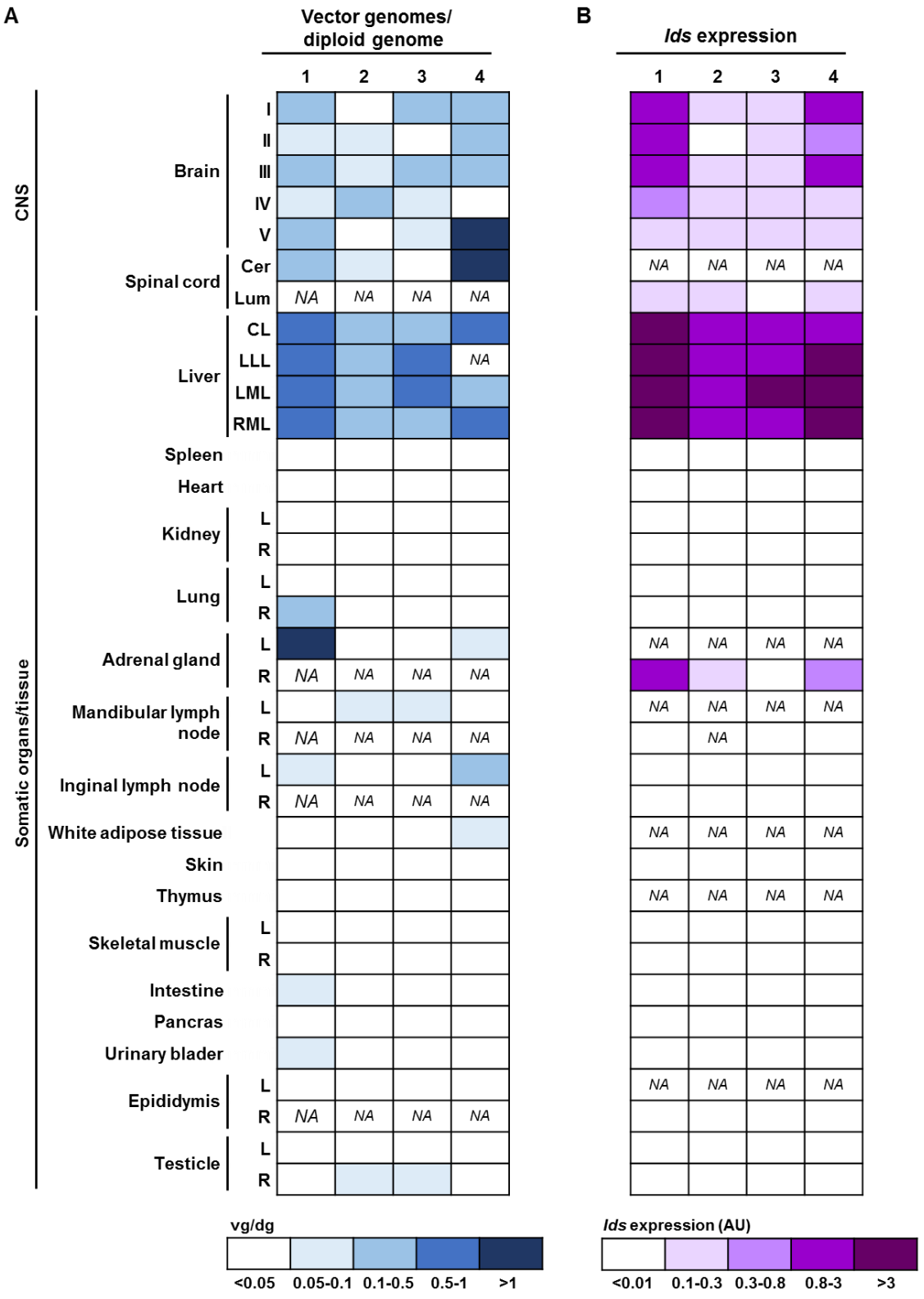


**Figure 23. Biodistribution of AAV9-*Ids* vectors and *Ids* expression following intra-CSF delivery to MPSII mice.** (**A**) Vector genome copy number per diploid genome (vg/dg) and (**B**) *Ids* mRNA expression in 4 individual MPSII mice 2 months after the intra-CSF administration of $5x10^{10}$ vg AAV9-*Ids*. The encephalon was sliced in 5 coronal sections (I-V). Cer, cervical; Lum, lumbar; CL, caudate lobe; LLL, left lateral lobe; LML, left medial lobe; RML, right medial lobe; L, left; R, right; AU, arbitrary unit; *NA*, non-available.

## 2. ASSESSMENT OF THE EFFICACY OF THE INTRA-CSF AAV9-*Ids* GENE THERAPY APPROACH

### 2.1. Experimental design of the AAV9-*Ids* gene therapy protocol

The gene therapy approach designed for MPSII was based on the delivery to the CSF of adeno-associated virus serotype 9 vectors containing the murine *Ids* CDS (AAV9-*Ids*) (Figure 24A).

MPSII mice of 2 months of age were treated with $5x10^{10}$ vg of AAV9-*Ids* vector by a single intra-CSF injection via the cisterna magna. As described in *Part I* of the present work, at that age, the CNS and somatic pathology is well established in this MPSII mouse model. As a control of the procedure, a separated cohort of MPSII males was treated with the same dose of a non-coding AAV9 vector (AAV9-Null). The genome of this "Null" vector contained all the elements of the expression cassette except for the *Ids* coding sequence. Age-matched wild-type littermates and untreated MPSII animals were used as controls. Four months after the treatment, i.e. at 6 months of age, a behavioural test was performed, animals were sacrificed and tissues were collected and subsequently analysed to assess the efficacy of the AAV9-*Ids* treatment (Figure 24B). In addition, 8 months after gene transfer, i.e. at 10 months of age, a thorough histopathological analysis of the CNS was performed. Finally, the effect of AAV9-*Ids* treatment on lifespan was also determined (Figure 24B).

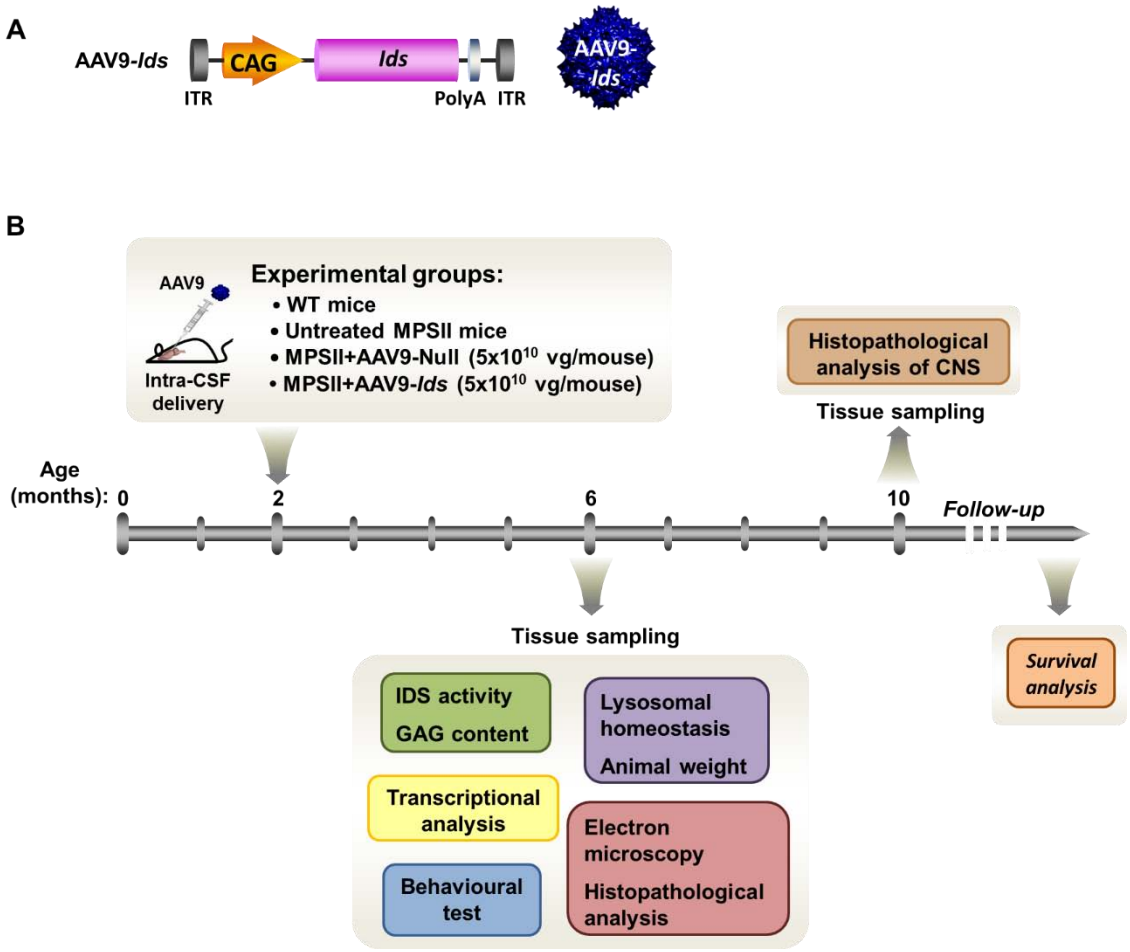


**Figure 24. Experimental design for the AAV9-*Ids* gene therapy protocol.** (**A**) Schematic representation of the modified genome of adeno-associated virus serotype 9 vector containing an optimized version of the murine *Ids* coding sequence and the polyA from the rabbit β-globin gene. The CAG promoter is a hybrid promoter composed of the early enhancer of cytomegalovirus (CMV), the chicken β-actin promoter and the chiken β-actin intron. ITR, inverted terminal repeats. The schematic representation is not to scale. (**B**) Experimental design for the administration of adeno-associated virus serotype 9 vectors containing the murine *Ids* coding sequence to 2-month-old MPSII male mice. The therapeutic efficacy was evaluated 4 and 8 months after the treatment. Additionally, the impact of the treatment on survival was also analysed.

## 2.2. Evaluation of the efficacy of intra-CSF AAV9-*Ids* gene therapy on the CNS pathology

### *2.2.1. IDS activity and GAG content in the encephalon*

To determine the effect of the intra-CSF delivery of AAV-*Ids* vectors on CNS pathology, IDS activity and GAG content were measured in encephalon samples (Figure 25). Four months after the treatment, i.e. at 6 months of age, animals were sacrificed and the encephalon was sectioned in 5 coronal regions (sections I to V). The intra-CSF administration of AAV9-*Ids* vectors to 2-month-old MPSII male mice led to restoration of IDS activity in all areas of

the encephalon analysed, from the most rostral (section I) to the most caudal parts (sections V), reaching levels that averaged around 40% of those observed in healthy WT littermates (Figure 25A). IDS activity remained undetectable in untreated MPSII mice and in MPSII mice treated with the Null vector (Figure 25A).

As a consequence of increased IDS activity, GAG content was completely normalized in all areas of the encephalon in AAV9-*Ids*-treated animals (Figure 25B). Null-injected MPSII mice showed, however, the same degree of GAG accumulation as untreated MPSII animals (Figure 25B).

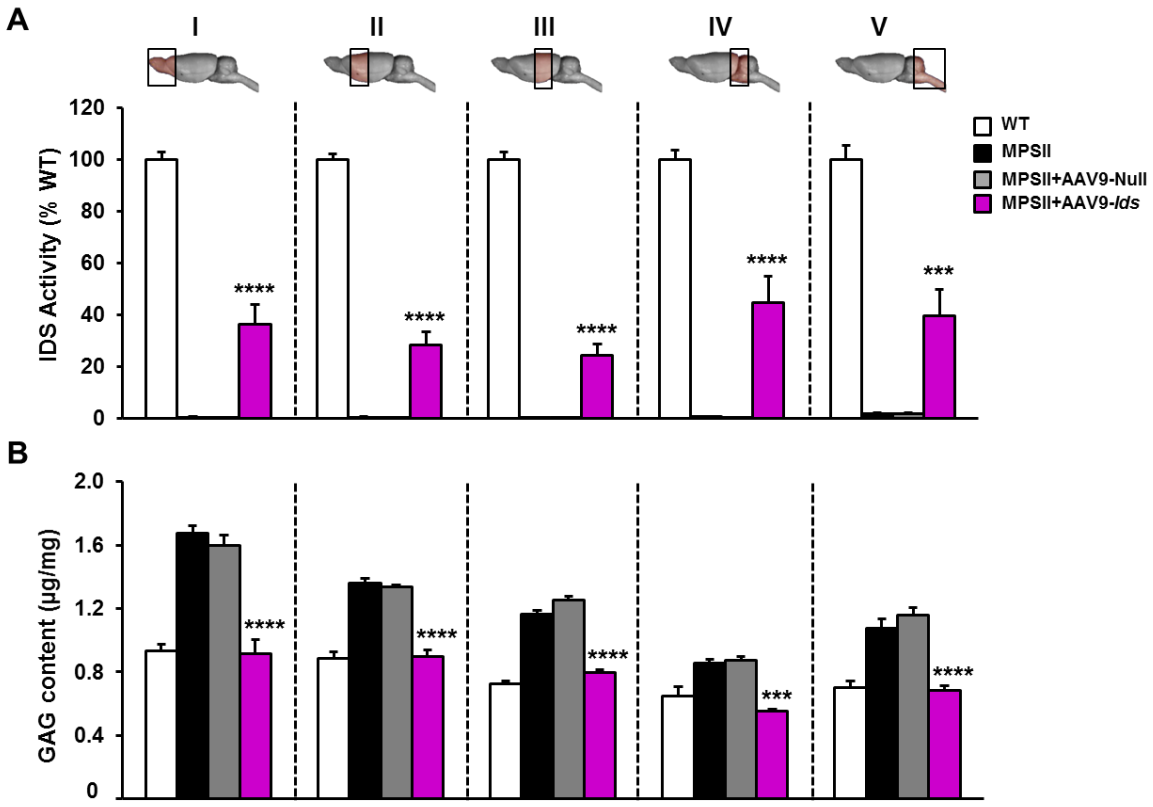


**Figure 25. Restoration of IDS activity and normalization of GAG content in the CNS of MPSII mice 4 months after intra-CSF AAV9-*Ids* delivery**. (**A**) Measurement of IDS activity in different regions of the encephalon of healthy wild-type (WT), untreated MPSII (MPSII) and MPSII mice injected in the CSF with $5x10^{10}$ vg/mouse of either Null vector (MPSII+AAV9-Null) or an equivalent dose of the therapeutic vector (MPSII+AAV9-*Ids*) at 2-months of age. Four months after treatment, i.e. at 6 months of age, the encephalon of each animal was dissected and sectioned in 5 coronal sections (I to V) as indicated in the diagram above the plot. IDS activity of WT mice was set to 100%. Administration of AAV9-*Ids* restored IDS activity throughout the encephalon of treated MPSII mice, whereas IDS activity was almost undetectable in untreated and Null-injected MPSII animals. (**B**) Quantification of GAG content in the same cohort of animals as in (A). AAV9-*Ids* delivery into the CSF resulted in full correction of GAG accumulation in all areas analysed. Values are shown as mean ± SEM of 4-5 animals/group. ***$P$<0.001 and ****$P$<0.0001 *vs.* MPSII+AAV9-Null.

### *2.2.2. Lysosomal pathology in the CNS*

To determine whether the administration of AAV9-*Ids* vectors into the CSF of 2-month-old MPSII mice resulted in any beneficial effect on the lysosomal pathology of the MPSII mouse model, immunostaining for the lysosomal marker LAMP2 was performed on encephalon tissue sections 4 months after gene transfer (Figure 26). At 6 months of age, an enlargement of the lysosomal compartment was clearly evident as increased LAMP2 signal in different areas of the encephalon from untreated nd AAV9-Null-treated MPSII mice in comparison with healthy WT littermates (Figure 26A). Consistent with the full normalization of GAG content, AAV9-*Ids* treatment led to a marked reduction in lysosomal distention in treated MPSII mice (Figure 26A). The correction of the lysosomal pathology in the CNS was further confirmed by quantification of the intensity of the LAMP2+ signal in different areas, which showed equivalent LAMP2+ signal intensity in AAV9-*Ids*-treated MPSII mice and healthy counterparts (Figure 26B).

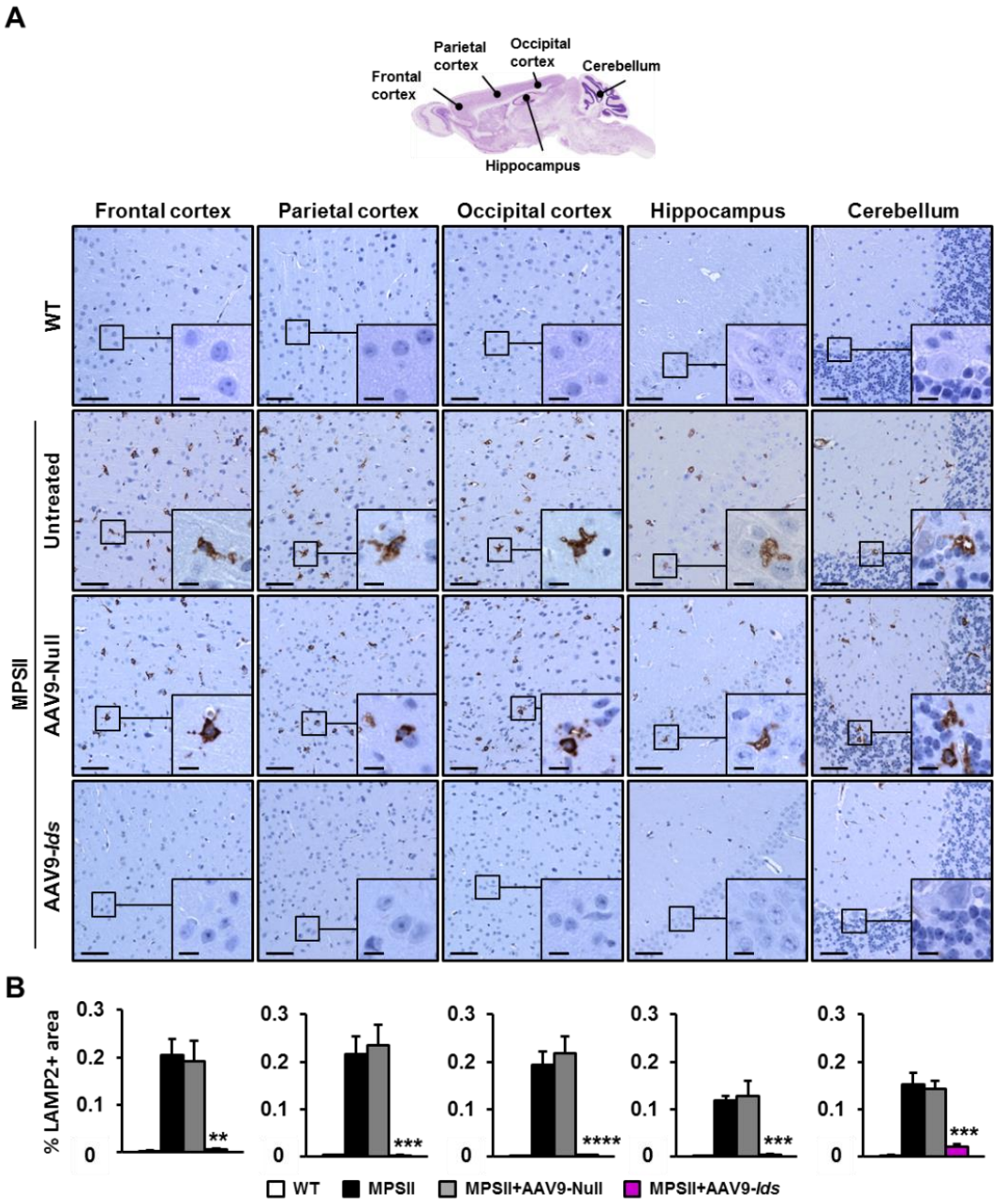


**Figure 26. Correction of lysosomal distention in the CNS of MPSII mice 4 months after intra-CSF AAV9-*Ids* delivery.** Immunostaining for the lysosomal marker LAMP2 to illustrate the size of the lysosomal compartment in different brain regions from 6-month-old healthy wild-type (WT), untreated MPSII (MPSII) and MPSII mice administered intra-CSF with Null (MPSII+AAV9-Null) or IDS-encoding vectors (MPSII+AAV9-*Ids*). (**A**) Representative photomicrographs of LAMP2 immunostaining of different areas of the encephalon as schematized in the above diagram. Scale bars are 50 µm, and 10 µm for insets. (**B**) Histograms depict the quantification of the percentage of LAMP2+ area in each brain region. A strong reduction in LAMP2+ signal, indicative of a reduction in the size of the lysosomal compartment, was achieved in all areas of MPSII mice treated with AAV9-*Ids* vectors. Results are shown as mean ± SEM of 4-5 animals per group. ***P*<0.01, ****P*<0.001 and *****P*<0.0001 *vs.* MPSII+AAV9-Null.

Moreover, when the effect of the AAV9-*Ids* treatment on lysosomal distention was evaluated 8 months after vector administration, i.e. at 10 months of age, the reduction in LAMP2+ signal intensity remained stable (Figure 27).

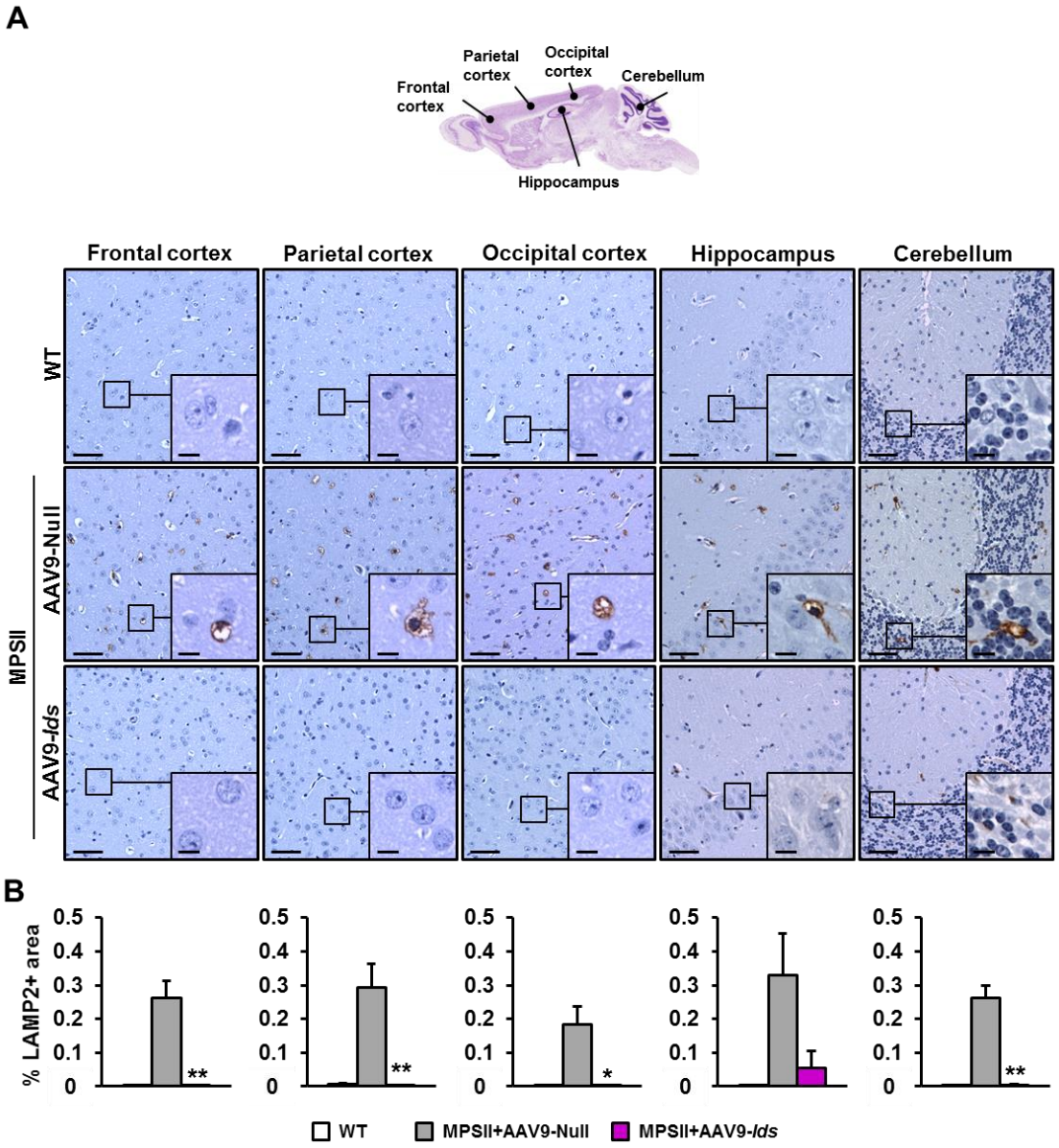


**Figure 27. Long-term correction of lysosomal distention in the CNS of MPSII mice by intra-CSF AAV9-*Ids* administration.** Immunostaining for the lysosomal marker LAMP2 in different brain areas from healthy wild-type (WT) and MPSII mice administered in the CSF with Null (MPSII+AAV9-Null) or IDS-encoding vectors (MPSII+AAV9-*Ids*) 8 months after vector delivery, i.e. at 10 months of age. (**A**) Representative photomicrographs of LAMP2 immunostaining of different areas of the encephalon as schematized in the above diagram. Scale bars are 50 µm, and 10 µm for insets. (**B**) Histograms depict the quantification of the percentage of LAMP2+ area in each brain region. The effect of the treatment on lysosomal distension remained stable 8 months after AAV9-*Ids* delivery. Results are shown as mean ± SEM of 2-6 animals per group. **P*<0.05 and ***P*<0.01 *vs.* MPSII+AAV9-Null.

To further confirm the correction mediated by the intra-CSF delivery of AAV9-*Ids* vectors of the MPSII lysosomal pathology present in this mouse model, ultrastructural analysis of the cerebral cortex was performed by transmission electron microscopy (TEM). Four months after intra-CSF administration of vectors, perineuronal glial cells of the cortex of MPSII mice injected with AAV9-Null vectors presented large electrolucent vacuoles that likely corresponded to lysosomes loaded with undegraded HS, DS and other compounds (Figure 28, middle panel). In contrast, perineuronal glial cells of MPSII mice treated with AAV9-*Ids* vectors showed a wild-type appearance, with no discernible storage vesicles in their cytoplasm (Figure 28, right panel), suggesting complete clearance of accumulated GAGs. Noteworthy, the presence of intracytoplasmic vacuoles were primarily localized in the perineuronal glial cells, while the juxtaposed cortical neurons barely showed signs of pathological storage (Figure 28); these results were in agreement with previous findings in other MPSs diseases (Ohmi et al., 2003; Ruzo et al., 2012a; Fraldi et al., 2007b; Haurigot et al., 2013; Ribera et al., 2015).

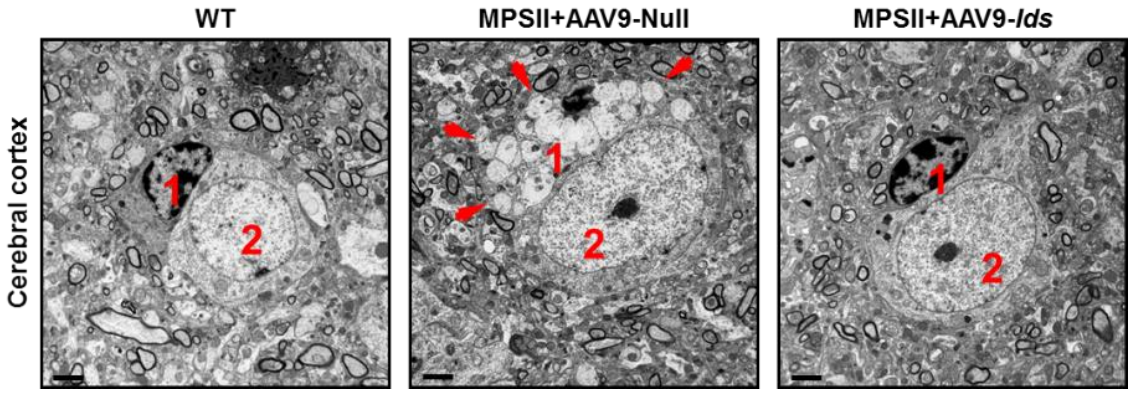


**Figure 28. Ultrastructural analysis of the cortex in MPSII mice 4 months after intra-CSF AAV9-*Ids* delivery.** Representative images of the ultrastructural analysis of cerebral cortex performed in wild-type (WT) or MPSII mice treated with either Null vector (MPSII+AAV9-Null) or therapeutic vector (MPSII+AAV9-*Ids*) 4 months after intra-CSF vector administration. AAV9-*Ids*-treated MPSII mice showed an evident reduction in the size and number of intracytoplasmic electrolucent vacuoles (indicated by red arrows) in perineuronal glial cells (1) associated to neurons (2) of the cerebral cortex. N=3. Scale bars are 2 μm.

The lysosomal homeostasis of the CNS was evaluated by measuring the activity of several hydrolases different from the lysosomal enzyme deficient in MPSII disease. In brain extracts of untreated or AAV9-Null injected MPSII mice aged 6 months, the activities of HGSNAT and β-HEXO were significantly increased, whereas SGSH and GALNS activities were reduced in comparison with wild-type levels (Figure 29). The activity of all these lysosomal enzymes returned to healthy wild-type levels 4 months after AAV9-*Ids*

treatment (Figure 29), suggesting a complete normalization of the lysosomal homeostasis through this gene therapy approach.

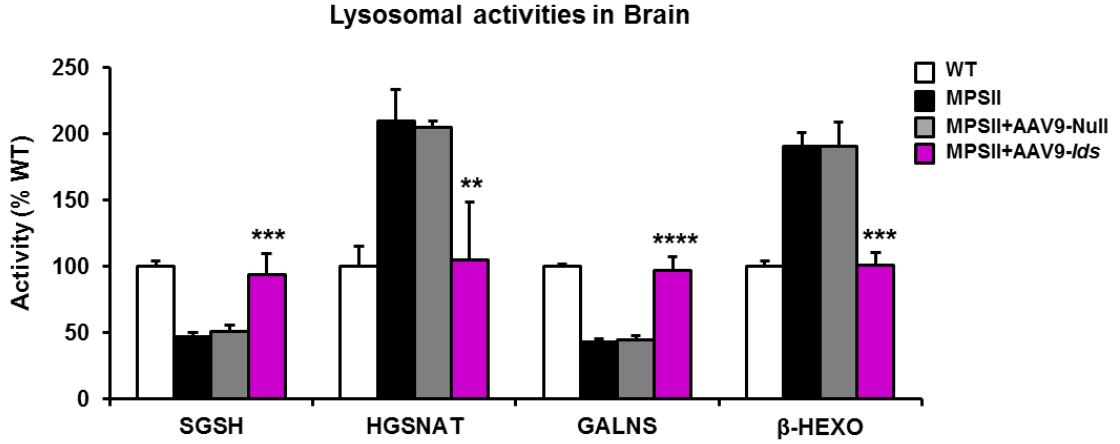


**Figure 29. Restoration of lysosomal homeostasis in the brain of MPSII mice after 4 months of intra-CSF AAV9-*Ids* delivery**. Measurement of the activity of other lysosomal enzymes different from IDS analysed in brain extracts 4 months after gene transfer. Intra-CSF delivery of AAV9-*Ids* vectors restored the activities of Sulfoglucosaminide N-sulfohydrolase (SGSH), Heparan α-glucosaminide N-acetyltransferase (HGSNAT), N-Acetylgalactosamine-6-sulfate-sulfatase (GALNS) and β-hexosaminidase (β-HEXO) in the brain of treated MPSII mice. Activities are expressed as % of WT activity, which was set to 100%. Results are shown as mean ± SEM of 4-5 animals per group. ***P*<0.01, ****P*<0.001 and *****P*<0.0001 *vs.* MPSII+AAV9-Null.

### *2.2.3. Effect of the treatment on neuroinflammation*

The effect of the therapy on the neuroinflammatory process characteristic of Hunter disease was also evaluated 4 months after AAV9-*Ids* gene transfer to MPSII mice. To this aim, immunohistochemistry for the specific marker of astrocytes, GFAP, and staining of microglia with the lectin BSI-B4 were performed on brain tissue sections.

At 6 months of age, untreated and AAV9-Null-treated MPSII mice showed intense GFAP signal in all the different areas of the encephalon evaluated, demonstrating a marked activation of astrocytes (Figure 30). By contrast, the administration of intra-CSF AAV9-*Ids* to MPSII mice resulted in the eradication of GFAP upregulation in all the regions of the brain evaluated; when quantified, the percentage of GFAP+ area of treated MPSII mice resembled that of healthy WT littermates (Figure 30B).

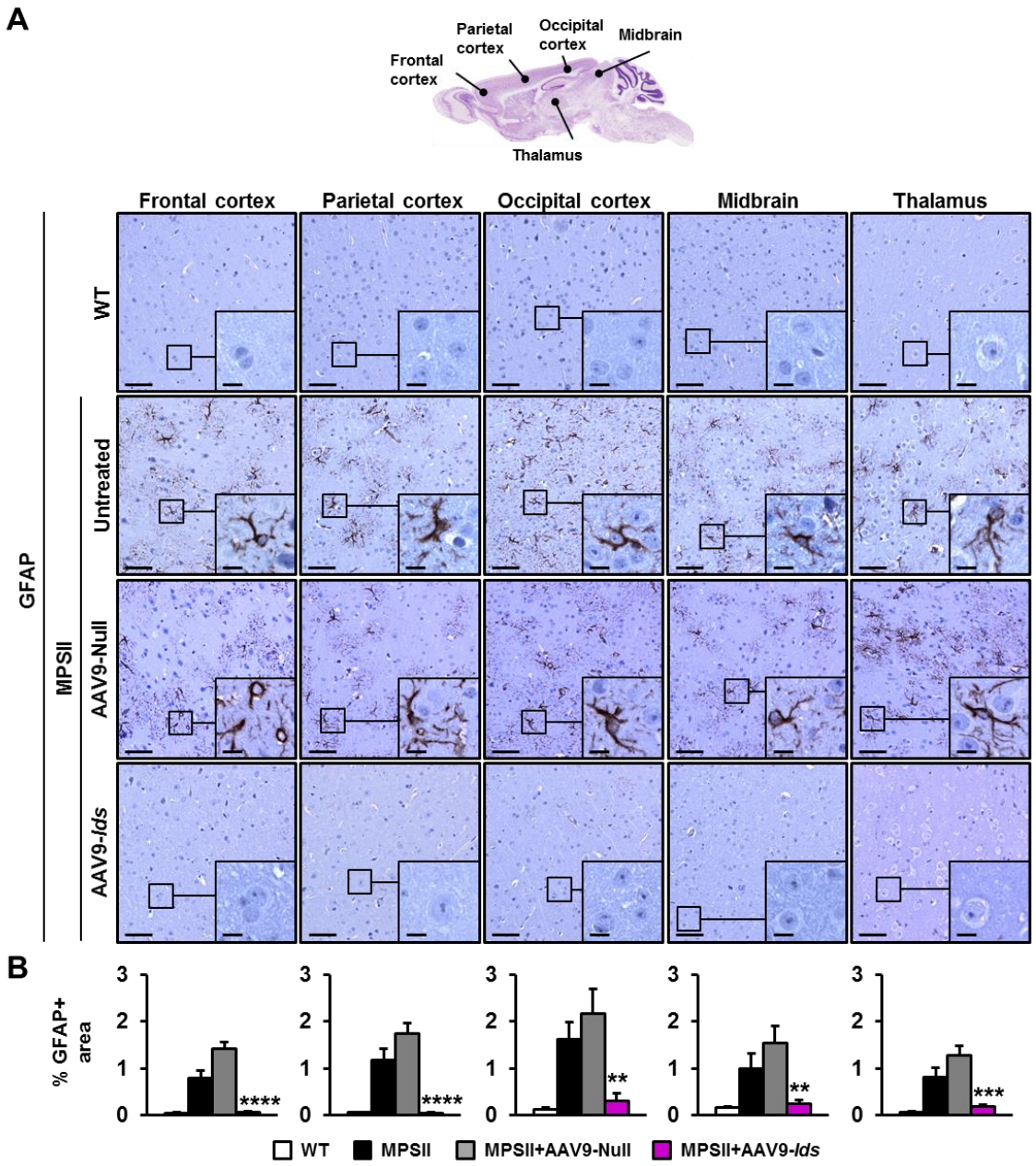


**Figure 30. Correction of astrogliosis in the CNS of MPSII mice 4 months after intra-CSF AAV9-*Ids* delivery.** Immunostaining for the specific marker for astrocytes, GFAP, in brain paraffin sections from 6-month-old healthy wild-type (WT), untreated MPSII (MPSII) and MPSII mice administered intra-CSF with Null (MPSII+AAV9-Null) or IDS-encoding vectors (MPSII+AAV9-*Ids*). (**A**) Representative photomicrographs of GFAP immunostaining of different areas of the encephalon as schematized in the diagram above. Scale bars are 50 µm, and 10 µm for insets. (**B**) Histograms depict the quantification of the percentage of GFAP+ area in each brain region. A strong reduction in GFAP+ signal, indicative of normalization of astrogliosis, was achieved in all areas of MPSII mice treated with AAV9-*Ids* vectors. Results are shown as mean ± SEM of 4-5 animals per group. ***P*<0.01, ****P*<0.001 and *****P*<0.0001 *vs.* MPSII+AAV9-Null.

The effect of AAV9-*Ids* treatment on astrogliosis was further confirmed by repeating the GFAP immunostaining on paraffin-embedded brain sections obtained from 10-month-old WT and MPSII mice treated either with Null vector (AAV9-Null) or the therapeutic vector (AAV9-*Ids*) (Figure 31). AAV9-Null-treated MPSII mice showed a strong positive signal for GFAP in all the different encephalon regions analysed, whereas the signal intensity in sections from treated MPSII mice resembled that of WT mice. The quantification of the GFAP+ signal intensity confirmed the reduction of the astrocytic activation in the CNS of AAV9-*Ids*-treated MPSII mice 8 months after gene transfer (Figure 31B).

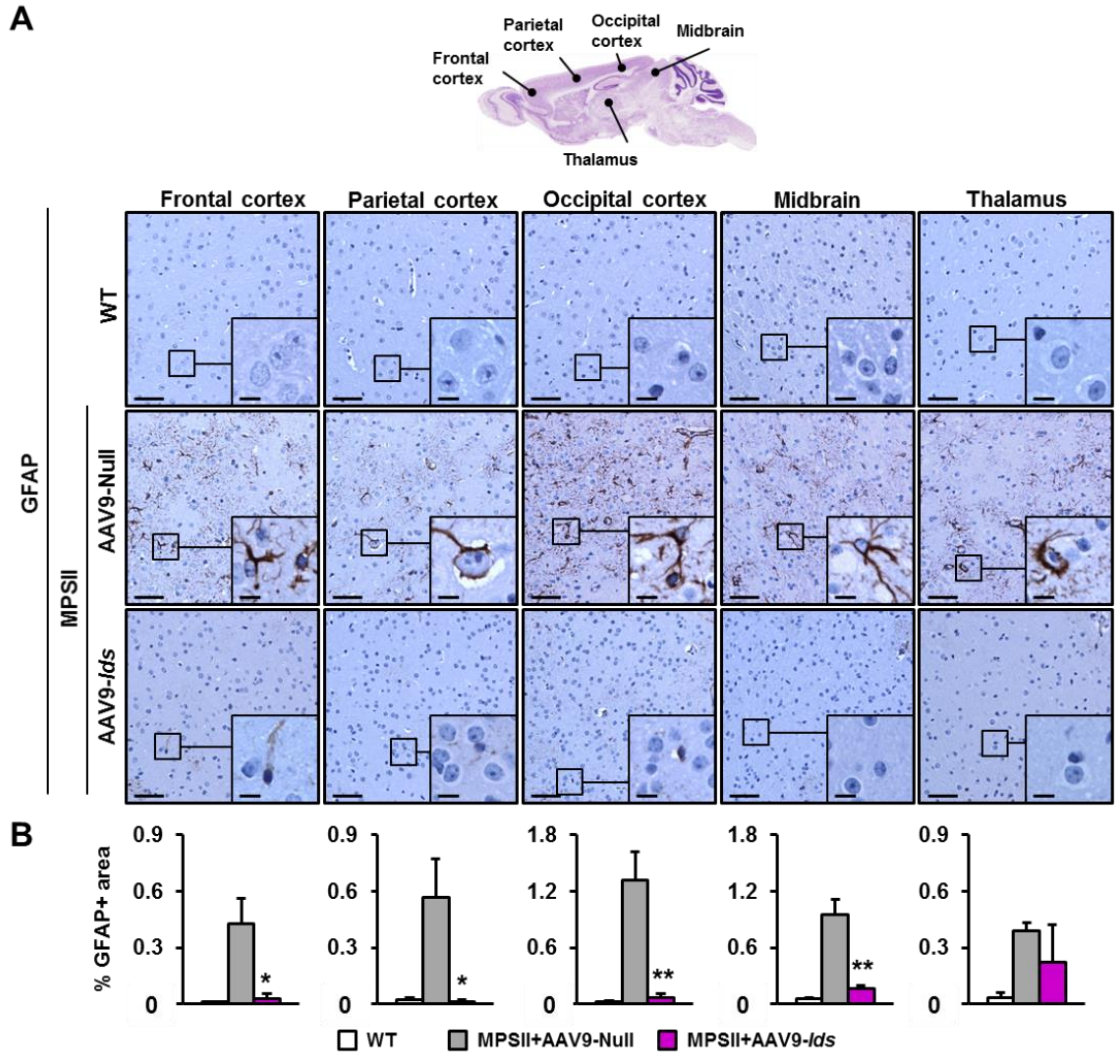


**Figure 31. Long-term correction of astrogliosis in the CNS of MPSII mice by intra-CSF AAV9-*Ids* administration.** Immunostaining for GFAP, a marker of activated astrocytes, in different brain areas of healthy wild-type (WT) and MPSII mice administered intra-CSF with Null (MPSII+AAV9-Null) or IDS-coding vectors (MPSII+AAV9-*Ids*) analysed 8 months after vector delivery, i.e. at 10 months of age. (**A**) Representative photomicrographs of GFAP immunostaining of different areas of the encephalon as schematized in the diagram above. Scale bars are 50 µm, and 10 µm for insets. (**B**) Histograms depict the quantification of the percentage of GFAP+ area in each brain region. Results are shown as mean ± SEM of 2-6 animals per group. **P*<0.05 and ***P*<0.01 *vs.* MPSII+AAV9-Null.

Similar to the results obtained with GFAP immunohistochemistry, the staining of microglial cells with the lectin BSI-B4 revealed that untreated and AAV9-Null-treated MPSII mice showed a strong positive signal for BSI-B4 in all encephalon areas analysed (Figure 32). Nonetheless, intra-CSF AAV9-*Ids* administration resulted in the normalization of BSI-B4+ signal intensity in all different encephalon areas analysed of MPSII mice, with values close to those measured in healthy WT counterparts (Figure 32B).

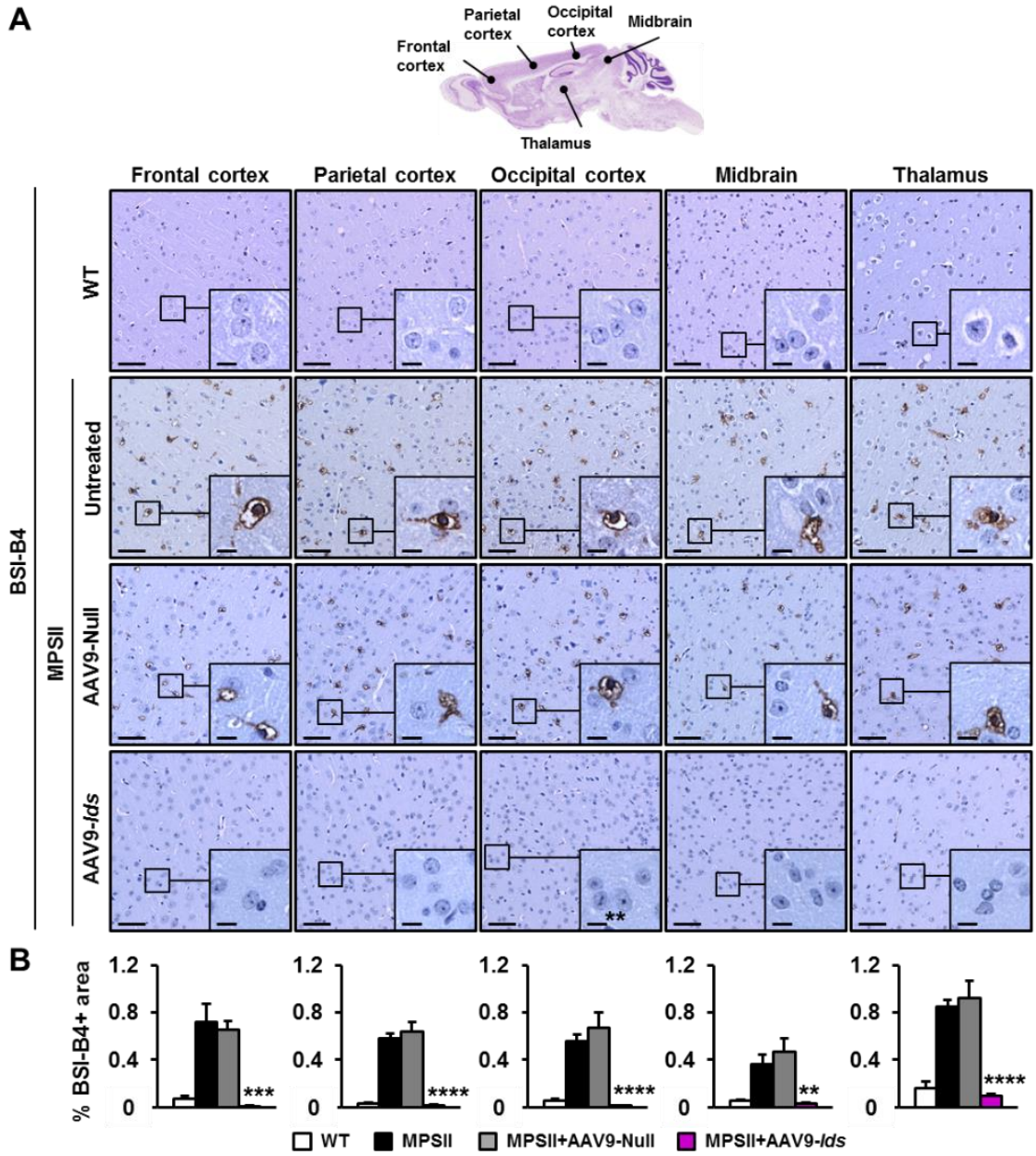


**Figure 32. Correction of microgliosis in the CNS of MPSII mice 4 months after intra-CSF AAV9-*Ids* delivery.** Staining with lectin BSI-B4, a marker of microglial cells, in brain paraffin-embedded sections from 6-month-old healthy wild-type (WT), untreated MPSII (MPSII) and MPSII mice administered intra-CSF with Null (MPSII+AAV9-Null) or IDS-coding (MPSII+AAV9-*Ids*) vectors. (**A**) Representative photomicrographs of BSI-B4 staining of different areas of the encephalon as schematized in the diagram above. Scale bars are 50 µm, and 10 µm for insets. (**B**) Histograms depict the quantification of the percentage of BSI-B4+ area in each brain region. Normalization of the intensity of BSI-B4 staining, indicative of absence of activated microglia, was achieved in all areas of MPSII mice treated with AAV9-*Ids* vectors. Results are shown as mean ± SEM of 4-5 animals per group. ***P*<0.01, ****P*<0.001 and *****P*<0.0001 *vs.* MPSII+AAV9-Null.

Furthermore, 8 months after vector delivery, the impact of AAV9-*Ids* treatment on microgliosis was sustained (Figure 33). While AAV9-Null-treated MPSII mice aged 10 months showed a strong positive signal for BSI-B4, this signal disappeared from all the areas of the encephalon of AAV9-*Ids*-treated MPSII mice (Figure 33).

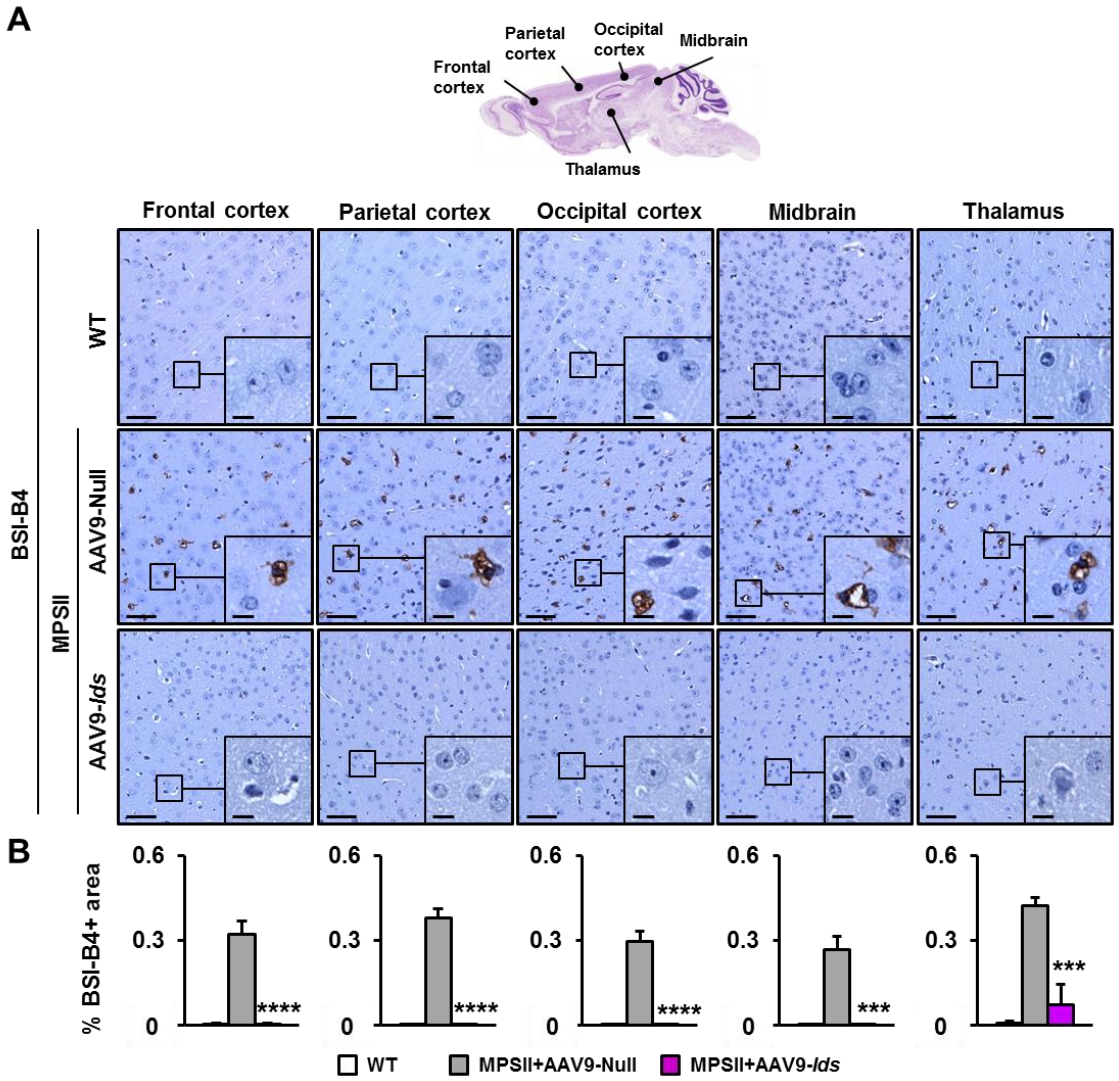


**Figure 33. Long-term correction of microgliosis in the CNS of MPSII mice by intra-CSF AAV9-*Ids* administration.** Staining for BSI-B4, a marker of activated microglia, in different brain areas of healthy wild-type (WT) and MPSII mice administered intra-CSF with Null (MPSII+AAV9-Null) or IDS-coding vectors (MPSII+AAV9-*Ids*) analysed 8 months after vector delivery, i.e. at 10 months of age. (**A**) Representative photomicrographs of BSI-B4 staining of different areas of the encephalon as schematized in the diagram above. Scale bars are 50 µm, and 10 µm for insets. (**B**) Histograms depict the quantification of the percentage of BSI-B4+ area in each brain region. A reduction of BSI-B4+ signal intensity persisted 8 months after AAV9-*Ids* treatment. Results are shown as mean ± SEM of 2-6 animals per group. ***$P$<0.001 and ****$P$<0.0001 *vs.* MPSII+AAV9-Null.

Altogether, these results indicated that the intra-CSF administration of AAV9-*Ids* vectors to MPSII mice with established disease could lead to full and long-term eradication of neuroinflammation.

### *2.2.4. CNS transcriptional signature*

To further evaluate the therapeutic effect of intra-CSF AAV9-*Ids* treatment on MPSII disease, genome microarray studies were carried out. To this aim, RNA was isolated from the encephalon of 6-month-old wild-type, AAV9-Null or AAV9-*Ids*-treated MPSII mice and subsequently analysed using the GeneChip Mouse Gene 2.1 ST 16 array plates (Affimetrix®). Focusing the analysis on known coding sequences, an initial list of 28427 genes was obtained. After data processing, 90 genes were found to be differentially expressed among the three experimental groups. The complete list of altered genes and their fold-change in comparison to WT is provided in Table 5.

**Table 5. List of the genes differentially expressed in the encephalon of Null-treated and AAV9-*Ids*-treated MPSII mice grouped according to the function of the encoded protein** *(Part I)*

| Gene name | Gene symbol | Fold change *vs.* WT | | AAV9-*Ids*-mediated % of correction |
|---|---|---|---|---|
| | | AAV9-*Ids* | AAV9-Null | |
| **Lysosomal enzyme** | | | | |
| Cathepsin D | *Ctsd* | 1.04 | 1.45 | 91.11 |
| Cathepsin S | *Ctss* | 1.22 | 2.2 | 81.67 |
| Cathepsin Z | *Ctsz* | 0.94 | 1.53 | 111.32 |
| Glucuronidase, beta | *Gusb* | 0.84 | 1.23 | 169.57 |
| Hexosaminidase B | *Hexb* | 1.1 | 1.63 | 84.13 |
| Heparanase | *Hpse* | 1.05 | 1.87 | 94.25 |
| **Monocyte/Macrophage linage** | | | | |
| CD109 antigen | *Cd109* | 1.04 | 1.49 | 91.84 |
| CD33 antigen | *Cd33* | 1.09 | 1.78 | 88.46 |
| CD63 antigen | *Cd63* | 1.09 | 1.45 | 80.00 |
| CD68 antigen | *Cd68* | 1.16 | 2.49 | 89.26 |
| Glycoprotein (transmembrane) nmb | *Gpnmb* | 1.15 | 2.17 | 87.18 |
| Lysozyme 2 | *Lyz2* | 1.32 | 3.02 | 84.16 |
| Macrophage expressed gene 1 | *Mpeg1* | 1.23 | 2.69 | 86.39 |
| Protein tyrosine phosphatase, non-receptor type 6 | *Ptpn6* | 1.22 | 1.54 | 59.26 |
| **Immune response** | | | | |
| Complement component 1, Q subcomponent, A chain | *C1qa* | 1.05 | 1.85 | 94.12 |
| Complement component 1, Q subcomponent, B chain | *C1qb* | 1.2 | 2.21 | 83.47 |
| Complement component 1, Q subcomponent, C chain | *C1qc* | 0.99 | 1.86 | 101.16 |
| Complement component 3a receptor 1 | *C3ar1* | 0.98 | 2.52 | 101.32 |
| Complement component 4B | *C4b* | 1.22 | 2.15 | 80.87 |
| Chemokine (C-C motif) ligand 3 | *Ccl3* | 0.98 | 2.95 | 101.03 |
| CD180 antigen | *Cd180* | 1.07 | 1.66 | 89.39 |
| Colony stimulating factor 3 receptor (granulocyte) | *Csf3r* | 1.01 | 1.57 | 98.25 |
| Defensin, alpha, related sequence 1 | *Defa-rs1* | 1.45 | 0.74 | 273.08 |
| Fc receptor, IgE, high affinity I, gamma polypeptide | *Fcer1g* | 0.86 | 1.7 | 120.00 |
| Fc receptor-like S, scavenger receptor | *Fcrls* | 1.42 | 2.6 | 73.75 |
| GTPase, IMAP family member 8 | *Gimap8* | 1.71 | 1.22 | -222.73 |
| Hepatitis A virus cellular receptor 2 | *Havcr2* | 1.09 | 1.69 | 86.96 |
| Interferon induced transmembrane protein 3 | *Ifitm3* | 1.25 | 1.54 | 53.70 |
| Interferon beta 1, fibroblast | *Ifnb1* | 0.65 | 0.64 | 2.78 |
| Immunoglobulin lambda variable 1 | *Iglv1* | 1.38 | 2.79 | 78.77 |
| Lymphocyte-activation gene 3 | *Lag3* | 1.26 | 2.23 | 78.86 |
| Lectin, galactose binding, soluble 9 | *Lgals9* | 1 | 1.54 | 100.00 |
| Leukocyte immunoglobulin-like receptor, subfamily B, member 4 | *Lilrb4* | 1.57 | 2.93 | 70.47 |
| Toll-like receptor 13 | *Tlr13* | 0.92 | 2.31 | 106.11 |
| T cell receptor alpha joining 12 | *Traj12* | 1.08 | 0.47 | 115.09 |
| T cell receptor beta, variable 13-1 | *Trbv13-1* | 1.43 | 0.82 | 338.89 |
| Triggering receptor expressed on myeloid cells 2 | *Trem2* | 1.05 | 2.1 | 95.45 |
| Thrombospondin 4 | *Thbs4* | 1.16 | 1.58 | 72.41 |
| TYRO protein tyrosine kinase binding protein | *Tyrobp* | 0.93 | 2.05 | 106.67 |
| Unc-93 homolog B1 | *Unc93b1* | 1.19 | 1.76 | 75.00 |
| **Ion transport** | | | | |
| FXYD domain-containing ion transport regulator 4 | *Fxyd4* | 1.44 | 0.72 | 257.14 |
| Predicted gene 5724 | *Gm5724* | 1.18 | 1.64 | 71.88 |
| Solute carrier family 22, member 27 | *Slc22a27* | 1.13 | 1.74 | 82.43 |
| Solute carrier family 7, member 11 | *Slc7a11* | 1.24 | 1.59 | 59.32 |

**Continuation Table 5. List of the genes differentially expressed in the encephalon of Null-treated and AAV9-*Ids*-treated MPSII mice grouped according to the function of the encoded protein** *(Part II)*

| Gene name | Gene symbol | Fold change *vs.* WT | | AAV9-*Ids*-mediated % of correction |
|---|---|---|---|---|
| | | AAV9-*Ids* | AAV9-Null | |
| **Miscellaneous** *(related function)* | | | | |
| Aquaporin 4 *(Water homeostasis)* | *Aqp4* | 1.28 | 1.46 | 39.13 |
| Astacin-like metalloendopeptidase, M12 family *(Metallopeptidase activity)* | *Astl* | 0.74 | 0.5 | 48.00 |
| Breast cancer 2, early onset *(Genome stability)* | *Brca2* | 0.94 | 1.44 | 113.64 |
| Copine III *(Glycerophospholipid synthesis)* | *Cpne3* | 1.17 | 1.45 | 62.22 |
| Cytochrome b-245, alpha polypeptide *(Oxidative stress)* | *Cyba* | 1.05 | 1.66 | 92.42 |
| 2-4-dienoyl-Coenzyme A reductase 2, peroxisomal *(Peroxixomal enzyme)* | *Decr2* | 0.88 | 1.37 | 132.43 |
| Enoyl-Coenzyme A delta isomerase 1 *(Lipid oxidation)* | *Eci1* | 0.82 | 1.42 | 142.86 |
| Egf-like module containing, mucin-like, hormone receptor-like 1 *(Chromosome segregation)* | *Emr1* | 0.92 | 1.87 | 109.20 |
| Forkhead box E3 *(Lens development)* | *Foxe3* | 0.54 | 0.68 | -43.75 |
| Glial fibrillary acidic protein *(Astrocytes)* | *Gfap* | 1.26 | 2.38 | 81.16 |
| Predicted gene 14484 *(Histones binding)* | *Gm14484* | 0.79 | 0.59 | 48.78 |
| Glutamate receptor, ionotropic, delta 1 *(Glutamate metabolism)* | *Grid1* | 1.19 | 1.45 | 57.78 |
| Hemoglobin, theta 1A *(Oxygen transport)* | *Hbq1a* | 0.66 | 0.47 | 35.85 |
| Interferon-induced protein 44 *(Structure)* | *Ifi44* | 1.7 | 2.1 | 36.36 |
| Kinase insert domain protein receptor *(Vasculare)* | *Kdr* | 1.15 | 1.55 | 72.73 |
| Kallikrein related-peptidase 7 *(Serine protease)* | *Klk7* | 0.79 | 0.68 | 34.38 |
| Olfactory receptor 152 *(Olfactory perception)* | *Olfr152* | 1.31 | 0.66 | 191.18 |
| Olfactory receptor 507 *(Olfactory perception)* | *Olfr507* | 1.05 | 0.53 | 110.64 |
| Olfactory receptor 544 *(Olfactory perception)* | *Olfr544* | 1 | 0.61 | 100.00 |
| Olfactory receptor 91 *(Olfactory perception)* | *Olfr91* | 0.61 | 0.72 | -39.29 |
| Phospholipase A2, group IID *(Lipid metabolism)* | *Pla2g2d* | 0.91 | 0.59 | 78.05 |
| Pleckstrin *(PKC signalling in platelets)* | *Plek* | 0.93 | 1.78 | 108.97 |
| Protein S, alpha *(Vascular signalling)* | *Pros1* | 1.23 | 1.85 | 72.94 |
| Protease, serine 41 *(Serine protease)* | *Prss41* | 1.1 | 0.59 | 124.39 |
| Ribonuclease T2A *(Ribonuclease)* | *Rnaset2a* | 1.02 | 1.33 | 93.94 |
| TATA-box binding protein associated factor 11 *(Transcription regulation)* | *Taf11* | 0.86 | 1.27 | 151.85 |
| Zinc finger protein 599 *(Transcription regulation)* | *Zfp599* | 1.07 | 1.6 | 88.33 |
| **Unknown function** | | | | |
| RIKEN cDNA 1700120C14 gene | *1700120C14Rik* | 1.32 | 2.45 | 77.93 |
| RIKEN cDNA 5930403L14 gene | *5930403L14Rik* | 1.29 | 1.75 | 61.33 |
| RIKEN cDNA 9230116N13 gene | *9230116N13Rik* | 0.66 | 0.8 | -70.00 |
| Carboxylesterase 2D, pseudogene | *Ces2d-ps* | 1.12 | 0.55 | 126.67 |
| RIKEN cDNA D930048G16 gene | *D930048G16Rik* | 0.64 | 1.13 | 376.92 |
| Predicted gene 10134 | *Gm10134* | 0.94 | 1.69 | 108.70 |
| Predicted gene 11009 | *Gm11009* | 0.69 | 0.58 | 26.19 |
| Predicted gene 11646 | *Gm11646* | 1.39 | 1.31 | -25.81 |
| Predicted gene 11725 | *Gm11725* | 1.33 | 0.89 | 400.00 |
| Predicted gene 12127 | *Gm12127* | 1.77 | 1.04 | -1825.00 |
| Predicted gene 15462 | *Gm15462* | 1.04 | 0.57 | 109.30 |
| Predicted gene 17421 | *Gm17421* | 1.2 | 0.72 | 171.43 |
| Predicted gene 4832 | *Gm4832* | 1.02 | 1.53 | 96.23 |
| RIKEN cDNA I830077J02 gene | *I830077J02Rik* | 1.22 | 1.9 | 75.56 |
| IQ motif containing F5 | *Iqcf5* | 0.73 | 0.53 | 42.55 |
| Putative E3 ubiquitin-protein ligase UNKL | *LOC101055995* | 1.73 | 0.24 | 196.05 |
| - | *LOC102638562* | 1.21 | 0.76 | 187.50 |
| Transmembrane protein 254b | *Tmem254b* | 1.82 | 1.95 | 13.68 |

Fold-change values >1 indicate gene up-regulation, whereas values <1 indicate gene down-regulation. WT gene expression was set to 1 to calculate AAV9-*Ids*-mediated % of correction. Source of related function: http://www.ncbi.nlm.nih.gov/gene and http://www.uniprot.org/.

Based on the complete list of differentially expressed genes, a hierarchical clustering of these genes and the corresponding heatmap were depicted (Figure 34). Four months after vector delivery, MPSII mice treated with AAV9-*Ids* presented an expression profile in the CNS that resembled that of healthy WT counterparts (Figure 34). Almost 80% of the genes differentially expressed in MPSII mice that received AAV9-Null vector showed a correction in their transcript levels of at least 50% following AAV9-*Ids* treatment, an in 60% of them the correction was of 75%.

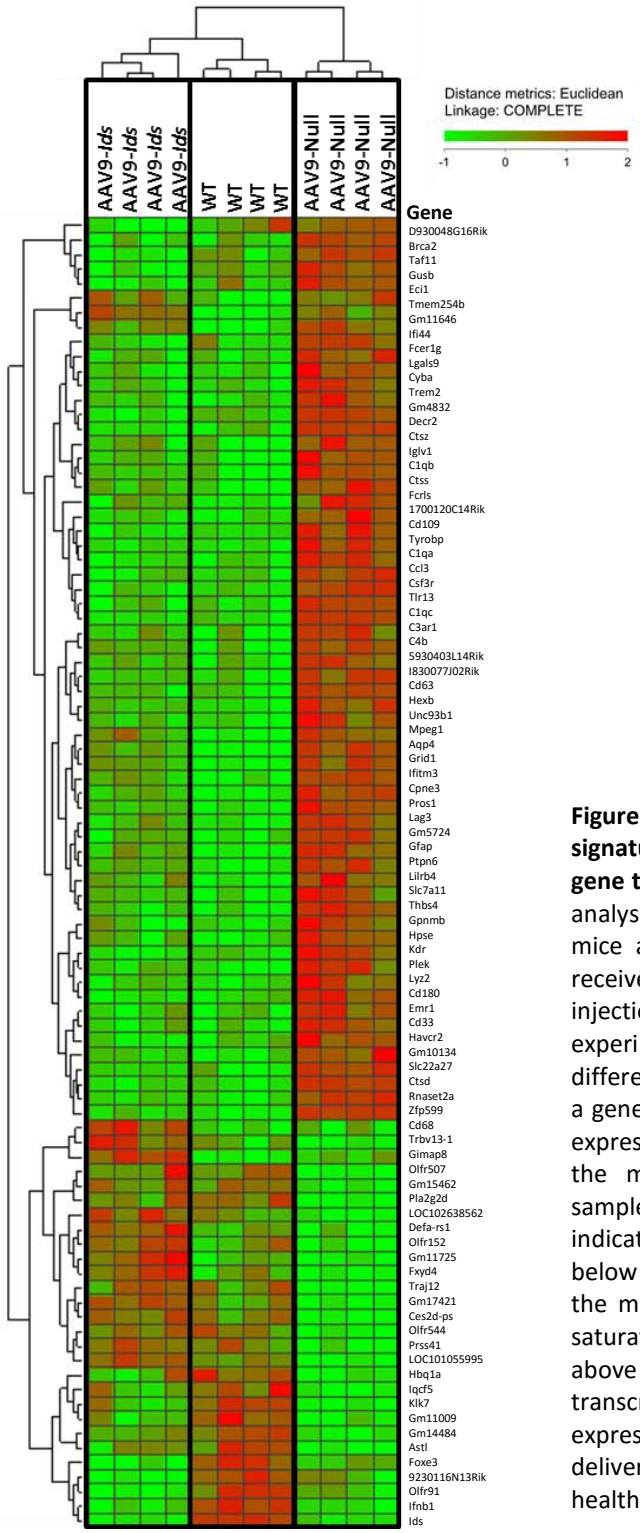


**Figure 34. Recovery of brain transcriptional signature after 4 months of intra-CSF AAV9-*Ids* gene therapy in MPSII mice.** Microarray expression analysis performed at 6 months of age in wild-type mice and MPSII littermates 4 months after they received either AAV9-Null or AAV9-Ids vector injections. Hierarchical clustering of all experimental groups based on the complete list of differentially expressed genes. Each row represents a gene and each column represents an animal. The expression of each gene is represented relative to the mean abundance of that gene across all samples in a colour scale in which red and green indicate, respectively, transcript levels above and below the mean. The magnitude of deviation from the mean is represented by the degree of colour saturation. The dendrogram of samples shown above the matrix represents overall similarities in transcript levels. Visibly, the profile of gene expression in MPSII animals treated by intra-CSF delivery of AAV9-*Ids* vectors resembled that of healthy, age-matched WT littermates.

To determine in which biological processes were these differentially expressed genes involved, Gene Ontology (GO) enrichment analysis was performed using the GeneCodis Tool 2.0 (genecodis2.dacya.ucm.es). GeneCodis is a web-based tool developed to perfom modular enrichment analysis orientated to group a list of genes into different functional clusters according to the standardized GO classification. When applied to the list of genes depicted in Table 5, the functional analysis classified the differentially expressed genes into 12 different GO categories; 83 of the 89 genes were annotated with corresponding ontologies (Figure 35). Noteworthy, a clear enrichment in biological processes associated with inflammation and innate immunity was observed in MPSII animals that received AAV9-Null vectors (Figure 35), likely owing to increased presence of immune cells involved in these processes, such as microglia, in the CNS of untreated MPSII animals.

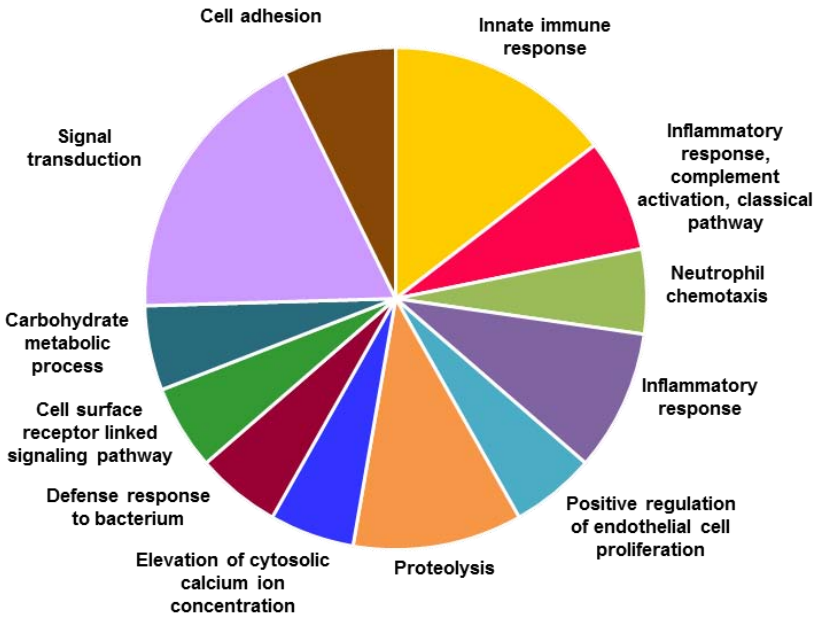


**Figure 35. Functional categorization of the genes differentially expressed based on Gene Ontology annotation.** 83 of the total list of 89 genes were annotated with corresponding ontology. Most of the categories depicted in the pie chart reflect processes associated with inflammation and innate immunity.

To confirm that microglial cells accounted for the majority of differentially expressed genes, Cell Type Enrichment (CTEN) analysis was performed to assess the contribution of different cell types to the observed changes in transcript levels. The CTEN software considers there is enrichment of a specific cell type if a software-defined score greater than 2 is obtained (http://www.influenza-x.org/~jshoemaker/cten/). When the 89 differentially expressed genes were analysed by the CTEN software, a high enrichment score (21.99) was obtained for the microglial population. Moreover, the transcript levels of genes assigned to microglia by the CTEN software were clearly normalized following the treatment with AAV9-*Ids* (Figure 36). These results support the established notion that microglia plays a key role in CNS pathology in all forms of MPS (Constantopoulos et al., 1980; Ohmi et al., 2003; Hamano et al., 2008; DiRosario et al., 2009; Archer et al., 2014). Moreover, these results demonstrate the efficacy of intra-CSF delivery of AAV9-*Ids* in eradicating neuroinflammation.

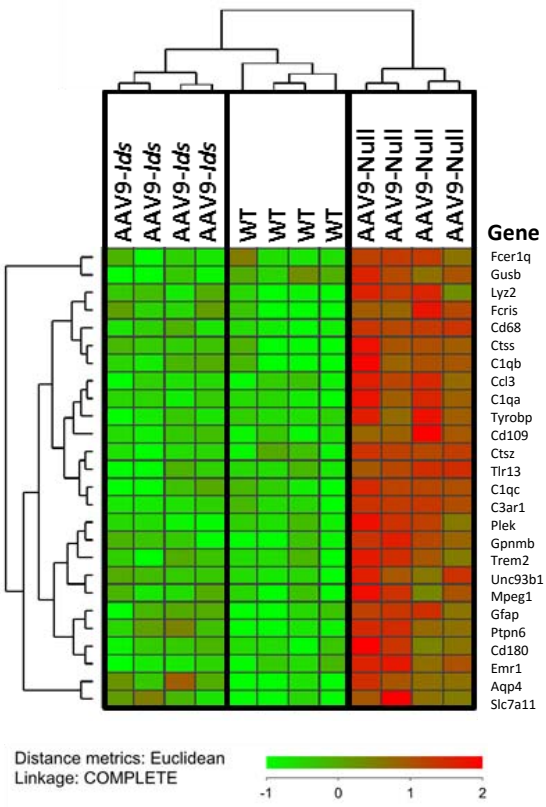


**Figure 36. Normalization of the expression of genes associated to microglia cells following intra-CSF AAV9-*Ids* gene therapy in MPSII mice.** Hierarchical clustering of the set of genes that the CTEN software assigned to microglia. Samples were obtained from 6-month-old healthy wild-type (WT) and MPSII mice that received either AAV9-Null or AAV9-*Ids* vectors at the age of 2 months. Each row represents a gene and each column represents an animal. The expression of each gene is represented relative to the mean abundance of that gene across all samples in a colour scale in which red and green indicate, respectively, transcript levels above and below the mean. The magnitude of deviation from the mean is represented by the degree of colour saturation. The dendrogram of samples shown above the matrix represents overall similarities in transcript levels. Visibly, the profile of gene expression in MPSII animals treated by intra-CSF delivery of AAV9-*Ids* vectors resembled that of healthy, age-matched WT littermates.

## 2.3. Evaluation of the efficacy of intra-CSF AAV9-*Ids* gene therapy on somatic pathology

### *2.3.1. IDS activity and GAG content in somatic tissues*

Previous studies reported by our laboratory demonstrated that after AAV9 vector administration to the cisterna magna, a portion of the delivered vector leaked to the circulation, which resulted in detection of vector genomes in somatic organs, mainly the liver, indicating that this organ had taken up the majority of the vectors (Haurigot et al., 2013). When AAV9-*Ids* vectors were administered to the CSF of MPSII mice at the dose of $5x10^{10}$vg/mouse, vector genomes and *Ids* expression were detected mainly in the liver (Figure 23), confirming our previous observation in other animal models. The liver can be an important source of circulating proteins. When the liver expresses secretable lysosomal enzymes, their enzymatic activity increases in serum, allowing for the correction of the disease in somatic organs by cross-correction (Haurigot et al., 2013; Ribera et al., 2015).

To determine whether the intra-CSF delivery of AAV9-*Ids* vectors to 2-month-old MPSII mice had any effect on somatic pathology, the enzymatic activity of Iduronate-2-sulfatase was measured in serum and in samples from several peripheral tissues, such as liver, lung and heart (Figure 37). At 6 months of age, i.e. 4 months after vector delivery, untreated and AAV9-Null-treated MPSII mice presented almost undetectable IDS activity in liver, serum, lung and heart (Figure 37). IDS activity was noticeably increased in liver (Figure 37A) and serum (Figure 37B). IDS activity was also increased in lung (Figure 37C) and was particularly high in heart (Figure 37D).

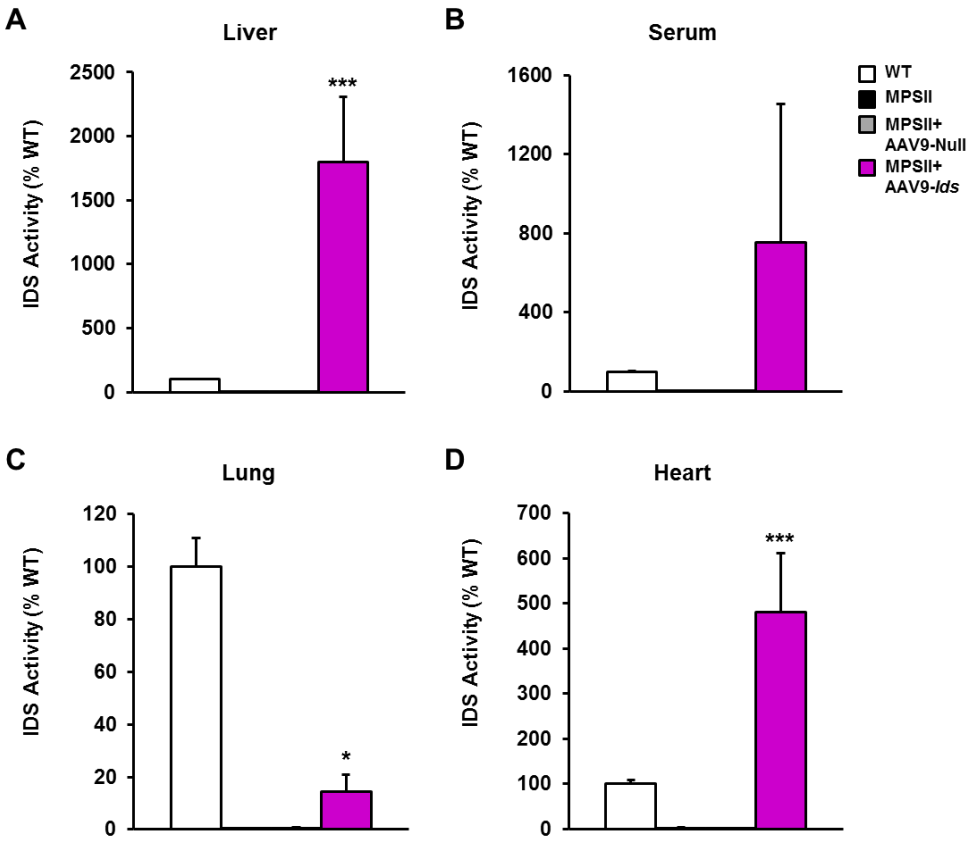


**Figure 37. Restoration of IDS activity in the periphery 4 months after intra-CSF AAV9-*Ids* delivery to MPSII mice**. Measurement of IDS activity in (**A**) liver, (**B**) serum, (**C**) lung and (**D**) heart of healthy wild-type (WT), untreated MPSII (MPSII) and MPSII mice injected in the CSF at 2 month Of age with either $5x10^{10}$ vg/mouse of Null vector (MPSII+AAV9-Null) or an equivalent dose of the therapeutic vector (MPSII+AAV9-*Ids*). Activity is expressed as % of WT activity, which was set to 100%. Administration of AAV9-*Ids* to the CSF of MPSII mice increased IDS activity in the liver, serum, lung and heart, whereas IDS activity was almost undetectable in untreated or Null-injected MPSII animals. Values are shown as mean ± SEM of 4-5 animals/group. **P*<0.05 and ****P*<0.001 *vs.* MPSII+AAV9-Null.

To determine the origin of the IDS activity detected in liver, lung and heart, vector genome copy number were measured in these organs (Table 6). Liver presented around 0.25 vector genomes/diploid genome (vg/dg), whereas lung and heart showed very low values, <0.007 vg/dg (Table 6), indicating lack of efficient transduction of these two organs following intra-CSF delivery of $5x10^{10}$ vg of AAV9-*Ids*. Hence, these results suggested cross-correction of IDS deficiency in lung and heart by uptake of IDS from circulation.

**Table 6. Vector genome copy numbers in somatic tissues 4 months after intra-CSF delivery of AAV9-*Ids* to MPSII mice**

| | Vector genome copy number/ diploid genome (vg/dp) | | | | | | |
|---|---|---|---|---|---|---|---|
| | Untreated MPSII | AAV9-*Ids*-treated MPSII | | | | | |
| | 1 | 1 | 2 | 3 | 4 | 5 | Mean ± SEM |
| **Liver** | 0.002 | 0.401 | 0.073 | 0.159 | 0.195 | 0.384 | **0.243 ± 0.064** |
| **Lung** | 0.002 | 0.004 | 0.003 | 0.004 | 0.003 | 0.005 | **0.004 ± 0.000** |
| **Heart** | 0.002 | 0.007 | 0.007 | 0.006 | 0.007 | 0.005 | **0.006 ± 0.000** |

Data represent 1 individual untreated MPSII mouse and the mean of 5 individual MPSII mice treated with $5x10^{10}$ vg of AAV9-*Ids* vectors. Samples were obtained 4 months after intra-CSF administration of vectors.

At 6 months of age, i.e. 4 months after gene transfer, GAG content was measured in several somatic tissues in order to evaluate whether the treatment with AAV9-*Ids* vectors delivered to the CSF of MPSII mice reverted the pathological storage of GAGs in the periphery. The circulating levels of IDS were sufficient to greatly reduce and, in the case of liver, spleen, heart, lung, testis, adipose tissue and skeletal muscle completely correct pathological GAG accumulation in AAV9-*Ids*-treated MPSII mice (Figure 38).

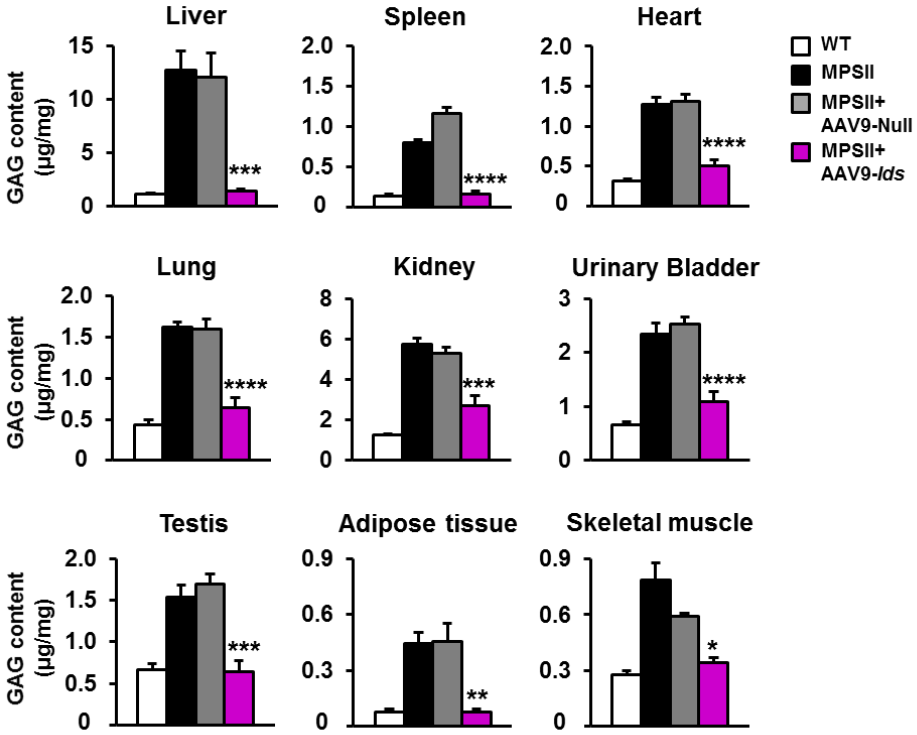


**Figure 38. Correction of GAG storage in somatic tissues of MPSII mice 4 months after intra-CSF delivery of AAV9-*Ids*.** Quantification of GAG content in several somatic tissues of healthy wild-type (WT), untreated MPSII (MPSII) and MPSII mice injected at 2 months of age in the CSF with either $5x10^{10}$ vg/mouse of Null vector (MPSII+AAV9-Null) or the therapeutic vector (MPSII+AAV9-*Ids*). Administration of AAV9-*Ids* to the CSF resulted in completely correction of GAG storage in almost all somatic tissues analysed. Values are shown as mean ± SEM of 4-5 animals/group. **P*<0.05, ***P*<0.01, ****P*<0.001 and *****P*<0.0001 *vs.* MPSII+AAV9-Null.

### *2.3.2. Lysosomal pathology in somatic tissues*

To study the effect of the intra-CSF AAV9-*Ids* treatment on the size of the lysosomal compartment in somatic tissues, immunohistochemistry for the lysosomal marker LAMP1 was performed in paraffin-embedded sections of liver, heart and lung (Figure 39). LAMP1 staining revealed a marked reduction in the size of the lysosomal compartment in peripheral tissues of AAV9-*Ids*-treated MPSII mice 4 months after gene transfer, whose samples showed a LAMP1 signal intensity that resembled that of WT counterparts (Figure 39).

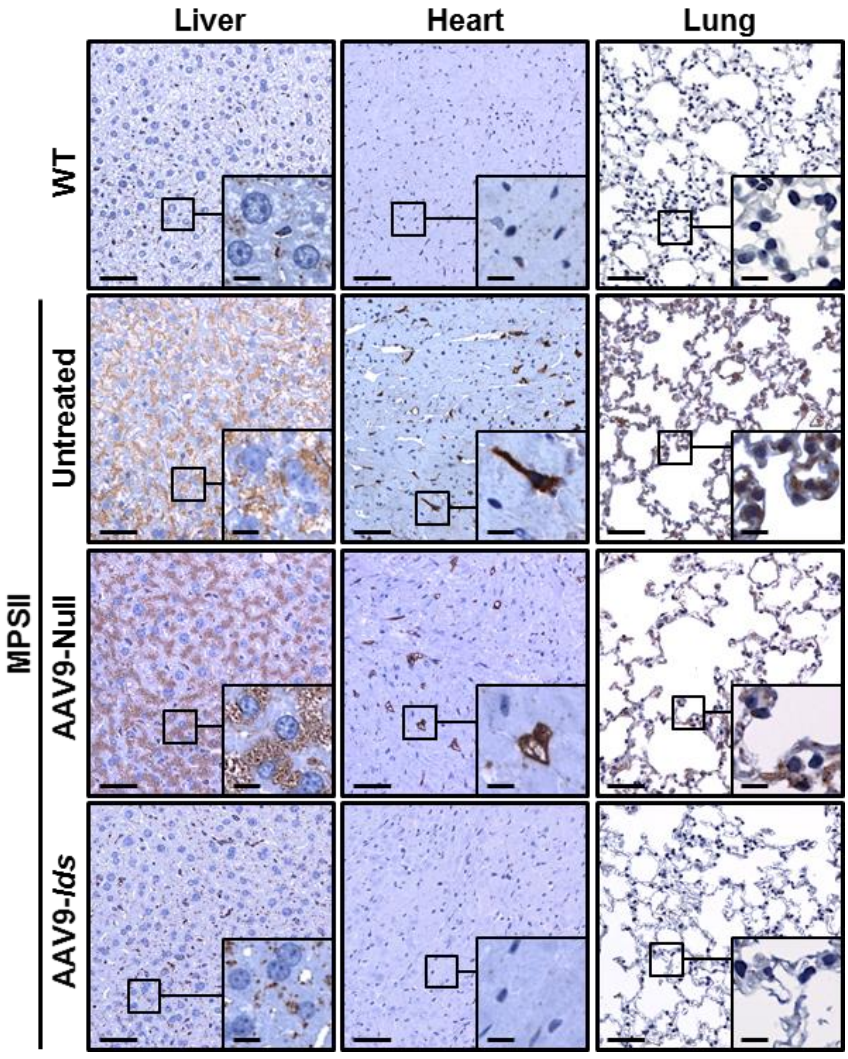


**Figure 39. Correction of the size of the lysosomal compartment in somatic tissues of MPSII mice 4 months after the intra-CSF delivery of AAV9-*Ids*.** Representative micrographs of LAMP1 immunostaining in liver, heart and lung tissue sections from healthy wild-type (WT), untreated MPSII (MPSII) and MPSII mice injected at 2 month of age in the CSF with either $5x10^{10}$ vg/mouse of Null vector (MPSII+AAV9-Null) or an equivalent dose of the therapeutic vector (MPSII+AAV9-*Ids*). Samples were obtained 4 months after gene transfer. Administration of AAV9-*Ids* intra-CSF clearly reduced the size of the lysosomal compartment in all somatic tissues analysed. Scale bars are 50 µm, and 10 µm for insets.

The efficacy of the intra-CSF delivery of AAV9-*Ids* vectors in treating somatic pathology was further confirmed by analysing by TEM the ultrastructure of several somatic tissues 4 months after gene transfer (Figure 40). Null-injected MPSII mice aged 6 months showed a large number of electrolucent vacuoles within hepatocytes (Figure 40, middle row). These storage vesicles provably accumulated undegraded HS, DS as well as other compounds (Resnick et al., 1994). Larger and more distended storage vesicles were observed in the cytoplasm of Kupffer cells, in ciliated cells of the pulmonary bronchus and in macrophage-like cells located around blood vessels of the myocardium or interspersed between cardiomyocites in the same group of animals (Figure 40, middle row). On the contrary, the cells of the liver, lung and heart of AAV9-*Ids*-treated MPSII mice showed no storage lesions (Figure 40, bottom row), and presented an aspect very similar to that oberved in healthy WT littermates (Figure 40, top row).

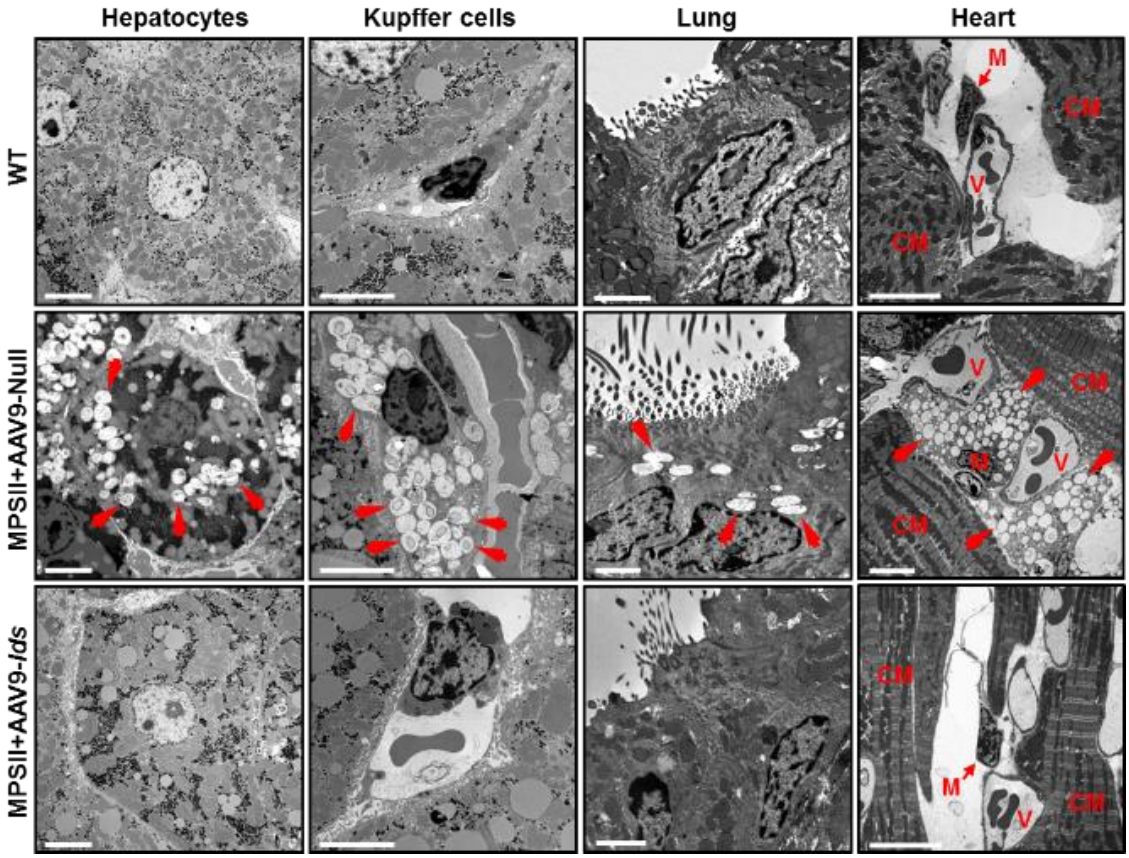


**Figure 40. Analysis of the ultrastructure of the liver, lung and heart in MPSII mice 4 months after intra-CSF delivery of AAV9-*Ids*.** Representative images of the ultrastructural analysis of hepatocytes and Kupffer cells of the liver, lung and heart performed by TEM in wild-type (WT) or MPSII mice treated with either Null vector (MPSII+AAV9-Null) or therapeutic vector (MPSII+AAV9-*Ids*). Samples were obteined 4 months after intra-CSF administration of vectors. AAV9-*Ids*-treated MPSII mice showed an evident reduction in the size and number of intracytoplasmic electrolucent vacuoles (indicated with red arrows) in all different tissues analysed. CM, Cardiac Myocite; V, Blood Vessel; M, Macrophage-like cell. N=3. Scale bars are 5 µm for hepatocytes and Kupffer cells, 2 µm for lung and 10 µm for heart.

### *2.3.3. Liver pathology and lysosomal functionality*

To further confirm the correction of somatic disease in MPSII mice after gene transfer, hepatomegaly was evaluated by measuring the weight of the liver (Figure 41). In agreement with the normalization of hepatic GAG content, the liver weight of AAV9-*Ids*-treated MPSII mice was similar to that of healthy WT counterparts, suggesting the AAV9-*Ids*-mediated correction of the hepatomegaly characteristic of MPSII (Figure 41).

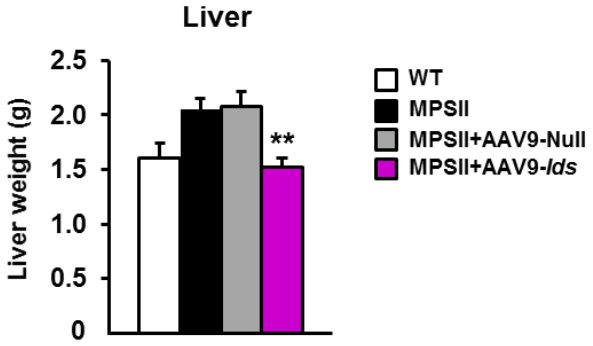


**Figure 41. Correction of hepatomegaly in MPSII mice 4 months after intra-CSF delivery of AAV9-*Ids*.** Wet weight of the liver of healthy wild-type (WT), untreated MPSII (MPSII) and MPSII mice injected at 2 month of age in the CSF with either $5x10^{10}$ vg/mouse of Null vector (MPSII+AAV9-Null) or the therapeutic vector (MPSII+AAV9-*Ids*). Intra-CSF administration of AAV9-*Ids* intra-CSF resulted in normalization of liver weight in MPSII mice. Values are shown as mean ± SEM of 14-22 animals/group. ***P*<0.01 *vs.* MPSII+AAV9-Null.

The activities of several lysosomal hydrolases different from the IDS were also measured in liver extracts to assess lysosomal homeostasis in this organ. Similar to the observations made in the encephalon, the activity of IDUA, NAGLU, HGSNAT, GALNS, GUSB and β-HEXO were altered in the liver of untreated and AAV9-Null-treated MPSII mice aged 6 months (Figure 42). This lysosomal dysfunction was completely corrected following intra-CSF delivery of AAV9-*Ids* vectors to MPSII mice (Figure 42), providing further evidence of the restoration of lysosomal homeostasis in the liver of treated animals.

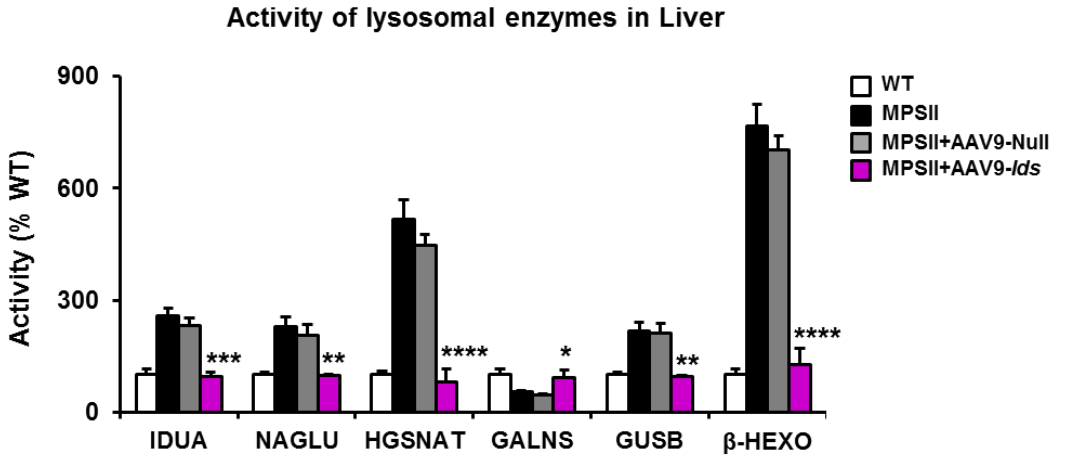


**Figure 42. Restoration of lysosomal homeostasis in the liver of MPSII mice 4 months after intra-CSF delivery of AAV9-*Ids***. Measurement of the activity of other lysosomal enzymes different from IDS analysed in brain extracts 4 months after gene transfer. Intra-CSF delivery of AAV9-*Ids* vectors restored the activities of α-L-Iduronidase (IDUA), α-N-Acetylglucosaminidase (NAGLU), Heparan α-glucosaminide N-acetyltransferase (HGSNAT), N-Acetylgalactosamine-6-sulfate-sulfatase (GALNS), β-Glucoronidase (GUSB) and β-hexosaminidase (β-HEXO) in the liver of healthy wild-type (WT), untreated MPSII (MPSII) and MPSII mice injected in the CSF with either Null vector (MPSII+AAV9-Null) or therapeutic vector (MPSII+AAV9-*Ids*). Activities are expressed as % of WT activity, which was set to 100%. Results are shown as mean ± SEM of 4-5 animals per group. **P*<0.05, ***P*<0.01, ****P*<0.001, and *****P*<0.0001 *vs.* MPSII+AAV9-Null.

The activity of β-hexosaminidase was also measured in serum of healthy wild-type, untreated MPSII and MPSII mice that received either AAV9-Null or AAV9-*Ids* vectors (Figure 43). At 6 months of age, serum β-HEXO activity was increased in untreated and MPSII-Null-treated mice as a consequence of lysosomal pathology (Figure 43). On the contrary, a complete normalization of serum β-HEXO activity was observed in AAV9-*Ids*-treated MPSII mice (Figure 43), providing evidence of whole-body correction of lysosomal functionality.

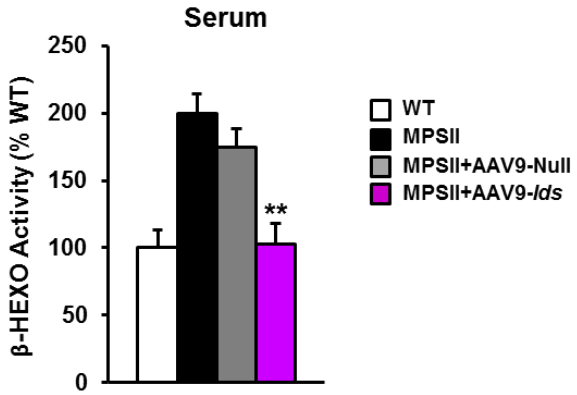


**Figure 43. Restoration of lysosomal functionality in MPSII mice 4 months after intra-CSF delivery of AAV9-*Ids***. Measurement of the activity of β-hexosaminidase (β-HEXO) in serum of healthy wild-type (WT), untreated MPSII (MPSII) and MPSII mice injected to the CSF with either Null vector (MPSII+AAV9-Null) or therapeutic vector (MPSII+AAV9-*Ids*). Activity is expressed as % of WT activity, which was set to 100%. Intra-CSF AAV9-*Ids* administration resulted in correction of β-HEXO activity in serum. Results are shown as mean ± SEM of 4-5 animals per group. ***P*<0.01 *vs.* MPSII+AAV9-Null.

## 2.4. Functional evaluation of the efficacy of intra-CSF AAV9-*Ids* gene therapy

### *2.4.1. Assessment of behaviour*

Hunter patients suffer from behavioural alterations, including hyperactivity and aggressiveness at initial stages of the disease, followed by hypoactive behaviour at later stages (Holt et al., 2011). Therefore, the impact of AAV9-*Ids* treatment on behaviour was evaluated 4 months after gene delivery with the Open Field test in naïve-tested MPSII mice that received either AAV9-Null or AAV9-*Ids* vectors together with age-matched wild-type and untreated MPSII mice. Untreated and Null-injected MPSII mice displayed reduced locomotor and exploratory activity when compared with age-matched healthy wild-type littermates, as evidenced by the reduced number of entries in the centre of the arena, reduced crossing of demarcated lines between the different areas and reduced total movements (Figure 44). Moreover, untreated and Null-injected MPSII mice showed anxiety-related behaviour, as they took longer to enter to centre of the arena for the first time, and spent less time in the centre region and more time in the periphery (Figure 44). Intra-CSF delivery of AAV9-*Ids* vectors completely corrected these behavioural deficits (Figure 44); there were no statistical differences in any of the parameters analysed between WT and AAV9-*Ids*-teated MPSII mice.

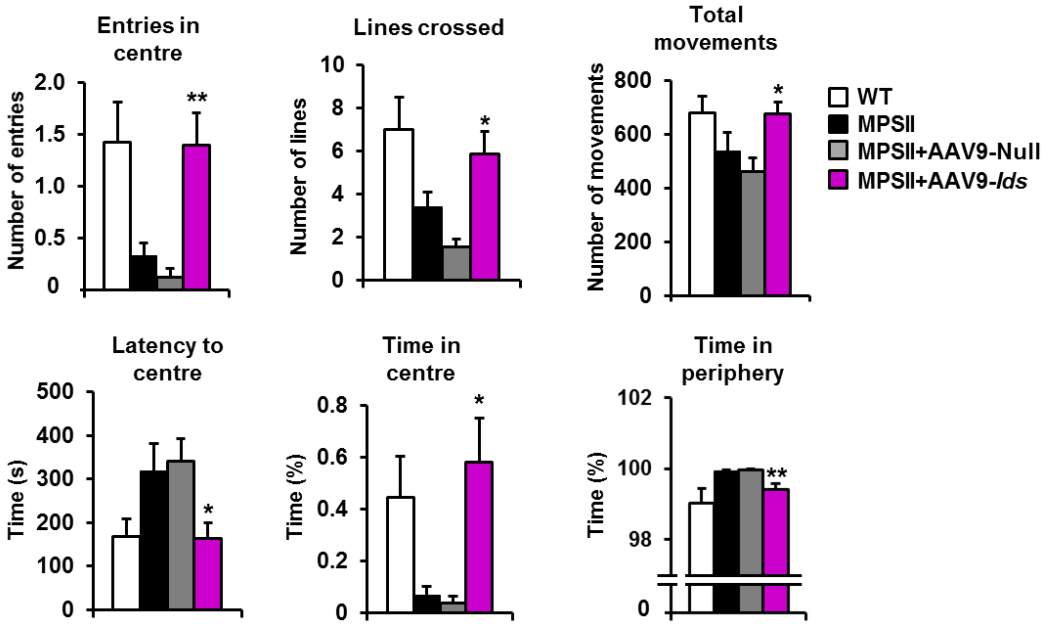


**Figure 44. Correction of behavioural alterations in MPSII mice 4 months after intra-CSF delivery of AAV9-*Ids***. Results of the Open Field test performed in naïve-tested healthy wild-type (WT), untreated MPSII (MPSII) and MPSII mice injected in the CSF with either Null vector (MPSII+AAV9-Null) or therapeutic vector (MPSII+AAV9-*Ids*). Histograms represent the mean ± SEM obtained during the first 3 minutes of recording for each parameter in groups of 16-22 animals/cohort. **P*<0.05 and ***P*<0.01 *vs.* MPSII+AAV9-Null.

### *2.4.2. Study of the impact of the gene therapy treatment on survival*

A survival study was performed to determine whether AAV9-*Ids* treatment had any effect on the lifespan of MPSII mice. Whilst at 17 months of age all untreated or Null-treated MPSII mice were dead, 76% of MPSII mice that received AAV9-*Ids* vectors were alive (Figure 45). Moreover, 65% of AAV9-*Ids*-treated MPSII mice were still alive at 22 months of age, whereas the % of wild-type animals alive at this age was 79% (Figure 45). Hence, the intra-CSF administration of AAV9-*Ids vectors* considerably prolonged the survival of MPSII mice.

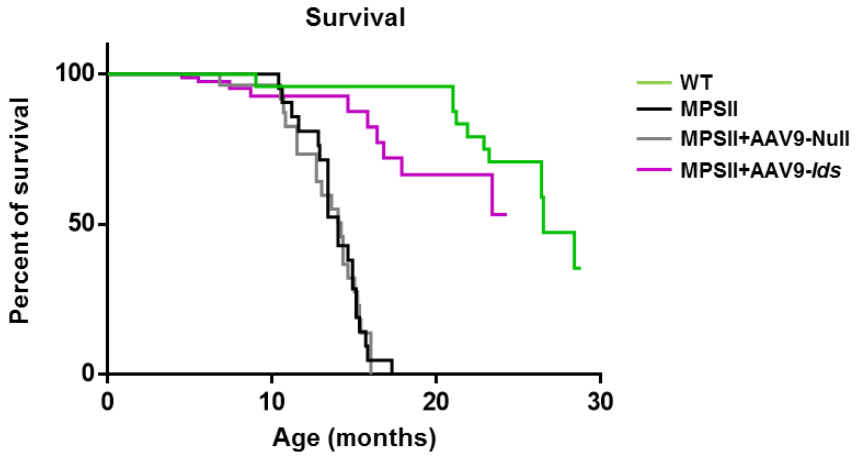


**Figure 45. Prolonged survival in MPSII mice after intra-CSF delivery of AAV9-*Ids***. Kaplan-Meier analysis of survival in healthy wild-type (WT), untreated MPSII (MPSII) and MPSII mice injected in the CSF with either Null vector (MPSII+AAV9-Null) or therapeutic vector (MPSII+AAV9-*Ids*). *Ongoing study*. The median survival of untreated MPSII and Null-treated MPSII mice was 14 and 14.2 months, respectively. In contrast, wild-type mice presented a median survival of 26.5 months. The median survival of AAV9-*Ids*-treated MPSII mice, however, could not be calculated because more than 50% of animals of this cohort were still alive. Analysis based on data from 24 WT, 22 untreated MPSII, 27 Null-treated MPSII and 91 AAV9-*Ids*-treated MPSII male mice. $P<0.0001$ for MPSII+AAV9-*Ids vs.* MPSII+AAV9-Null.

Altogether, these results provided evidence of simultaneous and long-term correction of neurological and systemic MPSII disease by administration of AAV9-*Ids* vectors directly to the CSF.

# PART III. Pre-clinical studies for the clinical translation of the intra-CSF AAV9-*Ids* gene therapy

As a first step in the translation of the intra-CSF AAV9-*Ids* gene therapy approach to the clinic, the third part of this work was centred on studying the therapeutic efficacy of AAV9 vectors encoding for human IDS in the MPSII mouse model.

## 1. VALIDATION OF THE HUMAN IDS-CODING CONSTRUCTS

Three different plasmids encoding for human IDS were generated (Figure 46). As with the murine IDS-coding constructs, the first engineered construct contained the wild-type human *IDS* CDS, while the other two constructs contained different optimized version of the human *IDS* CDS. As in *Part II* of the present work, the expression of all transgenes was under the control of the ubiquitous hybrid promoter CAG.

The functionality of the three constructs was evaluated in adult MPSII mice. A total dose of 30 µg of the plasmids pAAV-CAG-h*IDS*, pAAV-CAG-oh*IDS*-v1 and pAAV-CAG-oh*IDS*-v2 containing different versions of the *Iduronate-2-sulfatase* expressing cassette were administered to 3-month-old MPSII-affected mice via hydrodynamic tail vein injection. As a control of the technique, non-injected wild-type mice and MPSII mice injected with saline solution were used. One week after plasmid delivery, animals were sacrificed and tissues were harvested (Figure 46B).

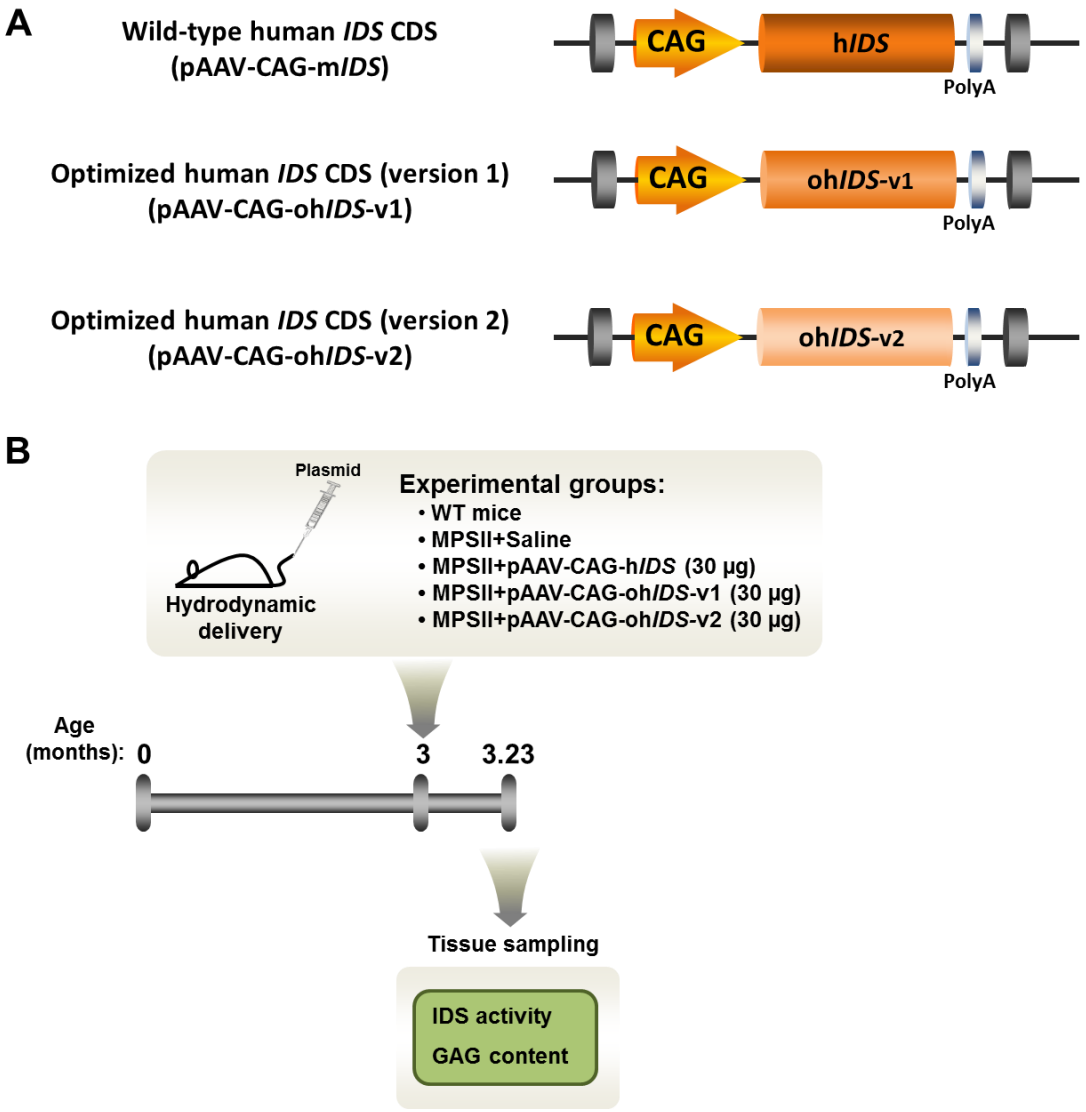


**Figure 46. Experimental design for the study of the plasmids containing human IDS-coding sequences.** (**A**) Schematic representation of the three generated constructs that contained the human *IDS* coding sequence (CDS)**.** The first plasmid contained the human wild-type *IDS* CDS, while the second and the third plasmid encoded for optimized versions of the human *IDS* CDS. CAG, hybrid CAG promoter. The schematic representation is not to scale. (**B**) Experimental design for the hydrodynamic administration of plasmids containing human IDS-encoding sequence to 3-month-old MPSII male mice. IDS activity and GAG content were evaluated 1 week after plasmid delivery.

Iduronate-2-sulfatase activity was measured in liver protein extracts and serum samples. All three Iduronate-2-sulfatase-containing plasmids mediated a substantial increase in IDS activity in comparison to MPSII animals that received saline injection (Figure 47). IDS activity in plasmid-injected MPSII mice ranged from 1200% to 2200% of WT levels in liver and from 2000% to 5700% of WT levels in serum (Figure 47). Noteworthy, the levels of IDS activity reached with the expression cassettes containing optimized versions of the *IDS* coding sequence were statistically higher than those mediated by the plasmid containing the wild-type *IDS* CDS (Figure 47).

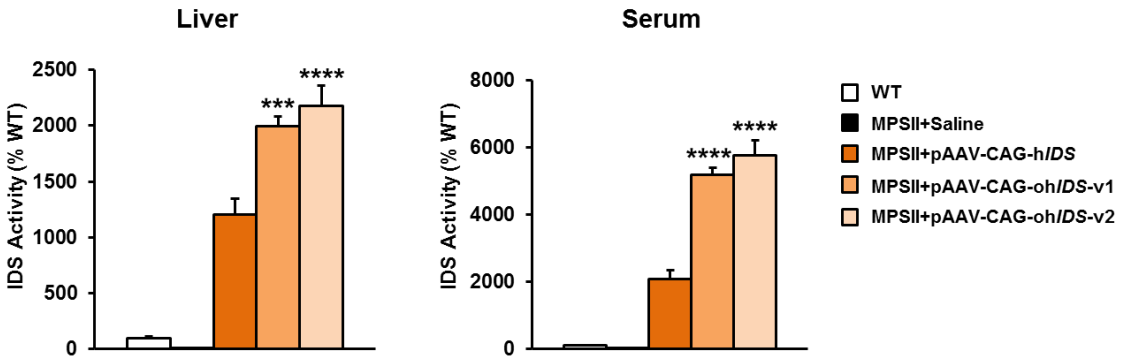


**Figure 47. IDS activity in liver and serum after hydrodynamic delivery of plasmids containing human IDS-coding sequences to adult MPSII mice.** Measurement of IDS activity in liver extracts and serum samples 1 week after the administration of the plasmids. Wild-type (WT) and saline-injected MPSII (MPSII+Saline) mice were used as controls. IDS activity of WT mice was set to 100%. IDS activity considerable increased over basal levels in both liver and serum 1 week after human IDS-encoding plasmid delivery. Data are shown as mean ± SEM of 5 animals/group. ***$P$<0.001 and ****$P$<0.0001 *vs.* MPSII+pAAV-CAG-h*IDS*.

In agreement with the high levels of IDS activity observed in liver and serum, the content of GAGs of MPSII mice that received any of the human IDS-coding plasmids was completely normalized in several somatic organs (Figure 48). In this case, however, no differences were observed between the different IDS-coding sequences likely because all constructs mediated the production of sufficient amount of IDS to overcome the threshold of activity necessary for full correction of pathological storage (Figure 48).

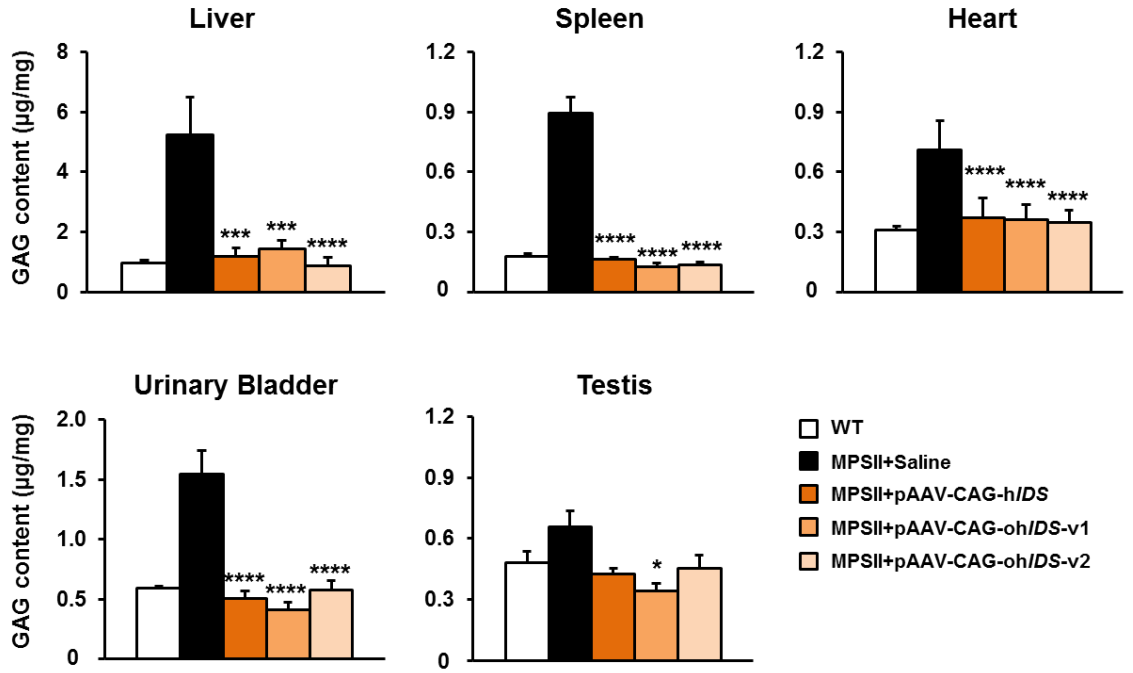


**Figure 48. GAG content after hydrodynamic delivery of IDS-containing plasmids to adult MPSII mice.** Quantification of the amount of GAGs in liver, spleen, heart, urinary bladder and testis 1 week after the administration of the plasmids. Wild-type (WT) and saline-injected MPSII (MPSII+Saline) mice were used as controls. All three human IDS-containing plasmids resulted in complete normalization of the pathological GAG accumulation observed in untreated MPSII mice. Data are shown as mean ± SEM of 5 animals/group. *$P$<0.05, ***$P$<0.001 and ****$P$<0.0001 *vs.* MPSII+pAAV-CAG-h*IDS*.

## 2. VALIDATION OF THE HUMAN IDS-CODING AAV VECTORS

To further analyse the functionality of human *IDS* baring constructs in MPSII mice, AAV9 vectors containing the wild-type, the optimized version1 or the optimized version2 of the human *IDS* sequences were generated (Figure 49A). MPSII mice aged 2 months received an intra-CSF injection of $5x10^{10}$ vg of AAV9 vectors containing either the wild-type or one of the optimized human *IDS* sequences. Separate cohorts of age-matched wild-type, untreated MPSII mice and MPSII mice receiving $5x10^{10}$ vg of a non-coding vector (AAV9-CAG-Null) were used as controls. At 3.5 months of age, i.e. 1.5 months after vector delivery, animals were sacrificed and samples were collected and analysed (Figure 49B).

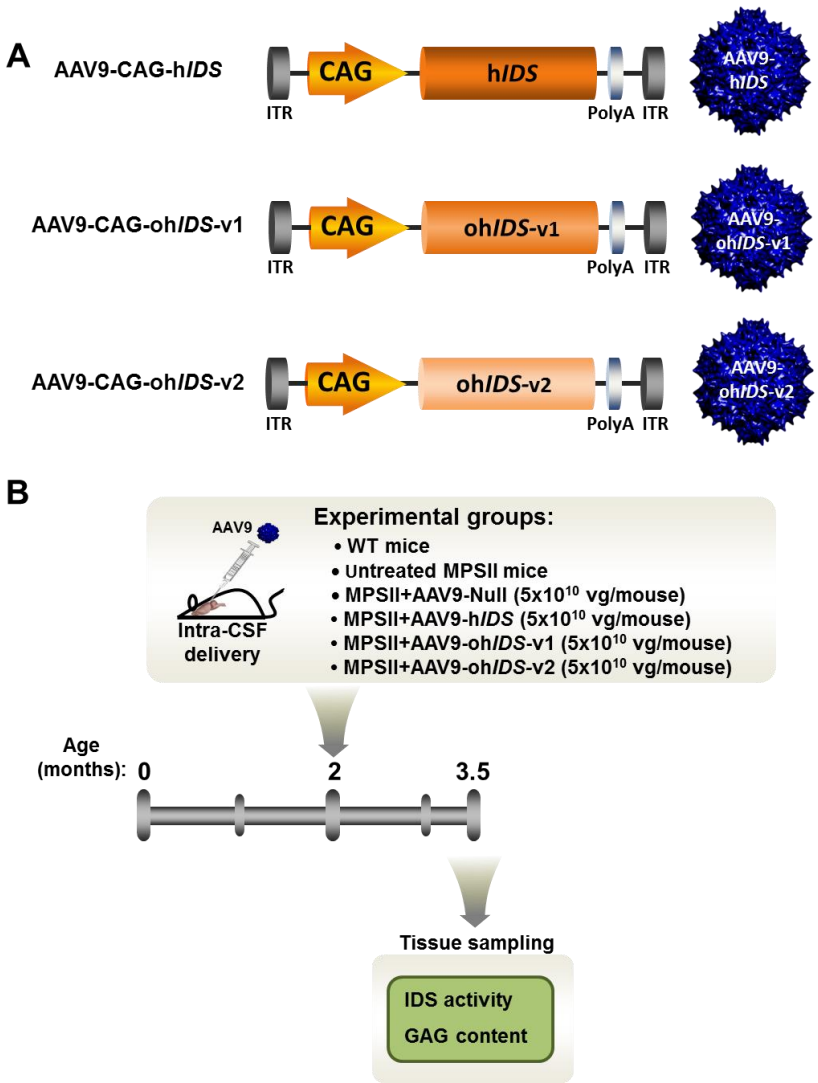


**Figure 49. Experimental design for the study of the AAV9 vectors containing human *IDS*-coding sequences.** (**A**) Schematic representation of the modified genome of adeno-associated virus serotype 9 vector containing the wild-type, the optimized version1 or the optimized version2 of the human *IDS* coding sequence and the polyA from the rabbit β-globin gene. CAG, hybrid CAG promoter. ITR, inverted terminal repeats. The schematic representation is not to scale. (**B**) Experimental design for the intra-CSF administration of AAV9 vectors containing human IDS-coding sequence to 2-month-old MPSII male mice. The therapeutic efficacy was evaluated 1.5 months after vector delivery.

A clear increase in IDS enzymatic activity was detected throughout the encephalon of MPSII mice treated with any of the human *IDS*-coding vectors (Figure 50A). This increase was, however, several folds higher in the case of the MPSII animals that received the AAV9 vectors containing optimized human *IDS* sequences than in those MPSII animals treated with wild-type human *IDS*-containing vectors (Figure 50A).

In agreement with the increase in IDS activity measured in brain, the accumulation of GAGs in the encephalon characteristic of MPSII disease was reduced in treated MPSII mice (Figure 50B). A complete normalization of GAG levels was achieved with all three *IDS*-coding constructs in all brain regions analysed, except for section V in which the reduction mediated by the wild-type *IDS*-containing vectors was not statistically significant (Figure 50B).

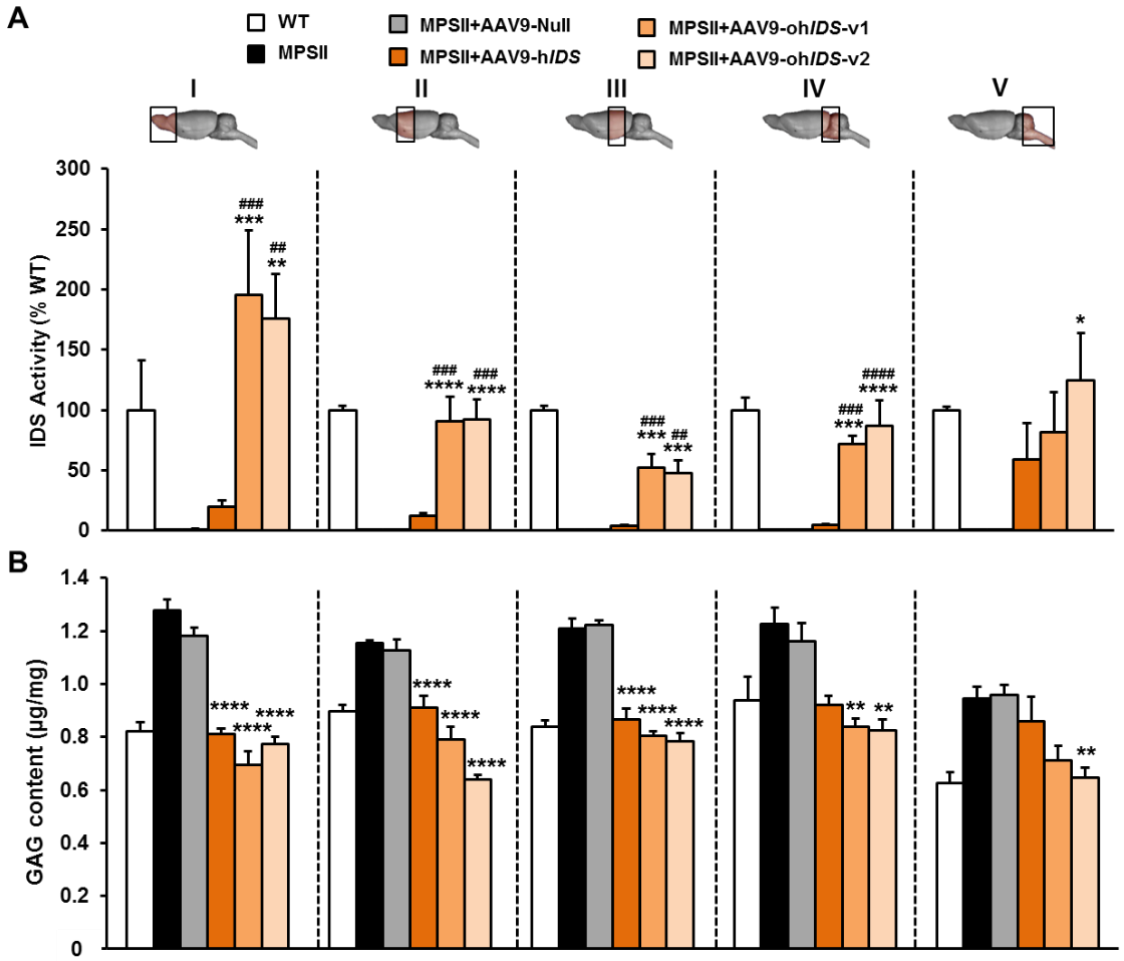


**Figure 50. Restoration of IDS activity and normalization of GAG content in MPSII mice after intra-CSF delivery of hIDS-encoding vectors**. MPSII mice aged 2 months were injected in the CSF with $5x10^{10}$ vg of AAV9 vectors encoding wild-type human *IDS* (AAV9-h*IDS*) or two different versions of optimized human *IDS* (AAV9-oh*IDS*-v1 and AAV9-oh*IDS*-v2). Wild-type (WT), untreated MPSII (MPSII) and MPSII mice administered with non-coding (Null) AAV9 vectors (MPSII+AAV9-Null) were used as controls. (**A**) Measurement of IDS activity in different parts of the brain (sections I to V as indicated in the diagram above the plot) analysed 1.5 months after vector delivery. IDS activity of WT mice was set to 100%. (**B**) Quantification of GAG content in the same animal cohorts and in the same regions of the brain as in (A). Results are shown as mean ± SEM of 5 mice per group. **P*<0.05, ***P*<0.01, ****P*<0.001 and *****P*<0.0001 *vs.* MPSII+AAV9-Null. $^{\#\#}P$<0.01, $^{\#\#\#}P$<0.001 and $^{\#\#\#\#}P$<0.0001 *vs.* MPSII+AAV9-h*IDS*.

When the effects of the human *IDS*-encoding vectors were evaluated at somatic level, a marked increase in IDS activity was observed in the liver of MPSII mice treated with any of the human *IDS*-encoding vectors (Figure 51). The increase was, again, significantly higher in the case of the MPSII animals that received the AAV9 vectors containing optimized human *IDS* sequences than in those MPSII animals treated with the wild-type *IDS*-coding vectors (Figure 51). In serum, only vectors carrying optimized versions of the transgene gave rise to quantificable increase in circulating IDS activity (Figure 51).

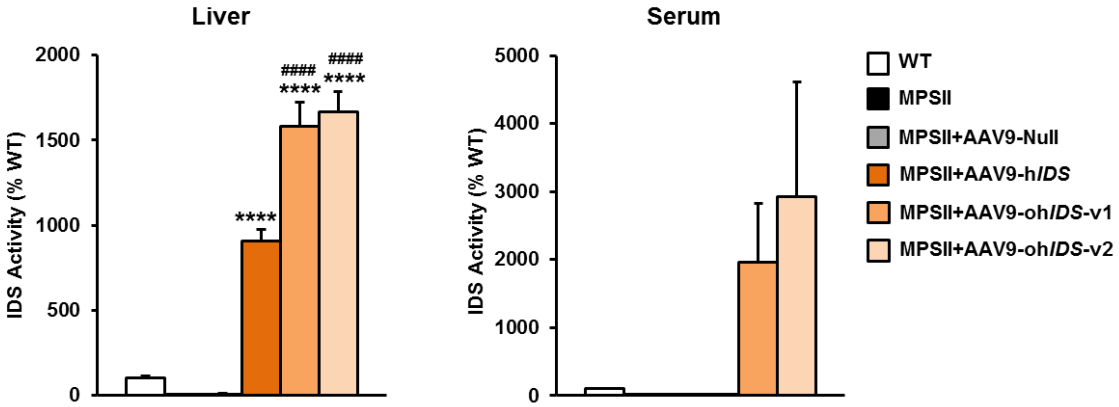


**Figure 51. Restoration of IDS activity in liver and serum in MPSII mice after intra-CSF delivery of hIDS-encoding vectors.** MPSII mice aged 2 months were injected in the CSF with $5x10^{10}$ vg of AAV9 vectors encoding wild-type human *IDS* (AAV9-h*IDS*) or two different versions of optimized human *IDS* (AAV9-oh*IDS*-v1 and AAV9-oh*IDS*-v2). Wild-type (WT), untreated MPSII (MPSII) and MPSII mice administered with non-coding (Null) AAV9 vectors (MPSII+AAV9-Null) were used as controls. Measurement of IDS activity in liver and serum 1.5 months after vector delivery. IDS activity of WT mice was set to 100%. Results are shown as mean ± SEM of 5 mice per group. ****$P$<0.0001 *vs.* MPSII+AAV9-Null. ####$P$<0.0001 *vs.* MPSII+AAV9-h*IDS*.

The quantification of the GAG content in different somatic organs revealed a full normalization of GAG levels in all tissues analysed of MPSII mice treated with any of the optimized human *IDS*-coding sequences (Figure 52). The wild-type human *IDS*-coding vector, however, resulted in a complete reversion of the pathological GAG accumulation in liver, heart, lung and spleen, but only a partial correction in testis, kidney, urinary bladder and adipose tissue (Figure 52). This observation was in agreement with the lower IDS activity recorded in animals treated with vectors carrying the wild-type human *IDS* coding sequence.

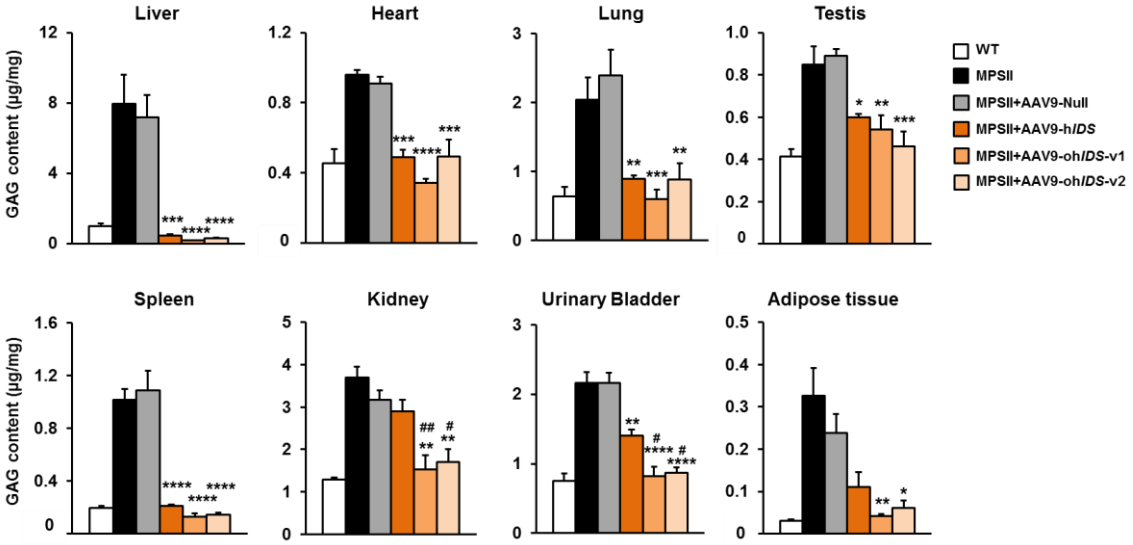


**Figure 52. Normalization of GAG accumulation in somatic tissues of MPSII mice after intra-CSF delivery of hIDS-encoding vectors.** MPSII mice aged 2 months were injected to the CSF with $5x10^{10}$ vg of AAV9 vectors encoding wild-type human *IDS* (AAV9-h*IDS*) or two different versions of optimized human *IDS* (AAV9-oh*IDS*-v1 and AAV9-oh*IDS*-v2). Wild-type (WT), untreated MPSII (MPSII) and MPSII mice administered with non-coding (Null) AAV9 vectors (MPSII+AAV9-Null) were used as controls. Measurement of GAG content in several somatic tissues 1.5 months after vector delivery. Results are shown as mean ± SEM of 5 mice per group. **P*<0.05, ***P*<0.01, ****P*<0.001 and *****P*<0.0001 *vs.* MPSII+AAV9-Null. $^{\#}P$<0.05 and $^{\#\#}P$<0.01 *vs.* MPSII+AAV9-h*IDS*.

Therefore, the observation of an increase of IDS activity and, consequently, a reduction or full normalization of pathological GAG accumulation at both CNS and somatic level in MPSII mice confirmed the functionality of the vectors carrying the human IDS transgene. These results highlighted the potential of this gene therapy approach for the treatment of MPSII based on the use of adeno-associated virus vectors of serotype 9 encoding for the human *IDS* gene and supported its clinical translation to MPSII patients.

# V. DISCUSSION

The treatment of the neurodegenerative disease, that characterizes the most severe and frequent form of MPSII, represents a highly unmet medical need and a therapeutic challenge. With the advent of ERT, came the possibility of correcting IDS deficiency through administration of recombinant enzyme. ERT is already commercially available for the treatment of MPSII. However, the delivery of proteins to the CNS has challenges and shortcomings. In a recent phase I/II clinical trial, monthly intrathecal ERT resulted in drastic and likely clinically meaningful reductions in CSF GAGs, but half of the patients involved in the study required surgical intervention due to problems with the device implanted to provide the enzyme, which included device dislocation, breakage, malfunction or implant site infection (Muenzer et al., 2015). On the other hand, although BMT offers therapeutic benefit to patients affected by other forms of MPS, such as MPSI, it does not improve the neurological outcome of MPSII patients with severe phenotype (Vellodi et al., 1999; Seto et al., 2001; Prasad and Kurtzberg 2010). Given these limitations, the main objective of this thesis was to develop a new effective therapeutic option for MPSII that directly address the CNS pathology of the severe phenotype of the disease. To this end, AAV9 vectors encoding IDS were administered through a minimally invasive procedure to the cerebrospinal fluid of MPSII mice. The results described in the present work provide evidence of the therapeutic efficacy of this approach to treat not only neurologic but also somatic pathology in MPSII animals with already established disease.

Previous attempts to treat neurologic MPSII disease with AAV vectors tested systemic vector delivery to achieve supraphysyological concentrations of circulating IDS (Cardone et al., 2006; Polito and Cosma, 2009). This strategy was based on earlier work with ERT for different forms of LSDs that suggested that when high levels of lysosomal enzyme were present in the bloodstream, a portion of the protein managed to cross the BBB (Vogler et al., 2005; Ou et al., 2014). Cardone *et al.* combined the capsid of adeno-associated virus serotype 8 vectors -a serotype with high tropism for hepatocytes (Wu et al., 2006)- and the thyroxin-binding globulin (TBG) promoter to drive the expression of IDS specifically to the liver. Following intravenous administration of $4x10^{12}$ vg/kg of recombinant AAV8-TBG-*IDS* vectors to adult MPSII mice, IDS activity in plasma was 16 to 70 fold higher than in WT counterparts, leading to complete correction of somatic disease (Cardone et al., 2006). However, the efficacy of the treatment on neurological pathology was limited, with only partial reduction of GAG accumulation observed in brain (Cardone et al., 2006), likely due to the small fractional amount of IDS that crossed the BBB despite

the high concentration of circulating enzyme. Similar observations have been reported in the MPSIIIA mouse model, in which the liver-targeted expression of the enzyme SGSH was insufficient to provide neurological benefit despite the high levels of enzyme in serum (Ruzo et al., 2012a). The same group that tested the AAV8-TBG-*IDS* approach later evaluated the intravenous administration of AAV5 vectors encoding for *IDS* to newborn (P2) MPSII mice (Polito and Cosma, 2009). In this study, the expression of *IDS* was driven by the strong viral promoter CMV (Xia et al., 2006). Although in this case the levels of circulating and brain IDS activity were much lower than those observed in their previous work, reaching only 1-2% of WT IDS activity in the brain, the impact on neurological disease seemed to be greater (Polito and Cosma, 2009). This neurological improvement could be attributed to the treatment of animals at an age at which the disease had barely manifested yet. It is worth noticing that this therapeutic effect was obtained using very high vector doses ($5x10^{13}$ vg/kg, assuming an average weight of 2 grams for a P2 mouse). In contrast, the results obtained in the present work demonstrate that a dose 25-fold lower ($5x10^{10}$ vg/mouse or $2x10^{12}$ vg/kg, assuming an average weight of 25 grams for an adult mouse) when delivered directly to the CNS of adult MPSII mice is sufficient to achieve levels of IDS activity in the brain of about 40% of WT levels. The use of the lowest possible therapeutic dose is always desirable in gene therapy with AAV vectors not only because capsid-directed immune responses are dose-dependent (Manno et al., 2006; Nathwani et al., 2014), but also because producing such high doses of GMP-quality vectors suitable for human administration represents a manufacturing challenge.

In this study, both murine and human *Iduronate-2-sulfatase* coding sequences were optimized to mediate the highest possible IDS activity. Several studies have demonstrated that the optimization of the coding sequence increases the expression of the gene of interest (Burgess-Brown et al., 2008; Foster et al., 2008; Kudla et al., 2009; Ward et al., 2011). Nonetheless, other works have challenged this affirmation (Zhou et al., 2013; Mauro and Chappell, 2014). In any case, the results provided in the present study demonstrated that with the optimization algorithms used, murine and human optimized *Iduronate-2-sulfatase* coding sequences led to higher levels of enzyme activity in comparison to those obtained when using the respective wild-type sequences.

The IDS-deficient mouse model used in the present work had not been phenotypically characterized before. For this reason, the first part of this study was

focused on the analysis of several markers of lysosomal pathology in 2-month-old animals. At this age, MPSII mice were phenotypically characterized, demonstrating established disease at this age that mimics Hunter pathology. The choice to treat 2-month-old MPSII animals with established disease was performed to mimic the situation of a child in whom diagnoses arrives after a few years of life.

There was a clear accumulation of glycosaminoglycans in the encephalon of MPSII mice at 2 months of age that resulted in distension of the lysosomal compartment and secondary alteration of the activity of several lysosomal hydrolases. A general increase in lysosomal activity is a common observation in many LSDs (Settember et al., 2013; Hinderer et al., 2015; Ribera et al., 2015) and is mediated through transcriptional activation by transcription factor EB (TFEB). TFEB is a master regulator of lysosomal biogenesis and function that translocates to the nucleus and activates the transcription of lysosomal-associated genes in response to aberrant lysosomal storage conditions (Sardiello et al., 2009; Ribera et al., 2015). Noticeably, in MPSII mice, while the activity of other hydrolases was increased, the activity of SGSH and GALNS was inhibited. This behaviour differed to what it was previously observed for SGSH in the brain of mice affected by MPSIIIB (Ribera et al., 2015). It has been described, however, that pathological accumulation of substrates can inhibit certain lysosomal enzymes. For instance, *in vitro* experiments have shown that HS inhibits GALNS activity in a dose-dependent manner (Rowan et al., 2013), a finding that could explain the reduction in GALNS activity observed in the present study. In agreement with this observation, the levels of keratan sulfate -a substrate of GALNS- in the sera of patients affected by several forms of mucopolysaccharidoses were significantly higher than in age-matched healthy patients (Tomatsu et al., 2005). Similarly, SGSH activity could be inhibited by other compounds. Therefore, the final profile of activity of lysosomal hydrolases seems to be a balance between the effects of TFEB activation and the inhibitions mediated by specific compounds. When MPSII mice were analysed at 6 months of age, i.e. 4 months after administration of AAV9-*Ids* vectors, the content of GAGs, the general and ultrastructural aspect, the size and function of brain lysosomes were all corrected in treated animals, but had worsened in MPSII non-treated animals or in those receiving non-coding AAV9-Null vectors. Moreover, the analysis of the lysosomal distension in different areas of the encephalon 8 months after delivery of AAV9-*Ids* vectors showed that the effects of the therapy persisted long-term after a single administration of the treatment.

Two-month-old untreated MPSII mice also showed pronounced astrocytosis and microgliosis throughout the encephalon, a hallmark finding in different animal models of mucopolysaccharidoses that manifest with neurodegeneration (Richard et al., 2008; Fu et al., 2012; Ruzo et al., 2012a; Ruzo et al., 2012b; Haurigot et al., 2013; Baldo G et al., 2015; Ribera et al., 2015) and in Hunter patients (Constantopoulos et al., 1980; Hamano et al., 2008). The effects of AAV9-mediated *Ids* gene transfer on the transcriptional signature and histological findings associated to microglial activation in 6-month-old animals were quite noticeable. These results were in agreement with previous observations in MPSIIIB mice that demonstrated the correspondence between CNS therapeutic efficacy and normalization of the CNS transcriptomic profile after CNS-directed gene transfer (Ribera et al., 2015). Several lines of evidence underscore the role played by the secondary activation of microglial/astroglial cells on the etiopathology of neurological dysfunction in LSDs (Constantopoulos et al., 1980; McGeer and McGeer, 1998; Ohmi et al., 2003; Walkley, 2007; Hamano et al., 2008; DiRosario et al., 2009; Archer et al., 2014; Cartier et al., 2014). The normalization of the markers of neuroinflammation that appear secondary to IDS deficiency provides further evidence of the resolution of the storage disease achieved through intra-CSF delivery of AAV9-*Ids* vectors. Furthermore, the inhibitory effects on neuroinflammation persisted 8 months after gene therapy, providing evidence of long-term therapeutic efficacy after a single dosing of the treatment.

In 2-month-old untreated MPSII mice there was also clear evidence of lysosomal pathology in all the somatic organs analysed, including liver, heart, lung and spleen. The accumulation of undegraded GAGs was particularly noticeable in liver, which presented a clear deregulation of the activity of lysosomal hydrolases. In addition, an increased weight of the liver was observed, being hepatomegaly a common manifestation that affects 75-90% of Hunter patients (Martin et al., 2008). Similar to the observations made in CNS, all of these pathological changes were corrected 4 months after the intra-CSF delivery of IDS-encoding AAV9. The therapeutic approach described in this work resulted in supraphysiological levels of the IDS enzyme in the liver and circulation, which allowed whole-body disease correction.

When the Open Field test was performed on 2-month-old animals, a tendency to suffer from anxiety and to have less exploratory activity was observed in IDS-deficient mice. However, no statistically significant differences with wild-type animals were reached

at this age. At the age of 6 months, however, untreated MPSII mice and MPSII mice that received non-coding AAV9-Null vectors showed statistically significant reductions in locomotor and exploratory activities and anxiety-related behaviour. These results were in agreement with the behavioural alterations described in Hunter patients, in whom hypoactivity has been reported at advanced stages of the disease when neurological impairment is evident (Holt et al., 2011). In agreement with the reversal of lysosomal pathology, 6-month-old MPSII mice that received AAV9-*Ids* vectors showed less anxiety and better locomotor performance, providing significant proof of functional correction following intra-CSF gene therapy protocol.

Further evidence of the improvement in the health condition of MPSII mice treated with AAV9-*Ids* vectors was provided by the survival analysis. A clear reduction of lifespan was observed in untreated MPSII mice or Null-treated MPSII mice when compared to wild-type animals, suggesting that the deficiency of IDS had similar consequences on life expectancy in mice as in humans (Neufeld and Muenzer, 2001; Jones et al., 2009). In contrast, AAV9-*Ids*-treated MPSII animals lived considerably longer than MPSII mice that did not receive the therapeutic vector. The prolonged extension of lifespan mediated by the treatment with AAV9-*Ids* vectors strongly support the clinical potential of this gene therapy strategy.

Since most of the pathological changes associated to the deficiency of IDS and consequently to the alteration of the lysosomal system were already present at the age of treatment (2 months of age), the results of the present work demonstrate that CNS-directed AAV9-mediated IDS gene transfer can reverse established MPSII pathology, at least to some extent. MPSII is, however, a progressive neurodegenerative disease, and probably there is a therapeutic window of opportunity after which full reversion of the disease will be hard to achieve.

Extensive biodistribution studies in mice and dogs have been previously conducted in our laboratory and determined that when AAV9 vectors are delivered to the CSF at the dose range used in the present study, vector genomes and transgene expression are found throughout the CNS and PNS (Haurigot et al., 2013; Ribera et al., 2015). Of particular relevance are the results obtained in dogs, an animal with a brain size closer to that of the target paediatric population. In one of these studies, the encephalon of 7 dogs was sampled in at least 30 fractions, covering the whole organ volume. Vector genomes and

transgene expression were detected in frontal, parietal, temporal and occipital cortexes, olfactory tract, striatum, hippocampus, piriform lobe, diencephalon, mesencephalon, pons, medulla oblongata, vermis and cerebellum (Haurigot et al., 2013). Moreover, vectors were detected in all portions of the spinal cord up to the cauda equina, and were present at relatively high copy numbers in trigeminal and cervical, thoracic and lumbar dorsal root ganglia (Haurigot et al., 2013). Regarding cellular tropism, co-localization studies demonstrated that in both mice and dogs, AAV9 vectors delivered to the CSF transduce primarily neurons, with scarce transduction of astrocytes and no transduction of microglia (Haurigot et al., 2013; Ribera et al., 2015). Efficient transduction of ependimocytes and leptomeninges was also observed (Haurigot et al., 2013). Importantly, our previous studies demonstrated in dogs that the intra-CSF administration of AAV9 vectors resulted in high and sustained levels (>41 months with observation ongoing) of the lysosomal enzyme in the CSF (Haurigot et al., 2013; Ribera et al., 2015); as mentioned before, ERT studies have demonstrated that intra-CSF delivery of enzyme results in substantial and potentially meaningful reductions in GAGs in MPSII patients (Muenzer et al., 2015). In addition, we and others have demonstrated that the intra-CSF administration of AAV9 vectors also results in leakage of a portion of the vector into circulation and transduction of the liver (Haurigot et al., 2013; Gray et al., 2013; Hinderer et al., 2014a; Hinderer et al., 2014b; Ribera et al., 2015), with low copy numbers detected in other peripheral tissues (Haurigot et al., 2013; Ribera et al., 2015). The present work confirmed the same pattern of AAV9 vector biodistribution and tropism following intra-CSF delivery to MPSII mice, with preferential transduction of neurons, spread of vectors throughout the CNS and transduction of the liver. Nevertheless, there is considerable variability in the literature regarding the main CNS cell type targeted by AAV9. Several factors have been held accountable for the different tropism observed, including the route of delivery (Gray et al., 2013; Hinderer et al., 2014a), the age at administration (Foust et al., 2009), the animal species (Bevan et al., 2011; Bucher et al., 2014; Jackson et al., 2015; Gurda et al., 2016), the doses used (Gray et al., 2011), the promoter used to drive the expression of the transgene (Duque et al., 2009; Snyder et al., 2011), the impact of the underlying disease, which may affect the distribution of the receptors used by the vector to enter the cell (Chen et al., 2012) and even the single or double stranded nature of the AAV (Donsante et al., 2016). Alternatively, the quality of vector preparations could play also an important role in determining vector tropism (Klein et al., 2008). To produce the AAV9 vectors that

were used in the present work, a second-generation, optimized CsCl protocol was followed, which results in markedly higher vector purity -comparable to good manufacturing practice (GMP) batches- and dramatically reduces the number of empty capsids (Ayuso et al., 2010a). Better transduction efficiency has been demonstrated for several AAV serotypes purified under this protocol, in multiple tissues and species (Ayuso et al., 2010a).

In contrast to diseases in which it is critical to transduce a particular cell type, LSDs in which the mutated gene encodes for a secreted lysosomal protein benefit from the possibility of cross-correction. The results described in the present study also provide strong evidence supporting the occurrence of cross-correction through IDS present in the CSF, serum or enzyme secreted by cells neighbouring non-transduced cells. First, the huge load of storage vesicles visible in the cytoplasm of cortical perineuronal glial cells was completely cleared from MPSII mice treated with AAV9-*Ids* vectors. As this cell type, typically recognized by microglial markers, is not transduced by AAV9, the observation suggests that the enzymatic deficiency in these cells was corrected through uptake of extracellular enzyme. Secondly, despite the fact that the liver is the only peripheral organ that it is efficiently transduced through this approach (Gray et al., 2013; Haurigot et al., 2013; Ribera et al., 2015), the content of GAGs was normalized or greatly reduced in all somatic organs analysed, suggesting efficient uptake of circulating enzyme and its appropriate trafficking to lysosomes. The detection of increased levels of IDS activity in heart and lung of AAV9-*Ids*-treated MPSII mice, two organs poorly transduced after intra-CSF delivery of AAV9 vectors at the doses used in this study, supports this notion. The demonstration that cross-correction occurred in MPSII mice following intra-CSF delivery of AAV9-*Ids* reinforces the potential of this approach to counteract the pathology characteristic of MPSII.

In summary, the present work provides the first evidence of simultaneous and long-term correction of neurological and systemic MPSII disease by CNS-directed gene therapy. Proof of efficacy was obtained through biochemical, histological, ultrastructural and functional analysis. Furthermore, as animals had established disease at the age of treatment, the results described in this study demonstrate that the tissue damage caused by excessive accumulation of undegraded heparan sulfate and dermatan sulfate is, to some extent, reversible. The data provided here support the clinical development of this

approach for the treatment of MPSII patients with somatic disease and any degree of CNS involvement.

Altogether, the results obtained along the three parts of the present work constitute the proof of concept that support the clinical development of this approach for the treatment of Hunter patients with cognitive impairment. This therapeutic has been granted the Orphan Drug Designation (ODD) by the EMA (European Medicines Agency, OD/076/15) and the FDA (Food and Drug Administration, Resolution number: 15-4863) in 2015 (Figure 53).


**Figure 53. Towards a gene therapy treatment for MPSII patients.** The preclinical results generated in the present work constituted the basis of the application for Orphan Drug Designation (ODD) for AAV9-h*IDS*. In 2015, EMA and FDA approved the ODD for the gene therapy medicinal product "Adeno-associated viral vector serotype 9 containing the Iduronate-2-sulfatase (*Ids*) for the treatment of mucopolysaccharidosis type II (Hunter syndrome)" (EMA, OD/076/15; FDA, Resolution number 15-4863).

# VI. CONCLUSIONS

1. At the age of 2 months, MPSII male mice showed a lack of IDS activity throughout the encephalon, liver and serum, resulting in pathological GAG accumulation, distention of the lysosomal compartment and disruption of lysosomal homeostasis in both CNS and somatic organs.

2. Neuroinflammation was already present in the brain of 2-month-old MPSII mice. Therefore, at this age the MPSII mouse model already presented a well-established pathology, which reassembled human Hunter syndrome.

3. The administration of AAV9-*Ids* vectors to the CSF resulted in broad distribution of the vector throughout the CNS and PNS. In somatic organs, vectors were mainly detected in the liver.

4. The intra-CSF delivery of AAV9-*Ids* vectors to 2-month-old MPSII mice led to the restoration of IDS activity throughout the encephalon. Consequently, GAG content and all lysosomal alterations were normalized 4 and 8 months post vector delivery.

5. The treatment with AAV9-*Ids* vectors reesulted in the reversion of neuroinflammation in 6-month-old MPSII animals. This therapeutic effect persisted long-term, i.e. whenMPSII mice were analysed at 10 months of age.

6. The brain from MPSII mice treated with AAV9-*Ids* vectors showed correction of the gene expression profile in almost 80% of the genes differentially expressed as a consequence of the disease. Many of the altered genes were related to immunological processes associated to the activation of microglial cells, confirming the key role played by this cell type in MPSII disease.

7. The delivery of AAV9-*Ids* vectors to the CSF resulted in the liver transduction, which produced the enzyme and secreted it to the circulation, providing a peripheral source of the therapeutic protein. By cross-correction, all somatic pathology characteristic of MPSII disease was reverted.

8. Correction of behavioural alterations and considerable prolongation of the lifespan of treated mice were achieved after AAV9-*Ids* vector administration.

**9.** Therefore, a single intra-CSF administration of AAV9-*Ids* vectors effectively corrected both neurologic and somatic mucopolysaccharidosis type II disease (Hunter syndrome). Since most of the pathological aspects of the disease were already present in mice at the age of treatment, this therapeutic approach reverted an established MPSII pathology.

**10.** Finally, the delivery of AAV9 vectors containing optimized human *IDS* coding sequences resulted in the restoration of IDS activity in the CNS and periphery of MPSII mice, leading to a completely normalization of phatological GAG storage. Altogether, these results support the clinical translation of this approach to Hunter patients.

# VII. MATERIALS AND METHODS

# 1. MATERIALS

## 1.1. Animals

Iduronate-2-sulfatase-deficient mouse (MPSII) model (129/SvEv-C57BL/6 genetic background) was purchased from Taconic (Model TF1838). Hemizygous male mice (*Ids*$^{Y/-}$) were originally generated by replacing exons 2 to 5 of the *Ids* murine gene by the selection cassette bGeo/Puro (Figure 54). The colony was established in a specific pathogen-free (SPF) animal facility of our center (SER-CBATEG) and was initially obtained from breeding of hemizygous males with heterozygous female founders. Afterwards, affected MPSII mice and healthy littermates were obtained by breeding from wild-type males with heterozygous females. Mice were fed *ad libitum* with standard diet (Teklad Global 18% Protein Rodent Diet, 2018S; Harland, now Envigo) and maintained under controlled temperature and light conditions (12-hour light-dark cycles, with lights on at 8:00 AM).

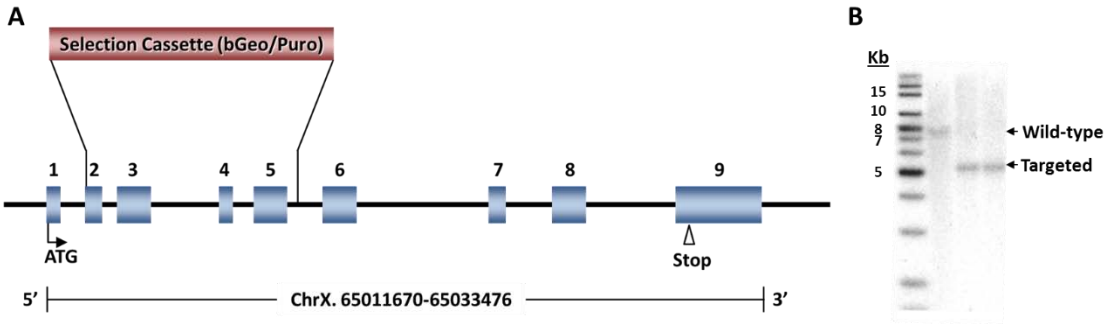


**Figure 54. Generation of the Iduronate-2-sulfatase deficient mouse. (A)** Schematic representation of the gene trap approach used to obtain the IDS-deficient mouse model. **(B)** Southern blot analysis of the targeted mutation. Adapted from Taconic.

Animal care and all experimental procedures were approved by the Ethics Committee for Animal and Human Experimentation of Universitat Autònoma de Barcelona (UAB) and following the Animal Research Reporting In Vivo Experiments (ARRIVE) guidelines.

## 1.2. Bacterial strains

The *E. coli XL2Blue* strain (Stratagene) was used to produce the different plasmid constructs of the present work. All plasmids contained the ampicillin resistance gene for selection. The bacterial culture was grown in LB medium (Miller's LB Broth, Laboratorios

Conda) in the presence of 50 g/ml of ampicillin (Sigma-Aldrich). When cells were grown on a solid medium, 2% agar was added to the LB medium.

### 1.3. Immunohistochemical reagents

Antibodies and other reagents used in the present work for immunohistochemical detections are listed in Table 7.

**Table 7: List of the antibodies used for immunohistochemical detections**

| Reagents | Host | Supplier | Reference | Dilution |
|---|---|---|---|---|
| **Primary antibodies** | | | | |
| BSI-B4 (Isolectin B4) | - | Sigma-Aldrich | L5391 | 1/100 |
| Anti-GFAP | Rabbit | Dako | Z0334 | 1/1000 |
| Anti-GFP | Goat | Abcam | Ab6673 | 1/300 |
| Anti-GFP | Chicken | Abcam | Ab13970 | 1/500 |
| Anti-Iba1 | Goat | Abcam | Ab5076 | 1/500 |
| Anti-LAMP1 | Rat | Santa Cruz Biotechnology | SC-19992 | 1/100 |
| Anti-LAMP2 | Rat | Abcam | Ab13524 | 1/500 |
| Anti-NeuN | Mouse | EMD-Millipore | MAB377 | 1/500 |
| **Secondary antibodies** | | | | |
| Anti-chicken 488 (FITC) | Donkey | Abcam | Ab63507 | 1/100 |
| Anti-goat IgG biotinilated | Donkey | Santa Cruz Biotechnolgoy | SC-2042 | 1/300 |
| Anti-mouse IgG biotinilated | Horse | Vector Laboratories | BA-2000 | 1/300 |
| Anti-rabbit IgG biotinilated | Goat | Pierce (Thermo Fischer Scientific Inc.) | 31820 | 1/300 |
| Anti-rat IgG biotinilated | Rabbit | Dako | E0467 | 1/300 |
| Streptoavidine Alexa Fluor 488 biotinilated | - | Molecular Probes | S-11223 | 1/300 |
| Streptoavidine Alexa Fluor 568 biotinilated | - | Molecular Probes | S-11226 | 1/300 |
| **Other reagents** | | | | |
| 3,3'-Diaminobenzidine tetrahydroghloride hydrate (DAB) | - | Sigma-Aldrich | D5637 | - |
| ABC Peroxidase Standard Staining Kit | - | Pierce (Thermo Fischer Scientific Inc.) | 32020 | 1/100 |
| Hoechst 33342 | - | Sigma-Aldrich | B2261 | 1/100 |
| Mayer's hemalum solution | - | Merck | 109249 | - |

### 1.4. Plasmids

The plasmids used in this study are summarized in Table 8.

**Table 8: List of the plasmids used in the present work**

| Name | Promoter | Gene of interest | Coding sequence optimized | WPRE | PolyA |
|---|---|---|---|---|---|
| pAAV-CAG-GFP-WPRE | GAG | GFP | No | Yes | Rabbit β-globin |
| pAAV-CAG-MCS | CAG | - | - | No | Rabbit β-globin |
| pAAV-CAG-Null | CAG | - | - | No | Rabbit β-globin |
| pAAV-CAG-m*Ids* | CAG | Murine *Ids* | No | No | Rabbit β-globin |
| pAAV-CAG-om*Ids*-version1 | CAG | Murine *Ids* | Yes | No | Rabbit β-globin |
| pAAV-CAG-om*Ids*-version2 | CAG | Murine *Ids* | Yes | No | Rabbit β-globin |
| pAAV-CAG-om*Ids*-version3 | CAG | Murine *Ids* | Yes | No | Rabbit β-globin |
| pAAV-CAG-h*IDS* | CAG | Human *IDS* | No | No | Rabbit β-globin |
| pAAV-CAG-oh*IDS*-version1 | CAG | Human *IDS* | Yes | No | Rabbit β-globin |
| pAAV-CAG-oh*IDS*-version2 | CAG | Human *IDS* | Yes | No | Rabbit β-globin |

MCS, Multiple-cloning site.

The CAG promoter is a hybrid promoter composed of the early enhancer of cytomegalovirus (CMV), the chicken β-actin promoter and the chiken β-actin intron. This promoter is able to drive a potent expression ubiquitously.

The woodchuck hepatitis virus post-transcriptional regulatory element (WPRE) is a hepadnavirus sequence that is widely used as a *cis*-acting regulatory module in various types of plasmid or viral gene vectors. When placed in the 3' untranslated region of gene transfer cassettes, the WPRE enhances the expression of the transgene by increasing both nuclear and cytoplasmic mRNA levels (Zanta-Boussif et al., 2009).

The pAAV-CAG-Null construct did not codify for any gene, and it was used to generate the AAV9-CAG-Null vector. This Null-vector worked as a control for the studies after intra-CSF administration.

The optimization of the sequence of the murine and human *Iduronate-2-sulfatase* gene was based on algorithms to maximize the efficiency of IDS protein production in mice through elimination of cryptic splice sites and RNA destabilizing sequence elements for increased RNA stability, addition of RNA stabilizing sequence elements, codon optimization, G/C content adaptation and avoidance of stable RNA secondary structures, among other changes.

# 2. METHODS

## 2.1. Basic DNA cloning techniques

### *2.1.1. Plasmid DNA preparations*

Minipreparations of plasmid DNA were obtained using the alkaline lysis protocol originally described by Birnboim and colleagues (Birnboim and Doly, 1979). When higher amounts of plasmid DNA were required, the PureYield™ MaxiPrep System (Promega Corporation), the EndoFree® Plasid Mega kit (Qiagen) or the EndoFree® Plasid Giga kit (Qiagen) were used.

### *2.1.2. DNA digestion with restriction enzymes*

Each restriction enzyme required specific reaction conditions of pH, ionic strength and temperature. Therefore, in each case, the manufacturer's instructions were followed (New England Biolabs, Roche, Promega Corporation or Fermentas). Generally, DNA was digested using 1 Unit of the enzyme per μg of DNA. Digestions were carried out for 1 hour in the specific buffer and the digestion products were analysed in agarose gels. When it was required to cleave the DNA with two restriction enzymes, the digestions were carried out simultaneously if both enzymes worked well at the same temperature and in the same buffer.

### *2.1.3. DNA resolution and purification*

Agarose gel electrophoresis was the standard method used to separate, identify and purify DNA fragments. An agarose gel of 1% was used to resolve DNA fragments between 0.2-8 kb. Gels were prepared by dissolving agarose in 1x TAE (1m M EDTA, 40 mM Tris acetate at pH 8.3) electrophoresis buffer containing 0.5 g/ml ethidium bromide. Samples were loaded in 10x loading dye and electrophoresed in 1x TAE electrophoresis buffer at 80 V. As DNA size marker, 1 kb or 100 bp DNA ladder (Invitrogen) was used. The location and relative size of DNA within the gel was determined by staining the gel with low concentrations of the fluorescent dye ethidium bromide, which intercalates between the two strands of DNA. The presence of DNA was visualised with low wavelength (310 nm) ultraviolet (UV) light using a transilluminator and camera system (Syngene). To extract and purify a DNA fragment from an agarose gel, the GeneJET Gel Extraction kit (Thermo Scientific) was used following the manufacturer's instructions. DNA was quantified using a Nanodrop 1000 spectrophotometer (Thermo Fisher Scientific Inc.).

#### *2.1.4. Ligation of DNA fragments*

The bacteriophage T4 DNA ligase was used for ligation reactions following the manufacturer's instructions (New England Biolabs). Reactions were carried out in the presence of ligation buffer with ATP at room temperature for either 2 hours or overnight, in the case of cohesive end fragments or blunt end fragmetns, respectively.

#### *2.1.5. Transformation of competent E. coli*

Plasmid DNA was introduced into competent *E. coli XL2Blue* bacteria by electroporation. Fourty µl of competent cells ($2x10^{10}$ cells/ml) were thawed on ice at the moment of use and 1 µl (approximately 10 ng) of the DNA ligation reaction or control DNA was added directly to the cells. Cells and DNA were mixed and incubated on ice for 5 minutes. Afterwards, cells were electroporated (Electroporator 2510, Eppendorf) at 2500 V. Then, 200 µl of LB medium were added and cells were plated in LB plates with the ampicillin antibiotic and incubated overnight at 37ºC.

### 2.2. Genotyping of MPSII mice

MPSII-deficient mice were identified on genomic DNA from tail-clipped samples by a specific touchdown PCR analysis that amplifies a sequence encompassing the targeted mutation.

#### *2.2.1. Genomic DNA isolation*

Genomic DNA was extracted from a tail sample of about 0.5 cm obtained from animals aged 3-4 weeks. Sample was digested overnight at 56ºC in 2% v/v Proteinase K (10 mg/ml, Roche) buffered solution (100 mM Tris at pH 8.0, 5 mM EDTA, 0.2% w/v SDS, 200 mM NaCl). This incubation allowed the digestion of the tissue by proteinase K and the release of genomic DNA from the cells. Digestion mixture was centrifuged at 16000 *g* for 5 minutes and the recovered supernatant (~500 µl) was mixed with 0.7 volumes of 2-propanol (Panreac Química) in order to precipitate genomic DNA. After 15 minutes of centrifugation at 12000 *g*, supernatant was aspirated by vacuuming the liquid out and the DNA pellet was resuspended in 800 µl of Mili-Q $H_20$ previously heated to 65ºC to facilitate the solubilisation of the DNA.

### *2.2.2. Touchdown PCR genotyping*

Once genomic DNA was obtained, analysis by specific touchdown PCR-based amplification of a region between the first wild-type intron and the second exon of the murine *Ids* gene allowed to discriminate between the presence or absence of the targeted mutation (Figure 55A).

The sequence of the respective sense and antisense oligonucleotide primers were: Forward primer (Fw): 5'-TTT TGT GTA CTC CAA CCC CG-3', Reverse wild-type primer (Rv WT): 5'-TGT CTC CAT AAC AGC CCA GG-3', Reverse mutation primer (Rv KO): 5'-GCC CTC ACA TTG CCA AAG GA-3'. GoTaq® DNA Polymerase (Promega Corporation) was used with the conditions detailed in Table 9.

**Table 9: Mix for touchdown PCR for MPSII mouse model genotyping**

| Reagents | Volume per reaction (µl) |
|---|---|
| 5x GoTaq® Flexi Green Buffer, Mg Free | 4 |
| $MgCl_2$ (25 mM) | 1.4 |
| Forward primer (Fw) (20 µM) | 0.3 |
| Reverse wild-type primer (Rv WT) (20 µM) | 0.3 |
| Reverse mutation primer (Rv KO) (20 µM) | 0.3 |
| dNTP (25 mM) | 0.2 |
| GoTaq® G2 Flexi DNA Polymerase (5 U/µl) | 0.1 |
| Mili-Q $H_2O$ | 11.9 |
| Genomic DNA (from *section 2.2.1.*) | 1.5 |
| Final volume | 20 |

Time and temperature conditions for MPSII genotyping touchdown PCR consisted of a first hot-start step of 94ºC for 4 minutes, a subsequent 10 rounds of amplification (15 seconds at 94ºC, 30 seconds at 65ºC and 30 seconds at 72ºC) followed by 40 cycles of a second amplification (15 seconds at 94ºC, 30 seconds at 55ºC and 30 seconds at 72ºC) and finalised with a hold step at 4ºC.

The resulting DNA fragments were run on a 2% agarose gel with ethidium bromide. The expected band size of the murine *Ids* locus fragment was 214 bp for wild-type ($Ids^{+/+}$) males and females (Figure 55B); whereas it was 312 bp for homozygous ($Ids^{-/-}$) females and hemizygous ($Ids^{Y/-}$) males. In DNA from heterozygous ($Ids^{+/-}$) females both214 and 312 bp fragments were amplified.

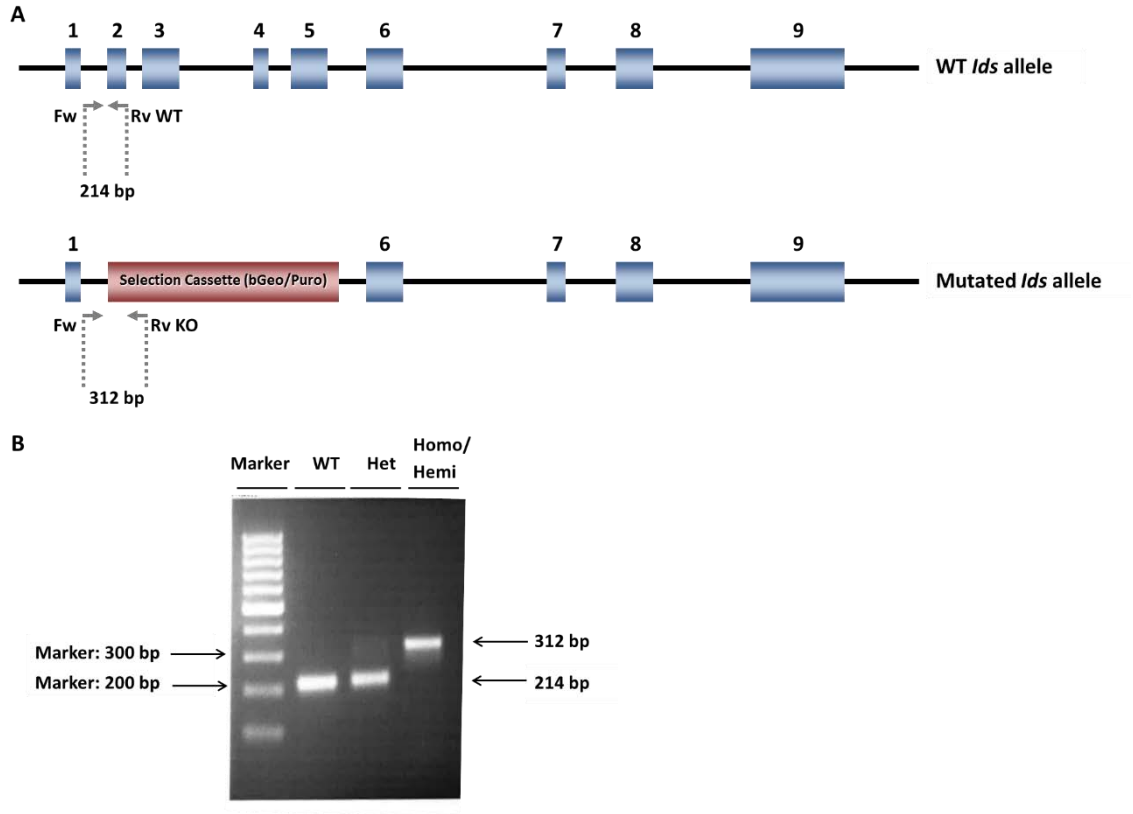


**Figure 55. Genotyping of the MPSII mouse model by touchdown PCR.** (**A**) Schematic representation of the strategy for the PCR-based amplification of the mutated region. The primers used for mouse genotyping are indicated in gray. The reverse mutation primer (Rv KO) hybridises specifically within the selection cassette (bGeo/Puro) of the knock-out mouse, and along with forward primer (Fw), which specifically hybridises within the first wild-type *Ids* intron, leads to the amplification of a 312 bp DNA fragment from mutated *Ids* allele. The reverse wild-type primer (Rv WT) was specific designed to anneal the second *Ids* exon, and together with the forward primer lead to the amplification of a 214 bp DNA fragment. The numbers above the boxes indicate the different exons. (**B**) Expected bands that allow the discrimination of each genotype. Their molecular size, as well as that of the marker bands running immediately before and after, are indicated by arrows. Bands are: 214 bp for wild-type (WT) mice, 312+214 bp for heterozygous (Het) mice, and 312 bp for homozygous or hemizygous (Homo/Hemi) mice for the mutation in the *Ids* gene.

## 2.3. Production, purification and characterization of AAV vectors

### *2.3.1. AAV vectors production and purification*

AAV vectors used in the present work were generated by helper virus-free transfection of HEK293 cells using three plasmids (Figure 56) (Matsushita et al., 1998; Ayuso et al., 2010b) and following an optimized procedure of purification previously described by our laboratory (Ayuso et al., 2010a). Briefly, cells were cultured to 70% confluence in roller bottles (RB) (Corning) in DMEM supplemented with 10% FBS and then co-transfected with 150 µg of: 1) a plasmid carrying the expression cassette of interest under the control of the desired promoter being all the construct flanked by the viral ITRs; 2) a packaging plasmid

pREP/CAP that encoded for the AAV Rep2 and the Cap9 genes; and 3) an adenoviral helper plasmid named pWEAD, which carried the adenovirus helper functions and was kindly provided by Dr. K. High, Children's Hospital of Philadelphia, USA. Three days after co-transfection, cells were harvested and centrifuged at 2500 *g* for 15 minutes at 4ºC. Cell pellet and medium were then processed separately. Cell pellet was thoroughly reconstituted in TMS (50 mM TrisHCl, 150 mM NaCl, 2 mM $MgCl_2$, pH 8.0). After sonication, cell lysate was centrifuged at 4000 *g* for 30 minutes at 4ºC. Supernatant from this centrifugation was added to the medium previously separated and vector suspension was subsequently purified.

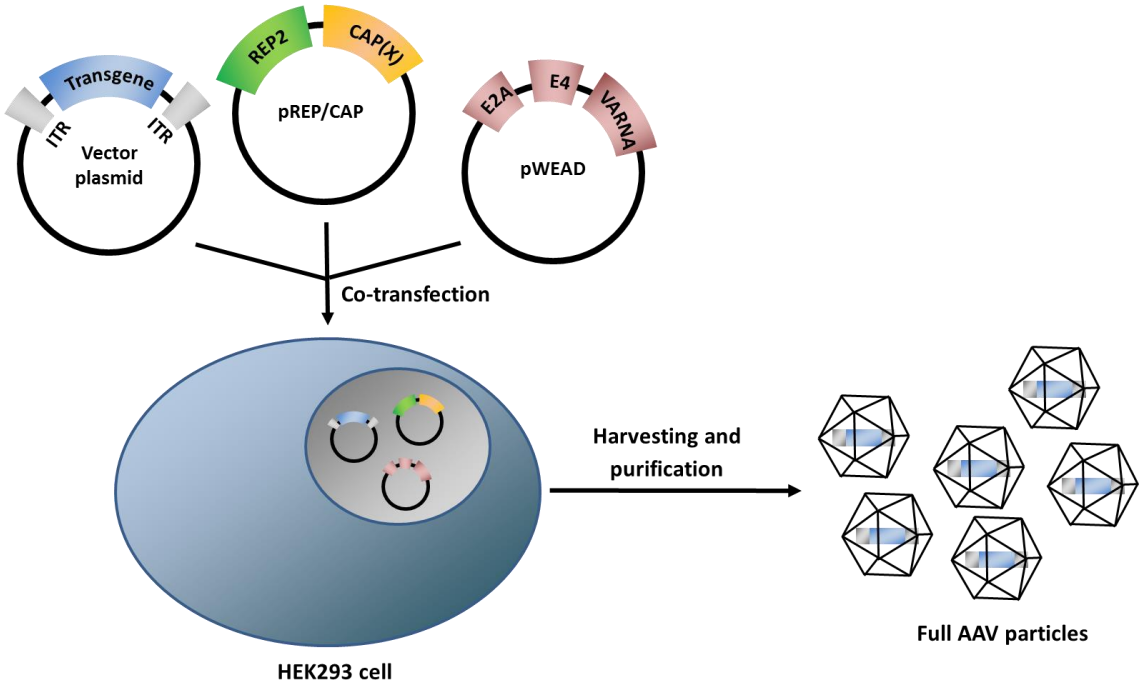


**Figure 56. Schematic representation of the production of AAV vectors**. Triple plasmid system transfection based in a first plasmid containing the vector genome flanked by ITR (from serotype 2), a second plasmid (pREP/CAP) that encodes Rep proteins, from serotype 2, and Cap proteins specific for serotype 9, and a third plasmid (pWEAD) that carries the minimal adenoviral genes (E2A, E4 and VARNA) required to support AAV replication. The schematic representation is not to scale. Adapted from Ayuso et al., 2012b.

To purify vector particles, they were precipitated by incubation with 8% of polyethylene glycol (PEG) 8000 (Sigma-Aldrich) overnight and then pelleted at 4000 *g* for 30 minutes at 4ºC. This pellet, now containing vectors from cells and medium, was thoroughly reconstituted in TMS (50 mM TrisHCl, 150 mM NaCl, 2 mM $MgCl_2$, pH 8.0), treated with benzonase (Merck) for 30 minutes at 37ºC and centrifuged at 10000 *g* for 10 minutes at 4ºC. The supernatant was loaded into 37.5 ml ultra clear tubes (Beckman)

containing 1.3 g/ml CsCl density step gradient, and centrifuged for 16 hours at 15ºC and 28000 rpm in a SW32Ti rotor (Beckman). This first CsCl gradient allowed the separation of full AAV vectors from the major part of protein impurities and empty AAV capsids (Figure 57). Viral bands were carefully collected using a 5 ml syringe and 18*G* needle and transferred to a new 12.5 ml ultraclear tube, which was filled up with 1.379 g/ml CsCl solution to generate a continuous gradient. Tubes were centrifuged at 31000 rpm for 48 hours at 15ºC in SW40Ti rotor (Beckman). This second CsCl gradient separated full AAV vectors from protein impurities of similar density than full AAV vectors, intermediate species and remaining empty AAV capsids. Finally, the band of full particles was collected and dialyzed in PBS + 0.001% Pluronic® F68 (Gibco) using Slide-A-Lyzer Dialysis chambers (Life Technologies) and filtered with 0.22 µm filters (EMD-Millipore). This PEG and CsCl-based purification protocol (Figure 57) dramatically reduced empty AAV capsids and DNA and protein impurities from the viral stock thus increasing AAV purity to >95%, which ultimately resultes in higher transduction *in vivo* (Ayuso et al., 2010a).

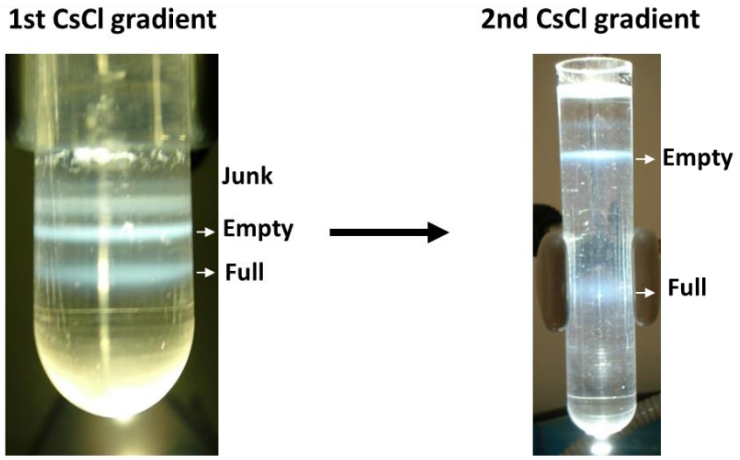


**Figure 57. Purification of AAV vectors**. The first CsCl gradient separated full AAV vectors from the major part of protein impurities and empty AAV capsids. The second CsCl gradient separated full AAV vectors from protein impurities of similar density than full AAV vectors, intermediate species and remaining empty AAV capsids. Adapted from Ayuso et al., 2010a.

### *2.3.2. Vector genomes quantification by qPCR*

Titers of vector genomes (vg/ml) were determined by quantitative PCR (qPCR) assay following the protocol described for the AAV2 Reference Standard Material using linearized plasmid DNA as standard curve (Lock et al., 2010) and using specific primers and probe for sequences present in the recombinant vector genome. A standard linealized plasmid pAAV-CAG-GFP-WPRE-rBGpA with known concentration was used to obtain a standard curve and internal reference AAV vector sample, also with known concentration,

was used as internal control of the technique. The AAV vector sample of unknown concentration and the internal reference AAV vector sample were quantified by interpolation from the standard curve.

To ensure that vector titer was not overestimated due to the presence of remaining DNA plasmids in the prep or DNA contaminants present outside AAV capsids, a DNAse treatment was performed prior to the qPCR reaction. Thus, 5 µl of each vector prep were added to 44.5 µl of DNAse buffer (13 mM TrisHCl, 5 mM $MgCl_2$, 0.12 mM $CaCl_2$, pH 7.5) and 0.5 µl of DNAse I (10 Units) (Roche). The mixture was incubated for 60 minutes at 37ºC.

Vector quantification was performed by using specific qPCR against the common rabbit β-globin polyA sequence (named rBGpA). Standard curve was generated from a linearized plasmid of known concentration diluted from $1x10^8$ to $1x10^3$ copies/µl. The sequence of the respective primers and probe were: Forward primer: 5'-CTT GAG CAT CTG ACT TCT GGC TAA T-3', Reverse primer: 5'-GAT TTG CCC TCC CAT ATG TCC-3' and Probe: 5'-/56-FAM/CCG AGT GAG AGA CAC AAA AAA TTC CAA CAC/BHQ1/-3'. LightCycler® 480 Probes Master (Roche) was used with the conditions detailed in Table 10.

**Table 10: Mix for qPCR used to determine the titer of viral preparations**

| Reagents | Volume per reaction (µl) |
|---|---|
| LightCycler® 480 Probes Master 2x | 5 |
| Forward primer (10 µM) | 0.2 |
| Reverse primer (10 µM) | 0.2 |
| Fluorescent probe (20 µM) | 0.1 |
| Mili-Q $H_2O$ | 2.5 |
| Standard plasmid/Internal reference/AAV vector sample | 2 |
| Final volume | 10 |

The time and temperature condition of qPCR reaction were based on the Mono Color Hydrolysis Probe – UPL Probe 384-II (Light Cycler® 480 II, Roche) programme, which consisted of a first pre-incubation period for 10 minutes at 95ºC, followed by 45 rounds of amplification (10 seconds at 95ºC, 30 seconds at 60ºC and 1 second at 72ºC), and finalised with a cooling step at 40ºC for 30 seconds.

The final titer from each viral preparation was calculated as the mean of three qPCR determinations within three different days.

### *2.3.3. Vector genomes quantification by silver staining*

Analysis of the viral preparations by protein electrophoresis and subsequent silver staining enables the quantification of the physical particles, which would provide another titer to be compared with the vector genome titer (*see section 2.3.2*.). Furthermore, this method not only can reveal if the preparation is contaminated with other non-viral proteins that might affect the transduction efficiency of the preparation (Figure 58) (Ayuso et al., 2010a), but also allows to calculate the percentage of empty capsids present in the sample (ratio viral particles/viral genome).

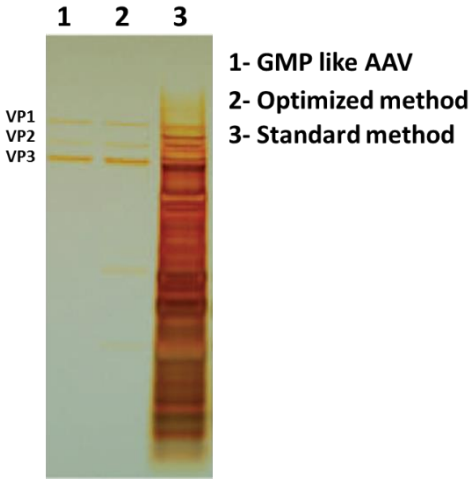


**Figure 58. Silver staining of SDS-PAGE gel of final purified preps.** Line 1, AAV vectors purified by GMP protocol. Line 2, AAV vectors purified according to the double CsCl optimized protocol. Line 3, AAV vectors purified by standard method. Adapted from Ayuso et al., 2010a.

Briefly, appropriate volumes of the tested vector and of several dilutions of a reference vector with known titer were mixed with 4x Novex® Tris-Glycine SDS Sample Buffer (Invitrogen) and 10x NuPAGE Sample Reducing Agent (Invitrogen) in a final volume of 20 µl. After 5 minutes boiling, samples were loaded into a 10% Novex® Tris-Glycine Mini Gel (Invitrogen) and run at 120 V for 1.5-2 hours. Gel was then stained using SilverXpress® Silver Staining Kit (Invitrogen) following manufacturer's instructions. Finally, the intensity of the bands was determined by densiometry and the titer of viral particles was calculated by extrapolation of the standard curve of the reference vector.

## 2.4. *In vivo* delivery of AAV vectors

### *2.4.1. Intra-CSF injection to mice*

For intra-CSF delivery of AAV vectors to mice, animals were anesthetized with an intraperitoneal injection of a mixture of 100 mg/kg ketamine (Imalgene®, Merial) and 10 mg/kg xylazine (Rompun®, Bayer). The skin of the posterior part of the head, from just behind the ears to approximately between the scapulas, was shaved. A 5 mm rostro-caudal incision was then made to expose the occiput and the C1-vertebra. Mice were positioned in prone position, immobilized with the thumb and midfinger, with head held in a slightly downward inclination (Reijneveld et al., 1999). Five µl of the appropriate vector dilution were injected into the cisterna magna with a 34*G* needle coupled to a 10 µl Hamilton syringe (Hamilton Bonaduz AG) under an angle of 45-55º. The injection was performed slowly to avoid an abrupt increase in intracranial pressure. After the delivery of vector solution, the incision was closed using Histoacryl® Topical Skin Adhesive (Aesculap Inc). Breathing rhythm was visually controlled after the injection for 30 seconds, and any alteration was reported. Those animals showing signs of wrong injection performance, breath alterations or tremor after the injection, were excluded from the study.

### *2.4.2. Hydrodynamic injection to mice*

Hydrodynamic tail vein injection to mice is a technique that targets expression of the delivered plasmid mainly to the liver (Liu et al., 1999). To perform it, the appropriate amount of plasmidic DNA (30 µg) was diluted in saline solution in a volume equal to ~10% of the body weight of the animal. Just prior to the hydrodynamic injection, each mouse was warmed under a 250 W infrared heat lamp for no more than 2 minutes to allow blood vessel dilatation and to facilitate the visualization of the caudal veins. Then, a rodent restrainer (Harvard Apparatus) was used to immobilize the mouse and the plasmidic DNA solution was immediately manually injected into the lateral tail vein in less than 5 seconds using a 26*G* needle (BD Microlance) coupled to 2.5-5 ml syringe (B. Braun).

### 2.5. Open Field test

The behaviour of mice was analysed with the Open Field test performed between 9:00 AM and 2:00 PM. Animals were placed in the lower left corner of a brightly lit chamber (41 x 41 x 30 cm) that was part of a Detection Unit equipped with a grid of infrared cells (LE8811, Panlab). This grid determined the magnitude of motor activity on the basis of the analysis of the position and frequency at which the experimental animal broke the infrared beams. The Detection Unit consisted of two 45 x 45 cm frames that emited the infrared beams placed at 2.5 cm from one another. The Detection Unit was connected to a Control Unit that transformed the disruption of the infrared beam to analytical data, and the Control Unit was connected to a computer.

The area, where mice were placed, was divided into three concentric square regions: centre (14 x 14 cm), periphery (27 x 27 cm) and border (41 x 41 cm) (Figure 59). Animal behavior was assessed with two softwares: SeDaCom 32 and Smart Junior (Panlab). SeDaCom 32 is designed to allow the direct communication and data sharing between the Control Unit and the computer. With this software, locomotor activity was measured. Smart Junior is a video-tracking software connected to a video camera, with which both locomotor and exploratory activities of animals were recorded during the first 15 minutes. Analysis of the data was performed within the first 3 minutes recorded.

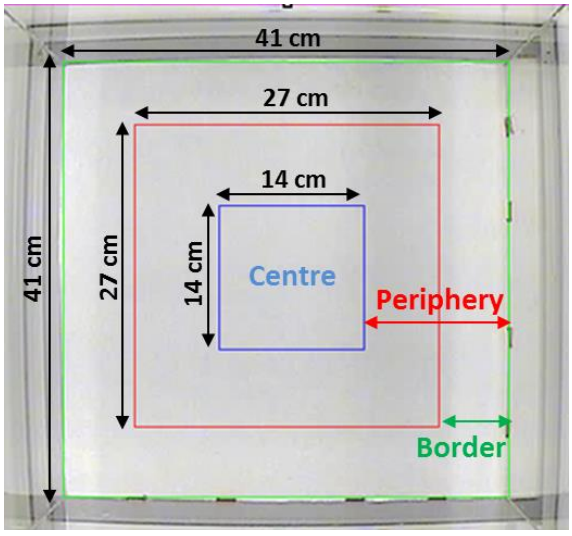


**Figure 59. Schematic division of the area of the Open Field.**

### 2.6. Obtention of *post-mortem* samples from mice

For tissue sampling, mice were anesthetized with an intraperitoneal injection of a mixture of 100 mg/kg ketamine (Imalgene®, Merial) and 10 mg/kg xylazine (Rompun®, Bayer). Blood was extracted by cardiac puncture and subsequently, animals were transcardially perfused with 12 ml of phosphate-buffered saline (PBS) to clear blood from tissues and to remove all traces of circulating IDS. Immediately, tissues of interest were carefully collected. Particularly, the liver was weighed and the encephalon was longitudinally divided into two pieces (left and right), and each piece was then coronal sectioned in five regions (I to V), being section I the most frontal and section V the most caudal (Figure 60). All collected samples were either snap frozen in liquid nitrogen and stored at -80ºC until analysis or immersed in formalin for subsequent histological analysis.

To separate serum from collected blood, blood samples were centrifuged for 10 minutes at 1200 *g* at 8ºC and the supernatant (serum fraction) was then collected and stored at -80ºC until processing.

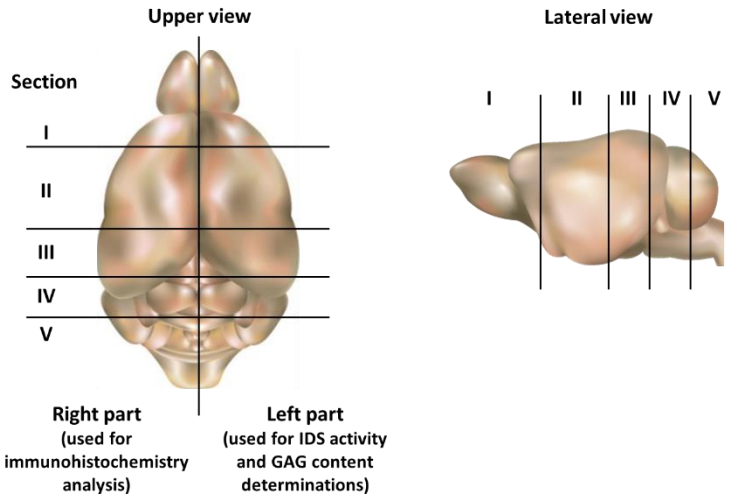


**Figure 60. Schematic representation of how the coronal sections of the encephalon were performed.**

### 2.7. Bradford method for total protein quantification

To quantify the protein content in a sample, the Bradford dye-binding method was used. This method is based on the shift in the colour of Coomassie brilliant blue G-250 dye when complexed with proteins. The dye binds to primarily basic (especially arginine) and

aromatic amino acid residues and the dye changes in response to the concentration of protein present in the sample. This colour shift leads to a change in the absorbance maximum from 495 nm to 595 nm.

Samples in which total protein was required to be quantified were homogenized by sonication in 300-500 µl of Mili-Q $H_2O$ with the Ultrasonic liquid processor (VC130PB, Sonics and Materials Inc.) for ≤ 5 seconds at 40 micron amplitude to allow tissue disruption. Then, mixtures were centrifuged for 10 minutes at 12000 *g* at 4ºC, and the supernatant was recovered as protein extract. Appropriate volumes of the protein extracts were diluted to 800 µl in Mili-Q $H_2O$, to which 200 µl of the Bradford reagent (Protein Assay, Bio-Rad Laboratories) were added. The same reaction was performed with different amounts (0-15 µg) of bovine serum albumin (BSA) to obtain the standard curve. After adding the Bradford reagent, samples were vigorously mixed and incubated for 5 minutes before measuring their absorbance at 595 nm in a spectophotmeter (PowerWave HT Microplate, BioTek Instruments).

### 2.8. Determination of IDS activity

Brain, liver, heart and lung samples were sonicated in 500 µl Mili-Q $H_2O$. Serum was analysed unprocessed. Iduronate-2-sulfatase activity was determined with a 4-methylumbelliferone-derived fluorogenic substrate (Moscerdam Substrates), as described previously (Voznyi et al., 2001). Briefly, 15 µg of total protein or 2 µl of serum were first incubated with 4-methylumbelliferyl-α-L-iduronide-2-sulphate.$Na_2$ (4-MU-αIdoA-2S, Moscerdam Substrates) for 4 hours at 37°C. This incubation allowed Iduronate-2-sulfatase present in the sample to remove sulfate groups from the fluorogenic substrate. A second incubation step was performed for 24 hours at 37ºC after the addition of 20 µl of PiCi-buffer (0.2M $Na_2HPO_4$/0.1M citric-acid buffer, pH 4.5 + 0.02% (w/v) Na-azide) and 10 µl of LEBT-solution (lysosomal enzymes purified from bovine testis, Moscerdam Substrates). This second incubation permitted the release of the fluorescent compound methylumbelliferone (MU) only from those substrate molecules that were de-sulfated by the Iduronate-2-sulfatase action during the first incubation step. Reaction was then stopped by increasing the pH with the addition of 200 µl of a carbonate buffer (0.5 M $NaHCO_3$ / 0.5 M $Na_2CO_3$ buffer, pH 10.7, 0.025% Triton X-100). The released fluorescence was measured with FLx800 fluorimeter (BioTek Instruments) using a 360/40 nm excitation

filter and a 460/40 nm emission filter. The IDS activity was calculated comparing the measured fluorescence with a standard curve consistent of serial dilutions of MU.

Brain, liver, heart and lung IDS activity levels were normalized against the total amount of protein, quantified using Bradford protein assay (Bio-Rad Laboratories, *see section 2.7.*). Serum activity was normalized against volume. IDS activity was expressed as nmol/4h/mg protein or nmol/4h/ml. All samples of the same tissue of interest were processed and analysed in parallel.

### 2.9. Determination of other lysosomal enzyme activities

Brain and liver samples were sonicated in 500 µl of Mili-Q $H_2O$ and cellular debris was removed by centrifugation at 12000 *g* for 10 minutes at 4ºC. Serum was analysed unprocessed. Enzyme activities were determined using 4-methylumbelliferone-derived fluorogenic substrates. α-L-iduronidase (IDUA) activity was assayed in 15 µg of protein incubated for 1 hour at 37ºC with 4-methylumbelliferyl α-L-iduronide (Glycosynth) (Stirling et al., 1978). Sulfoglucosamine N-sulfohydrolase (SGSH) activity was measured as previously described (Karpova et al., 1996; Haurigot et al., 2013). Briefly, 30 µg of protein were first incubated with 4-MU-αGlcNS (Enantia) for 17 hours at 47ºC. The second incubation was carried out in the presence of α-glucosidase (Sigma-Aldrich) at 10 U/ml in 0.2% BSA for 24 hours at 37ºC. For α-N-acetylglucosaminidase (NAGLU) activity, 30 µg of tissue protein extract were incubated with 4-methylumbelliferyl-α-N-acetyl-D-glucosaminide (Moscerdam Substrates) for 3 hours at 37ºC (Marsh and Fensom, 1985; Ribera et al., 2015). Heparan-α-glucosaminide N-acetyltransferase (HGSNAT) activity was determined in 30 µg of protein extract incubated with Acetyl-coenzyme A and 4-methylumbelliferyl-β-D-glucosamine (MU-βGlcNH$_2$, Moscerdam Substrates) for 17 hours at 37ºC (Voznyi et al., 1993). Galactosamine (N-acetyl)-6-sulfatase (GALNS) activity was assayed by a 2-step protocol using 10 µg of protein extract and 4-Methylumbelliferyl β-D-Galactopyranoside-6-sulfate Sodium salt (MU-βGal-6S, Toronto Research Chemical) during the first incubation for 17 hours at 37ºC. The second step was carried out adding Pi-buffer (0.9 M $Na_2HPO_4$/0.9 M $NaH_2PO_4$ buffer, pH 4.3 + 0.02% (w/v) Na-azide) and β-Galactosidase (β-Gal-Ao, Sigma-Aldrich) and incubating the mix for 2 hours at 37ºC (van Diggelen et al., 1990). The activity of β-glucuronidase (GUSB) enzyme was determined in

10 µg of protein extract incubated with 4-methylumbelliferyl-β-D-glucuronide (Sigma-Aldrich) at 37ºC for 1 hour. β-hexosaminidase (β-HEXO) activity was assayed by incubation of 0.1 µg of protein extract with 4-methylumbelliferyl N-acetyl-β-D-glucosaminide (Sigma-Aldrich) for 1 hour at 37ºC. After stopping reactions by increasing the pH, released fluorescence was measured with a FLx800 fluorimeter (BioTek Instruments). All brain and liver activity levels were normalized against the total amount of protein, quantified using Bradford protein assay (Bio-Rad Laboratories, *see section 2.7.*). Serum activity was normalized against volume. Activities of IDUA, NAGLU, GUSB and β-HEXO were expressed as nmol/h/mg protein or nmol/h/ml. Activities of SGSH, HGSNAT and GALNS were expressed as nmol/17h/mg protein. All samples of the same tissue of interest were processed and analysed in parallel.

### 2.10. Quantification of GAG content

The glycosaminoglycan quantification was determined in tissue extracts with the Blyscan™ Glycosaminoglycan Assay (Biocolor), following the manufacturer's instructions and using chondroitin 4-sulfate as standard. This method is based on the specific binding of the 1,9-dimethylmethylene blue dye (DMMB) to the sulfated polysaccharides component of proteoglycans or to the protein free sulfated glycosaminoglycan chains. Briefly, 40-70 mg of frozen tissue were digested overnight at 56ºC in 800 µl of phosphate buffer (0.1 M $KH_2PO_4$, 0.1 M $K_2HPO_4$, pH 8) with 150 µg/ml of Proteinase K solution (Roche). After digestion, proteinase K was inactivated at 90ºC for 10 minutes and then, solutions were clarified by centrifugation, for 10 minutes at 10000 *g* and at room temperature, and then filtrated (Ultrafree MC, EMD-Millipore). Different amounts (0-5 µg) of chondroitin 4-sulfate (Blyscan™ Glycosaminoglycan Assay, Biocolor) were preparated to obtain the standard curve. Appropriate volumes of the filtrates and standard curve were adjusted to 100 µl, to which 1 ml of Dye Reagent (Blyscan™ Glycosaminoglycan Assay, Biocolor) was addded. Mixes were shook at 1000-1500 rpm for 30 minutes to allow the formation of DMMB dye-GAG complex, after which the complexes were separated from the remaining excess of soluble dye by centrifugation the mixtures during 10 minutes at 12000 *g* and at room temperature. The supernatants were carefully discarded and the pellets were resuspended by adding 300 µl of Dissociation Reagent (Blyscan™ Glycosaminoglycan Assay, Biocolor). Samples were shook at 1000-1500 rpm for at least 10 minutes to release

the bound dye into the solution and finally, the absorbance at 656 nm and 550 nm was read in a microplate spectrophotometer (PowerWave HT Microplate, BioTek Instruments). Results were normalized to wet tissue weight and all samples of the same tissue of interest were processed and analysed in parallel.

### 2.11. Immunohistochemistry in paraffin-embedded tissue sections

Tissues were fixed for 12-24 hours in formalin (Panreac Química) and then embedded in paraffin following the steps detailed below to dehydrate the samples: tissue samples were placed in 70% v/v ethanol for 1 hour followed by two incubations in 96% v/v ethanol for 1 hour each one. Next, three incubations in 100% v/v ethanol for 1 hour were performed. Once dehydration was finished, samples were transferred successively to three incubations bath of xylol for 30, 30 and 60 minutes respectively and then, two paraffin incubation steps for 2 hours each one were performed. Finally, paraffin blocks were solidified and 3-5 μm were sectioned and mounted in coverplates.

For immunohistochemical detection, sections were deparaffinised and subjected to heat-induced epitope retrieval in citrate buffer (0.09 M $C_6H_8O_7$, 0.08 M $C_6H_5Na_3O_7 \cdot 2H_2O$, pH 6) when required (e.g. for LAMP2 immunohistochemistry). Afterwards, sections were blocked for 30 minutes with PBS solution containing 25% of normal serum and then incubated overnight at 4ºC with the specific primary antibody (*see Table 7, section 1.3.*) diluted in 10% normal serum PBS. After three washes of 5 minutes with PBS, samples were incubated for 1 hour at room temperature with the corresponding secondary antibodies (*see Table 7, section 1.3.*). After washing again, in sections later used for bright-field detections the antibody signal was amplified by incubating sections with ABC-Peroxidase staining kit (Pierce, Thermo Fischer Scientific Inc.), which employs 3',3'-Diaminobenzidine tetrahydroghloride hydrate (DAB, Sigma-Aldrich) as the substrate chromogen. Then, nucleis were counterstained in Mayer's hematoxylin (Merck). For fluorescence detection, sections were incubated with fluorochrome-conjugated antibodies (*see Table 7, section 1.3.*) for 1 hour at room temperature and nuclei were counterstained with Hoechst (Sigma-Aldrich). Brightfield-staining images were obtained with an optical microscope (Eclipse 90i; Nikon). Double fluorescence-immunostaining images were obtained with a confocal microscope (Leyca Microsystems).

### 2.12. Morphometric analysis

The NIS Elements Advanced Research 2.20 software was used to quantify LAMP2, GFAP, and BSI-B4 signal intensity in four images of each brain region (original magnification, X200) per animal, using the same signal threshold settings for all animals. Then, the percentage of positive area was calculated, i.e., the area, in pixels, with a positive signal over the total tissue area in the image.

### 2.13. Transmission electron microscopy

Samples for transmission electron microscopy were obtained from mice euthanized with an overdose of inhalator anaesthetic isofluorane (IsoFluo, Esteve). Mice were perfused via inferior vena cava with a 2.5% glutaraldehyde and 2% paraformaldehyde solution and then a small portion (approximately 1 $mm^3$) of the tissue of interest was sectioned and incubated for 2 hours at 4ºC in the same fixative. After washing in cold 0.1 M phosphate buffer, samples were post-fixed in 1% osmium tetroxide, stained in aqueous uranyl acetate, and then dehydrated through a graded ethanol series and embedded in epoxy resin. Resin blocks were ultrathin (600-800 Å) sectioned and subsequently stained using lead citrate. Samples were analysed with a Hitachi H-7000 transmission electron microscopy (Hitachi, Japan).

### 2.14. Transcriptomic analysis

Total RNA was isolated from encephalon mouse samples with mirVana™ miRNA Isolation Kit (Ambion). Briefly, 30 mg of liver and 250 mg of brain frozen samples were homogenised in 10 volumes of Lysis/Binding Buffer (mirVana™ miRNA Isolation Kit, Ambion) with a T10 Standard ULTRA TURRAX® PCR kit dispersing instrument (IKA). After the addition of 1/10 volumes of miRNA Homogenate Additive solution (mirVana™ miRNA Isolation Kit, Ambion), the mixture was kept on ice for 10 minutes. After the addition of one volume of Acid-Phenol:Chloroform equal to the lysate volume added before, mixtures were centrifuged at 10000 *g* for 5 minutes at room temperature. Then, the upper aqueous phase was recovered and 1.25 volumes of room temperature 100% v/v ethanol was added. The mixture was further purified using Filter Cartridge and following the

manufacturer's instructions (mirVana™ miRNA Isolation Kit, Ambion). After rinsing the columns with the buffers provided by the manufacturer, total RNA was eluted in 100 µl of nuclease-free water.

The concentration of each RNA sample was determined by measurement of the absorbance at 260 nm using a Nanodrop 1000 spectrophotometer (Thermo Fisher Scientific Inc.). Then, 7-10 µg of each sample were sent to Progenika Biopharma to continue the transcriptomic analysis protocol. After cDNA synthesis, samples were hybridized in GeneChip Mouse Gene 2.1 ST 16 array plates (Affymetrix) by Progenika Biopharma. Sample processing was performed following Affymetrix recommended protocols and equipment. Data normalization was done using Affymetrix® Expression Console TM tool with the RMA (Robust Multiarray Averaging) method, and log2 transformed normalized values were obtained. The analysis was focused on known coding sequences, which after data filtering resulted in an initial list of 28427 genes. For differentially expressed genes, the nominal significance level of each univariate test was set to $P \leq 0.001$. For clustering analysis, data was standardized and represented as heatmap using J-Express Pro (jexpress.bioinfo.no). Functional analysis was performed using Genecodis Tool 2.0 (genecodis2.dacya.ucm.es). Cell Type Enrichment (CTEN) analysis was performed using the software available at http://www.influenza-x.org/~jshoemaker/cten/.

## 2.15. Analysis of mRNA expression by qPCR

### *2.15.1. Total RNA isolation*

For total RNA extraction, tissues were rapidly removed after sacrificing the animal and then snap-frozen in liquid nitrogen. Frozen samples were homogenized in 1000 µl of TriPure Isolation Reagen (Roche) with a T10 Standard ULTRA TURRAX® PCR kit dispersing instrument (IKA). After the addition of 0.2 ml of chloroform, the mixture was centrifuged at 12000 *g* and at 4ºC during 15 minutes and the colourless upper aqueous phase was then recovered to proceed to RNA isolation based on a phenol-chloroform extraction. One volume of 70% v/v ethanol was added to the colourless upper aqueous phase and the mixture was further purified using adsorption columns for RNA purification (RNeasy Mini Kit, Qiagen) following the manufacturer's instructions. All samples were treated on-column with DNase I (RNase-Free DNase Set for on-column sample treatment, Qiagen)

and, after rinsing with buffers provided by the manufacturer, total RNA was eluted from the column with 30-50 µl of RNase-free distilled water.

Finally, the concentration of RNA in the different samples was determined by measurement of the absorbance at 260 nm using a Nanodrop 1000 spectrophotometer (Thermo Fisher Scientific Inc.).

### *2.15.2. cDNA synthesis*

cDNA synthesis was performed from 1 µg of total RNA, which was retrotranscribed to first-strand cDNA using the Transcriptor First Strand cDNA Synthesis Kit (Roche) following the instructions of the manufacturer. Oligo-dT and random hexamer oligonucleotides were used as primers for the reaction in the presence of protector RNase inhibitor.

### *2.15.3. Quantification of mRNA expression by qPCR*

Quantitative PCR was performed to quantify the mRNA expression of *Ids* using LightCycler® 480 Probes Master (Roche) with specific primers and probes (Integrated DNA Technologies) listed in Table 11.

**Table 11. Summary of the sequence of the respective forward primers, reverse primers and probes oligonucleotides primers used for the quantification of mRNA expression by qPCR**

| Gene | | Sequence |
|---|---|---|
| Murine *Ids* (optimized sequence) | Forward: | 5'-TGA CAT CGT CTT TAA ACC CCG-3' |
| | Reverse: | 5'-TGT CTG CTC CCA CAA TGA AG-3' |
| | Probe: | 5'-/5HEX/TGT CTT CCC/ZEN/TGG GCA TCA CGT C/3IABkFQ/-3' |
| Murine *Rplp0* (housekeeping gene, also known as 36b4) | Forward: | 5'-AGG ACC GTG GAC TAC AGA TAC-3' |
| | Reverse: | 5'-TGG ATG TCG CTG AAG TTG G-3' |
| | Probe: | 5'-/56-FAM/CAG GAA CTC/ZEN/GCT GGG GTC GAA TG/3IABkFQ/-3' |

In a final volume of 10 µl, qPCR was performed as it is described in Table 12.

**Table 12: Mix for the quantification of mRNA expression by qPCR**

| Reagents | Volume per reaction (µl) |
|---|---|
| LightCycler® 480 Probes Master (Roche) | 5 |
| Mix of forward primer, reverse primer and probe (10x) | 1 |
| Mili-Q $H_2O$ | 2 |
| cDNA (dilution 1/5, from *section 2.15.2.*) | 2 |
| Final volume | 10 |

The time and temperature conditions of qPCR reaction were based on the Dual Color Hydrolysis Probe – UPL Probe 384-II (Light Cycler® 480 II, Roche) programme, which consisted of a first pre-incubation period for 10 minutes at 95ºC, followed by 45 rounds of amplification (10 seconds at 95ºC, 30 seconds at 60ºC and 1 second at 72ºC) and finalised with a cooling step at 40ºC for 30 seconds.

To relatively quantify the expression of the *Ids* gene, *Abs Quant/2$^{nd}$ Derivative Max* (Light Cycler® 480 II, Roche) analysis was used to obtain Cts values. The threshold cycle or Ct indicated the fractional cycle number at which the amount of amplified target reached a fixed threshold. The Ct values obtained for the *Ids* gene were then normalized to the expression of the murine *Rplp0* gene.

## 2.16. Extraction and quantification of vector genome copy number

### *2.16.1. Extraction of total DNA from tissue*

After an overnight tissue digestion in Proteinase K (0.2 mg/ml), total DNA was isolated with MasterPure™ DNA Purification Kit (Epicenter) following the manufacturer's instructions. This commercial kit is based on a salt precipitation-method that allows an efficient DNA yield from any kind of samples.

### *2.16.2. Quantification of vector genome copy number by qPCR*

The vector genome copy numbers were determined in 20 ng of total DNA and the final values of vg/sample were interpolated from a standard curve built by serial dilutions of a linearized plasmid in which the molecules of DNA/µl were known.

#### *2.16.2.1. Generation of the standard curve*

The calibration curve was prepared by serial dilution of a linearized standard plasmid that contains the polyA sequence. Knowing the plasmid concentration and the base pairs of the construct that contains the polyA sequence, the number of molecules of DNA/µl was calculated using Equation 1.

$$Molecules\ of\ DNA/_{\mu l} = \frac{Plasmid\ concentration\ \left(\frac{g}{\mu l}\right) x\ 6.022x10^{23}\left(\frac{molecules}{mol}\right)}{Plasmid\ length\ (bp)\ x\ 622\ \left(\frac{g}{mol\ x\ bp}\right)}$$

**Equation 1. Equation to calculate the number of molecules of the linearized standard plasmid per µl.** Plasmid concentration, expressed in g/µl, is the concentration of the sample measured by spectrophotometry. $6.022x10^{23}$ molecules/mol corresponds to the Avogadro's number. Plasmid length is the number of base pairs of the standard plasmid. 622 g/(mol x bp) corresponds to a constant that define the grams of a mole of a base pair.

Then, serial dilutions (1/10) of the linearized standard plasmid were performed to obtain the standard curve composed of $1x10^7$, $1x10^6$, $1x10^5$, $1x10^4$, $1x10^3$, $1x10^2$ and $1x10^1$ molecules of DNA per µl. Since the concentration of plasmid in any point of the calibration curve is irrelevant when compared with the 20 ng/µl of DNA present in the samples to be analysed, stuffer DNA was added to the calibration curve in order to have the same amplification conditions as DNA samples.

#### *2.16.2.2. Quantification by qPCR*

Quantitative PCR with primers and probe specific for the HBB2 sequence, which was contained in the polyA segment, were used to quantify the vector genome copy number in 20 ng of total DNA. The sequence of the respective primers and probe were: Forward primer: 5'-CTT GAG CAT CTG ACT TCT GGC TAA T-3', Reverse primer: 5'-GAT TTG CCC TCC CAT ATG TCC-3' and Probe: 5'-/56-FAM/CCG AGT GAG AGA CAC AAA AAA TTC CAA CAC/BHQ1/-3'. LightCycler® 480 Probes Master (Roche) was used with the conditions detailed in Table 13.

**Table 13: Mix for qPCR used to determine the vector genome copy number**

| Reagents | Volume per reaction (µl) |
|---|---|
| LightCycler® 480 Probes Master 2x | 5 |
| Forward primer (10 µM) | 0.5 |
| Reverse primer (10 µM) | 0.5 |
| Fluorescent probe (20 µM) | 0.1 |
| Mili-Q $H_2O$ | 1.9 |
| Total DNA (20 ng, from *section 2.16.1.*) | 2 |
| Final volume | 10 |

The time and temperature condition of qPCR reaction were based on the Mono Color Hydrolysis Probe – UPL Probe 384-II (Light Cycler® 480 II, Roche) programme, which

consisted of a first pre-incubation period for 10 minutes at 95ºC, followed by 45 rounds of amplification (10 seconds at 95ºC, 30 seconds at 60ºC and 1 second at 72ºC) and finalised with a cooling step at 40ºC for 30 seconds.

The final values of vector genome copy number were calculated from the qPCR values interpolated to the standard curve and normalized by diploid genome (20 ng of total DNA contains 3115.26 diploid genomes of mouse).

### 2.17. Statistical analysis

All results were expressed as mean ± SEM (Standard Error of the Mean). Statistical comparison were made using 2-tailed Student's T-test for *Part I* and one-way analysis of variance (ANOVA) for *Part II and Part III*. Multiple comparisons between control and treated groups were made using Dunnett's post test, and between all groups using Tukey's post test. The Kaplan-Meier method was used for analysis of the survival, and the log-rank test was used for comparisons. Statistical significance was considered if $P<0.05$.

# VIII. BIBLIOGRAPHY

Akiyama, K., Shimada, Y., Higuchi, T., Ohtsu, M., Nakauchi, H., Kobayashi, H., Fukuda, T., Ida, H., Eto, Y., Crawford, B.E., et al. (2014). Enzyme augmentation therapy enhances the therapeutic efficacy of bone marrow transplantation in mucopolysaccharidosis type II mice. Mol. Genet. Metab. 111, 139–146.

Aldenhoven, M., Sakkers, R.J.B., Boelens, J., de Koning, T.J., and Wulffraat, N.M. (2009). Musculoskeletal manifestations of lysosomal storage disorders. Ann. Rheum. Dis. 68, 1659–1665.

Alroy, J., Garganta, C., and Wiederschain, G. (2014). Secondary biochemical and morphological consequences in lysosomal storage diseases. Biochem. Biokhimiia 79, 619–636.

Altarescu, G., Renbaum, P., Eldar-Geva, T., Brooks, B., Varshaver, I., Avitzour, M., Margalioth, E.J., Levy-Lahad, E., Elstein, D., Epsztejn-Litman, S., et al. (2011). Preventing mucopolysaccharidosis type II (Hunter syndrome): PGD and establishing a Hunter (46, XX) stem cell line. Prenat. Diagn. 31, 853–860.

Al Sawaf, S., Mayatepek, E., and Hoffmann, B. (2008). Neurological findings in Hunter disease: Pathology and possible therapeutic effects reviewed. J. Inherit. Metab. Dis. 31, 473–480.

Appelqvist, H., Wäster, P., Kågedal, K., and Öllinger, K. (2013). The lysosome: from waste bag to potential therapeutic target. J. Mol. Cell Biol. 5, 214–226.

Archer, I.M., Harper, P.S., and Wusteman, F.S. (1982). Multiple forms of iduronate 2-sulphate sulphatase in human tissues and body fluids. Biochim. Biophys. Acta 708, 134–140.

Archer, L.D., Langford-Smith, K.J., Bigger, B.W., and Fildes, J.E. (2014). Mucopolysaccharide diseases: a complex interplay between neuroinflammation, microglial activation and adaptive immunity. J. Inherit. Metab. Dis. 37, 1–12.

Ashworth, J.L., Biswas, S., Wraith, E., and Lloyd, I.C. (2006). Mucopolysaccharidoses and the eye. Surv. Ophthalmol. 51, 1–17.

Ayuso, E., Mingozzi, F., Montane, J., Leon, X., Anguela, X.M., Haurigot, V., Edmonson, S.A., Africa, L., Zhou, S., High, K.A., et al. (2010a). High AAV vector purity results in serotype- and tissue-independent enhancement of transduction efficiency. Gene Ther. 17, 503–510.

Ayuso, E., Mingozzi, F., and Bosch, F. (2010b). Production, purification and characterization of adeno-associated vectors. Curr. Gene Ther. 10, 423–436.

Bach, G., Eisenberg, F., Cantz, M., and Neufeld, E.F. (1973). The defect in the Hunter syndrome: deficiency of sulfoiduronate sulfatase. Proc. Natl. Acad. Sci. U. S. A. 70, 2134–2138.

Baehner, F., Schmiedeskamp, C., Krummenauer, F., Miebach, E., Bajbouj, M., Whybra, C., Kohlschütter, A., Kampmann, C., and Beck, M. (2005). Cumulative incidence rates of the mucopolysaccharidoses in Germany. J. Inherit. Metab. Dis. 28, 1011–1017.

Bailey, K., and Crawley, J. (2009). Anxiety-Related Behaviors in Mice. In Methods of Behavior Analysis in Neuroscience, Buccafusco JJ, ed. (Boca Raton (FL): CRC Press: Frontiers in Neuroscience),.

Bainbridge, J.W.B., Mehat, M.S., Sundaram, V., Robbie, S.J., Barker, S.E., Ripamonti, C., Georgiadis, A., Mowat, F.M., Beattie, S.G., Gardner, P.J., et al. (2015). Long-term effect of gene therapy on Leber's congenital amaurosis. N. Engl. J. Med. 372, 1887–1897.

Balakrishnan, B., and Jayandharan, G.R. (2014). Basic biology of adeno-associated virus (AAV) vectors used in gene therapy. Curr. Gene Ther. 14, 86–100.

Baldo, B.A. (2015). Enzymes approved for human therapy: indications, mechanisms and adverse effects. BioDrugs 29, 31–55.

Baldo, G., Giugliani, R., and Matte, U. (2014). Gene delivery strategies for the treatment of mucopolysaccharidoses. Expert Opin. Drug Deliv. 11, 449–459.

Baldo, G., Lorenzini, D.M., Santos, D.S., Mayer, F.Q., Vitry, S., Bigou, S., Heard, J.M., Matte, U., and Giugliani, R. (2015). Shotgun proteomics reveals possible mechanisms for cognitive impairment in Mucopolysaccharidosis I mice. Mol. Genet. Metab. 114, 138–145.

Ballabio, A., and Gieselmann, V. (2009). Lysosomal disorders: from storage to cellular damage. Biochim. Biophys. Acta 1793, 684–696.

Banecka-Majkutewicz, Z., Jakóbkiewicz-Banecka, J., Gabig-Cimińska, M., Węgrzyn, A., and Węgrzyn, G. (2012). Putative biological mechanisms of efficiency of substrate reduction therapies for mucopolysaccharidoses. Arch. Immunol. Ther. Exp. (Warsz). 60, 461–468.

Bekri, S. (2006). Laboratory diagnosis of lysosomal storage diseases. In Fabry Disease: Perspectives from 5 Years of FOS. Oxford: Oxford PharmaGenesis, A. Mehta, M. Beck, and G. Sunder-Plassmann, eds.

Berg, K., Danes, B.S., and Bearn, A.G. (1968). The linkage relation of the loci for the Xm serum system and the X-linked form of Hurler's syndrome (Hunter's syndrome). Am. J. Hum. Genet. 20, 398–401.

Bevan, A.K., Duque, S., Foust, K.D., Morales, P.R., Braun, L., Schmelzer, L., Chan, C.M., McCrate, M., Chicoine, L.G., Coley, B.D., et al. (2011). Systemic gene delivery in large species for targeting spinal cord, brain, and peripheral tissues for pediatric disorders. Mol. Ther. 19, 1971–1980.

Biffi, A. (2015). GENE THERAPY FOR lYSOSOMAL STORAGE DISORDERS: A GOOD START. Hum. Mol. Genet. 25, R65–R75.

Birnboim, H.C., and Doly, J. (1979). A rapid alkaline extraction procedure for screening recombinant plasmid DNA. Nucleic Acids Res. 7, 1513–1523.

Block, M.L., and Hong, J.-S. (2005). Microglia and inflammation-mediated neurodegeneration: multiple triggers with a common mechanism. Prog. Neurobiol. 76, 77–98.

Boado, R.J., Ka-Wai Hui, E., Zhiqiang Lu, J., and Pardridge, W.M. (2014). Insulin receptor antibody-iduronate 2-sulfatase fusion protein: pharmacokinetics, anti-drug antibody, and safety pharmacology in Rhesus monkeys. Biotechnol. Bioeng. 111, 2317–2325.

Bondeson, M.L., Malmgren, H., Dahl, N., Carlberg, B.M., and Pettersson, U. (1995). Presence of an IDS-related locus (IDS2) in Xq28 complicates the mutational analysis of Hunter syndrome. Eur. J. Hum. Genet. 3, 219–227.

Bonuccelli, G., Regis, S., Filocamo, M., Corsolini, F., Caroli, F., and Gatti, R. (1998). A deletion involving exons 2-4 in the iduronate-2-sulfatase gene of a patient with intermediate Hunter syndrome. Clin. Genet. 53, 474–477.

Boutin, S., Monteilhet, V., Veron, P., Leborgne, C., Benveniste, O., Montus, M.F., and Masurier, C. (2010). Prevalence of serum IgG and neutralizing factors against adeno-associated virus (AAV) types 1, 2, 5, 6, 8, and 9 in the healthy population: implications for gene therapy using AAV vectors. Hum. Gene Ther. 21, 704–712.

Brante, G. (1952). Gargoylism; a mucopolysaccharidosis. Scand. J. Clin. Lab. Invest. 4, 43–46.

Braulke, T., and Bonifacino, J.S. (2009). Sorting of lysosomal proteins. Biochim. Biophys. Acta 1793, 605–614.

Braun, S.E., Aronovich, E.L., Anderson, R.A., Crotty, P.L., McIvor, R.S., and Whitley, C.B. (1993). Metabolic correction and cross-correction of mucopolysaccharidosis type II (Hunter syndrome) by retroviral-mediated gene transfer and expression of human iduronate-2-sulfatase. Proc. Natl. Acad. Sci. U. S. A. 90, 11830–11834.

Braun, S.E., Pan, D., Aronovich, E.L., Jonsson, J.J., McIvor, R.S., and Whitley, C.B. (1996). Preclinical studies of lymphocyte gene therapy for mild Hunter syndrome (mucopolysaccharidosis type II). Hum. Gene Ther. 7, 283–290.

Braunlin, E.A., Harmatz, P.R., Scarpa, M., Furlanetto, B., Kampmann, C., Loehr, J.P., Ponder, K.P., Roberts, W.C., Rosenfeld, H.M., and Giugliani, R. (2011). Cardiac disease in patients with mucopolysaccharidosis: presentation, diagnosis and management. J. Inherit. Metab. Dis. 34, 1183–1197.

Broadhead, D.M., Kirk, J.M., Burt, A.J., Gupta, V., Ellis, P.M., and Besley, G.T. (1986). Full expression of Hunter's disease in a female with an X-chromosome deletion leading to non-random inactivation. Clin. Genet. 30, 392–398.

Bucher, T., Dubreil, L., Colle, M.-A., Maquigneau, M., Deniaud, J., Ledevin, M., Moullier, P., and Joussemet, B. (2014). Intracisternal delivery of AAV9 results in oligodendrocyte and motor neuron transduction in the whole central nervous system of cats. Gene Ther. 21, 522–528.

Buchlis, G., Podsakoff, G.M., Radu, A., Hawk, S.M., Flake, A.W., Mingozzi, F., and High, K.A. (2012). Factor IX expression in skeletal muscle of a severe hemophilia B patient 10 years after AAV-mediated gene transfer. Blood 119, 3038–3041.

Bunge S, Rathmann M, Steglich C, Bondeson ML, Tylki-Szymanska A, Popowska E, G.A. (1998). Homologous nonallelic recombinations between the iduronate-sulfatase gene and pseudogene cause various intragenic deletions and inversions in patients with mucopolysaccharidosis type II. Eur. J. Hum. Genet. 6, 492–500.

Burgess-Brown, N.A., Sharma, S., Sobott, F., Loenarz, C., Oppermann, U., and Gileadi, O. (2008). Codon optimization can improve expression of human genes in Escherichia coli: A multi-gene study. Protein Expr. Purif. 59, 94–102.

Burton, B.K., and Giugliani, R. (2012). Diagnosing Hunter syndrome in pediatric practice: practical considerations and common pitfalls. Eur. J. Pediatr. 171, 631–639.

Burton, B.K., and Whiteman, D.A.H. (2011). Incidence and timing of infusion-related reactions in patients with mucopolysaccharidosis type II (Hunter syndrome) on idursulfase therapy in the real-world setting: a perspective from the Hunter Outcome Survey (HOS). Mol. Genet. Metab. 103, 113–120.

Calcedo, R., Vandenberghe, L.H., Gao, G., Lin, J., and Wilson, J.M. (2009). Worldwide epidemiology of neutralizing antibodies to adeno-associated viruses. J. Infect. Dis. 199, 381–390.

Calcedo, R., Morizono, H., Wang, L., McCarter, R., He, J., Jones, D., Batshaw, M.L., and Wilson, J.M. (2011). Adeno-associated virus antibody profiles in newborns, children, and adolescents. Clin. Vaccine Immunol. 18, 1586–1588.

Calias, P., Papisov, M., Pan, J., Savioli, N., Belov, V., Huang, Y., Lotterhand, J., Alessandrini, M., Liu, N., Fischman, A.J., et al. (2012). CNS penetration of intrathecal-lumbar idursulfase in the monkey, dog and mouse: implications for neurological outcomes of lysosomal storage disorder. PLoS One 7, e30341.

Callejas, D., Mann, C.J., Ayuso, E., Lage, R., Grifoll, I., Roca, C., Andaluz, A., Ruiz-de Gopegui, R., Montané, J., Muñoz, S., et al. (2013). Treatment of diabetes and long-term survival after insulin and glucokinase gene therapy. Diabetes 62, 1718–1729.

de Camargo Pinto, L.L., Maluf, S.W., Leistner-Segal, S., Zimmer da Silva, C., Brusius-Facchin, A., Burin, M.G., Brustolin, S., Llerena, J., Moraes, L., Vedolin, L., et al. (2011). Are MPS II heterozygotes actually asymptomatic? A study based on clinical and biochemical data, X-inactivation analysis and imaging evaluations. Am. J. Med. Genet. A 155A, 50–57.

Cantz, M., Chrambach, A., Bach, G., and Neufeld, E.F. (1972). The Hunter corrective factor. Purification and preliminary characterization. J. Biol. Chem. 247, 5456–5462.

Capila, I., and Linhardt, R.J. (2002). Heparin-protein interactions. Angew. Chem. Int. Ed. Engl. 41, 391–412.

Cardone, M., Polito, V.A., Pepe, S., Mann, L., D'Azzo, A., Auricchio, A., Ballabio, A., and Cosma, M.P. (2006). Correction of Hunter syndrome in the MPSII mouse model by AAV2/8-mediated gene delivery. Hum. Mol. Genet. 15, 1225–1236.

Carpentier, P.A., Duncan, D.S., and Miller, S.D. (2008). Glial toll-like receptor signaling in central nervous system infection and autoimmunity. Brain. Behav. Immun. 22, 140–147.

de Carvalho, T.G., da Silveira Matte, U., Giugliani, R., and Baldo, G. (2015). Genome Editing: Potential Treatment for Lysosomal Storage Diseases. Curr. Stem Cell Reports 1, 9–15.

Chen, D., Zhao, M., and Mundy, G.R. (2004). Bone morphogenetic proteins. Growth Factors 22, 233–241.

Chen, Y.H., Claflin, K., Geoghegan, J.C., and Davidson, B.L. (2012). Sialic acid deposition impairs the utility of AAV9, but not peptide-modified AAVs for brain gene therapy in a mouse model of lysosomal storage disease. Mol. Ther. 20, 1393–1399.

Chira, S., Jackson, C.S., Oprea, I., Ozturk, F., Pepper, M.S., Diaconu, I., Braicu, C., Raduly, L.-Z., Calin, G.A., and Berindan-Neagoe, I. (2015). Progresses towards safe and efficient gene therapy vectors. Oncotarget 6, 30675–30703.

Civallero, G., Michelin, K., de Mari, J., Viapiana, M., Burin, M., Coelho, J.C., and Giugliani, R. (2006). Twelve different enzyme assays on dried-blood filter paper samples for detection of patients with selected inherited lysosomal storage diseases. Clin. Chim. Acta. 372, 98–102.

Clarke, L.A., and Hollak, C.E.M. (2015). The clinical spectrum and pathophysiology of skeletal complications in lysosomal storage disorders. Best Pract. Res. Clin. Endocrinol. Metab. 29, 219–235.

Clarke, J.T., Greer, W.L., Strasberg, P.M., Pearce, R.D., Skomorowski, M.A., and Ray, P.N. (1991). Hunter disease (mucopolysaccharidosis type II) associated with unbalanced inactivation of the X chromosomes in a karyotypically normal girl. Am. J. Hum. Genet. 49, 289–297.

Constantopoulos, G., Iqbal, K., and Dekaban, A.S. (1980). Mucopolysaccharidosis types IH, IS, II, and IIIA: glycosaminoglycans and lipids of isolated brain cells and other fractions from autopsied tissues. J. Neurochem. 34, 1399–1411.

Cox, T.M., and Cachón-González, M.B. (2012). The cellular pathology of lysosomal diseases. J. Pathol. 226, 241–254.

Cudry, S., Tigaud, I., Froissart, R., Bonnet, V., Maire, I., and Bozon, D. (2000). MPS II in females: molecular basis of two different cases. J. Med. Genet. 37, E29.

Daniele, A., Faust, C.J., Herman, G.E., Di Natale, P., and Ballabio, A. (1993). Cloning and Characterization of the cDNA for the Murine Iduronate Sulfatase Gene. Genomics 16, 755–757.

Deganuto, M., Pittis, M.G., Pines, A., Dominissini, S., Kelley, M.R., Garcia, R., Quadrifoglio, F., Bembi, B., and Tell, G. (2007). Altered intracellular redox status in Gaucher disease fibroblasts and impairment of adaptive response against oxidative stress. J. Cell. Physiol. 212, 223–235.

Dekaban, A.S., Constantopoulos, G., Herman, M.M., and Steusing, J.K. (1976). Mucopolysaccharidosis type V. (Scheie syndrome). A postmortem study by multidisciplinary techniques with emphasis on the brain. Arch. Pathol. Lab. Med. 100, 237–245.

Demitsu, T., Kakurai, M., Okubo, Y., Shibayama, C., Kikuchi, Y., Mori, Y., Sukegawa, K., and Mizuguchi, M. (1999). Skin eruption as the presenting sign of Hunter syndrome IIB. Clin. Exp. Dermatol. 24, 179–182.

Desnick, R.J. (2004). Enzyme replacement and enhancement therapies for lysosomal diseases. J. Inherit. Metab. Dis. 27, 385–410.

Diez-Roux, G., and Ballabio, A. (2005). Sulfatases and human disease. Annu. Rev. Genomics Hum. Genet. 6, 355–379.

DiFerrante, N., and Nichols, B.L. (1972). A case of the Hunter syndrome with progeny. Johns Hopkins Med. J. 130, 325–328.

van Diggelen, O.P., Zhao, H., Kleijer, W.J., Janse, H.C., Poorthuis, B.J., van Pelt, J., Kamerling, J.P., and Galjaard, H. (1990). A fluorimetric enzyme assay for the diagnosis of Morquio disease type A (MPS IV A). Clin. Chim. Acta. 187, 131–139.

DiRosario, J., Divers, E., Wang, C., Etter, J., Charrier, A., Jukkola, P., Auer, H., Best, V., Newsom, D.L., McCarty, D.M., et al. (2009). Innate and adaptive immune activation in the brain of MPS IIIB mouse model. J. Neurosci. Res. 87, 978–990.

Donsante, A., McEachin, Z., Riley, J., Leung, C.H., Kanz, L., O'Connor, D.M., and Boulis, N.M. (2016). Intracerebroventricular delivery of self-complementary adeno-associated virus serotype 9 to the adult rat brain. Gene Ther. 23, 401–407.

Dorfman, A., and Lorincz, A.E. (1957). Occurence of urinary acid mucopolysaccharides in the Hurler syndrome. Proc. Natl. Acad. Sci. U. S. A. 43, 443–446.

Duque, S., Joussemet, B., Riviere, C., Marais, T., Dubreil, L., Douar, A.-M., Fyfe, J., Moullier, P., Colle, M.-A., and Barkats, M. (2009). Intravenous administration of self-complementary AAV9 enables transgene delivery to adult motor neurons. Mol. Ther. 17, 1187–1196.

de Duve, C. (2005). The lysosome turns fifty. Nat. Cell Biol. 7, 847–849.

de Duve, C., Pressman, B.C., Gianetto, R., Wattiaux, R., and Appelmans, F. (1955). Tissue fractionation studies. 6. Intracellular distribution patterns of enzymes in rat-liver tissue. Biochem. J. 60, 604–617.

Ellis, R.W.B., Sheldon, W., and Capon, N.B. (1936). Gargoylism (chondro-osteo-dystrophy, corneal opacities, hepatosplenomegaly, and mental deficiency). QJM 5, 119–139.

Eng, L.F., and Ghirnikar, R.S. (1994). GFAP and astrogliosis. Brain Pathol. 4, 229–237.

Enns, G.M., and Huhn, S.L. (2008). Central nervous system therapy for lysosomal storage disorders. Neurosurg. Focus 24, E1–E12.

Ernst, S., Langer, R., Cooney, C.L., and Sasisekharan, R. (1995). Enzymatic degradation of glycosaminoglycans. Crit. Rev. Biochem. Mol. Biol. 30, 387–444.

Fabry, J. (1898). Ein Beitrag Zur Kenntnis der Purpura haemorrhagica nodularis (Purpura papulosa haemorrhagica Hebrae). Arch Dermatol Syph. 43, 187–200.

Faust, C.J., Verkerk, A.J., Wilson, P.J., Morris, C.P., Hopwood, J.J., Oostra, B.A., and Herman, G.E. (1992). Genetic mapping on the mouse X chromosome of human cDNA clones for the fragile X and Hunter syndromes. Genomics 12, 814–817.

Fenzl, C.R., Teramoto, K., and Moshirfar, M. (2015). Ocular manifestations and management recommendations of lysosomal storage disorders I: mucopolysaccharidoses. Clin. Ophthalmol. 9, 1633–1644.

Di Ferrante, N. (1980). N-acetylglucosamine-6-sulfate sulfatase deficiency reconsidered. Science 210, 448.

Filocamo, M., Bonuccelli, G., Corsolini, F., Mazzotti, R., Cusano, R., and Gatti, R. (2001). Molecular analysis of 40 Italian patients with mucopolysaccharidosis type II: New mutations in the iduronate-2-sulfatase (IDS) gene. Hum. Mutat. 18, 164–165.

Flomen, R.H., Green, E.P., Green, P.M., Bentley, D.R., and Giannelli, F. (1993). Determination of the organisation of coding sequences within the iduronate sulphate sulphatase (IDS) gene. Hum. Mol. Genet. 2, 5–10.

Foster, H., Sharp, P.S., Athanasopoulos, T., Trollet, C., Graham, I.R., Foster, K., Wells, D.J., and Dickson, G. (2008). Codon and mRNA sequence optimization of microdystrophin transgenes improves expression and physiological outcome in dystrophic mdx mice following AAV2/8 gene transfer. Mol. Ther. 16, 1825–1832.

Foust, K.D., Nurre, E., Montgomery, C.L., Hernandez, A., Chan, C.M., and Kaspar, B.K. (2009). Intravascular AAV9 preferentially targets neonatal neurons and adult astrocytes. Nat. Biotechnol. 27, 59–65.

Fraldi, A., Biffi, A., Lombardi, A., Visigalli, I., Pepe, S., Settembre, C., Nusco, E., Auricchio, A., Naldini, L., Ballabio, A., et al. (2007a). SUMF1 enhances sulfatase activities in vivo in five sulfatase deficiencies. Biochem. J. 403, 305–312.

Fraldi, A., Hemsley, K., Crawley, A., Lombardi, A., Lau, A., Sutherland, L., Auricchio, A., Ballabio, A., and Hopwood, J.J. (2007b). Functional correction of CNS lesions in an MPS-IIIA mouse model by intracerebral AAV-mediated delivery of sulfamidase and SUMF1 genes. Hum. Mol. Genet. 16, 2693–2702.

Fratantoni, J.C., Hall, C.W., and Neufeld, E.F. (1968). The defect in Hurler's and Hunter's syndromes: faulty degradation of mucopolysaccharide. Proc. Natl. Acad. Sci. U. S. A. 60, 699–706.

Fratantoni, J.C., Hall, C.W., and Neufeld, E.F. (1969). The defect in Hurler and Hunter syndromes. II. Deficiency of specific factors involved in mucopolysaccharide degradation. Proc. Natl. Acad. Sci. U. S. A. 64, 360–366.

Friso, A., Tomanin, R., Alba, S., Gasparotto, N., Puicher, E.P., Fusco, M., Hortelano, G., Muenzer, J., Marin, O., Zacchello, F., et al. (2005). Reduction of GAG storage in MPS II mouse model following implantation of encapsulated recombinant myoblasts. J. Gene Med. 7, 1482–1491.

Friso, A., Tomanin, R., Salvalaio, M., and Scarpa, M. (2010). Genistein reduces glycosaminoglycan levels in a mouse model of mucopolysaccharidosis type II. Br. J. Pharmacol. 159, 1082–1091.

Froissart, R., Millat, G., Mathieu, M., Bozon, D., and Maire, I. (1995). Processing of iduronate 2-sulphatase in human fibroblasts. Biochem. J. 309 (Pt 2), 425–430.

Froissart, R., Moreira da Silva, I., Guffon, N., Bozon, D., and Maire, I. (2002). Mucopolysaccharidosis type II--genotype/phenotype aspects. Acta Paediatr. Suppl. 91, 82–87.

Froissart, R., Da Silva, I.M., and Maire, I. (2007). Mucopolysaccharidosis type II: an update on mutation spectrum. Acta Paediatr. Suppl. 96, 71–77.

Fu, H., Dirosario, J., Killedar, S., Zaraspe, K., and McCarty, D.M. (2011). Correction of neurological disease of mucopolysaccharidosis IIIB in adult mice by rAAV9 trans-blood-brain barrier gene delivery. Mol. Ther. 19, 1025–1033.

Fu, H., Bartz, J.D., Stephens, R.L., and McCarty, D.M. (2012). Peripheral nervous system neuropathology and progressive sensory impairments in a mouse model of Mucopolysaccharidosis IIIB. PLoS One 7, e45992.

Fuller, M., Meikle, P.J., and Hopwood, J.J. (2006). Epidemiology of lysosomal storage diseases: an overview. In Fabry Disease: Perspectives from 5 Years of FOS, A. Mehta, M. Beck, and G. Sunder-Plassmann, eds. (Oxford PharmaGenesis), Chapter 2.

Fusar Poli, E., Zalfa, C., D'Avanzo, F., Tomanin, R., Carlessi, L., Bossi, M., Rota Nodari, L., Binda, E., Marmiroli, P., Scarpa, M., et al. (2013). Murine neural stem cells model Hunter disease in vitro: glial cell-mediated neurodegeneration as a possible mechanism involved. Cell Death Dis. 4, e906.

Futerman, A.H., and van Meer, G. (2004). The cell biology of lysosomal storage disorders. Nat. Rev. Mol. Cell Biol. 5, 554–565.

Gao, G., Vandenberghe, L.H., Alvira, M.R., Lu, Y., Calcedo, R., Zhou, X., and Wilson, J.M. (2004). Clades of Adeno-associated viruses are widely disseminated in human tissues. J. Virol. 78, 6381–6388.

Garcia, A.R., DaCosta, J.M., Pan, J., Muenzer, J., and Lamsa, J.C. (2007a). Preclinical dose ranging studies for enzyme replacement therapy with idursulfase in a knock-out mouse model of MPS II. Mol. Genet. Metab. 91, 183–190.

Garcia, A.R., Pan, J., Lamsa, J.C., and Muenzer, J. (2007b). The characterization of a murine model of mucopolysaccharidosis II (Hunter syndrome). J. Inherit. Metab. Dis. 30, 924–934.

Gaucher, P. (1882). De l'epithelioma primitif de la rate, hypertrophie idiopathique del la rate san leucemie. Thesis, Doctor of Medicine. Octave Doin, University of Paris, France.

Gaudet, D., Méthot, J., Déry, S., Brisson, D., Essiembre, C., Tremblay, G., Tremblay, K., de Wal, J., Twisk, J., van den Bulk, N., et al. (2013). Efficacy and long-term safety of alipogene tiparvovec (AAV1-LPLS447X) gene therapy for lipoprotein lipase deficiency: an open-label trial. Gene Ther. 20, 361–369.

Gelb, M.H., Turecek, F., Scott, C.R., and Chamoles, N.A. (2006). Direct multiplex assay of enzymes in dried blood spots by tandem mass spectrometry for the newborn screening of lysosomal storage disorders. J. Inherit. Metab. Dis. 29, 397–404.

Ginzburg, L., Kacher, Y., and Futerman, A.H. (2004). The pathogenesis of glycosphingolipid storage disorders. Semin. Cell Dev. Biol. 15, 417–431.

Giugliani, R., Federhen, A., Rojas, M.V.M., Vieira, T., Artigalás, O., Pinto, L.L., Azevedo, A.C., Acosta, A., Bonfim, C., Lourenço, C.M., et al. (2010). Mucopolysaccharidosis I, II, and VI: Brief review and guidelines for treatment. Genet. Mol. Biol. 33, 589–604.

Giugliani, R., Federhen, A., Vairo, F., Vanzella, C., Pasqualim, G., da Silva, L.M.R., Giugliani, L., de Boer, A.P.K., de Souza, C.F.M., Matte, U., et al. (2016). Emerging drugs for the treatment of mucopolysaccharidoses. Expert Opin. Emerg. Drugs 21, 9–26.

Gort, L., Chabás, A., and Coll, M.J. (1998). Hunter disease in the Spanish population: molecular analysis in 31 families. J. Inherit. Metab. Dis. 21, 655–661.

Gray, G., Claridge, P., Jenkinson, L., and Green, A. (2007). Quantitation of urinary glycosaminoglycans using dimethylene blue as a screening technique for the diagnosis of mucopolysaccharidoses: an evaluation. Ann. Clin. Biochem. 44, 360–363.

Gray, S.J., Matagne, V., Bachaboina, L., Yadav, S., Ojeda, S.R., and Samulski, R.J. (2011). Preclinical differences of intravascular AAV9 delivery to neurons and glia: a comparative study of adult mice and nonhuman primates. Mol. Ther. 19, 1058–1069.

Gray, S.J., Nagabhushan Kalburgi, S., McCown, T.J., and Jude Samulski, R. (2013). Global CNS gene delivery and evasion of anti-AAV-neutralizing antibodies by intrathecal AAV administration in non-human primates. Gene Ther. 20, 450–459.

Gritti, A., Parati, E.A., Cova, L., Frolichsthal, P., Galli, R., Wanke, E., Faravelli, L., Morassutti, D.J., Roisen, F., Nickel, D.D., et al. (1996). Multipotential stem cells from the adult mouse brain proliferate and self-renew in response to basic fibroblast growth factor. J. Neurosci. 16, 1091–1100.

Guillén-Navarro, E., Domingo-Jiménez, M.R., Alcalde-Martín, C., Cancho-Candela, R., Couce, M.L., Galán-Gómez, E., and Alonso-Luengo, O. (2013). Clinical manifestations in female carriers of mucopolysaccharidosis type II: a spanish cross-sectional study. Orphanet J. Rare Dis. 8, 92.

Gurda, B.L., De Guilhem De Lataillade, A., Bell, P., Zhu, Y., Yu, H., Wang, P., Bagel, J., Vite, C.H., Sikora, T., Hinderer, C., et al. (2016). Evaluation of AAV-mediated gene therapy for central nervous system disease in canine mucopolysaccharidosis VII. Mol. Ther. 24, 206–216.

Häcker, U., Nybakken, K., and Perrimon, N. (2005). Heparan sulphate proteoglycans: the sweet side of development. Nat. Rev. Mol. Cell Biol. 6, 530–541.

Hamano, K., Hayashi, M., Shioda, K., Fukatsu, R., and Mizutani, S. (2008). Mechanisms of neurodegeneration in mucopolysaccharidoses II and IIIB: analysis of human brain tissue. Acta Neuropathol. 115, 547–559.

Haskins, M.E. (2007). Animal models for mucopolysaccharidosis disorders and their clinical relevance. Acta Paediatr. Suppl. 96, 56–62.

Haurigot, V., Marcó, S., Ribera, A., Garcia, M., Ruzo, A., Villacampa, P., Ayuso, E., Añor, S., Andaluz, A., Pineda, M., et al. (2013). Whole body correction of mucopolysaccharidosis IIIA by intracerebrospinal fluid gene therapy. J. Clin. Invest. 123, 3254–3271.

Hauswirth, W.W., Aleman, T.S., Kaushal, S., Cideciyan, A. V, Schwartz, S.B., Wang, L., Conlon, T.J., Boye, S.L., Flotte, T.R., Byrne, B.J., et al. (2008). Treatment of leber congenital amaurosis due to RPE65 mutations by ocular subretinal injection of adeno-associated virus gene vector: short-term results of a phase I trial. Hum. Gene Ther. 19, 979–990.

Hers, H.G. (1965). INBORN LYSOSOMAL DISEASES. Gastroenterology 48, 625–633.

Higuchi, T., Shimizu, H., Fukuda, T., Kawagoe, S., Matsumoto, J., Shimada, Y., Kobayashi, H., Ida, H., Ohashi, T., Morimoto, H., et al. (2012). Enzyme replacement therapy (ERT)

procedure for mucopolysaccharidosis type II (MPS II) by intraventricular administration (IVA) in murine MPS II. Mol. Genet. Metab. 107, 122–128.

Hinderer, C., Bell, P., Vite, C.H., Louboutin, J.-P., Grant, R., Bote, E., Yu, H., Pukenas, B., Hurst, R., and Wilson, J.M. (2014a). Widespread gene transfer in the central nervous system of cynomolgus macaques following delivery of AAV9 into the cisterna magna. Mol. Ther. Methods Clin. Dev. 1, 14051.

Hinderer, C., Bell, P., Gurda, B.L., Wang, Q., Louboutin, J.-P., Zhu, Y., Bagel, J., O'Donnell, P., Sikora, T., Ruane, T., et al. (2014b). Intrathecal gene therapy corrects CNS pathology in a feline model of mucopolysaccharidosis I. Mol. Ther. 22, 2018–2027.

Hinderer, C., Bell, P., Louboutin, J.-P., Zhu, Y., Yu, H., Lin, G., Choa, R., Gurda, B.L., Bagel, J., O'Donnell, P., et al. (2015). Neonatal Systemic AAV Induces Tolerance to CNS Gene Therapy in MPS I Dogs and Nonhuman Primates. Mol. Ther. 23, 1298–1307.

Hobbs, J.R., Hugh-Jones, K., Barrett, A.J., Byrom, N., Chambers, D., Henry, K., James, D.C., Lucas, C.F., Rogers, T.R., Benson, P.F., et al. (1981). Reversal of clinical features of Hurler's disease and biochemical improvement after treatment by bone-marrow transplantation. Lancet (London, England) 2, 709–712.

Hobolth, N., and Pedersen, C. (1978). European Society of Human Genetics Abstracts from Symposium on "Clinical Genetics" Oslo, Norway: "Six cases of a mild form of the Hunter syndrome in five generations. Three affected males with progeny." Clin. Genet. 13, 121.

Hollak, C.E.M., and Wijburg, F.A. (2014). Treatment of lysosomal storage disorders: successes and challenges. J. Inherit. Metab. Dis. 37, 587–598.

Holt, J.B., Poe, M.D., and Escolar, M.L. (2011). Natural progression of neurological disease in mucopolysaccharidosis type II. Pediatrics 127, e1258–e1265.

Van Hoof, F., and Hers, H.G. (1968). The abnormalities of lysosomal enzymes in mucopolysacc- haridoses. Eur. J. Biochem. 7, 34–44.

Hopwood, J.J., Bunge, S., Morris, C.P., Wilson, P.J., Steglich, C., Beck, M., Schwinger, E., and Gal, A. (1993). Molecular basis of mucopolysaccharidosis type II: mutations in the iduronate-2-sulphatase gene. Hum. Mutat. 2, 435–442.

Hunter, C. (1917). A Rare Disease in Two Brothers. Proc. R. Soc. Med. 10, 104–116.

Hurler, G. (1919). Über einen Typ multipler Abartungen, vorwiegend am Skelettsystem. Z. Kinderheilkd. 24, 220–234.

Ito, D., Imai, Y., Ohsawa, K., Nakajima, K., Fukuuchi, Y., and Kohsaka, S. (1998). Microglia-specific localisation of a novel calcium binding protein, Iba1. Mol. Brain Res. 57, 1–9.

Jackson, K.L., Dayton, R.D., and Klein, R.L. (2015). AAV9 supports wide-scale transduction of the CNS and TDP-43 disease modeling in adult rats. Mol. Ther. Methods Clin. Dev. 2, 15036.

Jacobson, S.G., Cideciyan, A. V, Ratnakaram, R., Heon, E., Schwartz, S.B., Roman, A.J., Peden, M.C., Aleman, T.S., Boye, S.L., Sumaroka, A., et al. (2012). Gene therapy for leber congenital amaurosis caused by RPE65 mutations: safety and efficacy in 15 children and adults followed up to 3 years. Arch. Ophthalmol. (Chicago, Ill. 1960) 130, 9–24.

Jimenez, V., Muñoz, S., Casana, E., Mallol, C., Elias, I., Jambrina, C., Ribera, A., Ferre, T., Franckhauser, S., and Bosch, F. (2013). In vivo adeno-associated viral vector-mediated genetic engineering of white and brown adipose tissue in adult mice. Diabetes 62, 4012–4022.

Jones, S.A., Almássy, Z., Beck, M., Burt, K., Clarke, J.T., Giugliani, R., Hendriksz, C., Kroepfl, T., Lavery, L., Lin, S.-P., et al. (2009). Mortality and cause of death in mucopolysaccharidosis type II-a historical review based on data from the Hunter Outcome Survey (HOS). J. Inherit. Metab. Dis. 32, 534–543.

de Jong, J.G., Wevers, R.A., and Liebrand-van Sambeek, R. (1992). Measuring urinary glycosaminoglycans in the presence of protein: an improved screening procedure for mucopolysaccharidoses based on dimethylmethylene blue. Clin. Chem. 38, 803–807.

Jung, S.-C., Park, E.-S., Choi, E.N., Kim, C.H., Kim, S.J., and Jin, D.-K. (2010). Characterization of a novel mucopolysaccharidosis type II mouse model and recombinant AAV2/8 vector-mediated gene therapy. Mol. Cells 30, 13–18.

Jurecka, A., Krumina, Z., Żuber, Z., Różdżyńska-Świątkowska, A., Kłoska, A., Czartoryska, B., and Tylki-Szymańska, A. (2012). Mucopolysaccharidosis type II in females and response to enzyme replacement therapy. Am. J. Med. Genet. A 158A, 450–454.

Jurecka, A., Ługowska, A., Golda, A., Czartoryska, B., and Tylki-Szymańska, A. (2015). Prevalence rates of mucopolysaccharidoses in Poland. J. Appl. Genet. 56, 205–210.

Kampmann, C., Beck, M., Morin, I., and Loehr, J.P. (2011). Prevalence and characterization of cardiac involvement in Hunter syndrome. J. Pediatr. 159, 327–331.

Karpova, E.A., Voznyi YaV, Keulemans, J.L., Hoogeveen, A.T., Winchester, B., Tsvetkova, I. V, and van Diggelen, O.P. (1996). A fluorimetric enzyme assay for the diagnosis of Sanfilippo disease type A (MPS IIIA). J. Inherit. Metab. Dis. 19, 278–285.

Kasapkara, Ç.S., Tümer, L., Aslan, A.T., Hasanoğlu, A., Ezgü, F.S., Küçükçongar, A., Tunca, Z., and Köktürk, O. (2014). Home sleep study characteristics in patients with mucopolysaccharidosis. Sleep Breath. 18, 143–149.

Keulemans, J.L.M., Sinigerska, I., Garritsen, V.H., Huijmans, J.G.M., Voznyi, Y. V, van Diggelen, O.P., and Kleijer, W.J. (2002). Prenatal diagnosis of the Hunter syndrome and the introduction of a new fluorimetric enzyme assay. Prenat. Diagn. 22, 1016–1021.

Khan, S.A., Nelson, M.S., Pan, C., Gaffney, P.M., and Gupta, P. (2008). Endogenous heparan sulfate and heparin modulate bone morphogenetic protein-4 signaling and activity. Am. J. Physiol. Cell Physiol. 294, C1387–C1397.

Klein, R.L., Dayton, R.D., Tatom, J.B., Henderson, K.M., and Henning, P.P. (2008). AAV8, 9, Rh10, Rh43 vector gene transfer in the rat brain: effects of serotype, promoter and purification method. Mol. Ther. 16, 89–96.

Kloska, A., Jakóbkiewicz-Banecka, J., Tylki-Szymańska, A., Czartoryska, B., and Węgrzyn, G. (2011). Female Hunter syndrome caused by a single mutation and familial XCI skewing: implications for other X-linked disorders. Clin. Genet. 80, 459–465.

Kotin, R.M., Siniscalco, M., Samulski, R.J., Zhu, X.D., Hunter, L., Laughlin, C.A., McLaughlin, S., Muzyczka, N., Rocchi, M., and Berns, K.I. (1990). Site-specific integration by adeno-associated virus. Proc. Natl. Acad. Sci. U. S. A. 87, 2211–2215.

Kotterman, M.A., and Schaffer, D. V (2014). Engineering adeno-associated viruses for clinical gene therapy. Nat. Rev. Genet. 15, 445–451.

Kotterman, M.A., Chalberg, T.W., and Schaffer, D. V (2015). Viral Vectors for Gene Therapy: Translational and Clinical Outlook. Annu. Rev. Biomed. Eng. 17, 63–89.

Kowalewski, B., Lamanna, W.C., Lawrence, R., Damme, M., Stroobants, S., Padva, M., Kalus, I., Frese, M.-A., Lübke, T., Lüllmann-Rauch, R., et al. (2012). Arylsulfatase G inactivation causes loss of heparan sulfate 3-O-sulfatase activity and mucopolysaccharidosis in mice. Proc. Natl. Acad. Sci. U. S. A. 109, 10310–10315.

Krabbi, K., Joost, K., Zordania, R., Talvik, I., Rein, R., Huijmans, J.G.M., Verheijen, F. V, and Õunap, K. (2012). The live-birth prevalence of mucopolysaccharidoses in Estonia. Genet. Test. Mol. Biomarkers 16, 846–849.

Krivit, W., Sung, J.H., Shapiro, E.G., and Lockman, L.A. (1995). Microglia: the effector cell for reconstitution of the central nervous system following bone marrow transplantation for lysosomal and peroxisomal storage diseases. Cell Transplant. 4, 385–392.

Kudla, G., Murray, A.W., Tollervey, D., and Plotkin, J.B. (2009). Coding-sequence determinants of gene expression in Escherichia coli. Science 324, 255–258.

Lehtinen, M.K., Bjornsson, C.S., Dymecki, S.M., Gilbertson, R.J., Holtzman, D.M., and Monuki, E.S. (2013). The choroid plexus and cerebrospinal fluid: emerging roles in development, disease, and therapy. J. Neurosci. 33, 17553–17559.

Li, F., Shetty, A.K., and Sugahara, K. (2007). Neuritogenic Activity of Chondroitin/Dermatan Sulfate Hybrid Chains of Embryonic Pig Brain and Their Mimicry from Shark Liver:

Involvement of the pleiotrophin and hepatocyte growth factor signaling pathways. J. Biol. Chem. 282, 2956–2966.

Li, P., Bellows, A.B., and Thompson, J.N. (1999). Molecular basis of iduronate-2-sulphatase gene mutations in patients with mucopolysaccharidosis type II (Hunter syndrome). J. Med. Genet. 36, 21–27.

Lin, H.-Y., Lin, S.-P., Chuang, C.-K., Niu, D.-M., Chen, M.-R., Tsai, F.-J., Chao, M.-C., Chiu, P.-C., Lin, S.-J., Tsai, L.-P., et al. (2009). Incidence of the mucopolysaccharidoses in Taiwan, 1984-2004. Am. J. Med. Genet. A 149A, 960–964.

Link, B., de Camargo Pinto, L.L., Giugliani, R., Wraith, J.E., Guffon, N., Eich, E., and Beck, M. (2010). Orthopedic manifestations in patients with mucopolysaccharidosis type II (Hunter syndrome) enrolled in the Hunter Outcome Survey. Orthop. Rev. (Pavia). 2, e16.

Lisowski, L., Tay, S.S., and Alexander, I.E. (2015). Adeno-associated virus serotypes for gene therapeutics. Curr. Opin. Pharmacol. 24, 59–67.

Liu, F., Song, Y., and Liu, D. (1999). Hydrodynamics-based transfection in animals by systemic administration of plasmid DNA. Gene Ther. 6, 1258–1266.

Lloyd-Evans, E., Morgan, A.J., He, X., Smith, D.A., Elliot-Smith, E., Sillence, D.J., Churchill, G.C., Schuchman, E.H., Galione, A., and Platt, F.M. (2008). Niemann-Pick disease type C1 is a sphingosine storage disease that causes deregulation of lysosomal calcium. Nat. Med. 14, 1247–1255.

Lock, M., McGorray, S., Auricchio, A., Ayuso, E., Beecham, E.J., Blouin-Tavel, V., Bosch, F., Bose, M., Byrne, B.J., Caton, T., et al. (2010). Characterization of a recombinant adeno-associated virus type 2 Reference Standard Material. Hum. Gene Ther. 21, 1273–1285.

Lowry, R.B., Applegarth, D.A., Toone, J.R., MacDonald, E., and Thunem, N.Y. (1990). An update on the frequency of mucopolysaccharide syndromes in British Columbia. Hum. Genet. 85, 389–390.

Lyon, M.F. (1961). Gene action in the X-chromosome of the mouse (Mus musculus L.). Nature 190, 372–373.

Lyon, M., Deakin, J.A., Rahmoune, H., Fernig, D.G., Nakamura, T., and Gallagher, J.T. (1998). Hepatocyte growth factor/scatter factor binds with high affinity to dermatan sulfate. J. Biol. Chem. 273, 271–278.

Maguire, A.M., Simonelli, F., Pierce, E.A., Pugh, E.N., Mingozzi, F., Bennicelli, J., Banfi, S., Marshall, K.A., Testa, F., Surace, E.M., et al. (2008). Safety and Efficacy of Gene Transfer for Leber's Congenital Amaurosis. N. Engl. J. Med. 358, 2240–2248.

Maguire, A.M., High, K.A., Auricchio, A., Wright, J.F., Pierce, E.A., Testa, F., Mingozzi, F., Bennicelli, J.L., Ying, G., Rossi, S., et al. (2009). Age-dependent effects of RPE65 gene

therapy for Leber's congenital amaurosis: a phase 1 dose-escalation trial. Lancet (London, England) 374, 1597–1605.

Malavaki, C., Mizumoto, S., Karamanos, N., and Sugahara, K. (2008). Recent advances in the structural study of functional chondroitin sulfate and dermatan sulfate in health and disease. Connect. Tissue Res. 49, 133–139.

Malm, G., Lund, A.M., Månsson, J.-E., and Heiberg, A. (2008). Mucopolysaccharidoses in the Scandinavian countries: incidence and prevalence. Acta Paediatr. 97, 1577–1581.

Manno, C.S., Pierce, G.F., Arruda, V.R., Glader, B., Ragni, M., Rasko, J.J., Rasko, J., Ozelo, M.C., Hoots, K., Blatt, P., et al. (2006). Successful transduction of liver in hemophilia by AAV-Factor IX and limitations imposed by the host immune response. Nat. Med. 12, 342–347.

Marsh, J., and Fensom, A.H. (1985). 4-Methylumbelliferyl alpha-N-acetylglucosaminidase activity for diagnosis of Sanfilippo B disease. Clin. Genet. 27, 258–262.

Martin, R., Beck, M., Eng, C., Giugliani, R., Harmatz, P., Muñoz, V., and Muenzer, J. (2008). Recognition and diagnosis of mucopolysaccharidosis II (Hunter syndrome). Pediatrics 121, e377–e386.

Matalon, R., and Dorfman, A. (1966). Hurler's syndrome: biosynthesis of acid mucopolysaccharides in tissue culture. Proc. Natl. Acad. Sci. U. S. A. 56, 1310–1316.

Matos, L., Gonçalves, V., Pinto, E., Laranjeira, F., Prata, M.J., Jordan, P., Desviat, L.R., Pérez, B., and Alves, S. (2015). Functional analysis of splicing mutations in the IDS gene and the use of antisense oligonucleotides to exploit an alternative therapy for MPS II. Biochim. Biophys. Acta - Mol. Basis Dis. 1852, 2712–2721.

Matsumoto, K., and Nakamura, T. (1996). Emerging multipotent aspects of hepatocyte growth factor. J. Biochem. 119, 591–600.

Matsushita, T., Elliger, S., Elliger, C., Podsakoff, G., Villarreal, L., Kurtzman, G.J., Iwaki, Y., and Colosi, P. (1998). Adeno-associated virus vectors can be efficiently produced without helper virus. Gene Ther. 5, 938–945.

Mauro, V.P., and Chappell, S.A. (2014). A critical analysis of codon optimization in human therapeutics. Trends Mol. Med. 20, 604–613.

McCarty, D.M., Young, S.M., and Samulski, R.J. (2004). Integration of adeno-associated virus (AAV) and recombinant AAV vectors. Annu. Rev. Genet. 38, 819–845.

McGeer, P.L., and McGeer, E.G. (1998). Glial cell reactions in neurodegenerative diseases: pathophysiology and therapeutic interventions. Alzheimer Dis. Assoc. Disord. 12 Suppl 2, S1–S6.

McKusick, V.A. (1956). Heritable disorders of connective tissue. J. Chronic Dis. 3, 360–389.

Meikle, P.J., Hopwood, J.J., Clague, A.E., and Carey, W.F. (1999). Prevalence of lysosomal storage disorders. JAMA 281, 249–254.

Millat, G., Froissart, R., Maire, I., and Bozon, D. (1997). Characterization of iduronate sulphatase mutants affecting N-glycosylation sites and the cysteine-84 residue. Biochem. J. 326, 243–247.

Moreira, G.A., Kyosen, S.O., Patti, C.L., Martins, A.M., and Tufik, S. (2014). Prevalence of obstructive sleep apnea in patients with mucopolysaccharidosis types I, II, and VI in a reference center. Sleep Breath. 18, 791–797.

Moreira da Silva, I., Froissart, R., Marques dos Santos, H., Caseiro, C., Maire, I., and Bozon, D. (2001). Molecular basis of mucopolysaccharidosis type II in Portugal: identification of four novel mutations. Clin. Genet. 60, 316–318.

Mossman, J., Blunt, S., Stephens, R., Jones, E.E., and Pembrey, M. (1983). Hunter's disease in a girl: association with X:5 chromosomal translocation disrupting the Hunter gene. Arch. Dis. Child. 58, 911–915.

Muenzer, J. (2011). Overview of the mucopolysaccharidoses. Rheumatology (Oxford). 50 Suppl 5, v4–v12.

Muenzer, J., Lamsa, J.C., Garcia, A., Dacosta, J., Garcia, J., and Treco, D.A. (2002). Enzyme replacement therapy in mucopolysaccharidosis type II (Hunter syndrome): a preliminary report. Acta Paediatr. Suppl. 91, 98–99.

Muenzer, J., Wraith, J.E., Beck, M., Giugliani, R., Harmatz, P., Eng, C.M., Vellodi, A., Martin, R., Ramaswami, U., Gucsavas-Calikoglu, M., et al. (2006). A phase II/III clinical study of enzyme replacement therapy with idursulfase in mucopolysaccharidosis II (Hunter syndrome). Genet. Med. 8, 465–473.

Muenzer, J., Gucsavas-Calikoglu, M., McCandless, S.E., Schuetz, T.J., and Kimura, A. (2007). A phase I/II clinical trial of enzyme replacement therapy in mucopolysaccharidosis II (Hunter syndrome). Mol. Genet. Metab. 90, 329–337.

Muenzer, J., Beck, M., Eng, C.M., Escolar, M.L., Giugliani, R., Guffon, N.H., Harmatz, P., Kamin, W., Kampmann, C., Koseoglu, S.T., et al. (2009). Multidisciplinary management of Hunter syndrome. Pediatrics 124, e1228–e1239.

Muenzer, J., Beck, M., Eng, C.M., Giugliani, R., Harmatz, P., Martin, R., Ramaswami, U., Vellodi, A., Wraith, J.E., Cleary, M., et al. (2011). Long-term, open-labeled extension study of idursulfase in the treatment of Hunter syndrome. Genet. Med. 13, 95–101.

Muenzer, J., Bodamer, O., Burton, B., Clarke, L., Frenking, G.S., Giugliani, R., Jones, S., Rojas, M.V.M., Scarpa, M., Beck, M., et al. (2012). The role of enzyme replacement therapy in severe Hunter syndrome-an expert panel consensus. Eur. J. Pediatr. 171, 181–188.

Muenzer, J., Hendriksz, C.J., Fan, Z., Vijayaraghavan, S., Perry, V., Santra, S., Solanki, G. a., Mascelli, M.A., Pan, L., Wang, N., et al. (2015). A phase I/II study of intrathecal idursulfase-IT in children with severe mucopolysaccharidosis II. Genet. Med. 1–9.

Mullen, R.J., Buck, C.R., and Smith, A.M. (1992). NeuN, a neuronal specific nuclear protein in vertebrates. Development 116, 201–211.

Mulloy, B. (2005). The specificity of interactions between proteins and sulfated polysaccharides. An. Acad. Bras. Cienc. 77, 651–664.

Naldini, L. (2015). Gene therapy returns to centre stage. Nature 526, 351–360.

Di Natale, P., and Ronsisvalle, L. (1981). Identification and partial characterization of two enzyme forms of iduronate sulfatase from human placenta. Biochim. Biophys. Acta 661, 106–111.

Nathwani, A.C., Reiss, U.M., Tuddenham, E.G.D., Rosales, C., Chowdary, P., McIntosh, J., Della Peruta, M., Lheriteau, E., Patel, N., Raj, D., et al. (2014). Long-Term Safety and Efficacy of Factor IX Gene Therapy in Hemophilia B. N. Engl. J. Med. 371, 1994–2004.

Nayerossadat, N., Maedeh, T., and Ali, P.A. (2012). Viral and nonviral delivery systems for gene delivery. Adv. Biomed. Res. 1, 27.

Nelson, J. (1997). Incidence of the mucopolysaccharidoses in Northern Ireland. Hum. Genet. 101, 355–358.

Nelson, J., Crowhurst, J., Carey, B., and Greed, L. (2003). Incidence of the mucopolysaccharidoses in Western Australia. Am. J. Med. Genet. A 123A, 310–313.

Neufeld, E.F. (1991). Lysosomal storage diseases. Annu. Rev. Biochem. 60, 257–280.

Neufeld, E.F., and Cantz, M.J. (1971). Corrective factors for inborn errors of mucopolysaccharide metabolism. Ann. N. Y. Acad. Sci. 179, 580–587.

Neufeld, E.F., and Muenzer, J. (2001). The mucopolysaccharidoses. In The Metabolic and Molecular Basis of Inherited Disease, B. Scriver, C.R., Beaudet, A.L., Sly, W.S., Valle, D., Childs, B., Kinzler, K.W., and Vogelstein, ed. (New York: McGraw-Hill, Medical Publishing Division), pp. 3421–3454.

Nielsen, T.C., Rozek, T., Hopwood, J.J., and Fuller, M. (2010). Determination of urinary oligosaccharides by high-performance liquid chromatography/electrospray ionization-tandem mass spectrometry: Application to Hunter syndrome. Anal. Biochem. 402, 113–120.

Niemeyer, G.P., Herzog, R.W., Mount, J., Arruda, V.R., Tillson, D.M., Hathcock, J., van Ginkel, F.W., High, K.A., and Lothrop, C.D. (2009). Long-term correction of inhibitor-prone hemophilia B dogs treated with liver-directed AAV2-mediated factor IX gene therapy. Blood 113, 797–806.

Nja, A. (1946). A sex-linked type of gargoylism. Acta Paediatr. 33, 267–286.

Ohmi, K., Greenberg, D.S., Rajavel, K.S., Ryazantsev, S., Li, H.H., and Neufeld, E.F. (2003). Activated microglia in cortex of mouse models of mucopolysaccharidoses I and IIIB. Proc. Natl. Acad. Sci. U. S. A. 100, 1902–1907.

Okuyama, T., Tanaka, A., Suzuki, Y., Ida, H., Tanaka, T., Cox, G.F., Eto, Y., and Orii, T. (2010). Japan Elaprase Treatment (JET) study: idursulfase enzyme replacement therapy in adult patients with attenuated Hunter syndrome (Mucopolysaccharidosis II, MPS II). Mol. Genet. Metab. 99, 18–25.

Ou, L., Herzog, T., Koniar, B.L., Gunther, R., and Whitley, C.B. (2014). High-dose enzyme replacement therapy in murine Hurler syndrome. Mol. Genet. Metab. 111, 116–122.

Pardridge, W.M. (2015). Targeted delivery of protein and gene medicines through the blood-brain barrier. Clin. Pharmacol. Ther. 97, 347–361.

Parenti, G., Andria, G., and Ballabio, A. (2015). Lysosomal Storage Diseases: From Pathophysiology to Therapy. Annu. Rev. Med. 66, 471–486.

Pellett, P.E., Mitra, S., and Holland, T.C. (2014). Basics of virology. Handb. Clin. Neurol. 123, 45–66.

Penc, S.F., Pomahac, B., Winkler, T., Dorschner, R.A., Eriksson, E., Herndon, M., and Gallo, R.L. (1998). Dermatan sulfate released after injury is a potent promoter of fibroblast growth factor-2 function. J. Biol. Chem. 273, 28116–28121.

Piña-Aguilar, R.E., Zaragoza-Arévalo, G.R., Rau, I., Gal, A., Alcántara-Ortigoza, M.A., López-Martínez, M.S., and Santillán-Hernández, Y. (2013). Mucopolysaccharidosis type II in a female carrying a heterozygous stop mutation of the iduronate-2-sulfatase gene and showing a skewed X chromosome inactivation. Eur. J. Med. Genet. 56, 159–162.

Pinto, R., Caseiro, C., Lemos, M., Lopes, L., Fontes, A., Ribeiro, H., Pinto, E., Silva, E., Rocha, S., Marcão, A., et al. (2004). Prevalence of lysosomal storage diseases in Portugal. Eur. J. Hum. Genet. 12, 87–92.

Piotrowska, E., Jakóbkiewicz-Banecka, J., Tylki-Szymanska, A., Liberek, A., Maryniak, A., Malinowska, M., Czartoryska, B., Puk, E., Kloska, A., Liberek, T., et al. (2008). Genistin-rich soy isoflavone extract in substrate reduction therapy for Sanfilippo syndrome: An open-label, pilot study in 10 pediatric patients. Curr. Ther. Res. Clin. Exp. 69, 166–179.

Platt, F.M., Boland, B., and van der Spoel, A.C. (2012). The cell biology of disease: lysosomal storage disorders: the cellular impact of lysosomal dysfunction. J. Cell Biol. 199, 723–734.

Podetz-Pedersen, K.M., Karlen, A.D., P., M., Buckvold, Nan, Z., Slepushkin, V., Roy, A., Yakovief, G., Gong, Z., Muenzer, J., et al. (2013). The American Society of Gene & Cell Therapy Abstracts from the 16th Annual Meeting, Salt Lake City, Utha: "Prevention of

Neurocognitive Deficit by Ex Vivo Lentiviral Transduction of Hematopoietic Stem Cells in a Murine Model of Mucop. Mol. Ther. 21, S191.

Polito, V.A., and Cosma, M.P. (2009). IDS Crossing of the Blood-Brain Barrier Corrects CNS Defects in MPSII Mice. Am. J. Hum. Genet. 85, 296–301.

Polito, V.A., Abbondante, S., Polishchuk, R.S., Nusco, E., Salvia, R., and Cosma, M.P. (2010). Correction of CNS defects in the MPSII mouse model via systemic enzyme replacement therapy. Hum. Mol. Genet. 19, 4871–4885.

Poorthuis, B.J., Wevers, R.A., Kleijer, W.J., Groener, J.E., de Jong, J.G., van Weely, S., Niezen-Koning, K.E., and van Diggelen, O.P. (1999). The frequency of lysosomal storage diseases in The Netherlands. Hum. Genet. 105, 151–156.

Poupetová, H., Ledvinová, J., Berná, L., Dvoráková, L., Kozich, V., and Elleder, M. (2010). The birth prevalence of lysosomal storage disorders in the Czech Republic: comparison with data in different populations. J. Inherit. Metab. Dis. 33, 387–396.

Prasad, V.K., and Kurtzberg, J. (2010). Transplant outcomes in mucopolysaccharidoses. Semin. Hematol. 47, 59–69.

Ramamoorth, M., and Narvekar, A. (2015). Non viral vectors in gene therapy- an overview. J. Clin. Diagn. Res. 9, GE01–GE06.

Reijneveld, J.C., Taphoorn, M.J., and Voest, E.E. (1999). A simple mouse model for leptomeningeal metastases and repeated intrathecal therapy. J. Neurooncol. 42, 137–142.

Resnick, J.M., Whitley, C.B., Leonard, A.S., Krivit, W., and Snover, D.C. (1994). Light and electron microscopic features of the liver in mucopolysaccharidosis. Hum. Pathol. 25, 276–286.

Ribera, A., Haurigot, V., Garcia, M., Marcó, S., Motas, S., Villacampa, P., Maggioni, L., León, X., Molas, M., Sánchez, V., et al. (2015). Biochemical, histological and functional correction of mucopolysaccharidosis Type IIIB by intra-cerebrospinal fluid gene therapy. Hum. Mol. Genet. 24, 2078–2095.

Richard, M., Arfi, A., Rhinn, H., Gandolphe, C., and Scherman, D. (2008). Identification of new markers for neurodegeneration process in the mouse model of Sly disease as revealed by expression profiling of selected genes. J. Neurosci. Res. 86, 3285–3294.

Rivera, V.M., Gao, G.P., Grant, R.L., Schnell, M.A., Zoltick, P.W., Rozamus, L.W., Clackson T., W.J. (2005). Long-term pharmacologically regulated expression of erythropoietin in primates following AAV-mediated gene transfer. Blood 105, 1424–1430.

Roberts, S.H., Upadhyaya, M., Sarfarazi, M., and Harper, P.S. (1989). Further evidence localising the gene for Hunter's syndrome to the distal region of the X chromosome long arm. J. Med. Genet. 26, 309–313.

Rowan, D.J., Tomatsu, S., Grubb, J.H., Montaño, A.M., and Sly, W.S. (2013). Assessment of bone dysplasia by micro-CT and glycosaminoglycan levels in mouse models for mucopolysaccharidosis type I, IIIA, IVA, and VII. J. Inherit. Metab. Dis. 36, 235–246.

Rowlands, D., Sugahara, K., and Kwok, J.C.F. (2015). Glycosaminoglycans and glycomimetics in the central nervous system. Molecules 20, 3527–3548.

Ruijter, G.J.G., Goudriaan, D.A., Boer, A.M., Van den Bosch, J., Van der Ploeg, A.T., Elvers, L.H., Weinreich, S.S., and Reuser, A.J. (2014). Newborn screening for hunter disease: a small-scale feasibility study. JIMD Rep. 14, 23–27.

de Ruijter, J., Valstar, M.J., Narajczyk, M., Wegrzyn, G., Kulik, W., IJlst, L., Wagemans, T., van der Wal, W.M., and Wijburg, F.A. (2012). Genistein in Sanfilippo disease: A randomized controlled crossover trial. Ann. Neurol. 71, 110–120.

Ruzo, A., Garcia, M., Ribera, A., Villacampa, P., Haurigot, V., Marcó, S., Ayuso, E., Anguela, X.M., Roca, C., Agudo, J., et al. (2012a). Liver production of sulfamidase reverses peripheral and ameliorates CNS pathology in mucopolysaccharidosis IIIA mice. Mol. Ther. 20, 254–266.

Ruzo, A., Marcó, S., García, M., Villacampa, P., Ribera, A., Ayuso, E., Maggioni, L., Mingozzi, F., Haurigot, V., and Bosch, F. (2012b). Correction of pathological accumulation of glycosaminoglycans in central nervous system and peripheral tissues of MPSIIIA mice through systemic AAV9 gene transfer. Hum. Gene Ther. 23, 1237–1246.

Sakka, L., Coll, G., and Chazal, J. (2011). Anatomy and physiology of cerebrospinal fluid. Eur. Ann. Otorhinolaryngol. Head Neck Dis. 128, 309–316.

Samaranch, L., Salegio, E.A., San Sebastian, W., Kells, A.P., Foust, K.D., Bringas, J.R., Lamarre, C., Forsayeth, J., Kaspar, B.K., and Bankiewicz, K.S. (2012). Adeno-associated virus serotype 9 transduction in the central nervous system of nonhuman primates. Hum. Gene Ther. 23, 382–389.

Sands, M.S., and Davidson, B.L. (2006). Gene therapy for lysosomal storage diseases. Mol. Ther. 13, 839–849.

Sardiello, M., Palmieri, M., di Ronza, A., Medina, D.L., Valenza, M., Gennarino, V.A., Di Malta, C., Donaudy, F., Embrione, V., Polishchuk, R.S., et al. (2009). A gene network regulating lysosomal biogenesis and function. Science 325, 473–477.

Scarpa, M., Almássy, Z., Beck, M., Bodamer, O., Bruce, I.A., De Meirleir, L., Guffon, N., Guillén-Navarro, E., Hensman, P., Jones, S., et al. (2011). Mucopolysaccharidosis type II: European recommendations for the diagnosis and multidisciplinary management of a rare disease. Orphanet J. Rare Dis. 6, 72.

Schaap, T., and Bach, G. (1980). Incidence of mucopolysaccharidoses in Israel: is Hunter disease a “Jewish disease”? Hum. Genet. 56, 221–223.

Schwartz, I.V.D., Ribeiro, M.G., Mota, J.G., Toralles, M.B.P., Correia, P., Horovitz, D., Santos, E.S., Monlleo, I.L., Fett-Conte, A.C., Sobrinho, R.P.O., et al. (2007). A clinical study of 77 patients with mucopolysaccharidosis type II. Acta Paediatr. Suppl. 96, 63–70.

Schwartz, I.V.D., Pinto, L.L.C., Breda, G., Lima, L., Ribeiro, M.G., Mota, J.G., Acosta, A.X., Correia, P., Horovitz, D.D.G., Porciuncula, C.G.G., et al. (2009). Clinical and biochemical studies in mucopolysaccharidosis type II carriers. J. Inherit. Metab. Dis. 32, 732–738.

Seto, T., Kono, K., Morimoto, K., Inoue, Y., Shintaku, H., Hattori, H., Matsuoka, O., Yamano, T., and Tanaka, A. (2001). Brain magnetic resonance imaging in 23 patients with mucopolysaccharidoses and the effect of bone marrow transplantation. Ann. Neurol. 50, 79–92.

Settembre, C., Fraldi, A., Medina, D.L., and Ballabio, A. (2013). Signals from the lysosome: a control centre for cellular clearance and energy metabolism. Nat. Rev. Mol. Cell Biol. 14, 283–296.

Shen, J.-S., Meng, X.-L., Moore, D.F., Quirk, J.M., Shayman, J.A., Schiffmann, R., and Kaneski, C.R. (2008). Globotriaosylceramide induces oxidative stress and up-regulates cell adhesion molecule expression in Fabry disease endothelial cells. Mol. Genet. Metab. 95, 163–168.

Sietsema, W.K., and Schwen, R. (2007). Toxicology Testing for Products Intended for Pediatric Population. In Nonclinical Drug Safety Assessment: Practical Considerations for Successful Registration, (FDAnews), pp. 411–440.

da Silva, E.M.K., Strufaldi, M.W.L., Andriolo, R.B., and Silva, L.A. (2014). Enzyme replacement therapy with idursulfase for mucopolysaccharidosis type II (Hunter syndrome). Cochrane Database Syst. Rev. 1, CD008185.

Simonaro, C.M., Haskins, M.E., and Schuchman, E.H. (2001). Articular chondrocytes from animals with a dermatan sulfate storage disease undergo a high rate of apoptosis and release nitric oxide and inflammatory cytokines: a possible mechanism underlying degenerative joint disease in the mucopolysaccharidoses. Lab. Invest. 81, 1319–1328.

Simonaro, C.M., D'Angelo, M., Haskins, M.E., and Schuchman, E.H. (2005). Joint and bone disease in mucopolysaccharidoses VI and VII: identification of new therapeutic targets and biomarkers using animal models. Pediatr. Res. 57, 701–707.

Simonaro, C.M., D'Angelo, M., He, X., Eliyahu, E., Shtraizent, N., Haskins, M.E., and Schuchman, E.H. (2008). Mechanism of glycosaminoglycan-mediated bone and joint disease: implications for the mucopolysaccharidoses and other connective tissue diseases. Am. J. Pathol. 172, 112–122.

Simonelli, F., Maguire, A.M., Testa, F., Pierce, E.A., Mingozzi, F., Bennicelli, J.L., Rossi, S., Marshall, K., Banfi, S., Surace, E.M., et al. (2010). Gene therapy for Leber's congenital

amaurosis is safe and effective through 1.5 years after vector administration. Mol. Ther. 18, 643–650.

Skubis-Zegadło, J., Stachurska, A., and Małecki, M. (2013). Vectrology of adeno-associated viruses (AAV). Med. Wieku Rozwoj. 17, 202–206.

Snyder, B.R., Gray, S.J., Quach, E.T., Huang, J.W., Leung, C.H., Samulski, R.J., Boulis, N.M., and Federici, T. (2011). Comparison of adeno-associated viral vector serotypes for spinal cord and motor neuron gene delivery. Hum. Gene Ther. 22, 1129–1135.

Sohn, Y.B., Choi, E.W., Kim, S.J., Park, S.W., Kim, S.-H., Cho, S.-Y., Jeong, S.I., Huh, J., Kang, I.-S., Lee, H.J., et al. (2012). Retrospective analysis of the clinical manifestations and survival of Korean patients with mucopolysaccharidosis type II: emphasis on the cardiovascular complication and mortality cases. Am. J. Med. Genet. A 158A, 90–96.

Sohn, Y.B., Cho, S.Y., Park, S.W., Kim, S.J., Ko, A.-R., Kwon, E.-K., Han, S.J., and Jin, D.-K. (2013a). Phase I/II clinical trial of enzyme replacement therapy with idursulfase beta in patients with mucopolysaccharidosis II (Hunter Syndrome). Orphanet J. Rare Dis. 8, 42.

Sohn, Y.B., Lee, J., Cho, S.Y., Kim, S.J., Ko, A.-R., Nam, M.H., and Jin, D.-K. (2013b). Improvement of CNS defects via continuous intrathecal enzyme replacement by osmotic pump in mucopolysaccharidosis type II mice. Am. J. Med. Genet. A 161A, 1036–1043.

Sorrentino, N.C., Maffia, V., Strollo, S., Cacace, V., Romagnoli, N., Manfredi, A., Ventrella, D., Dondi, F., Barone, F., Giunti, M., et al. (2016). A Comprehensive Map of CNS Transduction by Eight Recombinant Adeno-associated Virus Serotypes Upon Cerebrospinal Fluid Administration in Pigs. Mol. Ther. 24, 276–286.

Spector, R., Robert Snodgrass, S., and Johanson, C.E. (2015). A balanced view of the cerebrospinal fluid composition and functions: Focus on adult humans. Exp. Neurol. 273, 57–68.

Stirling, J.L., Robinson, D., Fensom, A.H., Benson, P.F., and Baker, J.E. (1978). Fluorimetric assay for prenatal detection of Hurler and Scheie homozygotes or heterozygotes. Lancet 1, 147.

Streit, W.J., and Kreutzberg, G.W. (1987). Lectin binding by resting and reactive microglia. J. Neurocytol. 16, 249–260.

Sukegawa, K., Song, X.Q., Masuno, M., Fukao, T., Shimozawa, N., Fukuda, S., Isogai, K., Nishio, H., Matsuo, M., Tomatsu, S., et al. (1997). Hunter disease in a girl caused by R468Q mutation in the iduronate-2-sulfatase gene and skewed inactivation of the X chromosome carrying the normal allele. Hum. Mutat. 10, 361–367.

Sukegawa, K., Matsuzaki, T., Fukuda, S., Masuno, M., Fukao, T., Kokuryu, M., Iwata, S., Tomatsu, S., Orii, T., and Kondo, N. (1998). Brother/sister siblings affected with Hunter disease: evidence for skewed X chromosome inactivation. Clin. Genet. 53, 96–101.

Taylor, K.R., and Gallo, R.L. (2006). Glycosaminoglycans and their proteoglycans: host-associated molecular patterns for initiation and modulation of inflammation. FASEB J. 20, 9–22.

Testa, F., Maguire, A.M., Rossi, S., Pierce, E.A., Melillo, P., Marshall, K., Banfi, S., Surace, E.M., Sun, J., Acerra, C., et al. (2013). Three-year follow-up after unilateral subretinal delivery of adeno-associated virus in patients with Leber congenital Amaurosis type 2. Ophthalmology 120, 1283–1291.

Timms, K.M., Lu, F., Shen, Y., Pierson, C.A., Muzny, D.M., Gu, Y., Nelson, D.L., and Gibbs, R.A. (1995). 130 kb of DNA sequence reveals two new genes and a regional duplication distal to the human iduronate-2-sulfate sulfatase locus. Genome Res. 5, 71–78.

Tomatsu S, Okamura K, Maeda H, Taketani T, Castrillon SV, Gutierrez MA, Nishioka T, Fachel AA, Orii KO, Grubb JH, Cooper A, Thornley M, Wraith E, Barrera LA, Laybauer LS, Giugliani R, Schwartz IV, Frenking GS, Beck M, Kircher SG, Paschke E, Yamaguchi S, U, N.A. (2005). Keratan sulphate levels in mucopolysaccharidoses and mucolipidoses. J. Inherit. Metab. Dis. 28, 187–202.

Trowbridge, J.M., and Gallo, R.L. (2002). Dermatan sulfate: new functions from an old glycosaminoglycan. Glycobiology 12, 117R – 125R.

Tuschl, K., Gal, A., Paschke, E., Kircher, S., and Bodamer, O.A. (2005). Mucopolysaccharidosis type II in females: case report and review of literature. Pediatr. Neurol. 32, 270–272.

Vafiadaki, E., Cooper, A., Heptinstall, L.E., Hatton, C.E., Thornley, M., and Wraith, J.E. (1998). Mutation analysis in 57 unrelated patients with MPS II (Hunter's disease). Arch. Dis. Child. 79, 237–241.

Valayannopoulos, V., and Wijburg, F.A. (2011). Therapy for the mucopolysaccharidoses. Rheumatology (Oxford). 50 Suppl 5, v49–v59.

Vellodi, A. (2005). Lysosomal storage disorders. Br. J. Haematol. 128, 413–431.

Vellodi, A., Young, E., Cooper, A., Lidchi, V., Winchester, B., and Wraith, J.E. (1999). Long-term follow-up following bone marrow transplantation for Hunter disease. J. Inherit. Metab. Dis. 22, 638–648.

Villani, G.R.D., Di Domenico, C., Musella, A., Cecere, F., Di Napoli, D., and Di Natale, P. (2009). Mucopolysaccharidosis IIIB: oxidative damage and cytotoxic cell involvement in the neuronal pathogenesis. Brain Res. 1279, 99–108.

Vitner, E.B., Platt, F.M., and Futerman, A.H. (2010). Common and uncommon pathogenic cascades in lysosomal storage diseases. J. Biol. Chem. 285, 20423–20427.

Vogler, C., Levy, B., Grubb, J.H., Galvin, N., Tan, Y., Kakkis, E., Pavloff, N., and Sly, W.S. (2005). Overcoming the blood-brain barrier with high-dose enzyme replacement therapy in murine mucopolysaccharidosis VII. Proc. Natl. Acad. Sci. U. S. A. 102, 14777–147782.

Voznyi, Y. V, Keulemans, J.L., and van Diggelen, O.P. (2001). A fluorimetric enzyme assay for the diagnosis of MPS II (Hunter disease). J. Inherit. Metab. Dis. 24, 675–680.

Voznyi YaV, Karpova, E.A., Dudukina, T. V, Tsvetkova, I. V, Boer, A.M., Janse, H.C., and van Diggelen, O.P. (1993). A fluorimetric enzyme assay for the diagnosis of Sanfilippo disease C (MPS III C). J. Inherit. Metab. Dis. 16, 465–472.

Waehler, R., Russell, S.J., and Curiel, D.T. (2007). Engineering targeted viral vectors for gene therapy. Nat. Rev. Genet. 8, 573–587.

Wakabayashi, T., Shimada, Y., Akiyama, K., Higuchi, T., Fukuda, T., Kobayashi, H., Eto, Y., Ida, H., and Ohashi, T. (2015). Hematopoietic Stem Cell Gene Therapy Corrects Neuropathic Phenotype in Murine Model of Mucopolysaccharidosis Type II. Hum. Gene Ther. 26, 357–366.

Walkley, S.U. (1998). Cellular pathology of lysosomal storage disorders. Brain Pathol. 8, 175–193.

Walkley, S.U. (2007). Pathogenic mechanisms in lysosomal disease: a reappraisal of the role of the lysosome. Acta Paediatr. 96, 26–32.

Wang, D.B., Dayton, R.D., Henning, P.P., Cain, C.D., Zhao, L.R., Schrott, L.M., Orchard, E.A., Knight, D.S., and Klein, R.L. (2010). Expansive gene transfer in the rat CNS rapidly produces amyotrophic lateral sclerosis relevant sequelae when TDP-43 is overexpressed. Mol. Ther. 18, 2064–2074.

Ward, N.J., Buckley, S.M.K., Waddington, S.N., Vandendriessche, T., Chuah, M.K.L., Nathwani, A.C., McIntosh, J., Tuddenham, E.G.D., Kinnon, C., Thrasher, A.J., et al. (2011). Codon optimization of human factor VIII cDNAs leads to high-level expression. Blood 117, 798–807.

Weinreb, N.J. (2013). Oral small molecule therapy for lysosomal storage diseases. Pediatr. Endocrinol. Rev. 11 Suppl 1, 77–90.

Wilkerson, M.J., Lewis, D.C., Marks, S.L., and Prieur, D.J. (1998). Clinical and morphologic features of mucopolysaccharidosis type II in a dog: naturally occurring model of Hunter syndrome. Vet. Pathol. 35, 230–233.

Wilson, P.J., Morris, C.P., Anson, D.S., Occhiodoro, T., Bielicki, J., Clements, P.R., and Hopwood, J.J. (1990). Hunter syndrome: isolation of an iduronate-2-sulfatase cDNA clone and analysis of patient DNA. Proc. Natl. Acad. Sci. U. S. A. 87, 8531–8535.

Wilson, P.J., Meaney, C.A., Hopwood, J.J., and Morris, C.P. (1993). Sequence of the human iduronate 2-sulfatase (IDS) gene. Genomics 17, 773–775.

Winchester, B., Young, E., Geddes, S., Genet, S., Hurst, J., Middleton-Price, H., Williams, N., Webb, M., Habel, A., and Malcolm, S. (1992). Female twin with Hunter disease due to nonrandom inactivation of the X-chromosome: a consequence of twinning. Am. J. Med. Genet. 44, 834–838.

Wolf, D.A., Banerjee, S., Hackett, P.B., Whitley, C.B., McIvor, R.S., and Low, W.C. (2015). Gene therapy for neurologic manifestations of mucopolysaccharidoses. Expert Opin. Drug Deliv. 12, 283–296.

Wooten, W.I., Muenzer, J., Vaughn, B. V, and Muhlebach, M.S. (2013). Relationship of sleep to pulmonary function in mucopolysaccharidosis II. J. Pediatr. 162, 1210–1215.

Wraith, J.E., Scarpa, M., Beck, M., Bodamer, O.A., De Meirleir, L., Guffon, N., Meldgaard Lund, A., Malm, G., Van der Ploeg, A.T., and Zeman, J. (2008a). Mucopolysaccharidosis type II (Hunter syndrome): a clinical review and recommendations for treatment in the era of enzyme replacement therapy. Eur. J. Pediatr. 167, 267–277.

Wraith, J.E., Beck, M., Giugliani, R., Clarke, J., Martin, R., and Muenzer, J. (2008b). Initial report from the Hunter Outcome Survey. Genet. Med. 10, 508–516.

Wright, B.L.C., Lai, J.T.F., and Sinclair, A.J. (2012). Cerebrospinal fluid and lumbar puncture: a practical review. J. Neurol. 259, 1530–1545.

Wu, Z., Asokan, A., and Samulski, R.J. (2006). Adeno-associated virus serotypes: vector toolkit for human gene therapy. Mol. Ther. 14, 316–327.

Wyatt, K., Henley, W., Anderson, L., Anderson, R., Nikolaou, V., Stein, K., Klinger, L., Hughes, D., Waldek, S., Lachmann, R., et al. (2012). The effectiveness and cost-effectiveness of enzyme and substrate replacement therapies: a longitudinal cohort study of people with lysosomal storage disorders. Health Technol. Assess. 16, 1–543.

Xia, W., Bringmann, P., McClary, J., Jones, P.P., Manzana, W., Zhu, Y., Wang, S., Liu, Y., Harvey, S., Madlansacay, M.R., et al. (2006). High levels of protein expression using different mammalian CMV promoters in several cell lines. Protein Expr. Purif. 45, 115–124.

Yamada, Y., Tomatsu, S., Sukegawa, K., Suzuki, Y., Kondo, N., Hopwood, J.J., and Orii, T. (1993). Mucopolysaccharidosis type II (Hunter disease): 13 gene mutations in 52 Japanese patients and carrier detection in four families. Hum. Genet. 92, 110–114.

Yatziv, S., Erickson, R.P., and Epstein, C.J. (1977). Mild and severe Hunter syndrome (MPS II) within the same sibships. Clin. Genet. 11, 319–326.

Yayon, A., Klagsbrun, M., Esko, J.D., Leder, P., and Ornitz, D.M. (1991). Cell surface, heparin-like molecules are required for binding of basic fibroblast growth factor to its high affinity receptor. Cell 64, 841–848.

Zanta-Boussif, M.A., Charrier, S., Brice-Ouzet, A., Martin, S., Opolon, P., Thrasher, A.J., Hope, T.J., and Galy, A. (2009). Validation of a mutated PRE sequence allowing high and

sustained transgene expression while abrogating WHV-X protein synthesis: application to the gene therapy of WAS. Gene Ther. 16, 605–619.

Zhou, M., Guo, J., Cha, J., Chae, M., Chen, S., Barral, J.M., Sachs, M.S., and Liu, Y. (2013). Non-optimal codon usage affects expression, structure and function of clock protein FRQ. Nature 495, 111–115.

Zincarelli, C., Soltys, S., Rengo, G., and Rabinowitz, J.E. (2008). Analysis of AAV serotypes 1-9 mediated gene expression and tropism in mice after systemic injection. Mol. Ther. 16, 1073–1080.